Targeting the epigenome and immune system for diagnosis and treatment of malignancies

Ali Mehdi

Department of Human Genetics

Faculty of Medicine and Health Sciences

McGill University, Montreal

September 2022

A thesis submitted to McGill University in partial fulfillment of the requirements of the degree of Doctor of Philosophy

DEDICATION

This thesis is dedicated to my parents (Iqbal Baqer and Mahlaqa Bano), my siblings (Ali Imran, Arooj Fatima, Heera Fatima, Dua Fatima and Ali Asghar) and my wife (Hira Sana). Thank you for always encouraging me, believing in me, and giving me hope and guidance when I was lost.

TABLE OF CONTENTS

ABSTRACT

Early detection of common cancers including prostate cancer (PCa) remains a challenge due to limitations of current diagnostic techniques. A promising strategy is to utilize cancer immunosurveillance system, including T cells, that target pre-malignant and malignant cells in early stages of tumorigenesis. This targeting by T cells may alter their DNA methylome. Hence, an epigenome-wide methylation analysis of peripheral T cells was performed in healthy controls and PCa patients. DNA methylation changes were enriched in genes involved in immunosurveillance pathways. A DNA methylation signature was also identified that could not only distinguish between healthy controls and PCa patients, but also different stages of PCa.

Aberrant methylomes drive carcinogenesis especially in melanoma and are responsible for emerging resistance mechanisms against immune checkpoint inhibitors (CPIs). Although CPIs such as anti-PD-1 antibody have caused a paradigm shift in cancer treatments, 60-70% of the patients do not respond to such therapies. Accordingly, combination therapies are being proposed to enhance CPIs response. S-adenosylmethionine (SAM) is a methyl donor that targets hypomethylated DNA and has significant anti-cancer effects in several malignancies. However, the effect of SAM had never been investigated in melanoma. Hence, SAM alone and in combination with CPI was used to target melanoma.

SAM caused significant decrease in proliferation and metastatic ability of melanoma cells. SAM directed phenotype switching of heterogeneous invasive and proliferative melanoma cells towards differentiation characterized by increased melanogenesis, immunogenicity, and reduced stemness ability. Transcriptome analysis of SAM treated YUMMER1.7 cells showed significant reduction in cell cycle genes/pathways while upregulation of immunostimulatory genes/pathways. SAM alone caused significant reduction of tumor growth and progression of BRAF wild-type B16-B6 and BRAF mutant YUMMER1.7-B6 mice. Intriguingly, SAM and anti-PD-1 antibody combination caused superior anti-cancer efficacy in both melanoma mouse models. Transcriptome analysis of B16 tumors treated with combination showed marked downregulation of core melanoma genes and pathways while upregulation of tumor suppressor genes. In YUMMER1.7-B6 mice, the combination also had high anti-cancer efficacy and increased survival of mice compared to all groups. Immunophenotyping revealed that the combination treated B16 and YUMMER1.7 tumors had high $CD8^+$ T cells' activation, effector functions, and polyfunctionality.

Cumulatively, this is the first direct evidence of the beneficial anti-cancer efficacy of SAM alone and in unique combination with anti-PD-1 antibody against melanomas.

Luminal B subtype of breast cancer (BCa) is immunogenically low and unresponsive to CPI. It also metastasizes to skeletal and non-skeletal sites. Hence, the anti-cancer efficacy of SAM+anti-PD-1 combination was further tested in luminal B BCa. The combination had highest anti-cancer efficacy in Eo771 luminal B BCa mice compared to all groups. The combination significantly reduced skeletal lesion area and protected the tibial integrity from tumor osteolytic damage in bone metastasis model. Transcriptome analysis of the Eo771 primary tumors revealed significant downregulation of pro-metastatic genes and pathways, and upregulation of infiltration and cytotoxicity of $CD8^+$ T cells, and immunostimulatory genes and pathways in the combination treated tumors. Hence combining SAM with CPI has potential to treat luminal B BCa.

In summary, the present thesis leveraged power of DNA methylation alterations in peripheral T cells for cancer diagnosis. It provides first evidence of the superior anti-cancer efficacy of a novel SAM and anti-PD-1 antibody combination. Since both agents are approved, this novel therapeutic strategy provides immense potential to be translated into clinic in reducing cancer associated morbidity and mortality.

RÉSUMÉ

La détection précoce des cancers courants, dont le cancer de la prostate (CPa), reste un défi en raison des limites des techniques de diagnostic actuelles. Une stratégie prometteuse consiste à utiliser le système d'immunosurveillance du cancer, notamment les cellules T, qui ciblent les premiers stades de la tumorigenèse. Une analyse de la méthylation des cellules T périphériques à l'échelle de l'épigénome a montré que les changements de méthylation de l'ADN étaient enrichis dans les voies/gène de signalisation de l'immunosurveillance. Une signature de méthylation de l'ADN a également été identifiée, ce qui permet non seulement de distinguer les témoins sains mais aussi les différents stades du cancer du sein.

Les méthylomes aberrants sont responsables des mécanismes de résistance émergents contre les inhibiteurs de point de contrôle immunitaire (IPC). Bien que les IPC tels que l'anticorps anti-PD-1 aient entraîné un changement de paradigme dans le traitement du cancer, 60 à 70 % des patients ne répondent pas à ces thérapies. En conséquence, des thérapies combinées sont proposées pour améliorer la réponse aux IPC. S-adénosylméthionine (SAM) cible l'hypométhylation de l'ADN, en traitement seul et en combinaison avec l'IPC a été utilisée pour cibler le mélanome. SAM a provoqué une diminution significative de la prolifération et de la capacité métastatique des cellules de mélanome, a induit un changement de phénotype vers une différenciation caractérisée par une augmentation de la mélanogénèse, de l'immunogénicité, et une réduction de la croissance cellulaire à caractère ‘souche’. L'analyse du transcriptome des cellules YUMMER1.7 traitées avec SAM a montré une réduction des voies de signalisation du cycle cellulaire/gènes et une augmentation des voies de signalisation des immunostimulateurs/gènes. SAM seule a entraîné une réduction significative de la croissance et de la progression tumorales chez les souris B16-B6 de type BRAF sauvage et YUMMER1.7-B6 mutant BRAF alors que la combinaison de SAM avec d'anticorps anti-PD-1 a entraîné une efficacité supérieure. L'analyse du transcriptome des tumeurs B16 traitées par l'association a révélé une baisse marquée des voies de signalisation/gène essentiels du mélanome et une augmentation des gènes suppresseurs de tumeurs et a augmenté la survie des souris. L'immunophénotypage a révélé que les tumeurs B16 et YUMMER1.7 traitées par l'association présentaient une activation des fonctions effectrices et une polyfonctionnalité élevées des cellules T CD8+. Il s'agit de la première preuve directe de l'efficacité anticancéreuse bénéfique de SAM seul et en combinaison avec l'anticorps anti-PD-1 contre les mélanomes. Le sous-type

Luminal B du cancer du sein (BCa) est immunologiquement faible et ne répond pas à l'IPC. Par conséquent, l'efficacité anticancéreuse de l'association SAM+anti-PD-1 a été testée plus tôt. L'association a présenté une plus grande efficacité anticancéreuse chez les souris Eo771 luminal B, a réduit la surface des lésions squelettiques et a protégé l'intégrité du tibia des dommages ostéolytiques de la tumeur. L'analyse du transcriptome des tumeurs primaires Eo771 a révélé une baisse significative des voies pro-métastatiques /gènes, et une augmentation de l'infiltration et de la cytotoxicité des cellules T CD8+, une augmentation des voies immunostimulantes/gènes dans les tumeurs traitées par l'association. Par conséquent, la combinaison de la SAM avec l'IPC a un potentiel dans le traitement du BCa.

En résumé, la présente thèse a exploité le pouvoir des altérations de la méthylation de l'ADN des cellules T périphériques dans le diagnostic du cancer. Elle fournit les premières preuves de l'efficacité anticancéreuse supérieure d'une nouvelle combinaison de SAM et d'anticorps anti-PD-1. Cette nouvelle stratégie thérapeutique offre un immense potentiel pour être appliquée en clinique et réduire la morbidité et la mortalité associées au cancer.

LIST OF ABBREVIATIONS

Ags	Antigens	**MFI**	Mean fluorescence intensity
APCs	Antigen presenting cells	**MGDB**	The melanoma gene database
AUC	Area under curve	**MHC class I**	Major histocompatibility complex class I
BCa	Breast cancer	**MHC class II**	Major histocompatibility complex class II
BCR	B cell receptor	**MICs**	Melanoma initiating cells
BH	Benjamini-hochberg	**MITF**	Microphthalmia-associated transcription factor or melanocyte inducing transcription factor
BLS	Bone lesion score	**MMP**	Matrix metalloproteinase
BMIQ	Beta-mixture quantile	**NK**	Natural killer
BRAF	V-raf murine sarcoma viral oncogene homolog B1	**NRP2**	Neuropilin 2
CD	Cluster of differentiation	**NSG**	Next-generation sequencing
ChAMP	Chip analysis methylation pipeline	**PBMCs**	Peripheral blood mononuclear cells
CPIs/ ICPi	Immune checkpoint inhibitors	**PCa**	Prostate cancer
CREB	Camp-response element binding protein	**PD-1**	Programmed cell death 1
CSCs	Cancer stem cells	**PDGFA**	Platelet-derived growth factor alpha
CTLA-4	Cytotoxic T-lymphocyte-associated protein 4	**PD-L1**	Programmed death ligand 1
CTLs	Cytotoxic T lymphocytes	**PI3K**	Phosphoinositide-3-kinase
DC	Dendritic cells	**PLAU/ uPA**	Urokinase plasminogen activator
DEGs	Differentially expressed genes	**PMA**	Phorbol 12-myristate 13-acetate
DMBT1	Deleted in malignant brain tumors 1	**PMEL/ GP100**	Pre-melanosome protein/ Glycoprotein 100
DMP	Differentially methylated probes	**PMS**	Polygenic methylation score
DNMT	DNA methyltransferase	**PTEN**	Loss of phosphatase and tensin homolog
DNMTi	DNA methyltransferase inhibitors	**ROC**	Receiver operating characteristic
ECM	Extracellular matrix	**rPD-1**	Recombinant PD-1
EGFR	Epidermal growth factor receptor	**RSEM**	RNA-Seq by Expectation Maximization
EMT	Epithelial to mesenchymal transition	**RT-qPCR**	Reverse transcriptase quantitative real-time PCR
ENCODE	The Encyclopedia of DNA Elements	**SAM**	S-adenosylmethionine
FANTOM5	Functional Annotation of the Mammalian Genome 5	**SOX10**	SRY-box transcription factor 10

FDA	Food and drug administration	**SRE**	Skeletal-related events
FDR	False discovery rate	**SVD**	Singular value decomposition
FMO	Fluorescence minus one	**TAMS**	Tumor-associated macrophages
GEMMs	Genetically engineering mouse models	**TCGA**	The cancer genome atlas
H&E	Hematoxylin and Eosin	**TCR**	T cell receptor
HCC	Hepatocellular carcinoma	**TGI**	Tumor growth inhibition
HDACi	Histone deacetylase inhibitors	**Th1**	$CD4^+$ T helper 1 cells
HGPCa	High gleason prostate cancer	**Th17**	$CD4^+$ T helper 17 cells
IFNγ	Interferon-gamma	**Th2**	$CD4^+$ T helper 2 cells
IGV	Integrative genomics viewer	**TILs**	Tumor infiltrating lymphocytes
IHC	Immunohistochemistry	**TIM-3**	T cell immunoglobulin and mucin domain-containing protein 3
IL-2	Interleukin 2	**TMB**	Tumor mutational burden
irAEs	Immune-related adverse events	**TME**	Tumor microenvironment
LAG-3	Lymphocyte-activation gene 3	**TNFα**	Tumor-necrosis factor alpha
LAT	Linker for activation of T cells	**Tregs**	Regulatory T cells
LCK	Lymphocyte-specific protein tyrosine kinase	**TSGs**	Tumor suppressor genes
LGPCa	Low gleason prostate cancer	**TYR**	Tyrosinase
MAAs	Melanoma associated antigens	**TYRP1**	Tyrosinase-related protein 1
MAPK	Mitogen-activated protein kinase	**TYRP2/ DCT**	Tyrosinase-related protein 2/ dopachrome tautomerase
MART1/ MELAN-A	Melanoma antigen recognized by T cells 1	**VEGF**	Vascular endothelial growth factor
MDAs	Melanoma differentiation antigens	**WBCs**	White blood cells

LIST OF FIGURES AND TABLES

CHAPTER ONE

CHAPTER TWO

CHAPTER THREE

CHAPTER FOUR

Figure 6: Combination of SAM with anti-PD-1 antibody results in significant higher anti-cancer efficacy in melanoma mouse models.

Figure 7: SAM in combination with anti-PD-1 antibody enhances $CD8^+$ T cells' tumor infiltration, activation, cytokine production and polyfunctionality in the TME.

Figure 8: SAM elevates $CD4^+$ T helper cell responses in the TME.

CHAPTER FIVE

Figure 1: Effect of SAM on proliferation, colony-formation (survival), and invasion of luminal B BCa cell lines.

Figure 2: PD-L1 expression and effect of PD-L1 intracellular signaling on cell proliferation of murine BCa cells.

Figure 3: SAM, anti-PD-1 antibody, and the combination treatment decreased primary tumor growth in Eo771 tumor-bearing mice.

Figure 4: SAM, anti-PD-1 antibody, and the combination treatment decreased lung metastasis in Eo771 tumor-bearing mice.

Figure 5: The SAM and anti-PD-1 antibody combination decreases bone metastasis and protects the bone from damage caused by aggressively growing tumor lesions.

Figure 6: Tumors treated with the SAM and anti-PD-1 antibody combination show reduced expression of key oncogenes and pro-metastasis genes, and elevated expression of immunostimulatory genes.

CHAPTER SEVEN

Figure 1: SAM and anti-PD-1 antibody combination reduces tumor growth, progression, and metastasis, and enhances the anti-cancer immunity in melanoma.

ACKOWLEDGEMENTS

I truly believe that in life no one can succeed alone. I feel my PhD candidacy is no different. There are many people that have helped me in various aspects during my PhD time.

I would like to pay my sincere gratitude to my supervisor, Dr. Shafaat A. Rabbani, for providing me the opportunity and the resources to work in his laboratory. I am thankful to Dr. Rabbani for his consistent guidance and mentorship throughout the duration my degree. Dr. Rabbani fostered essential skills such as critical thinking, problem-solving and independence that were not only important during my PhD but also in future for my career growth. I would like to thank my supervisory committee members, Dr. Andrew Bateman and Dr. Ioannis Ragoussis, for their immense support, constructive feedback and scholarly discussions.

I would like to thank our laboratory manager, Ani Arakelian, for training me in various experimental techniques especially *in vivo* mouse work which were pivotal to my PhD. Also, for helping me tackle problems related to experimental techniques. I would also like to thank our former laboratory mate Dr. Niaz Mahmood for scholarly discussions and solving some of the problems I faced during PhD. I would also like to thank all the members of the Calcium laboratory for their help whenever I needed it, and special thanks to Loan for translating my thesis abstract. I would also like to thank Patricia and all the administrative staff, ARD, immunophenotyping staff, and immunohistochemistry staff at the RI-MUHC.

I would also like to thank our collaborator Dr. Moshe Szyf and his laboratory personnel Dr. David Cheishvili, Daniel, Farida and Sergiv for allowing me to use their laboratory resources and teaching me laboratory techniques related to methylation. Special thanks to Dr. Szyf for his constructive feedback and meticulous review of all my manuscripts.

Special thanks to our collaborator Dr. Ciriaco. A. Piccirillo and his student, Mikhael Attias, for carrying out immunophenotyping work and teaching me some of the latest techniques in immunophenotyping using flow cytometry. I would also like to thank them for their advice and expert feedback on immunology.

I would also like to thank all the members of the Human Genetics department especially Ross MacKay and Rimi Joshi for their consistent help, guidance, and support through out my PhD.

I would also like to specially thank my friend Dr. Mohanachary Amaravadi for his excellent mentorship, constant guidance and support for my PhD and my career path. Dr. Amaravadi also provided his constructive feedback for the thesis as well. I would also like to thank my friend Pubudu for his constant help and support in bioinformatics analysis.

I want to also acknowledge all the funding agencies for their financial support including the Department of Human Genetics, Queen Elizabeth II Scholarship program from Genome Quebec, and Fonds de recherche du Québec-Santé (FRQ-S).

Finally, I would like to thank my parents, siblings and my wife for their constant emotional support, encouragement, and unconditional love throughout my life and during my PhD time.

CONTRIBUTION TO ORIGINAL KNOWLEDGE

- Provided for the first-time a potential role of DNA methylation changes in peripheral T cells of patients with prostate cancer (PCa). Indeed, the DNA methylation changes occurred at essential immune recognition and activation pathways.
- Identified a non-invasive DNA methylation signature in peripheral T cells that may allow for early intervention and stratification of patients into different diagnostic groups to reduce PCa associated morbidity from repeat invasive prostate biopsies and design therapeutic strategy to reduce PCa associated mortality.
- Demonstrated for the first time that a universal methyl donor and a nutraceutical supplement, S-adenosylmethionine (SAM), causes anti-cancer effects in BRAF wild-type (WT) and BRAF mutant melanoma (*in vitro* and *in vivo*) which together represent 80-85% of the melanoma patients. SAM alone reduces primary tumor growth and progression of both BRAF WT B16-B6 and BRAF mutant YUMMER1.7-B6 syngeneic (immunocompetent) mouse models of melanoma.
- Reported for the first time, a novel and highly effective combination of SAM with immune checkpoint inhibitor (CPI), anti-PD-1 antibody, in reducing primary tumor growth and metastasis of melanoma mouse models.
- Unveiled using transcriptome analysis of BRAF WT B16 tumors that the SAM and anti-PD-1 antibody combination regulates a large number of genes. In combination treated tumors compared to control, genes and pathways involved in tumorigenesis of melanoma were significantly downregulated whereas the genes and pathways involved in immune stimulation were significantly upregulated.
- Showed that the oncogenes (including *NRP2*) that are typically upregulated in primary tumor and metastatic tissues of human melanoma patients (and associated with poor survival) were significantly downregulated by the SAM and anti-PD-1 antibody combination treatment in B16 tumors, whereas vice versa trend was noticed for the expression of tumor suppressor genes (including *DMBT1*).
- Discovered the role of SAM and anti-PD-1 antibody combination in stimulating the anti-cancer immunity in tumor microenvironment (TME) of low immunogenic BRAF WT B16-B6 melanoma mouse model. Together SAM and anti-PD-1 antibody combination unleashes highly effective anti-cancer immune responses including increased infiltration

of $CD8^+$ T cells into the TME, and activation, proliferation (clonal expansion), cytokine production as well as polyfunctionality of cytotoxic $CD8^+$ T cells.

- Uncovered the role of SAM in phenotype switching of melanoma cells. SAM directed cells from invasive and proliferative state into differentiated state by regulating MITF expression and inducing melanogenesis.
- Revealed that SAM increases the immunogenicity and sensitivity of melanoma cell lines and tumors which contributes to enhanced anti-cancer immunity and response to CPI.
- Discovered that SAM alone stimulates anti-cancer immune responses in TME of immunogenic BRAF mutant YUMMER1.7-B6 melanoma mouse model, and together with anti-PD-1 antibody enhances the anti-cancer immune responses including increased infiltration of $CD8^+$ T cells into the TME, and activation, cytokine production and increased polyfunctionality of cytotoxic $CD8^+$ T cells.
- Uncovered an unusual role of SAM in increasing the density and frequency of $CD4^+$ Th17 cells in YUMMER1.7 TME.
- Demonstrated that SAM and anti-PD-1 antibody combination can reduce lung metastasis in B16-B6 lung metastasis mouse model.
- For the first time, demonstrated the potential of combining SAM with anti-PD-1 antibody in treatment of luminal B BCa. SAM and anti-PD-1 antibody significantly reduced tumor growth and progression of Eo771-B6 mouse model.
- Uncovered that combining SAM with anti-PD-1 antibody can significantly reduce metastasis of luminal B BCa to skeletal and non-skeletal sites. Combination significantly reduced skeletal lesion area and protected the tibial integrity from tumor osteolytic damage in Eo771-B6 bone metastasis model.
- Revealed using transcriptome analysis of Eo771 primary tumors that the SAM and anti-PD-1 antibody combination significantly downregulated oncogenes and pathways including matrix metalloproteinases (MMPs) whereas upregulated infiltration and cytotoxicity (elevated granzymes) of $CD8^+$ T cells, and immunostimulatory genes and pathways.

FORMAT OF THE THESIS AND PUBLICATIONS

This thesis follows a manuscript (article) based format in line with the thesis preparation guidelines provided by the Human Genetics department and the Faculty of Graduate and Postdoctoral Studies, McGill University. The thesis is prepared by Ali Mehdi and supervised by Dr. Shafaat A. Rabbani. This thesis includes seven Chapters. Chapter One provides a general introduction including rationale, hypotheses, and objectives, and a literature review that contains excerpts from a review article that the author had published as a first author during his Ph.D. tenure. Chapter Six and Seven provides general discussion, conclusions, and prospects. Chapter One, Six and Seven follows a uniform referencing style and has the bibliography at the end. Chapters Two to Five are original research articles that were published by the author as a first author during his Ph.D. tenure. Chapters Two to Five have their own title, abstract, introduction, materials and methods, results, discussion and conclusion, references, and supplementary material sections. For Chapters Two to Five, there is a preface at the beginning which briefly describes the justification and perspective of each chapter and acts as a bridging text to logically connect the chapters. The references for prefaces are also in the bibliography at the end.

Published articles included in the thesis:

- **Mehdi, A**. and S.A. Rabbani, *Role of Methylation in Pro- and Anti-Cancer Immunity.* Cancers (Basel), 2021. **13**(3). ***(Chapter One includes excerpts from this review)***
- **Mehdi, A**., D. Cheishvili, A. Arakelian, T.A. Bismar, M. Szyf, and S.A. Rabbani, *DNA methylation signatures of Prostate Cancer in peripheral T-cells.* BMC Cancer, 2020. **20**(1): p. 588. ***(Chapter Two of the thesis)***
- **Mehdi, A**., M. Attias, N. Mahmood, A. Arakelian, C. Mihalcioiu, C.A. Piccirillo, M. Szyf, and S.A. Rabbani, *Enhanced Anticancer Effect of a Combination of S-adenosylmethionine (SAM) and Immune Checkpoint Inhibitor (ICPi) in a Syngeneic Mouse Model of Advanced Melanoma.* Front Oncol, 2020. **10**: p. 1361. ***(Chapter Three of the thesis)***
- Mehdi, A., M. Attias, A. Arakelian, M. Szyf, C.A. Piccirillo, and S.A. Rabbani, *S-adenosylmethionine blocks tumorigenesis and with immune checkpoint inhibitor enhances anti-cancer efficacy against BRAF mutant and wildtype melanomas.* Neoplasia, 2023. **36**: p. 100874. ***(Chapter Four of the thesis)***

- **Mehdi, A**., M. Attias, A. Arakelian, C.A. Piccirillo, M. Szyf, and S.A. Rabbani, *Co-Targeting Luminal B Breast Cancer with S-Adenosylmethionine and Immune Checkpoint Inhibitor Reduces Primary Tumor Growth and Progression, and Metastasis to Lungs and Bone.* Cancers, 2023. **15**(1): p. 48. ***(Chapter Five of the thesis)***

Published articles not included in the thesis:

- **Mehdi, A**. and Y. Riazalhosseini, *Epigenome Aberrations: Emerging Driving Factors of the Clear Cell Renal Cell Carcinoma.* Int J Mol Sci, 2017. **18**(8).

CONTRIBUTION OF AUTHORS

CHAPTER ONE

Chapter One contains excerpts from the following published literature review.

- **Mehdi, A**. and S.A. Rabbani, *Role of Methylation in Pro- and Anti-Cancer Immunity.* Cancers (Basel), 2021. **13**(3).

Ali Mehdi researched, wrote, and prepared all the figures for the review and Dr. Shafaat A. Rabbani revised the literature review.

CHAPTER TWO

- **Mehdi, A**., D. Cheishvili, A. Arakelian, T.A. Bismar, M. Szyf, and S.A. Rabbani, *DNA methylation signatures of Prostate Cancer in peripheral T-cells.* BMC Cancer, 2020. **20**(1): p. 588.

Drs. Shafaat A. Rabbani and Moshe Szyf conceived the study and experimental design. Ali Mehdi and Ani Arakelian carried out the experimental procedures. Ali Mehdi carried out all the experiments involved with pyrosequencing. Illumina 850K was carried out by Genome Quebec. All data analysis, including Illumina 850K analysis, was carried out by Dr. David Cheishvili and Ali Mehdi. Ali Mehdi wrote the manuscript with Drs. Shafaat A. Rabbani and Moshe Szyf. Dr. Tariq A. Bismar selected subjects, provided access to samples and assisted in manuscript revisions. The revisions were carried out by Ali Mehdi and Drs. Moshe Szyf and Shafaat A. Rabbani. All authors read and approved the final manuscript. Dr. David Cheishvili is a post-doctoral fellow and a co-author of this paper.

CHAPTER THREE

- **Mehdi, A**., M. Attias, N. Mahmood, A. Arakelian, C. Mihalcioiu, C.A. Piccirillo, M. Szyf, and S.A. Rabbani, *Enhanced Anticancer Effect of a Combination of S-adenosylmethionine (SAM) and Immune Checkpoint Inhibitor (ICPi) in a Syngeneic Mouse Model of Advanced Melanoma.* Front Oncol, 2020. **10**: p. 1361.

Ali Mehdi, Dr. Shafaat A. Rabbani, and Dr. Moshe Szyf conceived the study and experimental design. Ali Mehdi carried out the *in vitro* studies except invasion assay which was carried out by Ali Mehdi and Ani Arakelian. The *in vivo* studies were performed by Ali Mehdi and Ani Arakelian except immunophenotyping which was done by Ali Mehdi, Ani Arakelian, Niaz Mahmood, and Mikhael Attias, and data analysis was carried out by Ali Mehdi and Mikhael Attias. All the bioinformatics, including RNA-sequencing and pathway analysis, and clinical data analysis was carried out by Ali Mehdi. Manuscript and figures were prepared by Ali Mehdi and edited by Dr. Shafaat A. Rabbani, Dr. Moshe Szyf, Mikhael Attias, and Dr. Ciriaco A. Piccirillo. The revisions for the manuscript were carried out by Ali Mehdi and Dr. Shafaat A. Rabbani. All authors read and approved the final manuscript.

CHAPTER FOUR

- Mehdi, A., M. Attias, A. Arakelian, M. Szyf, C.A. Piccirillo, and S.A. Rabbani, *S-adenosylmethionine blocks tumorigenesis and with immune checkpoint inhibitor enhances anti-cancer efficacy against BRAF mutant and wildtype melanomas.* Neoplasia, 2023. **36**: p. 100874.

Ali Mehdi and Dr. Shafaat A. Rabbani conceived the study and experimental design. Ali Mehdi carried out all *in vitro* and *in vivo* experiments. Ani Arakelian helped in all *in vivo* studies. Immunophenotyping experiments were performed by Ali Mehdi, Ani Arakelian and Mikhael Attias, and the data analysis for immunophenotyping was carried out by Mikhael Attias. All the bioinformatics, including RNA-sequencing and pathway analysis, and clinical data analysis was carried out by Ali Mehdi. Ali Mehdi wrote the first draft of the manuscript and prepared the figures. Dr. Shafaat A. Rabbani, Dr. Moshe Szyf, Mikhael Attias, and Dr. Ciriaco A. Piccirillo edited and provided feedback for the manuscript. The revisions for the manuscript were carried out by Ali Mehdi and Dr. Shafaat A. Rabbani. All authors read and approved the final manuscript.

CHAPTER FIVE

- **Mehdi, A**., M. Attias, A. Arakelian, C.A. Piccirillo, M. Szyf, and S.A. Rabbani, *Co-Targeting Luminal B Breast Cancer with S-Adenosylmethionine and Immune Checkpoint Inhibitor Reduces Primary Tumor Growth and Progression, and Metastasis to Lungs and Bone.* Cancers, 2023. **15**(1): p. 48.

Ali Mehdi, Dr. Shafaat A. Rabbani, and Dr. Moshe Szyf conceived the study, experimental design and conceptualization. Ali Mehdi carried out all *in vitro* and *in vivo* experiments except invasion assay which was carried out by Ali Mehdi and Ani Arakelian. Ani Arakelian helped in all *in vivo* studies. All the bioinformatics, including RNA-sequencing and pathway analysis, and clinical data analysis was carried out by Ali Mehdi. Ali Mehdi wrote the first draft of the manuscript and prepared the figures. Dr. Shafaat A. Rabbani, Dr. Moshe Szyf, Mikhael Attias, and Dr. Ciriaco A. Piccirillo edited and provided feedback for the manuscript. The revisions for the manuscript were carried out by Ali Mehdi and Dr. Shafaat A. Rabbani. All authors read and approved the final manuscript.

CHAPTER ONE: INTRODUCTION AND LITERATURE REVIEW

Preface

Chapter One provides a literature review and general introduction including the rationale, hypotheses, and objectives of the thesis. Chapter One contains excerpts from the following published literature review.

- **Mehdi, A**. and S.A. Rabbani, *Role of Methylation in Pro- and Anti-Cancer Immunity.* Cancers (Basel), 2021. **13**(3).

EPIGENETICS AND CANCER

Cancer is a complex disease involving progressive transformation of normal cells into a neoplastic state acquiring biological capabilities known as hallmarks of cancer [1]. Although several hallmarks have been identified, the acquisition of these hallmarks relies primarily upon genome instability that occurs through abnormal genetic and/or epigenetic mechanisms [1]. Whereas genetic mutations result in the activation/inactivation of certain genes playing a pivotal role in carcinogenesis, abnormalities in the epigenetic landscape can lead to altered gene expression and function, genomic instability, and malignant cellular transformation (Figure 1) [2, 3]. Epigenetic modifications are heritable changes regulating cellular gene expression patterns required for normal development and maintenance of various tissue functions [2, 4, 5]. The three most studied epigenetic mechanisms that result in cancer are alterations in DNA methylation, histone modification, and non-coding RNA (ncRNA) expression.

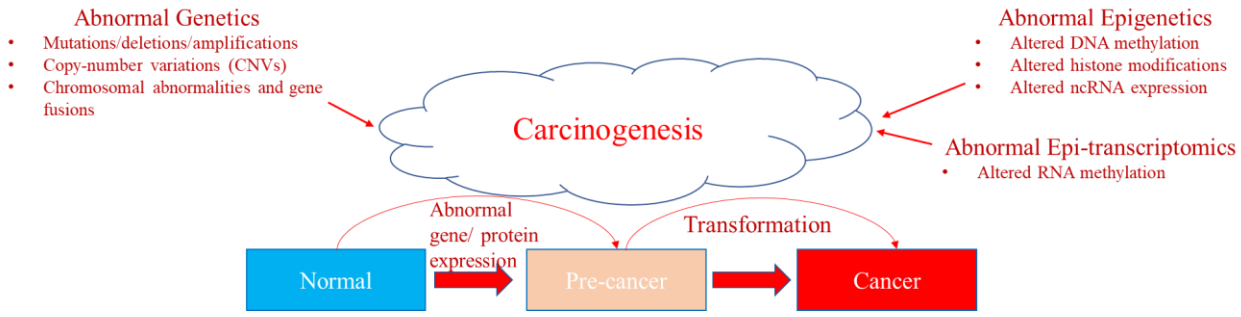

Figure 1: Mechanisms driving carcinogenesis. Abnormal genetic modifications such as gene mutations, deletions, amplifications, copy-number variations (CNVs), chromosomal abnormalities, or instability and gene fusions can all result in abnormal expression of genes and proteins leading to transformation of a normal cell into a pre-cancer state and/or cancer stage. Similarly, abnormal epigenetics, such as aberrant DNA methylation patterns, histone modifications, and ncRNA expression (e.g., miRNA) levels, also cause tumorigenesis. Recently, abnormal RNA methylation patterns, such as m^6A RNA post-transcriptional modifications (epi-transcriptomics), have been shown to result in the initiation and progression of cancer. Adapted from [6].

DNA Methylation

DNA methylation is the most well-characterized epigenetic mechanism, and was linked to cancer as early as the 1980s [7]. Specific DNA methylation patterns are crucial for parental imprinting, genomic stability, and importantly, regulation of gene expression [8, 9]. DNA methylation is covalent addition of a methyl (-CH3) group at the cytosine (C) base adjacent to 5' of a guanosine (G) [10, 11]. The methyl donor for this methylation reaction is S-adenosylmethionine (SAM). In the human genome, more than 28 million CpG dinucleotides exist, and 60%–80% show methylation in any given cell [12]. In contrast, there are specific regions where CpG dinucleotides are enriched, called CpG islands, which are primarily located near gene promoters [12]. Increased methylation at CpG islands is typically associated with gene silencing. However, varying levels of DNA methylation at other regions, including gene bodies, enhancers, 5' and 3' UTRs, and partially methylated domains (PMDs), can also differentially affect gene expression to regulate dynamic biological processes [13-16]. In mammals, addition of methyl groups to DNA is carried out by "writers", DNA methyltransferase (DNMT) 1, DNMT3A, and DNMT3B converting unmodified C into 5-methyl-cytosine (5mC) [2, 3]. DNMT3A and DNMT3B adds methyl groups to DNA without template DNA and hence undertake *de novo* methylation, whereas DNMT1, maintenance DNMT, adds methyl groups to hemi-methylated DNA by copying DNA methylation patterns from the parental strand to the daughter strand during cell division [2, 3]. DNMTs utilize methyl groups from SAM, which is a universal methyl donor and acts as a co-factor in this reaction [2, 3].

Aberrant DNA methylation in Cancer

Alterations in methylation have been strongly associated with the initiation and progression of cancer [17]. Compared to normal control tissues, in tumors DNA hypomethylation occurs at global and gene-specific levels, which results in genomic instability and activation of silenced oncogenes [18]. In contrast, DNA hypermethylation occurs at the promoter regions of tumor suppressor genes (TSGs), which leads to their silencing [18].

DNA hypermethylation in Cancer

Several studies have reported increased tumorigenesis following silencing of certain TSGs in cell cycle, mismatch repair, cell growth and metastasis pathways [19]. A key example is the

hypermethylation of the promoter region of *CDKN2A* (p16) and its reduced expression in esophageal adenocarcinoma [20]. Being a crucial cyclin-dependent kinase inhibitor, p16, inhibits cell cycle and avoids hyper-proliferation [19]. Significant reduction in p16 expression was observed in esophageal adenocarcinoma and other common human cancers. Interestingly, loss of functional mutations in *CDKN2A* gene also occurs in a variety of human cancers, and this acts in synchrony with hypermethylation of *CDKN2A* gene resulting in loss of both alleles (1 by genetic and 1 by epigenetic mechanism) of p16 gene [19, 20]. This pattern of loss of function of a gene is parallel to the Knudson's hypothesis wherein lack of gene function is due to mutations in both alleles of a gene [19]. However, in this case, one abnormality is by DNA methylation. Moreover, this loss of gene function pattern is reported in various other cancers including *RB* and retinoblastoma, and *VHL* and renal cancers, *BRCA1* and breast cancer, *APC* and colorectal cancer [19]. Another example of promoter hypermethylation and subsequent TSG silencing is of a mismatch repair gene *MLH1* which is typically observed in colorectal cancers. Hypermethylation of *MLH1* leads to loss of functional MLH1 protein which results in increased mutational rates and microsatellite instability phenotype [19]. Treatment of colorectal cancer cell lines using DNA methyl-transferase inhibitor (DNMTi) have been shown to reverse the MLH1 protein expression and mismatch repair capacity [19]. Hypermethylation and reduced expression of the estrogen receptor (ER) which increases the aggressiveness of breast cancer (BCa) has been reported [19]. Similarly, androgen receptor (AR) promoter hypermethylation and inactivation of AR has been detailed in prostate cancer (PCa) [19].

DNA hypomethylation in Cancer

DNA hypomethylation refers to a loss of DNA methylation at specific loci or globally which is typically methylated in normal physiological conditions. DNA hypomethylation was the first epigenetic mechanism to be identified in cancer in 1983 [7, 21, 22]. Using methylation-specific restrictions enzymes and HPLC methods, compared to normal cells and tissues, it was found that reduction in DNA methylation occurs at specific regions of the genome and at a global level, respectively [7, 21, 22]. Moreover, DNA methylation levels decrease globally as the cancer progresses from localized primary tumors to metastatic malignant neoplasms which suggested the involvement of DNA hypomethylation in tumor metastasis [7, 21, 22]. Surprisingly, DNA hypomethylation was largely understudied for decades and was often overshadowed by DNA

hypermethylation studies. One of the major reasons for this was the experimental design that followed investigating DNA methylation at gene specific loci which are usually unmethylated but becomes methylated in cancer [23]. Due to this bias, it was not possible to detect a reduction in methylation as the sites were already unmethylated [24]. However, advancements in DNA methylation technologies and next-generation sequencing (NSG) have accumulated strong evidence in identifying gene-specific and global DNA hypomethylation playing a crucial role in the initiation and progression of cancer [9, 18].

Consequences of DNA hypomethylation

DNA hypomethylation can have several consequences on the aberrant transcriptional re-programming and genome instability which can ultimately lead to carcinogenesis. These impacts of DNA methylation include: (a) activation of oncogenes and pro-metastatic genes; (b) activation of repetitive elements; and (c) genome instability.

(a) Activation of oncogenes and pro-metastatic genes

DNA hypomethylation can occur at the regulatory transcriptional elements including promoter, intergenic and intronic regions that ultimately results in activation of oncogenes and pro-metastatic genes [18, 24]. Pioneering studies carried out by our laboratory and others have shown that several pro-metastatic genes are hypomethylated at the promoter region. For example, the urokinase plasminogen activator (*PLAU/uPA*), which plays a key role in tumor invasion and metastasis, is hypomethylated, activated and overexpressed in various cell lines and surgical biopsies of patients with BCa and PCa [25, 26]. The high expression of uPA was also associated with aggressiveness of BCa [25]. Furthermore, DNA hypomethylation and activation of several other genes has been linked to tumorigenesis including cancer-testis genes, heparinase (*HPSE*), mesothelin (*MSLN*), S100 calcium binding proteins A4 and P (*S100A4/P*), claudin 4 (*CLDN4*), *synuclein-γ*, *H-Ras*, *c-Myc*, *VEGF, trefoil factor 2 (TFF2), maspin (SERPINB5),* and several pro-metastatic genes (including matrix metalloproteinases (MMPs)-- *MMP2*, *MMP3, MMP10*, *MMP9*) [18, 27-31]. Lastly, certain imprinted genes, including *IGF2*, *H19* and *KCNQ1*, are activated via DNA hypomethylation or demethylation and expressed in high levels [18, 32].

(b) Activation of repetitive elements

In addition to gene-specific loci, DNA hypomethylation and activation of repetitive elements including transposable elements has been widely reported [18, 33]. Hypomethylation of interspersed repeats and tandem repeats are incidentally observed in various cancers and accelerates carcinogenesis by fostering DNA rearrangements resulting in mutagenesis and genomic instability [18, 33]. For instance, DNA hypomethylation at the promoter of the LINE1 repetitive element activates LINE1 enabling subsequent retro-transposition. Upon activation, repetitive elements can alter transcription of other oncogenes and TSGs thereby accelerating carcinogenesis. For example, a well-known oncogene *Met* was overexpressed due to DNA hypomethylation related activation of LINE1 [34, 35].

(c) Genome instability

Genome instability is one of the prominent hallmarks of cancer [1, 36]. Studies utilizing DNMT deficient mice or DNMTi (*in vitro* and *in vivo*) have suggested loss of DNA methylation is crucial for carcinogenesis [18, 37]. For instance, knock-out of *Dmnt1* in mouse embryonic stem cells led to higher mutational rates which increased chromosomal translocations [38]. Similarly, *Dmnt1* mutant hypomorphic mice that developed genome-wide DNA hypomethylation were more susceptible to develop T cell lymphomas linked to chromosomal instability [39]. Additionally, there is a strong correlation between DNA hypomethylation in human cancer models and chromosomal rearrangements leading to genomic instability [18, 24]. Rodents fed with methyl-deficient diet had decreased levels of SAM, had global DNA hypomethylation, and developed liver tumors [18, 24, 40]. In one study, breaks in genomic DNA (genome instability) and within *p53* gene was associated with hypomethylation in liver of methyl-deficient rodents [41]. Another study reported that if methyl-deficient diets are given over prolonged period, change in DNA methylation levels in these animals could be irreversible [40]. Several studies have also demonstrated that DNA hypomethylation or demethylation of Sat2 and Sat3 heterochromatin regions of chromosomes can result in chromosomal abnormalities resulting in genome instability and aneuploidy [18, 24].

Therefore, from a large body of evidence, it is evident that DNA hypomethylation plays a key role in tumor initiation and progression and can serve as a viable and effective therapeutic target to block tumor growth, progression, and metastasis (Figure 2).

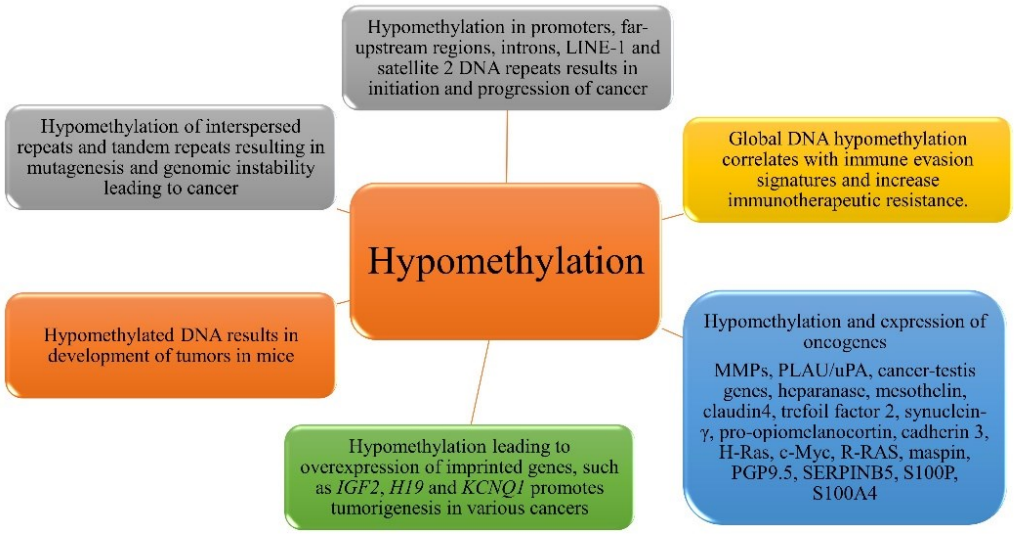

Figure 2: Role of DNA hypomethylation in cancer. DNA hypomethylation can lead to genomic instability, abnormal gene expression and immune evasion that can eventually lead to initiation and progression of cancer.

Targeting methylation as an anti-cancer strategy

With our increasing understanding of the role of methylation in cancer and immunity, further efforts are being aimed at its translational potential to develop new therapeutic strategies that can alter the methylation landscape. Towards these goals, both DNA hypo- and hyper-methylation can serve as viable targets which, unlike genetic changes, are both dynamic and reversible. Moreover, DNA methylation can be corrected by either therapies or dietary interventions [42]. Therefore, targeting DNA methylation is an attractive anti-cancer therapy with immense potential [24, 43].

Targeting DNA hypermethylation

Several DNA hypomethylating agents have been developed that target DNA hypermethylation. However, among these DNMTi, 5-azacytidine (Vidaza®) and 5-aza-2'deoxycytidine (Decitabine, Dacogen®), have been approved by the Food and Drug Administration (FDA) [24]. Because multiple hematologic malignancies are linked to abnormal DNA methylation patterns, DNMTi were first tested in these cancers. Among these, myelodysplastic syndromes (MDS) comprising a group of hematologic disorders derived from

abnormal progenitor cells were the first to be evaluated. Patients with MDS have hypo-proliferative bone marrow and a risk of developing different forms of acute leukemia [44]. The inhibitor 5-azacytidine was first tested on MDS patients, where it showed improved response rates, lower transformation to acute leukemia, and prolonged survival [45], and 5-aza-2'deoxycytidine showed similar clinical outcomes [46]. Both 5-azacytidine and 5-aza-2'deoxycytidine have also shown success in a clinical setting for acute myeloid leukemia (AML) and chronic myelomonocytic leukemia (CMML) [24]. Following the clinical success of DNMTi with hematologic malignancies, DNMTi were also tested in solid tumors [47-49].

Although DNMTi showed a good response in patients with ovarian cancer and non-small cell lung cancer (NSCLC), the response was highly variable and less effective in other solid tumors [47-49]. Moreover, DNMTi have various disadvantages limiting its use especially in solid tumor. For instance, response to treatment of cancer patients with DNMTi have been considerably low in solid tumors [47-49]. Furthermore, various adverse effects have been reported in patients treated with DNMTi including bleeding, anemia, and joint pain [48]. Improving DNMTi efficacy and reducing related adverse events is an active area of research, however, due to lack of sufficient knowledge about the precise mechanism of action of DNMTi in various cancer types, this has been challenging [47-49]. DNMTi primary mechanism of action is hypomethylation of the DNA, targeting promoter regions of TSGs and other genomic regions to induce its anti-cancer effect [47-52]. However, there are reports on DNMTi increasing the expression of silenced oncogenes and pro-metastatic genes (including *uPA*) via DNA hypomethylation that could result in increased risk of metastasis [53, 54]. For instance, recently, demethylation and upregulation of a well-known oncogene, *SALL4*, by DNMTi treatment was demonstrated in patients and cell lines [55]. SALL4 plays an essential role in tumorigenesis of solid tumors including liver, breast, and lung cancer, and in hematologic cancers including MDS and AML [55, 56]. In a meta-analysis, reactivation, and high expression of SALL4 has been strongly associated with worse outcome [56]. Therefore, it is critical to further elucidate the molecular mechanism of action of DNMTi including its downstream targets in cancer.

Targeting DNA hypomethylation

In cancer, promoter hypermethylation of TSGs and silencing of TSGs resulting in tumorigenesis has been the focus of the last few decades, resulting in the discovery of FDA-

approved DNMTis [50-52, 57]. By comparison, a phenomenon that is relatively underestimated is genome-wide DNA hypomethylation, which occurs in various solid tumors [18, 37]. As detailed above, several studies have also demonstrated that gene-specific and global hypomethylation play a crucial role in the initiation and progression of cancer [9, 18]. However, there is still no approved agent that targets DNA hypomethylation. Currently, the most studied approach to target DNA hypomethylation uses SAM.

SAM as an anti-cancer agent

SAM has a nodal position in three major pathways including transmethylation, transsulfuration, and aminopropylation [58-61]. SAM is a natural and universal methyl donor of all methylation reactions and is present ubiquitously in all living cells [30, 58]. In the transmethylation pathway, SAM donates its methyl group to key cellular components including proteins, nucleic acids (RNA and DNA), lipids, and secondary metabolites to modulate several physiological functions [30, 58, 59]. SAM's ability to donate methyl groups stems from its chemical structure which has a high energy sulfonium moiety that is attached to three carbon atoms which are prone to nucleophilic substitution making it highly reactive and a co-factor mediator in many biochemical reactions (Figure 3) [60]. In the transsulfuration pathway, SAM is converted to cysteine thereby producing major cellular antioxidants such as glutathione [58-61]. In the aminopropylation pathway, SAM donates the aminopropyl groups to generate polyamines such as spermidine and spermine which are required for cell growth [58-61]. SAM has such diverse and versatile physiological functions that it has been suggested to be only second to adenosine triphosphate (ATP) [61]. Currently, SAM is used as an approved natural food supplement and preventive agent for mood disorders, fibromyalgia, and joint pain [30, 59].

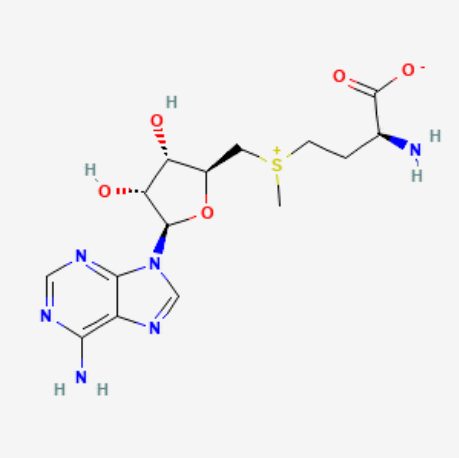

Figure 3: The two-dimensional chemical structure of SAM. The structure was generated on PubChem [261].

Aberrant methylome is a common consequence of a disrupted SAM cycle associated with transformation of cells towards tumorigenesis [58, 62, 63]. Since SAM is the most prominent methyl donor, disturbances in SAM levels can lead to changes in methylation patterns of DNA and proteins and cellular transformation [58, 62]. Moreover, abnormal methylation can affect activity and stability of transcription factors and other proteins [58, 63]. SAM, which increases DNA methylation and inhibits demethylation, causes significant anti-cancer effects in osteosarcoma, BCa, PCa, hepatocellular cancer, gastric cancer, and colon cancer [25, 30, 58, 62-66]. Although SAM increases methylation levels globally, it also increases methylation levels at specific loci affecting gene transcription selectively and thereby causing its anti-tumor and anti-metastatic effects [25, 30, 58, 62-66]. Effect of SAM on various cancer cell lines and mouse models along with genes affected are summarized in Table 1.

Table 1: Effect of SAM on various cancer cell lines and mouse models

Cancer	Model	Genes affected	Effect	
Osteosarcoma	LM-7 and MG-63. LM-7 xenograft (SCID) mouse model.	*MMP2, MMP9, VEGF, PAI-1, uPA, TGF-β, RUNX2, EXOC7, PCGF3, PDGFA.*	*In vitro*: Reduced cell proliferation, migration, and invasion. *In vivo*: Reduced bone and lung metastasis.	[64]

Prostate	PC-3 and DU-145. PC3-xenograft (SCID) mouse model.	*uPA, MMP2, TGF-β, TGFBR2* and *RUNX2.* *CTSH, TTC23, STAT3, STAT5A, STAT5B, NXN, SRY, MIER2* and *HSFY1. TMEM52, TMEM171, IGFBP3, MKX, MATK, CBS* and *ADM2*	*In vitro*: Reduced cell proliferation, migration, and invasion. *In vivo*: Reduced bone metastasis.	[62, 67]
Gastric	MGC-803 cells and HT-29 cells. SGC-7901 and MKN-45 cells. SGC-7901 xenograft (balb/c) mouse model	*c-Myc* and *H-Ras.* *c-Myc* and *uPA*	*In vitro*: Reduced cell proliferation. *In vivo*: Reduced tumor growth and progression.	[66, 68]
Colon	SW-620 cells. Carcinogens-induced inflammation induced colon cancer mouse (balb/c) model.	*TIMP-2, MMP-2, MT1-MMP, uPA, VEGF* *IL-6, IL-10, STAT3.*	*In vitro*: Reduced cell proliferation migration, and invasion. Increased apoptosis and caused cell cycle arrest. *In vivo*: Reduced tumor load (growth).	[69, 70]
Breast	MDA-MB-231, Hs578T, PyMT-R221A, Eo771 cells. MDA-MB-231 xenograft and MMTV-PyMT mouse models.	*uPA, MMP2, MUC1, FABP7, SPARC, HAS2, HAS3, SOX4.* *VEGFA, TFPI2, GSTP1, FADS2, MCL1, ITPR3, AGRN, KLF4, DUSP1, CXCR4,*	*In vitro*: Increased apoptosis. Reduced cell proliferation, colony formation, migration, and invasion. *In vivo*: Reduced tumor growth, progression and metastasis to lungs and tibia.	[30, 54, 71]

		IRF7/9, STAT1, IFNγ genes, etc.		
Liver	HepG2 and SKhep1 cells.	*DDIT3, TAF15, MTHF2, ITGA6, NFIB, PBK, MIA, PDK1, CLIC4, SLC2A1, STMN1, NFIL3, RAN, TRIB3, PEG10, CDT1, DYNC1H1, RRM2, E2F1, HAT1, CBS, MYC, MCM3*	*In vitro*: Reduced cell proliferation, colony formation and invasion.	[72]

Uncontrolled cellular proliferation is a core hallmark of cancer [1, 36]. One of the major pathways with which SAM causes its anti-cancer effects is inhibition of cell proliferation by inhibiting cell cycle progression (Table 1). Cancer cells thrive on growth factors such as polypeptides for their rapid cell proliferation. Our laboratory has demonstrated that SAM decreased expression of crucial growth factors including transforming growth factor β (TGF-β), vascular endothelial growth factor (VEGF), platelet-derived growth factor alpha (PDGFA) required by PCa and osteosarcoma cells to proliferate [62, 64].

Apoptosis, a programmed cell death, is controlled by pro and anti- apoptotic proteins and pathways. Intriguingly, SAM demonstrated the ability of causing apoptosis in BCa cells by increasing and decreasing the expression of pro-apoptotic (BAX) and anti-apoptotic (BCL-2) proteins, respectively [30, 73]. In addition, SAM caused cell cycle arrest at the G_2M phase of PCa, BCa and osteosarcoma cell lines [62, 64, 73-75]. Accordingly, SAM reduced expression of key cell cycle regulators including cyclin A, B, D and E that progress the cell cycle and increased expression of cell cycle inhibitors such as p21, p27 and p53 [73-75].

SAM was demonstrated to affect survival pathways in cancer cells. For instance, methylome profiling using Illumina Infinium 450K array demonstrated that SAM hypermethylated the promoter of *STAT3* leading to its reduced expression in PCa [62]. In addition, promoter

hypermethylation and reduction in expression of proto-oncogenes, *MYC* and *HRAS,* was also demonstrated in gastric and colorectal cancers [66, 68].

SAM was also found to decrease tumor growth and progression in mouse models of gastric and colorectal cancers [66, 68]. Recently, we have demonstrated that SAM decreases cell proliferation *in vitro* and *in vivo* (given orally) in xenograft, transgenic and syngeneic BCa mouse models [30, 54, 71]. SAM decreased number of cells in culture plates, caused cell cycle arrest and reduced colony formation in anchorage-independent assays (*in vitro*) while, in *in vivo* studies, SAM decreased tumor volume and ki67 proliferation marker in tumor cells [30, 54, 71].

Most cancers if diagnosed in early stages have relatively better clinical outcomes compared to cancers that have metastasized. Metastasis is a multi-step process including invasion and migration of cancer cells through the extracellular matrix (ECM), intravasation into the blood vessels, survival in blood, extravasation, and colonization into the distant organ [76]. Metastasis is the major cause of cancer-associated death [76, 77]. SAM has demonstrated significant ability to reduce metastasis in different cancer models *in vitro* and *in vivo*. One of the earliest studies of our laboratory showed that SAM decreased the expression of a key pro-metastatic gene, *uPA/PLAU*, which is significantly involved in inducing metastasis together with MMPs. Our laboratory demonstrated that SAM reduced the invasive ability of PCa and osteosarcoma cells by downregulating pro-metastatic genes, *uPA* and *MMP2* [30, 65]. Our laboratory has also shown that SAM decreases the invasion and migration of BCa cells using transwell Boyden chamber invasion assay and wound-healing assay, respectively [30, 54, 71]. Recently, our laboratory has suggested that orally given SAM can also cause anti-metastatic effects *in vivo* in xenograft and transgenic BCa mouse models [30, 54, 71]. These anti-metastatic effects were demonstrated by lower metastatic nodule formation in the lungs, and lower metastatic burden in the liver, spleen, and tibia [30, 54, 71]. Parallel to this, a high number of genes involved invasion, metastasis and in epithelial to mesenchymal transition (EMT) pathways were found to be downregulated by SAM [30, 54, 71]. Others have also reported that SAM targets miRNAs (miRNA-34a and b) and decreased the metastatic ability of colon cancer cells [78].

SAM has also demonstrated its anti-cancer effects in combination with other chemotherapeutic or chemo-preventive drugs. SAM was reported to synergize with Doxorubicin, a well-established chemotherapeutic agent, thereby increasing apoptosis and reducing cell

proliferation of BCa cell lines [79]. In addition, SAM when combined with an autophagy inhibitor chloroquine showed synergistic effect in reducing cell growth and inducing apoptosis [75]. Moreover, SAM in combination with another nutraceutical agent, Vitamin D (25-hydroxyvitamin D), showed reduction in cell proliferation and colony formation (*in vitro*) in various BCa cell lines. Furthermore, the combination demonstrated significant reduction in tumor growth and metastasis of primary BCa tumors, and lung and skeletal metastasis, respectively, in BCa mouse models [71]. Interestingly, DNA hypomethylation was also shown to reduce the response to radiation therapy in doxorubicin-resistant BCa cells, and SAM increased radiation sensitivity of the cancer cells by reversing DNA hypomethylation of the radiation-resistant BCa cells [80]. All the above studies establish the role of SAM in reducing tumorigenesis *in vitro* and *in vivo* alone or in combination with other anti-cancer agents.

Leveraging DNA methylation and immune system for cancer risk stratification and diagnosis

Apart from being an attractive therapeutic target, DNA methylation is being actively evaluated as an early cancer diagnostic and prognostic biomarker. DNA methylation is a stable marker, has a higher frequency than genetic mutations, and can be studied from even fresh frozen formalin-fixed paraffin-embedded samples [30, 81, 82]. Various components of the tumor cells (cell-free DNA, circulating tumor cells), and immune cells can be utilized as cancer biomarkers [81, 82]. However, the focus of our laboratory has been to identify DNA methylome alterations that occurs early in the malignant transformation. Therefore, we focused on the cancer immunosurveillance system.

Cancer immunosurveillance system carries out vital functions by eradicating and controlling tumor cells (discussed in detail below). Cancer immunosurveillance system includes components of innate and adaptive immune system that can directly kill malignant cells. One of the key peripheral immune cells are the T cells that can detect and eliminate transformed cells even before they have become malignant [83, 84]. Detection and elimination of pre-malignant tumor cells requires changes in DNA methylome that results in activation, proliferation (clonal expansion) and elevated effector functions of T cells in order to eliminate the pre-malignant and malignant cells. These alterations caused by pre-malignant/malignant cells can be detected by

using advanced DNA methylation technologies such as pyrosequencing and Illumina Infinium 850K. Therefore, T cells can serve as potential candidates for early detection of cancers and act as efficient biomarkers. Interestingly, DNA methylation differences in the leukocytes and cell-free DNA of the patient versus healthy controls have been suggestive of tumorigenesis [85, 86].

Recently, our laboratory identified DNA methylation differences in the $CD3^+$ T cells of healthy controls and BCa patients (from stage I-IV) [87]. Six CpG sites were identified to be differentially methylated in BCa patients compared to healthy individuals. In addition, DNA methylation signatures in PBMCs and T cells in hepatocellular carcinoma (HCC) was identified that discriminates early HCC stage from chronic hepatitis B and C and healthy controls, and strengthens with progression of HCC [88]. These novel findings may have a major impact in the early diagnosis and risk stratification of cancer patients. This is because these DNA methylation signatures in T cells have the potential to predict pre-malignant and malignant cells. Furthermore, analyzing DNA methylome of T cells can be carried out using simple non-invasive drawing of blood like taking out PBMCs and WBCs. Interestingly, in our laboratory, DNA methylation is also being evaluated as a biomarker for response to immunotherapy. Therefore, there is immense potential in identifying precise DNA methylation alterations in T cells and other immune cells that can further establish signatures which could distinguish cancer patients from healthy individuals or at least stratify high risk individuals that could potentially develop tumors.

IMMUNE SYSTEM AND CANCER

Immune system: Pro- and Anti-Cancer Immunity

After a century of controversy, it has now been established that a functional cancer immunosurveillance system indeed exists, and acts as a tumor suppressor or killer (Figure 4) [83, 89-92]. Humans have evolved their cancer immunosurveillance system, including the innate and adaptive immune systems, to combat a broad range of diseases, including cancer (Figure 4)[89-91]. Interestingly, both innate and adaptive immune systems can recognize and eliminate malignant cells thereby regressing or killing tumor cells. However, cancer cells employ immune evasive mechanisms to hi-jack components of the immune system that act as pro-tumor or create immunosuppressive tumor microenvironment (TME), helping tumor growth and progression [89, 93]. The next section discusses principal components of the TME which can be either anti-tumor or pro-tumor.

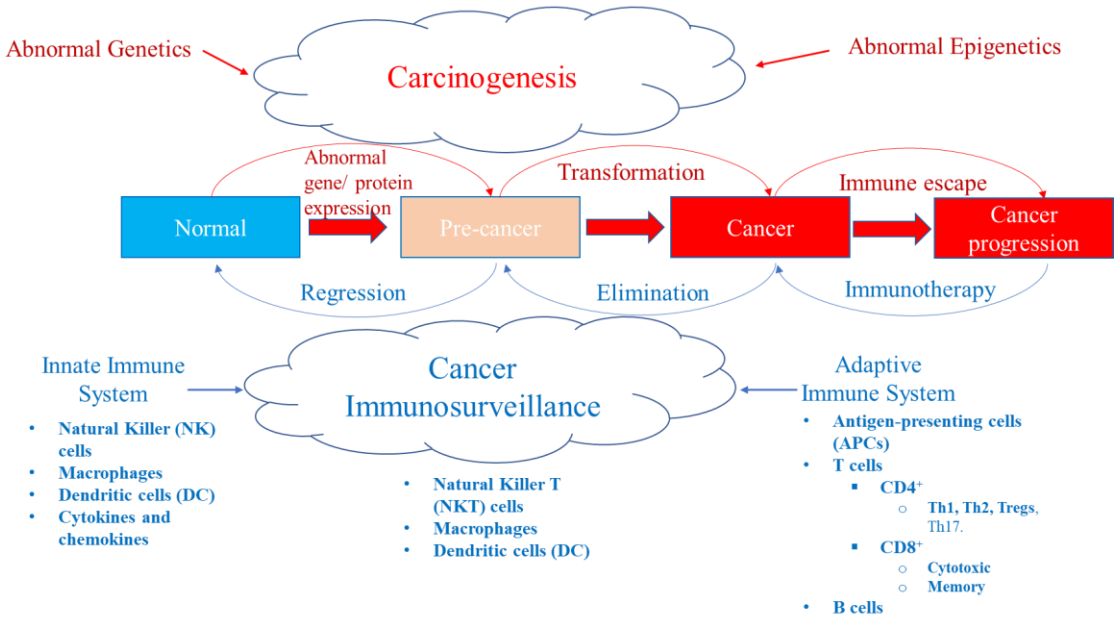

Figure 4: A balance between carcinogenesis and cancer immunosurveillance system. Although the aberrant genetics and epigenetics mechanisms promote tumorigenesis, the cancer immunosurveillance system acts as a tumor suppressor working against the formation of pre-malignant and cancer cells. The cancer immunosurveillance system is comprised of the innate and adaptive immune system that has various components that help to regress or eliminate tumor cells. However, some immune cells can be pro-tumor, which paradoxically help tumor progression in

the TME. Cancer can evolve and escape the immune system by developing immunosuppressive escape mechanisms (such as high expression of PD-L1) that allow it to progress. This state can be reversed with immunotherapy, such as immune checkpoint inhibitors (CPIs). Adapted from [6].

1. Innate immunity

The innate immune system consists of immune cells including natural killer (NK) cells, dendritic cells (DC), macrophages, and neutrophils. The innate immune system is typically the first line of defense, has a nonspecific and immediate response against pathogens, and exhibits germline inheritance [89-91]. Innate immune cells use pattern recognition receptors (PRRs), such as toll-like receptors (TLRs), and identify pathogens based on non-specific molecular patterns including single stranded RNAs or lipopolysaccharide.

1.1. Dendritic cells (DCs)

DCs and macrophages are the first innate immunity cell types which are triggered for defense against pathogen invasion. DCs are professional antigen presenting cells (APCs) that are essential for triggering adaptive T cell responses in an antigen (Ag) specific manner. DCs can undergo marked changes in their phenotype and function under various stimuli and inflammatory conditions [94]. For instance, DCs can be polarized towards producing specific type of cytokines (e.g., IL-12, IL-23) and Notch ligands (e.g., DLL1/4) to induce different effector CD4 (Th1, Th2, Th17) and CD8 (cytotoxic) T cells [94].

1.2. Macrophages

Macrophages are myeloid cells that have a spectrum of phenotypes in which M1 or M2 subtypes are the extreme ends. M1 cells are “classically activated” by IFNγ and destroy tumor cells through their production of nitric oxide and type 1 cytokines and chemokines [89, 95]. Moreover, M1 act as APCs to activate cytotoxic $CD8^+$ T cells in an Ag-specific manner. M2 cells are activated by “alternative” pathways via IL-4, IL-13, and/or TGFβ [89, 95]. M2 secrete type II chemokines and cytokines, thereby promoting tumor growth and progression. Stromal and tumor-associated factors in the TME can shift macrophages to M2 types, specifically the tumor-associated macrophages (TAMs) type, that promote angiogenesis, tumor progression, and metastasis [95-97].

1.3. Natural Killer (NK) cells

NK cells can directly lyse MHC class I-deficient tumor cells [89, 92]. NK cells have activating receptors that identify malignant cells expressing stress-induced ligands (e.g., MICA) [89, 92]. NK cells kill the tumor cells by making them undergo apoptosis through either expressing death ligands (e.g., Fas ligand) that, when binding to death receptors (e.g., Fas) on tumor cells, causes tumor cell apoptosis, or releases granzymes and perforin [89, 92]. NK cells together with cytotoxic $CD8^+$ T cells are most potent in killing tumor cells.

2. Adaptive Immunity

The adaptive immune system, by comparison to innate immune system, is highly specific and forms immunological memory. Adaptive immunity is comprised of lymphocytes, T and B cells, which produce cytokines and antibodies to counter pathogens [89-91]. A large number of extremely diverse but highly specific receptors on T cells—T cell receptors (TCRs)—and B cells—B cell receptors (BCR)—which recognize and differentiate self from non-self-antigens are extremely useful in response to foreign pathogens. Long-lasting memory cells generated after pathogen clearance provide a rapid and robust pathogen control upon re-exposure to the same pathogen.

(i) Antigen recognition

Adaptive immunity as mentioned above is highly specific and hence requires presentation of specific peptides or Ags. These peptides or Ags represent state of every cell for recognition by the immune cells. These Ags are presented onto MHC I by all the nucleated cells or MHC II exclusively by APCs such as macrophages, B lymphocytes, and DCs. In general, the Ags for MHC I are derived from intracellular space of normal cells or malignant and mutated proteins in cancer cells; whereas Ags for MHC II are derived from digestion of necrotic cells and cell debris and therefore represent the immediate microenvironment and not APCs itself [98, 99]. However, Ags derived from exogenous sources can be presented by APCs on MHC I to $CD8^+$ T cells by a process known as cross-presentation [98, 99].

(ii) Immunological synapse

The major players in adaptive immunity are the $CD3^+$ T cells which can be either $CD4^+$ or $CD8^+$ T cells [89]. Both $CD4^+$ and $CD8^+$ T cells have TCR that bind to Ag-bound MHC II and I, respectively. Multiple ligands and receptor interactions are required for activation of T cells at immunological synapse [89, 98, 99]. Firstly, binding of the TCR present on T cells to the Ag-MHC complex (signal 1) expressed on target cell or APCs is essential for the activation of naive T cells [98-100]. Secondly, additional binding of positive co-stimulatory molecules present on activated APCs, called signal 2 (e.g., CD80/86 and B7RP1 on APCs onto CD28 and ICOS on T cells, respectively), helps in proper activation. It is essential that both signals 1 (Ag-MHC and TCR interaction) and 2 (CD28-CD80/CD86 interaction) are activated to cause T cell activation and priming by APCs [89, 98-100].

(iii) TCR activation

Details of TCR activation process can be referred elsewhere [89, 98-100]. Essentially, during TCR activation, LCK kinase binds to CD8 or CD4 co-receptor and is recruited to the TCR by co-binding of CD8 and CD4 to MHC class I and II complexes, respectively. LCK phosphorylates tyrosine at CD3ζ chains, enabling the docking and activation of the tyrosine kinase, ZAP70 [98, 99]. ZAP70 phosphorylates LAT, leading to recruitment of multiple adaptors and effector molecules and the formation of the LAT signalosome [98, 99]. Activation of LAT-associated effector molecules results in activation of; (1) Ca^{2+}–calcineurin (NFAT leading to nuclear translocation of the REL and NF-κB transcription factors); (2) Mitogen-activated protein kinase (MAPK) pathways leading to actin polymerization and FOS, JUN and AP-1 transcription factors activation; and (3) Nuclear factor-κB (NF-κB) signaling pathways [98, 99]. In addition, signal 2 (CD28-CD80/CD86 interaction) leads to activation of phosphoinositide-3-kinase (PI3K) signaling which helps in proliferation and survival of T cells [98, 99]. Therefore, TCR activation is a multistep process that leads to an intracellular signaling cascade that results in activation, differentiation, proliferation (clonal expansion), and survival of T cells, and transforms them into effector cells producing cytokines [98, 99].

(iii) Inhibition of T-cell responses

Long-term activation of T cells can result in unnecessary damage to healthy cell and tissues and further lead to autoimmunity [89, 98-100]. Therefore, upon activation of T cells, there is an upregulation of co-inhibitory molecules which try to limit the activation and function of T cells,

upon engagement to their subsequent partners, resulting in T cell anergy, dysfunction and even apoptosis. These co-inhibitory proteins include cytotoxic T-lymphocyte-associated protein 4 (CTLA-4), programmed death 1 (PD-1), lymphocyte activation gene 3 (LAG-3), T cell immunoglobulin and mucin domain-containing protein 3 (TIM-3) [89, 98-100]. This process is known as contraction of the T cell responses and upon pathogen clearance the number of Ag-specific activated T cells decreases. However, memory T cells remain in a certain number for protection against re-challenge of the pathogen [89, 98-100].

2.1. $CD4^+$ T cells

$CD4^+$ T cells are unique T cells that can, depending on the nature of Ag signal and type of cytokine stimulation, differentiate into various subtypes including helper T cell 1, 2 and 17 (Th1, Th2, and Th17) and regulatory T cells (Tregs).

2.1.1. T helper 1 (Th1) and T helper 2 (Th2) cells

Th1 produce type I cytokines, including IL-2 and IFNγ, facilitating optimal expansion, trafficking, and effector functions of $CD8^+$ T cells, thereby reducing tumor growth and progression [89, 93, 101]. In contrast, Th2 produce type II cytokines (IL-4, IL-5, and IL-13) and polarize immunity towards tumor progression [89, 93, 101]. The differentiated $CD4^+$ T cells then regulate downstream immune functions, such as enhancement of $CD8^+$ T cells, macrophages, and B cell effector functions, and immunological memory.

2.1.2. Regulatory T cells (Tregs)

Tregs can be natural (nTreg), i.e., derived from the thymus, or Ag-induced (iTreg), i.e., differentiated from naïve T cells by TGF-β and IL-2 in the periphery [89, 93, 101]. Tregs typically act as pro-tumor, are immunosuppressive, and are associated with poorer prognosis in several cancer types [92, 102]. Tregs block the activation of $CD8^+$ T cells through expressing CTLA-4, which is an inhibitory molecule for $CD8^+$ T cells [89, 102]. In addition, inflammation enhances Treg function because prostaglandin E2 (PGE2) causes differentiation of Tregs. Tregs were also reported to block killing by NK cells, and thus down-regulate both adaptive and innate anti-tumor immunity [89, 103].

2.1.3. Th17 cells

Th17 cells are characterized by increased production of IL-17. Th17 cells have demonstrated both pro-cancer and anti-cancer effects depending on the TME [89, 104]. Th17 cells have shown to promote angiogenesis by increasing expression of VEGF, PGE2, and activating Stat3 signaling [89, 104]. In contrast, Th17 cells have shown to help recruitment of DCs, $CD4^+$ T cells, cytotoxic $CD8^+$ T cells and NK cells into the TME and promote anti-tumor immune responses [104]. Furthermore, Th17 have demonstrated to have direct tumor cells killing effect through IFNγ [104].

2.2. $CD8^+$ T cells

$CD8^+$ T cells control tumor growth and kill tumor cells directly in an Ag-specific manner [89, 93, 101]. The $CD8^+$ T cells upon recognizing an Ag can undergo activation and clonal expansion, thereby carrying out effector functions, such as cytokine production (IFNγ, TNFα) [89, 93, 98, 101]. $CD8^+$ T cells are the most potent Ag-specific cytotoxic cells that cause tumor lysis. The activated cytotoxic $CD8^+$ T cells can cause direct lysis or apoptosis of the target cells (e.g. tumor cells) by producing cytokines (e.g. IFNγ), proteases (e.g. granzymes and perforin) and by interaction of Fas and Fas-ligand [89, 98-100].

If an Ag is exposed to $CD8^+$ T cells for a long time, for example in cancer or other chronic pathologies, $CD8^+$ T cells can become non-functional or exhausted, resulting in reduced effector functions, such as decreased cytokine production (IFNγ and TNFα) and/or loss of cytotoxicity (e.g., low granzyme production). Exhausted T cells generally have high surface expression of multiple inhibitory molecules, such as PD-1, TIM-3, LAG-3, TIGIT, and 2B4, and transcription factors; T-bet, Eomes and Yin Yang 1 (YY1) [105-107]. YY1 is a key transcription factor that can regulate the inhibitory molecules PD-1, TIM-3, LAG-3, and was shown to have downregulated IL-2 via EZH2 activation, features characteristic of exhausted T cells [105-107]. This exhaustive state can be reversed by immunotherapy such as CPIs (Figure 4).

Summary of the factors that result in pro-tumor or anti-tumor immune responses

Solid tumors typically have immune cells that can be either anti-tumor or pro-tumor as a result of factors including differentiation (Figure 5).

In summary, pro-tumor factors include [89-91, 93, 99, 101, 108-113]:

- typically, low or exhausted tumor infiltrating lymphocytes (TILs) (immunologically cold tumor)
- high type II M2 macrophages
- high $CD4^+$ Tregs
- high type II $CD4^+$ Th2 cells
- low antigenicity and immunogenicity of the tumor cells

In contrast, anti-tumor factors include [89-91, 93, 99, 101, 108-113]:

- typically, high or activated/functional TILs (immunologically hot tumor)
- high NK cells
- high type I M1 macrophages
- high type I $CD4^+$ Th1 cells
- low Tregs
- high tumor infiltrating $CD8^+$ T cells (memory, cytotoxic)
- high type I cellular immune response (e.g., IFNγ, IL-2, TNF, granzyme B)
- high antigenicity and immunogenicity of the tumor cells

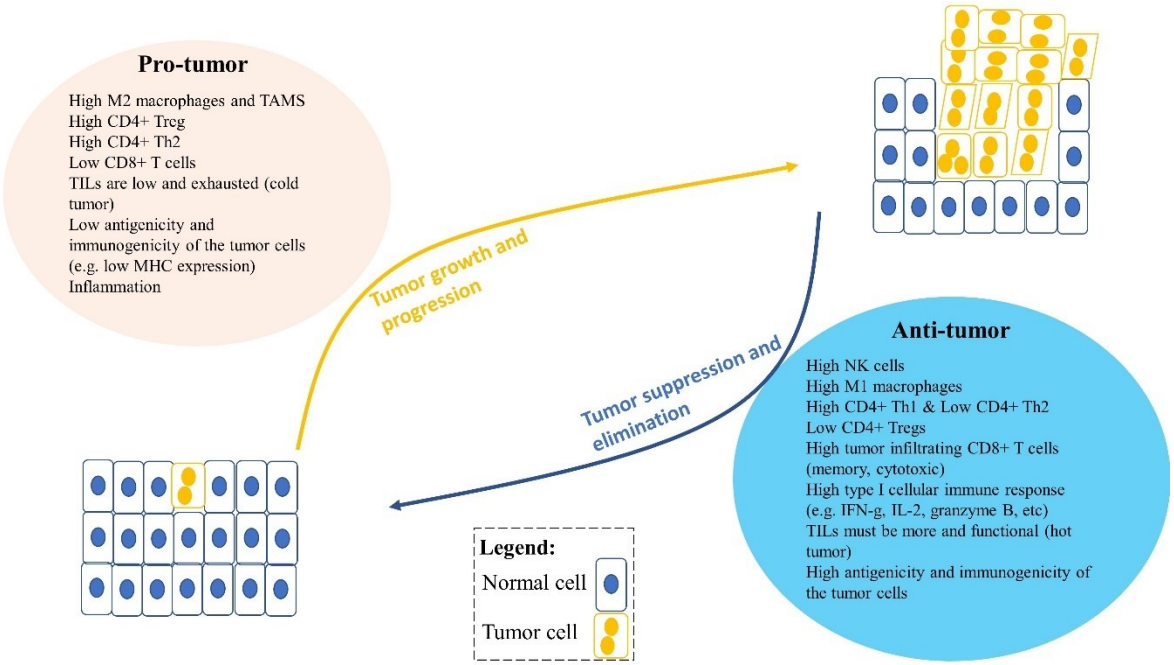

Figure 5: An imbalance between pro-tumor and anti-tumor immune cells and factors in the tumor microenvironment (TME) can lead to tumor growth and progression or tumor suppression and elimination. Pro-tumor immune cells can promote tumor progression, including type II M2 or TAMs (tumor-associated macrophages), regulatory T cells (Tregs), and type II Th2 cells. Moreover, factors that influence tumor progression are low tumor infiltrating lymphocytes (TILs) in the TME, low antigenicity and immunogenicity of tumor cells, and inflammation. Anti-tumor immune cells can reduce tumor growth and suppress tumor progression in the TME. These include $CD8^+$ T cells, type I Th1 cells, NK cells, and type I M1 cells and their type I cytokines such as IFNγ, TNFα, IL-2, and granzyme B. Furthermore, anti-tumor immune factors can also influence tumor suppression, including high infiltration of functional TILs, and greater antigenicity and immunogenicity of the tumor cells, such as high MHC-I expression and tumor-associated antigen expression. Reproduced from [6].

Targeting Immune system as an anti-cancer strategy- Immunotherapy

Immunotherapy has revolutionized treatment of cancer. In the 19th century, the first case of treating cancer by harnessing the power of immune system came from William B. Coley, who is known as the father of immunotherapy [114]. Coley treated tumors using Coley's toxin (live and inactivated bacteria) that induced sepsis-related durable immune response in several malignancies leading to complete remissions. However, due to risk involved in injecting live pathogenic bacteria and incompletely understood mechanisms, oncologist relied upon surgery and radiotherapy as therapeutic strategies against cancers [115]. Next considerable immunotherapy strategy was treatment with high doses of IL-2 in late-stage renal cell carcinoma and melanoma that resulted in moderate response and remissions. However, IL-2 therapy success was succumbed by significant adverse events. Paradigm shift in immunotherapy came from the discovery of immune checkpoints including CTLA-4 and PD-1 which led to 2018 Nobel prize in Physiology or Medicine to Drs. James P. Allison and Tasuku Honjo.

Immune checkpoint inhibitors (CPIs)

In normal physiology, a balance between co-stimulatory and co-inhibitory molecules is required to regulate the TCR response of T cells [92, 116, 117]. PD-1, an essential surface checkpoint receptor, act as co-inhibitory molecule that reduces the TCR response of T cells by binding onto it's ligand PD-L1 (Programmed death ligand 1) [92, 116, 117]. PD-1 functions to

reduce the activity of T cells during inflammation, limits overactivation and autoimmunity [92, 116, 117]. However, tumor cells evade T cells by increasing surface expression of, co-inhibitory molecule, PD-L1. PD-L1 on tumor cells bind to PD-1 on the T cells triggering inhibitory pathways that make T cells inert or tolerant towards them [92, 100, 118]. This binding results in inhibition of T cells proliferation, cytokine production, and ultimately results in their dysfunction or apoptosis [119-121]. This loss of immunological control is considered as a hallmark of cancer [1]. Therefore, blocking these interactions is one of the ways of making T cells more active towards tumor cells and reversing the immunologically tolerant state. These antibody blockers, such as anti-PD-1 and anti-PD-L1 antibody, are called CPIs [92, 100, 122]. CPIs represent one of the most successful approaches that has emerged in the treatment of cancer in recent years [122, 123]. This is evident as CPIs have been approved by FDA for the frontline treatment of multiple cancers including metastatic melanoma, NSCLC, renal cell carcinoma (RCCs), and bladder cancer [122]. Indeed, countless clinical trails have started that use CPIs for the treatment of several other cancers such as breast, colon, colorectal, ovarian, lung, head and neck cancer, and several other solid or hematological malignancies [122]. There are multiple immune checkpoints including LAG-3, TIM-3, CTLA-4, and PD-1. However, antibodies against CTLA-4 (Ipilimumab) and PD-1 (Nivolumab and Pembrolizumab) are most effective and are already approved by FDA for several cancers [100, 122, 124].

CPI therapy in Melanoma and Breast cancer

Melanomas are the most lethal type of skin cancers causing 80% of skin cancer deaths. Melanoma accounts for 232,100 (1.7%) cases of all newly diagnosed primary malignant cancers and causes about 55,500 cancer deaths annually [124]. Melanoma can be genetically stratified into four major subgroups in which patient tumors contain; (1) activating BRAFV600 mutations (~50%); (2) *N/H/K-RAS* mutations (15–20%), (3) inactivating mutations of *NF1* (~10%), and (4) wild-type *BRAF*, wild-type *RAS* and wild-type *NF1* (30–35 %) [125, 126]. Typically, non-sun exposed melanomas are strongly associated with the activating driver BRAFV600E mutation, and these patients develop melanoma early in life, whereas sun exposed melanomas are characterized by genetic mutations in *NRAS*, *NF1* and *KIT* [124-126]. Other frequent genetic mutations contributing to melanomagenesis include mutations in *CDKN2A*, *PTEN*, *P53*, and aberrant

pathways such as β-catenin, MAPK/ERK, and PI3K/AKT signaling pathways [124-126]. For patients with BRAF mutant melanoma, a response rate of ~76% has been observed with the combination of BRAF and MEK inhibitors [124-126]. However, 80% of patients relapse on the BRAF inhibitor (BRAFi) or MEK inhibitors (MEKi), where then the only option is CPI therapy. The CPI therapy, combining anti-CTLA-4 and anti-PD-1 antibodies, has shown less impressive response rates (~50%) compared to targeted therapy (~76%), but show long lasting responses in a group of patients (up to 40% show a progression-free survival after 4 years), and has led to a paradigm shift in treating all melanoma genotypes [127-130].

Breast cancer (BCa) has a high prevalence with estimated 2.3 million new cases (11.7% of all cancer) and accounting for 685,000 deaths [131, 132]. The 10-year survival rate is reduced from 88% in stage I/II BCa to 10-40% in stage III patients, with less than 10% for stage IV BCa [133]. High rates of morbidity and mortality are primarily due to increased metastasis to lungs, brain and especially to skeleton [133]. In fact, it has been estimated that metastasis can account for up to 90% of cancer related deaths [134, 135]. BCa is a heterogeneous cancer with four major molecular subtypes; Luminal A (ER^{high},$PR^{high/low}$, $HER2^{low}$); Luminal B (ER^{high}, $PR^{high/low}$, $HER2^{high/low}$ki-67^{high}); HER2 enriched (ER^{low},PR^{low}, $Her2^{high}$) and triple-negative BCa (ER^{low},PR^{low} and $HER2^{low}$)[136]. Luminal A and B account for 70% of invasive BCa [132]. Compared to luminal A, luminal B tumors show higher proliferation and are associated with a higher cumulative incidence of distant metastasis [137, 138]. Importantly, patients with luminal B BCa subtype have the highest probability to form bone metastasis leading to skeletal-related events (SREs) that include hypercalcemia, intractable bone pain, nerve compression, increased bone fragility which collectively increases cancer associated morbidity and mortality [139-142]. Objective response rate to CPI is highly correlated to mutational burden ($p< 0.001$)[143, 144]. BCa is generally considered to be less immunogenic due to low mutational load (around 1/Mb) compared to melanoma and lung cancer (10/Mb) [144, 145]. Moreover, BCa usually have high immunosuppressive Tregs infiltration in TME [146]. Although there is some clinical success with triple negative BCa subtype (5-30% overall response rate), luminal A and B which are the least immunogenic of all BCas subtypes had limited clinical success [147, 148]. However, combining CPI with radiotherapy or chemotherapy or epi-therapy that increase the immunogenicity (elevated

tumor mutational burden) and tumor infiltrating immune cells can potentially increase the efficacy of CPI in all BCa subtypes [147-149].

To understand the strategies that could increase the effectiveness of CPI therapy, it is imperative to comprehensively identify factors that could determine the response to CPI therapy which are discussed in the next section of the thesis.

Factors determining the response to CPIs

Apart from the aforementioned factors that provide a generally effective anti-tumor immunity and are desired for a better clinical outcome (Figure 5), there are specific factors that predict better CPI response. In era of precision medicine, selecting patients that would highly benefit from the CPI therapy is essential as this would avoid unnecessary CPI treatment administration to non-responding patients and avoid suffering of patients due to severe adverse events. Although there are various factors that determine the response to CPI therapy, the most essential tumor and immune factors are detailed below.

(i) Tumor Mutational Burden (TMB) and Neoantigen expression

TMB is the somatic mutations per length of DNA. TMB is a major determining factor identified that is associated with response of CPIs [150, 151]. In several clinical trials, TMB was shown to correlate with enhanced efficacy of CPIs strongly and positively in tumors with high TMB such as melanoma and NSCLC [150, 151]. In fact, analysis of 27 common cancer types showed a strong correlation between TMB and objective response rates with CPIs (anti-PD-1 and anti-PD-L1 antibodies) [144]. Accordingly, BCa (especially luminal subtypes) and PCa have low TMB and therefore tend to have a low response to CPI and this trend is opposite for high TMB cancer types including melanoma, NSCLC, and colon cancer. Consistently, tumors that have defects or loss of functional mutations in DNA repair genes or inability to repair DNA such as microsatellite instability (MSI) phenotype, tend to have higher response to CPIs [150, 151].

The reason for the high response to tumors with high TMB is due to higher immunogenicity of the tumor cells. Typically, tumor with high mutation rates will lead to generation of greater number of tumor specific or associated antigens (TSAs or TAAs) [150]. These TSAs, termed as neoantigens, will be recognized by the immune cell as foreign and will elicit an immune response

[150]. Furthermore, tumor cells tend to downregulate expression of TSAs and self-antigens to avoid immune destruction. For instance, BRAF mutant melanomas have suppressed expression of melanocyte differentiation antigens (MDAs) including Melanoma antigen recognized by T cells 1 (MART-1 or MELAN-A), pre-melanosome (PMEL or GP100), tyrosinase (TYR) and tyrosinase-related protein 1 and 2 (TYRP1 and TYRP2). Accordingly, BRAF/MEK inhibition upregulated the expression of MDAs thereby increasing the immunogenicity of the tumor cells. This led to enhanced anti-cancer immune responses including a higher $CD8^+$ T cell infiltration, activation, cytokine (IFNγ) and cytotoxic proteases (granzyme B and perforin) production [152, 153]. Therefore, increasing TSA, TAA, and MDAs (in melanoma) on tumor cells can uplift recognition by anti-cancer immunity and lead to higher anti-cancer immune responses including CPI response.

(ii) PD-L1 expression

As mentioned above, one of the major tumor escape mechanisms adopted by tumor cells is to upregulate PD-L1 expression and inhibit killing by cytotoxic Ag-specific $CD8^+$ T cells. Consistently, higher PD-L1 expression is correlated to poor prognosis in several cancer types including melanoma and BCa [150, 151]. In contrast, higher PD-L1 is an excellent biomarker for predicting response to CPIs, and PD-L1 immunohistochemistry (IHC) has been approved by FDA to be used in conjunction with diagnosis for patient selectivity for CPI therapy [150, 151]. For instance, in a meta-analysis it was demonstrated that melanoma and NSCLC patient tumors that had high expression of PD-L1 showed a better response to anti-PD-1 antibody (Nivolumab and Pembrolizumab) [150, 151]. Moreover, several other cancer types have shown that the higher the levels of PD-L1 the higher response to anti-PD-1 antibody compared to other biomarkers including PD-1 or PD-L2 [150, 151, 154]. Additionally, PD-L1 expression on immune cells is also predictive of response to anti-PD-L1 antibody. However, absence or low expression of PD-L1 doesn't necessarily mean poor response to CPIs blockade as some patients (11-20%) with low or negative PD-L1 expression have demonstrated high clinical efficacy with response up to 41% and 54% with Nivolumab and Nivolumab + Ipilimumab, respectively [150, 151, 155, 156]. This discrepancy could be attributed to various factors. Firstly, poor uniformity in the PD-L1 IHC as different thresholds for PD-L1 positivity and different staining techniques with different antibodies are utilized in different labs [150, 151]. Secondly, it could be due to intra-patient and intra-tumoral heterogeneity which would mean that different tumor sites (or sampling) and/or different time

points can reflect different state of PD-L1 expression from the same patient [150, 151]. Thirdly, it can be attributed to the effect that CPIs have on IFNγ as IFNγ regulates PD-L1 expression. Lastly, the variability could be because PD-L1 is regulated by transcriptional factors, multiple pathways including MAPK and PI3K/AKT pathways, PD-L1 expression by several immune cells, and epigenetic factors [150, 151]. Therefore, the paradoxical predictive value of PD-L1 is useful but not a definitive biomarker [150, 151].

(iii) Tumour-infiltrating lymphocytes (TILs)

Typically, higher TILs (immunologically hot tumors) have been associated with improved survival rates in several cancers including melanoma, colorectal cancer, and NSCLC. In general, clinical benefit of most immunotherapies, such as high dose of IL-2, was associated with higher TILs within the TME and this is true for CPIs as well. A higher TILs had significantly higher clinical activity with anti-CTLA-4 (Ipilimumab) and anti-PD-1 (Pembrolizumab) antibodies in clinical trials with melanoma patients [150, 151]. This association was even more significant after the CPIs treatment was started. Although these studies do point out TILs to be predictive of CPI therapy, it was hard to find the cut off between responders and non-responders solely based on baseline lymphocyte infiltration [150, 151].

(iv) T cell receptor (TCR) clonality

TCR clonality is another factor of TILs that could predict better response to CPIs. TCR repertoire of all the uniquely rearranged variable TCR β-chain regions of the TILs was studied in melanoma patients in response to anti-PD-1 antibody (Pembrolizumab) [157]. It was demonstrated that the patients that responded to anti-PD-1 antibody had a more restricted TCR β chain usage, meaning that they had more clonal and less diverse T cell population, than non-responders. In addition, these clonal T cells (T cells specific to a set of Ags) increased 10 folds in responders after receiving anti-PD-1 treatment compared to non-responders [157]. Although very intriguing findings, this phenomenon needs further validation with a larger group of patients and in other types of cancers.

(v) Immune gene signatures

Another tumor intrinsic factor that can determine response of CPIs is a particular gene expression signature. For instance, in a retrospective analysis, total RNA was isolated from pre-

treatment tumor (n= 50) of advanced melanoma patients undergoing anti-CTLA-4 antibody (Ipilimumab) treatment [158]. Then the patients were divided into responders and non-responders based on clinical activity or no clinical activity with anti-CTLA-4 antibody, respectively. The significant genes that were differentially upregulated in responder (compared to non-responders) were genes that stimulate anti-cancer immunity and inflammation [150, 158]. Essential genes of cytotoxic $CD8^+$ T cells (including granzyme B (*GZMB*) and perforin 1 (*PFR1*)), $CD4^+$ Th1 effector function, antigen expression, and other immune-related genes (*NKG7*, *IDO1*) were upregulated [150, 158].

IFNγ is one of the most powerful cytokines that can cause anti-tumor activity and is characteristic feature of cytotoxic T cells that produce perforin and granzymes [159-161]. IFNγ and its related gene signature are also key factors that determine success of CPIs [159]. In several clinical trails, it was demonstrated that the IFNγ (*IFNG*) and its pathway genes were strongly correlated with best overall response to CPIs, and progression-free survival [150, 162]. Furthermore, IFNγ also stimulates expression of PD-L1 and therefore contributes to better response to anti-PD-1 antibody as described earlier [150]. Other immune related genes (from 28-gene signature) that have been highly associated with better response to CPIs were granzyme A and B (*GZMA* and *GZMB*), and *PFR1*, *IDO1*, and *LAG-3* [150, 162].

Current challenges and limitations of CPIs

Although CPIs led to marked success in the clinic, around two-third of the patients do not respond to CPIs and there is a large variation in response to CPIs. For instance, the response rate generally is only 10–15% with anti-CTLA-4 (Ipilimumab) and only around 30-40% for anti-PD-1 antibody treatment in metastatic melanoma [151]. Immune-related adverse events (irAE) are often caused by CPIs blockade therapy because they result from non-specific activation of immune cells. The most frequent irAE is fatigue and possibly fatal inflammatory pneumonitis. Some patients can experience a high grade irAE which would result in immediate withdrawal from CPIs [151]. Nevertheless, PD-1/PD-L1 blockade is preferable due to a more restricted spectrum of T-cell activation at effector stage that results in lower incidence of irAE compared to CTLA-4 blockade [163, 164].

The variable responses are due to tumor intrinsic immune evasive mechanisms, primary and secondary resistance, and together with irAE, limit the use of CPIs. Therefore, understanding

the resistance mechanisms and countering them may help improve the patient outcome. In the next section, resistance mechanisms to CPIs are discussed.

Tumor primary (intrinsic) resistance

Tumor inhibition or progression depends on TME factors, which can be anti- or pro-tumorigenic. Tumor progression is suppressed or eliminated by the cancer immunosurveillance system, however, tumor cells can evolve and develop mechanisms that allow them to evade or escape the immune system (Figures 4 and 5) [89, 93, 101].
There are three main immune escape mechanisms [112]:

(i) Loss of antigenicity—tumor cells increase defects in Ag processing and presentation machinery resulting in lower presentation of Ags to immune cells. For examples, downregulation of MHC class I molecules is observed in ~20-60% of common solid malignancies, including melanoma, lung cancer, BCa, renal cancer, PCa, and bladder cancer.

(ii) Loss of immunogenicity—tumor cells produce low levels of immunogenic tumor Ags (TSA or TAA) and high levels of immunosuppressive ligands. For example, upregulation of the immunoinhibitory molecule PD-L1 on malignant cells.

(iii) Creating an immunosuppressive TME—tumor cells transform to cause alterations in oncogenes and TSGs to increase inflammation and recruitment of pro-tumor immune cells in TME. For instance, increased infiltration and differentiation of M2 macrophages/TAMs, myeloid-derived suppressor cells (MDSC), and Tregs in TME.

The resistance mechanisms result in pro-tumor TME as discussed in Figure 5. In addition, PTEN and activation of PI3K-AKT pathway in tumor cells have been associated with inability of the T cells to infiltrate the TME (T cell exclusion) and function within the TME [112, 151]. Moreover, tumor cells activate WNT/β-catenin signaling pathway that makes DCs non-functional and hence they are unable to prime and activate the $CD8^+$ T cells [112, 151]. Lastly, tumor cells can also activate EGFR pathway which leads to an immunosuppressive TME resulting from increased pro-tumor cytokines and inhibitory checkpoint expression including PD-1, PD-L1, and CTLA-4 [112, 151]. All the above mechanisms result in tumor growth and progression.

Tumor secondary (acquired) resistance

In clinical studies, some patients who initially responded to CPI therapy relapsed and acquired resistance to CPIs [100, 112, 165, 166]. Pathways involved in Ag presentation and processing (MHC I expression) or IFNγ responsive pathways were found to be either mutated or defective in these patients that acquired resistance to CPI [165, 166]. JAK1 and JAK2 which are involved in IFNγ response were consistently identified to be mutated in these patients. Moreover, mutations in IFNγ receptors IFNGR1/2 have been identified as modes of acquired resistance by cancer cells [100, 165, 166]. In addition, mutations in IFNγ responsive pathways were also found to have primary resistance to CPIs as non-responding patients also had mutations in JAK1 or interacting genes. As explained above, MHC I expression is pivotal in cytotoxic $CD8^+$ T cells recognition, activation, clonal expansion, and effector functions such as tumor cell lysis. Downregulation of MHC class I molecules is observed in ~20-60% of common solid malignancies [112]. Therefore, this has been proposed as a major resistance mechanism to CPIs. Loss of function mutations in β2-microglobulin (B2M), a key component of MHC I, has been extensively reported [100, 112, 165, 166]. Thus, active research focus is to identify pathways that can enhance the response to CPI by either increasing immunogenicity, Ag presentation and processing, and/or increasing IFN response pathways activation.

Combination therapies for a superior anti-cancer efficacy

To counter resistance to CPI, active research has focused on identifying therapies that could enhance the effectiveness of CPIs and multiple clinical trials are on-going. There are hundreds of combinations that can be established; however, the following sections will focus on combinations with most potential in the clinic.

Targeted therapy with CPI

Effect of targeted therapy on the immune system has been either immune suppressive or immune stimulating. Although targeted therapies are designed to inhibit proliferation or cause apoptosis, targeted therapies have demonstrated to enhance immune response [152, 153]. BRAFi (including Vemurafenib) and MEKi are approved by FDA for treating melanoma patients with hyperactive MAPK pathway. It was demonstrated in numerous pre-clinical and clinical studies that BRAFi/MEKi can upregulate MDAs and enhance anti-cancer immune response including $CD8^+$ T cell infiltration and $CD8^+$ T cells' activation and cytokine/cytotoxic proteases (granzyme B and perforin) production [152, 153]. However, there was also increase in expression of PD-1 on

T cells and PD-L1 expression on tumor cells [152, 153]. The high PD-L1 on tumor cells and PD-1 on T cells would hinder recognition and killing by $CD8^+$ T cells. Hence, even though increasing Ag expression increases immunogenicity of tumor cells, the PD-1/PD-L1 pathway may cause T cell dysfunction, and thus blocking PD-L1 or PD-1 using CPIs would revive pre-existing Ag recognition and anti-cancer immunity. This provided the rationale for combining BRAFi with CPI therapy [152, 153].

Based on these studies, numerous pre-clinical studies were carried out and it is now well established that BRAF-targeted therapy synchronizes with CPI therapy [152, 153]. These pre-clinical studies led to clinical trials in human melanoma patients. For instance, a clinical trial on previously untreated BRAF mutated metastatic melanoma patients have demonstrated that the combination of BRAFi (Vemurafenib) and MEKi (Cobimetinib) with anti-PD-L1 antibody (Atezolizumab) treatment had 76% objective response rate including three patients that were complete responders (CR) [153]. Moreover, the adverse events from the combination treatment were tolerable. Another clinical trial involved treating BRAF-mutant and BRAF-wild-type metastatic melanoma patients with anti-PD-L1 antibody (Durvalumab) and BRAFi (Dabrafenib) and MEKi (Trametinib) [167]. This trial had 3 treatment arms; (1) BRAF-mutant patients received anti-PD-L1 antibody with BRAFi and MEKi until progressive disease; (2) BRAF-WT patients received treatment with anti-PD-L1 antibody with MEKi until progressive disease; (3) BRAF-WT patients received treatment with MEKi in a 4-weeks lead-in followed by addition of anti-PD-L1+MEKi concurrently for 2 weeks followed by anti-PD-L1 antibody until progressive disease. The overall response rates for Arm 1, 2 and 3, were 69%, 21%, and 13%, respectively. Furthermore, almost 90% of Arm 1 patients continued to derive clinical benefit in a 50-week follow up. Adverse effects were as excepted for individual drugs. Post-treatment immune markers demonstrated that BRAF-mutant melanoma patients treated with BRAFi and MEKi had a strong immune response.

Apart from melanoma, targeted therapy in combination with CPI are being explored in other cancers [152, 153]. For instance, in c-kit mutant gastrointestinal stromal tumors (GIST), a c-kit inhibitor (Imatinib) has shown enhanced anti-tumor immunity [152, 153]. This has provided the rationale for initiation of clinical trials combining c-kit inhibitor with CPI (Ipilimumab) in patients with metastatic GIST. Another attractive targeted therapy with CPI combination is

blocking HER2 using HER2 inhibitor or monoclonal antibody and combine with anti-CTLA-4 or anti-PD-1 antibody [152, 153]. A HER2-targeting antibody (Trastuzumab deruxtecan) was demonstrated to improve antitumor immune responses by increasing MHC I expression in tumor cells and stimulating DCs function [152]. Indeed, HER2 targeting antibody combined with either anti-CTLA-4 or anti-PD-1 antibodies showed enhanced adaptive anti-tumor immune responses *in vivo* in BCa mouse models [152]. In addition, a clinical trial combining a novel HER2 monoclonal antibody (Margeuximab) with anti-PD-1 antibody (Pembrolizumab) in the treatment of HER2-positive gastro-oesophageal adenocarcinoma showed objective response in 18% (17/92) of patients [168]. However, serious adverse events were reported in 9 patients. Together the *in vitro*, *in vivo*, and clinical trials data shows the immense potential of combining targeted therapy with immunotherapy. However, the adverse effects and acquired resistance could hinder the success of the targeted therapy with CPI combination.

Chemotherapy with CPI

Effect of chemotherapies on the immune system has been either immune suppressive or immune stimulating. There is some potential of chemotherapy to be used in combination with CPI as they can stimulate immunogenic cell death (ICD) [111, 169]. ICD can be induced by cyclophosphamides and anthracyclines resulting in adaptive stress response that involves the ER, Toll-like receptor 3/4 (TLR3/4) signaling, type I interferon (IFN) response, and/or autophagy. All these effects lead to attracting DCs and T cells into the TME and activates the adaptive immune cells against TAAs [111, 169]. Apart from ICD, anthracyclines and cyclophosphamide can, respectively, reduce MDSCs and Treg cells resulting in the restoration of T and NK cell functions thereby enhancing immunity [111, 169]. Although there is some potential, most chemotherapies which are currently approved in the clinic are unable to stimulate immunity by ICD or are immunosuppressive or have heightened adverse events rendering them less attractive to be used in combination with CPIs [111, 169].

Radiation therapy with CPI

Compelling pre-clinical evidence have suggested that radiation therapy, apart from its cytotoxic effects in causing tumor cell death, can also stimulate anti-cancer immunity [170, 171]. Two major pathways have been demonstrated. (i) Firstly, radiation causes ICD that leads to release of high amounts of TAAs. Furthermore, ICD also releases signals such as high mobility group box

1 (HMGB1) protein which is a chemoattractant for immune cells and leads to greater tumor immune infiltration [171, 172]. Moreover, HMGB1 helps in DC activation and maturation and further helps in presentation and cross-presentation of Ags to other immune cells such as $CD8^+$ T cells [171, 172]. (ii) Secondly, radiation can cause an increase in immunogenicity and increased sensitivity of the tumor cells by increasing expression of Ags and antigen presentation machinery (APM) such as MHC class I molecules, FAS and ICAM-1 [173-175]. As explained above, this would result in Ag-specific tumor lysis by $CD8^+$ T cells [173-175]. These are rationale to combine radiotherapy with immunotherapy/CPIs, and consistently, pre-clinical studies have demonstrated synergistic anti-cancer efficacy. However, there is limited clinical evidence with significant overall response supporting this combination [170, 171]. Additionally, challenges remain in treating radiation resistant cells, and finding optimal radiation dose and timing that would synergize with immunotherapy [170, 171, 176]. Moreover, current challenges also include identifying biomarker that would elevate effectiveness of this combination therapy [170, 171]. Lastly, radiation therapy can negatively affect T cells in peripheral blood and in tumors and induce lymphopenia which can not only cause adverse effects but also undermine CPI's efficacy [170].

Epi-therapy with CPI

Some epigenetic drugs such as DNMTi tend to upregulate expression of immune signalling pathways in cancer cells thereby improving immune recognition and immunogenicity [177-181]. Combining epigenetic with immunotherapy has been proved in both clinical studies [182-185] and animal models [186-190]. Recently, studies have established that malignant cells escape host immune recognition by acquiring immune evasive phenotype through epigenetically downregulating essential molecules for cancer and immune interactions [92]. For instance, these mechanisms include suppression of TAAs, reducing expression of many components of APM, and decreasing co-stimulatory molecules, stress-induced ligands, and death receptors [92]. DNMTi and histone deacetylase inhibitors (HDACi) reverse the immune evasive phenotype, for example, by upregulating the expression of TAAs and APM components on tumor cells, which helps the immune system to recognize and eliminate tumor cells [92, 177, 180, 181]. Additionally, T cell exhaustion can also be reversed using DNMTi in mouse models, resulting in enhanced anti-cancer immunity [191, 192]. DNMTi can also trigger a state of "viral mimicry" by activating dsRNAs, thereby increasing type I interferon responses [92, 193]. In addition, DNMTi and HDACi

increased cytotoxic activity of $CD8^+$ T cells and NK cells and increased these anti-tumor cells' immune infiltration in the TME while reducing pro-tumor macrophage infiltration in a murine ovarian cancer model [194]. These anticancer effects were further elevated in triple combination with CPI (anti-PD-1 antibody), which reduced the tumor burden and provided longest overall survival. Collectively, the above studies indicate priming of the immune system by DNMTi (and HDACi), thereby increasing the efficacy of CPI therapy. However, DNMTi have various disadvantages including adverse events and upregulating silenced oncogenes (including *SALL4*) and pro-metastatic genes (including *uPA*) which could result in increased risk of metastasis [53, 54]. The adverse events become a real challenge when combined with CPI as CPI have their own irAEs. In order to lower adverse events related to DNMTi, the precise mechanism of action is warranted which is rather challenging to find due to the fact that DNMTi have non-specific effects including cytotoxic effects and DNA replication inhibition which is not related to its DNA demethylating activity [18]. Therefore, novel therapeutic strategies with lower adverse effects are warranted in combination with CPIs to reduce cancer associated morbidity and mortality.

Potential of SAM enhancing CPI response

Although studies investigating the effect of SAM on immune system are still lacking, SAM has been shown to modulate the immune system [195-208]. Interestingly, a few studies have shown that SAM is essential for T cell activation and proliferation [200-204]. In activated T cells, both the SAM quantity and the rate of SAM utilization increase dramatically via increased transcription of *MAT2A,* which encodes the catalytic subunit of MATII and is vital for SAM biosynthesis [202, 203, 205, 206]. Blockage of SAM synthesis resulted in blocked T cell proliferation [201]. Furthermore, SAM was shown to be indispensable for T cell proliferation and activation by decreasing both caspase-3 activity and apoptosis in ethanol-related activation-induced cell death (AICD) [200]. Moreover, SAM was shown to lower the suppressive capacity of Tregs by methylating the *FOXP3* gene, thereby reducing its protein and mRNA expression in a dose-dependent manner [209]. SAM was also found to decrease expression of an immunosuppressive cytokine, IL-10, and increase expression of IFNγ [209]. SAM in combination with vitamin D was also shown to upregulate immune-related genes and pathways particularly type I IFN (IFNα/β) pathways in BCa [71].

As discussed above, TMB is a predictive factor of successful response to CPI. TMB increases due to increased mutations in rapidly dividing cancer cells during consecutive rounds of cell divisions [176, 210, 211]. Similarly, global DNA hypomethylation (or methylation loss) also accumulates due to inability of the cells' methylation machinery to quickly methylate the newly formed daughter strands during rapid DNA replications, and due to reduced SAM availability within TME [176, 210, 211]. Global methylation regulates essential genes and pathways which provide resistance to therapy. In addition to the immune evasive mechanisms detailed above, studies have found that the altered methylome of cancer cells confers resistance to CPIs [176, 212-214]. In a pioneering study, it was demonstrated that global DNA hypomethylation was strongly linked to increase in genome instability (aneuploidy) and TMB in a pan-cancer analysis of TCGA data [214]. Importantly, global hypomethylation levels were strongly associated with immune evasion signatures independently of aneuploidy and TMB. These immune genes include markers of tumor infiltrating $CD8^+$ T cells, MHC expression, APM, interferon signalling, and cytokine–cytokine receptor interaction and signaling. The immune genes were concentrated in late replicating partially methylated domains reassuring that methylation loss in these regions activates immune evasive genes. Next, to test if global DNA hypomethylation affects the clinical benefit of immunotherapy, the authors utilized lung cancer and melanoma cohorts for which CPIs therapy data was available. They showed that global DNA hypomethylation (or demethylation) predicts response to CPIs, increases immunotherapeutic resistance, and counteracts the contribution of TMB to CPI response. This study, therefore, demonstrated DNA hypomethylation (or demethylation) as an essential biomarker which could predict response to CPIs and can also provide a tumor immune evasive mechanism and resistance to CPIs [214]. Results from this study were further supported by the findings that SAM levels are depleted by cancer cells through various mechanisms, such as increased conversion of SAM to by-products, which reduces the methylation potential of immune and cancer cells [212, 213]. Parallel to this, a recent study demonstrated that an essential immune evasive mechanism used by tumor cells is depriving $CD8^+$ T cells of methionine (the pre-cursor of SAM) in the TME. This makes $CD8^+$ T cells non-functional and unresponsive to CPIs as $CD8^+$ T cells require SAM for their activation, proliferation, and survival [200-204, 212]. Therefore, the effect of SAM must be studied not only on tumor/cancer cells but also on anti-cancer immunity comprehensively in future studies as SAM has the potential to enhance immunity in general and elevate CPI responses.

RATIONALE AND HYPOTHESIS

Cancer immunosurveillance system, including T cells, act as tumor suppressors eliminating and controlling the formation of pre-malignant and malignant cells. Recognition, activation, and cytotoxic transformation of T cells to recognize and kill pre-malignant and malignant cells may alter their DNA methylome. DNA methylation differences in T cells between healthy controls and BCa patients were demonstrated recently by our laboratory. Many studies did not yet extensively address the intriguing question of whether DNA methylation patterns would be altered in peripheral T cells in response to cancers, such as PCa, and during cancer progression. In addition, a challenge remains in diagnosing PCa early due to limitations of currently employed tests. Since T cells are involved in eliminating pre-malignant and malignant cells, the hypothesis is that the DNA methylation changes in the peripheral T cells will be different between healthy controls and PCa patients. Hence, epigenome-wide DNA methylation changes were investigated in peripheral T cells of negative-biopsy controls and positive-biopsy PCa patients. These DNA methylation changes can be further used to distinguish between controls and PCa patients, and different stages of PCa.

A balance remains between the cancer immunosurveillance system and carcinogenesis due to the latter regressing and eliminating rapidly growing cancer cells. However, cancer utilizes immune evasive mechanisms including immune checkpoints such as PD-L1 to escape killing from cytotoxic $CD8^+$ T cells and other anti-cancer immune cells. CPIs which block co-inhibitory checkpoints and restore the cancer immunosurveillance system (such as cytotoxicity of $CD8^+$ T cells), have revolutionized the cancer treatment. However, a high proportion of patients are still unresponsive to CPIs due to primary and acquired resistance, and immunosuppressive TME. As recently reported, the resistance to CPIs could be due to DNA hypomethylation of tumors. SAM targets DNA hypomethylation and is essential for activation, proliferation, and survival of T cells. SAM was reported to be present in low levels in the TME. Indeed, deprivation of $CD8^+$ T cells of methionine (a pre-cursor of SAM) in the TME was suggested to be another essential immune evasive mechanism that makes $CD8^+$ T cells non-functional and unresponsive to CPIs.

Apart from being a resistance mechanism, global DNA hypomethylation is a well-established phenomenon that have been associated with genomic instability, activation of oncogenes and repetitive elements, which ultimately leads to cancer initiation, progression, and

metastasis. DNA methylation serves as an attractive target because, unlike genetic changes, DNA methylation changes are reversible and can be altered by either dietary interventions or therapeutic strategies. Our laboratory has previously targeted DNA hypomethylation using SAM in treatment of BCa, PCa, and osteosarcoma. However, the direct effect of SAM has never been investigated in melanoma. Moreover, effect of SAM on cancer immunosurveillance components such as $CD8^+$ T cells has never been extensively studied. The hypothesis is that SAM would have beneficial anti-cancer effects against melanoma and SAM would enhance anti-cancer immunity against melanoma and other cancers. Moreover, SAM in combination with CPIs such as anti-PD-1 antibody would have a superior anti-cancer efficacy. Overall, this novel therapeutic strategy would be beneficial against tumor growth, progression, and metastasis of melanoma and BCa.

OBJECTIVES

- To investigate epigenome-wide DNA methylation changes that occur in peripheral T cells of PCa patients compared to healthy controls. To identify a non-invasive DNA methylation signature that could distinguish between PCa patients and healthy controls.
- To investigate the anti-cancer effects of SAM in BRAF WT and BRAF mutant melanoma cell lines and immunocompetent syngeneic mouse models.
- To test the combinatorial effect of SAM and CPIs (anti-PD-1 antibody) on tumor growth and progression, and metastasis of BRAF mutant and BRAF WT melanomas.
- To delineate the potential molecular pathways affected by the SAM alone and in combination with anti-PD-1 antibody in melanoma.
- To understand the tumor immune cells interactions and determine the effect of SAM alone and SAM and anti-PD-1 antibody combination on immune cells within the TME of melanoma tumors.
- To determine the effect of the SAM and anti-PD-1 antibody monotherapies and combination on tumor growth, anti-cancer immunity, and metastasis to skeletal and non-skeletal organs, of luminal B BCa subtype.

CHAPTER TWO: DNA methylation signatures of Prostate Cancer in peripheral T-cells

Preface

One of the major challenges in most common cancers is the early diagnosis or risk prediction of an individual developing cancer. This is especially true for prostate cancer (PCa) as the 5-year survival rate decreases drastically from 99% for a localized tumor to only 30% for metastasized PCa [77]. This warrants the urgent need to develop techniques for early intervention in detecting PCa. Early detection of cancer is limited by the lesion area or tumor mass. Currently, accurate early diagnosis of PCa patients remains a challenge. We rely upon digital rectal examination, prostate specific antigen levels, and prostate biopsies. Each of these tests have limitations, and prostate biopsies although accurate, are invasive, can provide false-negative results and do not examine the whole prostate. Furthermore, the surgical removal of prostate tumor tissue by biopsy can also increase the risk of patient developing metastasis. Moreover, digital rectal examination and prostate biopsies can also have a delay in early detection of PCa because they rely upon a certain tumor volume to be detected. T cells can detect and eliminate transformed cells even before they become malignant. Hence, T cells can serve not only as potential candidates for early detection of cancers but also as efficient biomarkers. Another unanswered question is whether the presence of pre-malignant or malignant cells alter DNA methylation patterns in peripheral T cells of PCa patients, and whether this intensifies with higher tumor stage or aggressiveness of PCa. To address these challenges, we investigated epigenome-wide DNA methylation status of peripheral blood T cells of healthy subjects or controls (negative biopsy having benign prostate tissue) and subjects with positive biopsy for PCa. T cells DNA was isolated and subjected to global Illumina Infinium methylation EPIC array and validated using Illumina amplicon sequencing and pyrosequencing platforms.

Chapter Two follows the author generated version of the manuscript which was published in BMC cancer journal and is referenced below.

- **Mehdi, A**., D. Cheishvili, A. Arakelian, T.A. Bismar, M. Szyf, and S.A. Rabbani, *DNA methylation signatures of Prostate Cancer in peripheral T-cells.* BMC Cancer, 2020. **20**(1): p. 588.

Abstract

Background: Prostate Cancer (PCa) is the second most common cancer in men where advancements have been made for early detection using imaging techniques, however these are limited by lesion size. Immune surveillance has emerged as an effective approach for early detection and to monitor disease progression. In recent studies, we have shown that host peripheral blood immune cells undergo changes in DNA methylation in liver and breast cancer.

Methods: In the current study, we examined the DNA methylation status of peripheral blood T cells of men with positive biopsy for PCa versus men with negative biopsy having benign prostate tissue, defined as controls. T cells DNA was isolated and subjected to Illumina Infinium methylation EPIC array and validated using Illumina amplicon sequencing and pyrosequencing platforms.

Results: Differential methylation of 449 CG sites between control and PCa T cell DNA showed a correlation with Gleason score ($p < 0.05$). 223 differentially methylated CGs between control and PCa ($\Delta\beta$ +/- 10%, $p < 0.05$), were enriched in pathways involved in immune surveillance system. Three CGs which were found differentially methylated following DMP (Differentially methylated probes) analysis of ChAMP remained significant after BH (Benjamini-Hochberg) correction, of which, 2 CGs were validated. Predictive ability of combination of these 3 CGs (polygenic methylation score, PMS) to detect PCa had high sensitivity, specificity and overall accuracy. PMS also showed strong positive correlation with Gleason score and tumor volume of PCa patients.

Conclusions: Results from the current study provide for the first-time a potential role of DNA methylation changes in peripheral T cells in PCa. This non-invasive methodology may allow for early intervention and stratification of patients into different prognostic groups to reduce PCa associated morbidity from repeat invasive prostate biopsies and design therapeutic strategy to reduce PCa associated mortality.

Keywords: Prostate cancer, DNA methylation, T cells, blood, diagnosis, immune.

Background

Prostate Cancer (PCa) is the second most common cancer in men and has been estimated to affect more than a million men worldwide in 2018 [1-4]. PCa is graded using the Gleason score (ranging from 2-10) that examines the differentiation of cancer cells according to their histological pattern [1-5]. In its early stage, tumor cells are androgen sensitive however, in advanced stages they are androgen insensitive, metastasize to distant organs and have limited therapeutic strategies available [3, 5]. Therefore, there is an urgent need to identify sensitive biomarkers which can detect initial and recurrent PCa early to allow for effective intervention. Diagnosis for PCa includes digital rectal examination and determination of the levels of prostate specific antigen however, each of these tests have limitations [6, 7]. On the other hand, prostate biopsies are invasive, can provide false-negative results and do not examine the whole prostate [5, 6, 8, 9].

DNA methylation has emerged as a major area of investigation for the identification of cancer specific biomarkers at an early time point which can be utilized as a diagnostic or prognostic biomarker in numerous cancers including PCa [10-18]. DNA methylation alterations are highly common and are particularly able to provide a high degree of sensitivity using plasma and urine of PCa patients [12, 19]. However, these studies were limited in scope due to their focus on a single or few gene loci. Collectively a multi-faceted approach is required to accurately predict and detect PCa for early intervention and develop effective therapeutic strategies.

Host immuno-surveillance plays an important role in the recognition and elimination of transformed and tumor cells [20-22]. T-cells are the most prominent component of this system that control tumor growth [20-22] and hence have the potential of being effective cancer biomarkers [23-25]. In previous studies, we have identified a DNA methylation signature in peripheral blood mononuclear cells and T cells in hepatocellular carcinoma (HCC) which distinguished HCC from chronic hepatitis B and C versus healthy controls [25]. Similarly, DNA methylation signature in T cells of breast cancer patients showed strong correlation with breast cancer progression compared to healthy controls [24].

In the current study, we have carried out genomic DNA methylation assay using peripheral blood T cells from negative-biopsy men having benign prostate tissue, defined as controls, and positive biopsy PCa patients. T cells DNA isolated from control and PCa subjects was analyzed by Illumina Infinium methylation EPIC array platform and validated using amplicon- and pyro-

sequencing. We have identified a DNA methylation signature that not only distinguishes healthy controls from PCa patients but also different stages of PCa according to Gleason score.

Methods

Study populations

The study design was approved by the ethics committee of Alberta PCa Research Initiative (APCaRI). Buffy coats for positive-biopsy PCa patients and healthy negative-biopsy, having benign prostate tissue defined as controls, men were obtained through APCaRI. All patients were enrolled at the time of diagnosis before initiation of any treatment and had strict exclusion criterion of any autoimmune disease, asthma or infection which could alter T cells characteristics. The study had 12 controls and 20 PCa samples; 9 of which were low Gleason PCa (LGPCa) having a Gleason score ≤7 and; 11 of which were high Gleason PCa (HGPCa) having a Gleason score >7 (Cohort 1) (Supplementary Figure 1A and Supplementary Table 1). We used an older cohort (Cohort 2) which had 11 controls and 13 LGPCa samples for some analysis (described below) (Supplementary Table 1). The controls (mean age of 58.0 years) and the PCa patients (mean age of 62.4 years) had no significant difference between mean age ($p > 0.05$). The percentage tumor volume (%) was calculated as the total volume of positive cores divided by all cores tissue and is reflective of the potential cancer volume in the prostate gland.

T-cell isolation, Methylome assay and Pyrosequencing

Firstly, CD3+ T cells were isolated using anti-CD3 immuno-magnetic beads (Dynabeads®, Invitrogen) from the buffy coats of PCa and healthy controls according to manufacturer's protocol. Genomic DNA was extracted from the T cells using AllPrep DNA/RNA mini kit (Qiagen, Canada) according to manufacture's protocol as previously described [24, 25].

Methylome assay was performed on the genomic DNA (gDNA) extracted from T cells using Infinium® MethylationEPIC BeadChip assay from Illumina (Illumina Inc., CA, USA). Following sodium bisulfite conversion of gDNA Infinium® MethylationEPIC BeadChip assay was carried out as previously described [24, 25].

Pyrosequencing was performed according to PyroMark Q24 (QIAGEN) following manufacturer's protocol except a few modifications according to Tost et al. [24-26]. All data were expressed as mean ± standard error of the mean (SEM). Primers used for the analysis are listed in Supplementary Table 2.

Amplicon sequencing (using Illumina MiSeq)

The bisulfite converted DNA was quantified by a Nanodrop Spectrophotometer (Thermo Fisher Scientific, MA, USA) followed by two rounds of polymerase chain reaction (PCR) targeting the cg14713996 and cg05133736 regions using Bio-Rad C1000 Touch Thermal Cycler (Bio-Rad Laboratories, CA, USA) for multiplex sequencing. The pooled library was then purified twice using AMPure XP Beads (Beckman Coulter Life Sciences, CA, USA) and quantified by RealTime PCR using NEBNext® Library Quant Kit for Illumina (New England Biolabs, MA, USA) and sequencing was performed on the Illumina platform using MiSeq Reagent Nano Kit V2 (Illumina, CA, USA).

Data and Statistical analysis

Data analysis was performed in R software using the ChAMP pipeline from Bioconductor at default setting and quality controlled using BMIQ and SVD while batch corrected with ComBat [27, 28]. Indeed, significant ($P < 0.05$) variation arising from the Slide variable were completely removed after running the ComBat function (Supplementary Figure 2)**.** We carried out further QC as previously described by us and others [24, 25]. Subsequently, Differentially Methylated Probes (DMPs) between PCa and negative-biopsy controls was run in ChAMP with Benjamini-Hochberg (BH) and False Discovery Rate (FDR) as < 0.05. We performed Pearson correlation between the normalized DNA methylation beta values and Gleason score using the Pearson correlation function in R and corrected for multiple testing using BH method (FDR <0.05). Next, we used an older small cohort (cohort 2) for which we had 11 control and 13 LGPCa T cell DNA samples (Supplementary Table 1). For this cohort, we had run Illumina Infinium Human Methylation 450K BeadChip in the past but there were no significantly differentially methylated CGs between the groups after BH correction (FDR<0.05). However, several CG methylation levels were

significantly correlated with the Gleason score. Hence, we combined the CGs in 450K and 850K cohorts that correlated with the Gleason score and plotted a Heatmap and Boxplot of these CGs.

We shortlisted differentially methylated CGs which had delta-beta value of +/- 10% in between the groups and plotted a Heat-map. Then the genes associated with these CGs were subjected to a pathway analysis using ConsensusPath DB (with $p<0.01$ and $q<0.05$)[29]. The flow chart of experimental approaches are outlined in Supplementary Figure 1B. Heatmaps were generated using GENE-E of broad institute [30].The statistical analyses were performed using the computing environment R version 3.4.4 and GraphPad Prism 6.0 (GraphPad Software Inc., California, US).

Results

Differentially methylated genes in T-cells of PCa patients are enriched in immune-related pathways

We delineated 223 differentially methylated CGs between the two groups of healthy individuals and PCa patients, using the Bioconductor package Limma, implemented in ChAMP [31, 32] with a delta beta threshold of +/- 10% (Supplementary File S1) and plotted a heatmap (Figure 1A). The differentially methylated genes were subjected to pathway analysis. Notably, genes associated with differentially methylated CG sites were enriched in the pathways involved in immuno-editing and immune-surveillance systems (Figure 1B).

Correlation between DNA methylation levels and Gleason score in PCa

To delineate a set of differentially methylated CGs that are correlated with Gleason score progression, we performed a Pearson correlation analysis (Hmisc R) (0 for healthy individuals and 6, 8 and 9 for Gleason score 6, 8, 9). We corrected for multiple testing using the FDR (Q of <0.05) Benjamini-Hochberg method. This analysis revealed a signature of DNA methylation comprised of 449 CGs which correlates with Gleason scores in T cells from PCa patients (Figure 2A-D). 416 CGs, out of 449 CGs, were hypermethylated (Figure 2A and B) and 33 were hypomethylated (Figure 2C and D). Boxplot of the methylation values of the differentially methylated sites included in the signature demonstrates the magnitude and progressive change in average DNA methylation as the Gleason score progresses from normal individuals to PCa patients with the

highest differences observed at the highest Gleason score of 9 (Figure 2A and C). Heatmap and hierarchical clustering analysis of 416 hypermethylated and 33 hypomethylated sites accurately grouped normal and PCa patients with Gleason score 6, 8 and 9 with exception of one PCa patient in Figure 2B and two normal in Figure 2D.

We next performed a Pearson analysis between methylation levels and Gleason scores of 354,692 CG sites that were also included in a 450K Illumina bead array analysis of a different cohort (cohort 2) which we performed earlier (hereafter Combined cohort) (Supplementary Table 1). 11,722 CG sites showed a statistically significant correlation after FDR correction (Supplementary File S2); 8,478 were hypermethylated and 3,244 were hypomethylated. We shortlisted 1,181 (Supplementary File S3) progressively methylated CGs that had a 10% difference in methylation level between average DNA methylation of PCa patients with Gleason score 9 and in normal individuals. 749 out of 1,181 were hypermethylated and 432 hypomethylated (Figure 2E-H). As demonstrated by the heatmap in Figure 2F and H, the methylation profile correlates with increasing Gleason score from 6, 7, 8 to 9. We next overlapped 184 out of 449 differentially methylated CGs from EPIC (850K) cohort with 11,722 differentially methylated in combined cohort (265 CGs were excluded as being specific to EPIC array CG list). This analysis resulted in 89 CGs that were significantly correlated with Gleason score in both (hypergeometric, $p= 1.56e-90$).

A genome-wide distribution on IGV browser [33] of 1181 differentially methylated CGs whose methylation changed progressively with Gleason score ($p < 0.05$) is shown in Supplementary Figure 3. Most sites were hypermethylated, as Gleason score progress from 6 to 9, while a small fraction was hypomethylated. These data are consistent with our previous data in breast and liver cancer and support the hypothesis that epigenome-wide methylation changes occur in T cells genome as the cancer progress [24, 25]. Interestingly, there was significant overlap ($p = 8.93e-42$) between the list of progressively changed methylation of CG sites as cancer progresses in prostate and liver, but not between prostate and breast or breast and liver (Supplementary Figure 4).

Differentially Methylated Regions (DMRs)

We analyzed differentially methylated regions (DMRs) utilizing the DMR function in ChAMP pipeline. We found 10 DMRs between the PCa patients and controls (Supplementary

Table 3 and Supplementary Figure 5). We visualized these DMRs in IGV using the reference genome Human Hg19 to identify genes overlapping with or nearby these regions (Supplementary Table 3). The DMRs were present near genes at different sites including transcriptions start sites (TSS), intergenic and intragenic regions. Pathway analysis on these genes showed only apoptosis pathway significantly different from control samples (data not shown). Although DMR function provides a good overview of DMRs around the genome, however, we were interested in CGs that could distinguish between healthy and PCa patients specifically. Thus, we moved to differentially methylated probes (DMPs) analysis in ChAMP pipeline.

Differentially Methylated Probes (DMPs) between PCa and normal progressively change with Gleason score

We next performed differentially methylation analysis between healthy individuals and PCa patients with both, high and low Gleason score (HGPCa and LGPCa) using stringent criteria of keeping BH correction at FDR<0.05. This analysis resulted in three significant CGs (cg14713996, cg02701909, cg05133736) whose methylation levels discriminated between healthy controls and PCa patients (Table 1 and Figure 3).

We then determined whether a polygenic methylation score of these 3 sites could serve as an accurate predictor of PCa. We calculated the regression coefficient of each CG and intercept using a multivariate linear regression model that included three methylation positions: polygenic methylation score (PMS) = ([β1*27.184+β2*28.842+β3*24.57)-58.774]; where β1=methylation level of cg14713996, β2= methylation level of cg02701909 and β3= methylation level of cg05133736). This polyvariable linear regression equation, composed of weighted methylation level of three CG sites, was highly significant for the prediction of Gleason score in PCa patients (r = 0.89, $p = 7.1e^{-12}$) as demonstrated in Figure 3A and B.

We generated receiver operating characteristic (ROC) curves and measured sensitivity, specificity and the area under the ROC curve (AUC) for each CG (cg14713996, cg02701909, cg05133736) and for PMS. Figure 3C shows ROC curves plotting the clinical performance of polygenic methylation markers for the detection of PCa. The combination of the 3 CGs (PMS) had higher sensitivity, specificity and overall accuracy particularly using Illumina EPIC (Table 2 and Figure 3C).

Percentage tumor volume, which is reflective of the potential cancer volume in the prostate gland of PCa patients, also showed a strong significant positive correlation with Gleason score (Supplementary Figure 6A; r^2= 0.4032; *p<0.0001*). However, the data points best fit was a non-linear exponential curve (Supplementary Figure 6B; r^2= 0.8344). Indeed, when stratified into healthy controls (Ctrl), LGPCa and HGPCa, the HGPCa showed significantly higher mean tumor volumes (%) than both the other groups (Figure 3D). Moreover, PMS also showed strong significant positive correlation with tumor volume (Figure 3E; r^2= 0.3351; *p<0.001*) indicating that PMS was able to predict progressiveness of the tumor. Hence, a higher PMS in peripheral T cells' DNA would potentially indicate a higher tumor volume in the prostate of that patient and vice versa.

Validation of differentially methylated cg14713996 and cg05133736

We next validated cg14713996 and cg05133736 using pyrosequencing and amplicon sequencing and due to insufficient amount of T cells DNA we couldn't validate cg02701909 for amplicon sequencing and some samples for pyrosequencing (Figure 4, Figure 5 and Supplementary Figure 7). The validation set included 20 PCa patients and 12 healthy controls.

cg14713996 showed a 12% (± 1.45%) difference in methylation between the controls and PCa in the Illumina EPIC (850K) assay (Figure 4A; Table 2). The methylation level of this site progressively changes between controls, LGPCa and HGPCa (Figure 4B). We examined correlation between Illumina EPIC array, amplicon sequencing and pyrosequencing assays (r^2 = 0.55 and r^2 = 0.618, respectively, *P <0.0001),* as well as amplicon sequencing and pyrosequencing (r^2 = 0.5032, *P <0.0001*) (Figure 4C).

cg05133736 showed an 8% (± 1.15%) difference in DNA methylation between the controls and PCa in the Illumina EPIC (850K) assay (Figure 5A; Table 2). Validations and correlations were performed for cg05133736 as well (Figure 5A-C). Lastly, both cg14713996 and cg05133736 had high sensitivity, specificity and overall accuracy particularly using Illumina EPIC (Table 2, and Figure 4D and 5D, respectively).

Discussion

DNA methylation alterations in leukocytes have been reported by us and others in many cancers including head and neck squamous cell carcinoma, ovarian [34, 35], colorectal [36], breast [24], and HCC [25, 37]. We focused on T cells which are essential for controlling tumorigenesis and epigenetic changes like DNA methylation which are likely to occur first in T cell as they are activated even before malignant transformation. Detection of these approaches which are highly sensitive, specific and non-invasive will allow stratification of men for the risk of developing or having PCa [24, 25]. In the current study, identified genes and CGs were enriched in signaling pathways implicated in immune-editing and -surveillance which allowed differentiation of control and PCa subjects, and also PCa subjects with various Gleason scores. Consistent with immune-editing theory, these results provide additional support that the DNA methylation signature can be utilized in assessing risk of early stages of PCa.

Previous studies have shown differential methylation of individual gene promoters in PCa. A study investigating clinical significance of gene promoter DNA methylation in blood DNA found six genes promoter methylation of PCa patients to be significantly different from controls [38]. However, we did not see such differences which could be due to several reasons; firstly, T cells DNA was used in our study while blood DNA was used in previous study [38]; secondly, previous study was carried out in African American men while our study had mostly Caucasian men [38]. Also, using whole blood DNA, no association between the DNA methylation on all CG sites and risk of PCa or aggressive disease was observed [39]. Similarly, in a small cohort, we also did not find any CG site with differential methylation between controls and PCa patients T cell DNA (data not shown) which could be due to small sample size and use of Illumina 450K which does not include FANTOM5 and ENCODE enhancer regions and many other sites that were added in EPIC (850K) array [40]. Our previous studies in breast and liver cancer validated the use of T cells to distinguish between control and cancer and also differentiated between different disease stages [24, 25]. Similarly, our study is not only consistent in distinguishing between negative and positive biopsy for PCa but also according to Gleason score.

Despite these convincing results we are aware of the limitation of our study due to the small sample size. However, these results are robust in differentiating normal and PCa subjects, identifying several CGs which were validated using amplicon sequencing and pyrosequencing [26,

27, 41-43]. In addition, our previous study involving T cells from breast cancer had smaller sample size of 19 samples, but was able to distinguish between healthy controls and cancer patients [24]. Our DNA methylation signature gets stronger between controls and PCa patients across various Gleason scores and the highest difference is seen between Gleason score of 9 and control subjects. Importantly, the PMS was able to not only predict PCa patients from healthy controls, but also Gleason score indicating progressive stages of PCa with strong predictive power of PMS with high sensitivity, specificity and accuracy (Figure 3C and Table 2). Indeed, the PMS in the T cells' DNA showed strong correlation with tumor volume of PCa patients that is strongly associated with Gleason score as showed herein and previously (Figure 3 and Supplementary Figure 6). While all subjects had no history of immune disorders or infection, due to the samples size we were unable to take into account additional confounding states including smoking and alcohol intake which can affect the state of DNA methylation [44-48].

Results of this study are the first to identify the DNA methylation signature in immune cells of PCa subjects using non-invasive approach for early detection and stratification of PCa. It is imperative to carry out follow up studies using a larger cohort of subjects which will also consider history of smoking, alcohol intake and stratify the subjects based on their racial background. Future studies will also monitor differences among different T cells, PCa sub-types, stages and Gleason score. It is anticipated that the T cell DNA methylation signature will be identifiable in whole blood for large scale screens, active surveillance, early intervention with targeted therapies including the use of epigenetic based therapeutic agents.

Conclusions

The current study provides for the first-time a potential role of DNA methylation changes in peripheral T cells in PCa. Using this non-invasive approach, changes in the DNA methylation status of T cells can predict men at risk of developing PCa and disease progression. Furthermore, the non-invasive methodology may allow for early intervention and stratification of patients into different prognostic groups to reduce PCa associated morbidity from repeat invasive prostate biopsies and design therapeutic strategy to reduce PCa associated mortality.

Figures (Chapter Two)

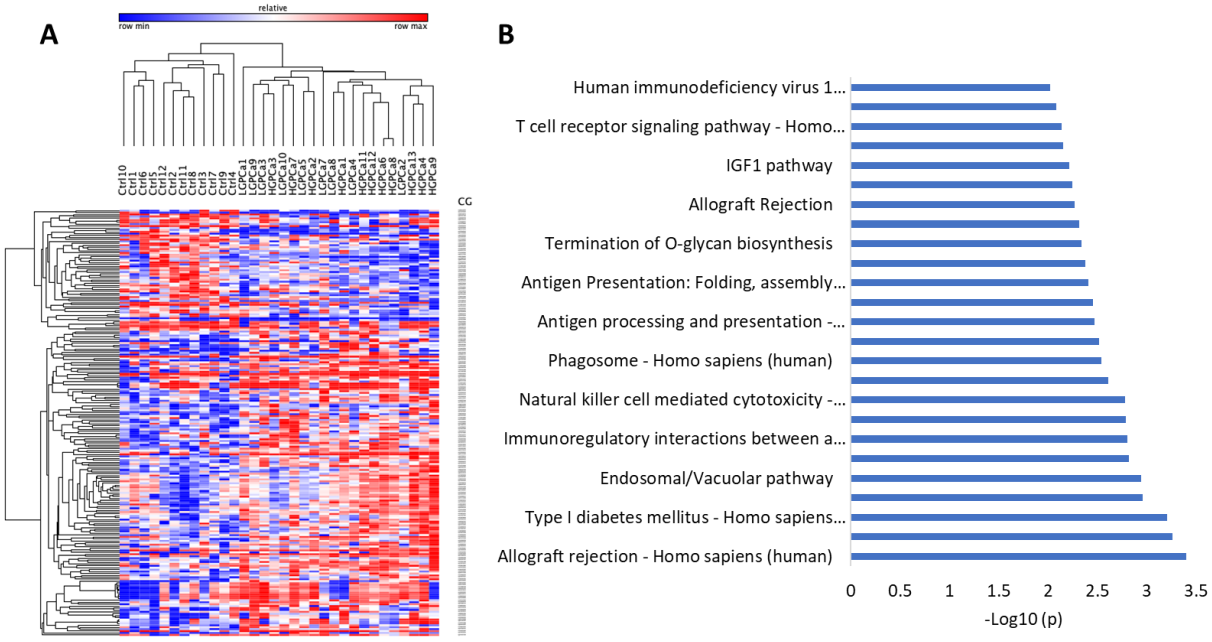

Figure 1: Differentially methylated CGs and respective gene-related pathways deregulated in PCa compared to the controls. A total of 223 statistically significant CGs which had 10% methylation difference in T cell DNA between Ctrl and PCa ($p<0.05$). (A) Heatmap of the 223 CGs shown for each sample. The scale bar shows methylation levels where highest is 100% and lowest is 0% of that CpG; Blue; hypomethylation; Red; hypermethylation. (B) Differentially methylated genes nearby 105 CGs showed various pathways involved in immune system and immuno-surveillance system. These pathways were obtained by conducting an overrepresentation analysis of the genes nearby 105 CGs utilizing ConsensusPath DB. The pathways have been plotted against -log10 of the *p* value.

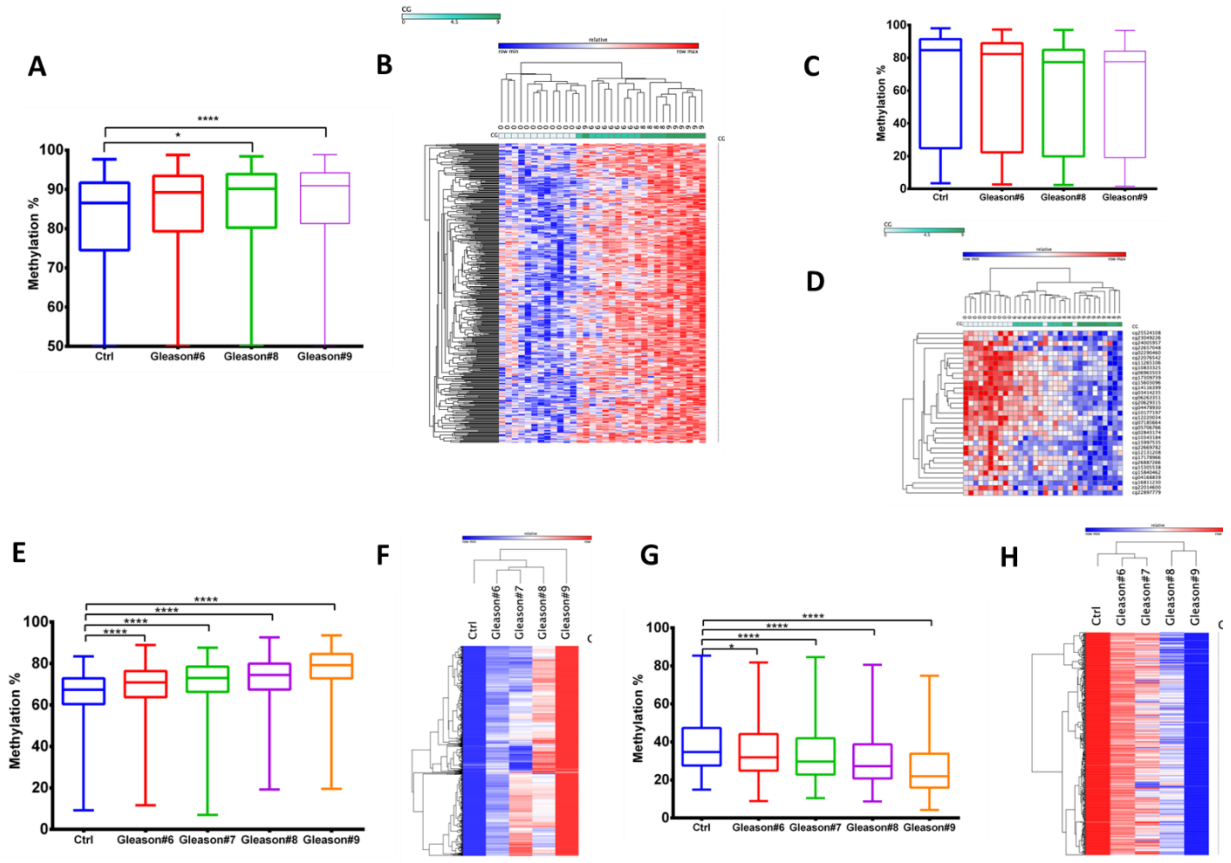

Figure 2: Pearson correlation between CG methylation levels (delta beta>0.1) and Gleason score. (A-D) A total of 449 CGs' T cell DNA methylation levels showed to be significantly (Q< 0.05 after FDR correction) correlated with Gleason score (0 for healthy individuals and 6, 8 and 9 for Gleason score 6, 8, 9). Boxplots of mean percentage methylation of the 416 and 33 CGs increasing or decreasing with respect to Gleason score, respectively. (B and D) Heatmaps of the methylation levels of 416 and 33 CGs that correlate with Gleason score either positively or negatively, respectively. (E-H) A total of 1181 CGs whose methylation levels significantly (Q< 0.05) correlated with Gleason score when the two cohorts, Cohort 1 and 2, were combined (Combined cohort). (E and F): Boxplots of mean percentage methylation of the 749 and 432 CGs increasing or decreasing with respect to Gleason score, respectively (G and H). Heatmaps of methylation levels of 749 and 432 CGs that correlate with Gleason score either positively or negatively, respectively.

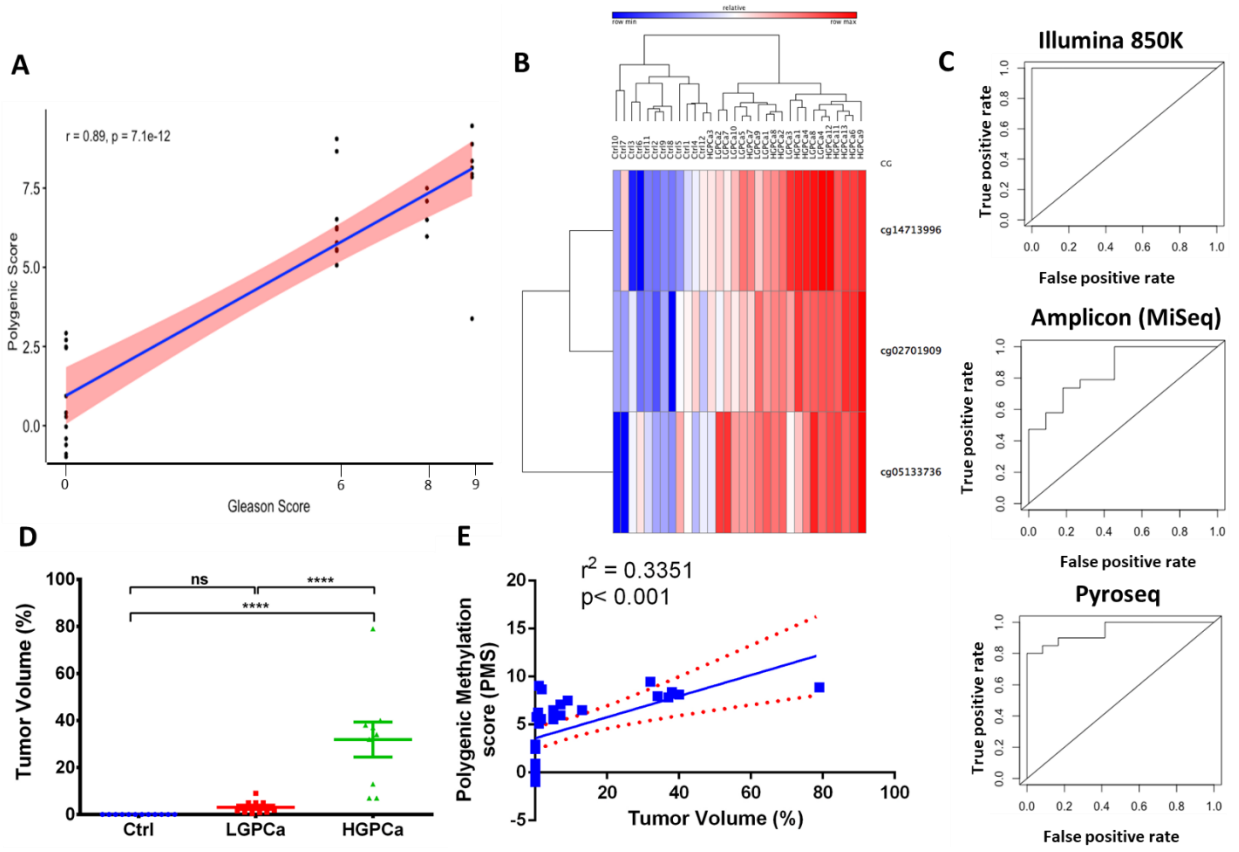

Figure 3: Polygenic methylation score (PMS) for detection of PCa. (A) Pearson correlation analysis of a weighted PMS of three target CGs (DMPs) in T cell DNA and Gleason score. DMPs were identified using ChAMP package in R. These three DMPs were combined to calculate a PMS for each sample which was plotted against Gleason score using a multivariate linear regression model as described in the Results section. (B) Heatmap of the T cell DNA methylation levels of the 3 DMPs for all negative-biopsy controls and positive-biopsy PCa patients (High methylation Red; Low methylation, Blue). (C) ROC curve showing the sensitivity and specificity of PMS score. (D) Mean percentage tumor volume (%) of control (Ctrl), LGPCa (Low Gleason PCa) and HGPCa (High Gleason PCa) samples predicted from core prostate biopsies as described in Methods. Ctrl (Control, Blue); LGPCa (Red); and HGPCa (Green). (E) Linear regression analysis of the PMS from T cell DNA with percentage tumor volume. The red dotted lines show the 95% confidence band of the line of best fit. The negative-biopsy control samples were assumed to have a tumor volume of 0% and a Gleason score of 0.

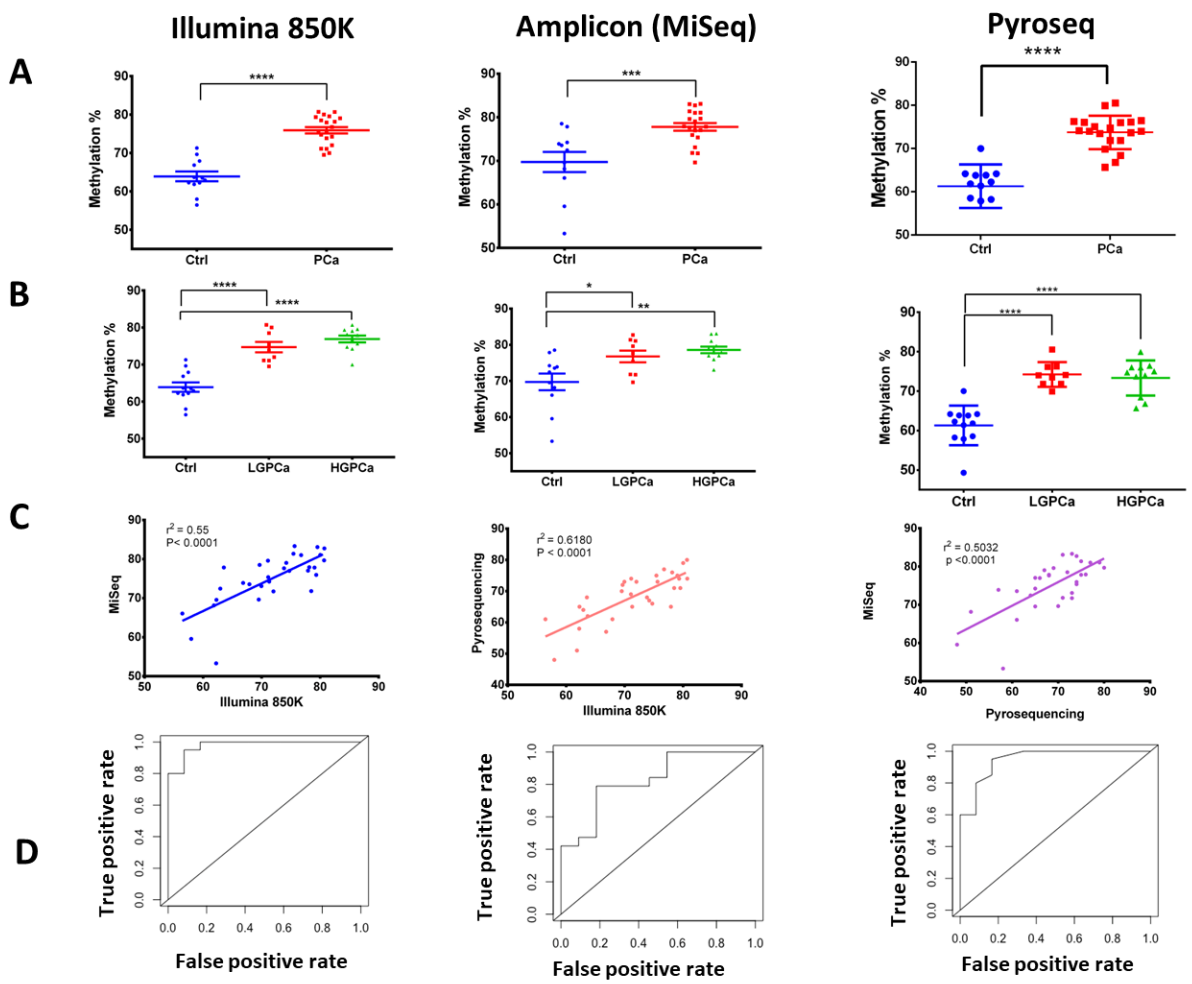

Figure 4: Identification and validation of cg14713996 as a DNA methylation marker using Illumina EPIC (850K), amplicon sequencing (using MiSeq system) and pyrosequencing. (A-B) Percentage methylation of T cell DNA of each sample at cg14713996 plotted as; (A) Ctrl (Control, Blue) and PCa (PCa, Red); (B) Ctrl (Control, Blue), LGPCa (Low Gleason PCa, Red) and HGPCa (High Gleason PCa, Green). Statistical significance was obtained in GraphPad Prism and are represented by asterisks (*$P < 0.05$; **$P < 0.01$, ***$P < 0.001$, ****$P < 0.0001$). (C) Correlation graphs between Illumina EPIC (850K), amplicon sequencing and pyrosequencing. (D) ROC curve showing the sensitivity and specificity of cg14713996 for detection of PCa.

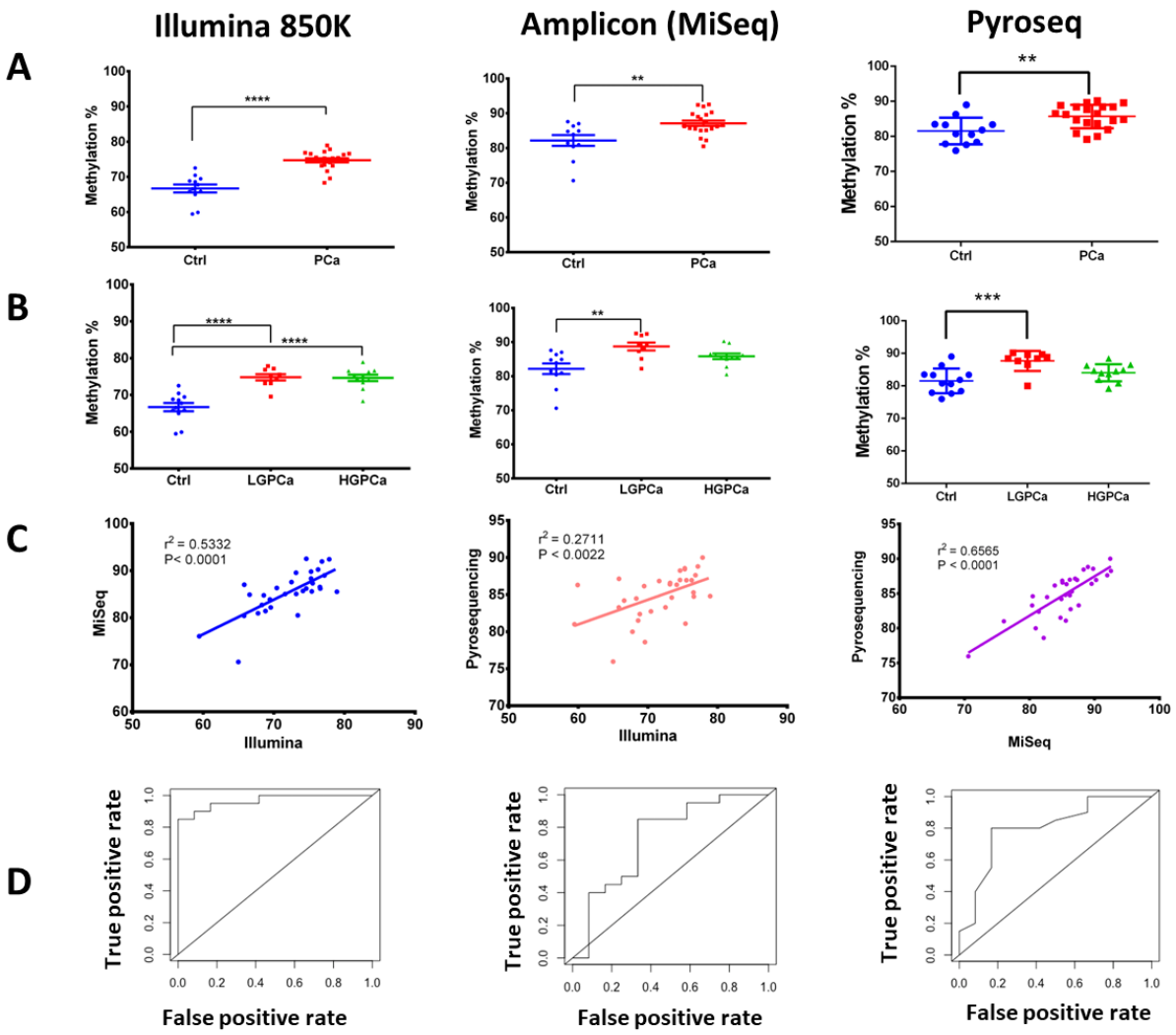

Figure 5: Identification and validation of cg05133736 as a DNA methylation marker using Illumina EPIC (850K), amplicon sequencing (using MiSeq system) and pyrosequencing systems. (A-B) Percentage methylation of T cell DNA of each sample at cg05133736 plotted as; (A) Ctrl (Control, Blue) and PCa (PCa, Red); (B) Ctrl (Control, Blue), LGPCa (Low Gleason PCa, Red) and HGPCa (High Gleason PCa, Green). Statistical significance was obtained in GraphPad Prism and are represented by asterisks (*$P < 0.05$; **$P < 0.01$, ***$P < 0.001$, ****$P < 0.0001$). (C) Correlation graphs between Illumina EPIC (850K), amplicon sequencing and pyrosequencing. (D) ROC curve showing the sensitivity and specificity of cg05133736 for detection of PCa.

Tables (Chapter Two)

Table 1: Differentially methylated probes (DMPs) between negative-biopsy controls and positive-biopsy PCa patients identified by Illumina EPIC methylation assay.

CpG	Chromosome Location	Gene nearby	Delta Beta /LogFC	FDR	Site of differential methylation	CGI
cg14713996	X		0.12	0.01	IGR	opensea
cg02701909	1	CTRC	0.03	0.03	1stExon	opensea
cg05133736	10		0.08	0.04	IGR	opensea
cg06915331	11	PDE2A	0.03	0.12	Body	shore
cg01235591	13	ATP11A	0.03	0.12	3'UTR	shore

Table 2: Sensitivity, specificity, accuracy and the area under the ROC curve (AUC) for each CG and for PMS, tested for Illumina EPIC (850K), amplicon sequencing and pyrosequencing platforms.

		Sensitivity	Specificity	Accuracy	AUC
Illumina 850K	cg14713996	0.95	0.92	0.94	0.98
	cg02701909	0.95	0.92	0.94	0.98
	cg05133736	0.9	0.92	0.9	0.97
	PMS	1	1	1	1
Pyrosequencing	cg14713996	0.95	0.83	0.9	0.95
	cg02701909	na	na	na	na
	cg05133736	0.8	0.83	0.81	0.8
	PMS	0.85	0.92	0.87	0.95
Amplicon sequencing	cg14713996	0.79	0.82	0.8	0.83
	cg02701909	na	na	na	na
	cg05133736	0.85	0.66	0.78	0.73
	PMS	0.74	0.82	0.83	0.85

List of Abbreviations

PCa: Prostate Cancer

LGPCa: Low Gleason Prostate Cancer

HGPCa: High Gleason Prostate Cancer

ChAMP: Chip Analysis Methylation Pipeline

DMP: Differentially methylated probes

BH: Benjamini-Hochberg

HCC: Hepatocellular carcinoma

PCR: Polymerase Chain Reaction

BMIQ: Beta-Mixture Quantile

SVD: Singular Value Decomposition

FDR: False Discovery Rate

IGV: Integrative Genomics Viewer

ROC: Receiver Operating Characteristic

AUC: Area Under Curve

FANTOM5: Functional Annotation of the Mammalian Genome 5

ENCODE: The Encyclopedia of DNA Elements

PMS: Polygenic Methylation Score

Declarations and other statements

Ethics approval and consent to participate

The study design was approved by the ethics committee of Alberta PCa Research Initiative (APCaRI) and informed consents were obtained in writing from all subjects for the APCaRI.

Consent for publication

Not applicable

Availability of data and material

All data generated or analysed during this study are included in this published article [and its supplementary information files].

Competing interests

MS and DC are co-founders of Montreal Epiterapia Inc. TAB is an Editorial Board member for the journal. The remaining authors declare that they have no conflict on interest.

Funding

This work was supported by grants from the Canadian Institutes for Health Research (PJT-156225) to SAR. There was no role of funding agency in the design of the study and collection, analysis, and interpretation of data and in writing the manuscript.

Authors' contributions

SAR and MS conceived the study and experimental design. AM and AA carried out experimental procedures. All data analysis was carried out by DC and AM. AM wrote the manuscript with SAR and MS. TAB provided access to samples and assisted in manuscript revisions. All authors read and approved the final manuscript.

Acknowledgements

Ali Mehdi is the recipient of Queen Elizabeth II scholarship.

References

1. Society, C.C. *Prostate cancer statistics - Canadian Cancer Society*. 2020 1 April 2020]; Available from: http://www.cancer.ca/en/cancer-information/cancer-type/prostate/statistics/?region=qc.
2. Research, A.I.f.C. *Prostate cancer statistics*. 2018 2018-08-22 1 April 2020]; Available from: https://www.wcrf.org/dietandcancer/cancer-trends/prostate-cancer-statistics.
3. Gandhi, J., et al., *The molecular biology of prostate cancer: current understanding and clinical implications.* Prostate Cancer Prostatic Dis, 2018. **21**(1): p. 22-36.
4. Siegel, R.L., K.D. Miller, and A. Jemal, *Cancer statistics, 2017.* CA: A Cancer Journal for Clinicians, 2018. **67**(1): p. 7-30.
5. Litwin, M.S. and H.J. Tan, *The Diagnosis and Treatment of Prostate Cancer: A Review.* Jama, 2017. **317**(24): p. 2532-2542.
6. Carter, H.B., et al., *Early detection of prostate cancer: AUA Guideline.* J Urol, 2013. **190**(2): p. 419-26.
7. Lilja, H., D. Ulmert, and A.J. Vickers, *Prostate-specific antigen and prostate cancer: prediction, detection and monitoring.* Nat Rev Cancer, 2008. **8**(4): p. 268-78.
8. Gaudreau, P.O., et al., *The Present and Future of Biomarkers in Prostate Cancer: Proteomics, Genomics, and Immunology Advancements.* Biomark Cancer, 2016. **8**(Suppl 2): p. 15-33.
9. Stabile, A., et al., *MRI in prostate cancer diagnosis: do we need to add standard sampling? A review of the last 5 years.* Prostate Cancer Prostatic Dis, 2018. **21**(4): p. 473-487.
10. Bird, A., *The essentials of DNA methylation.* Cell, 1992. **70**(1): p. 5-8.
11. Baylin, S.B., et al., *Alterations in DNA methylation: a fundamental aspect of neoplasia.* Adv Cancer Res, 1998. **72**: p. 141-96.
12. Hoque, M.O., *DNA methylation changes in prostate cancer: current developments and future clinical implementation.* Expert Rev Mol Diagn, 2009. **9**(3): p. 243-57.
13. Merlo, A., et al., *5' CpG island methylation is associated with transcriptional silencing of the tumour suppressor p16/CDKN2/MTS1 in human cancers.* Nat Med, 1995. **1**(7): p. 686-92.

14. Hoque, M.O., et al., *Quantitative methylation-specific polymerase chain reaction gene patterns in urine sediment distinguish prostate cancer patients from control subjects.* J Clin Oncol, 2005. **23**(27): p. 6569-75.
15. Cooper, C.S. and C.S. Foster, *Concepts of epigenetics in prostate cancer development.* Br J Cancer, 2009. **100**(2): p. 240-5.
16. Nelson, W.G., et al., *Abnormal DNA methylation, epigenetics, and prostate cancer.* Front Biosci, 2007. **12**: p. 4254-66.
17. Dobosy, J.R., et al., *The expanding role of epigenetics in the development, diagnosis and treatment of prostate cancer and benign prostatic hyperplasia.* J Urol, 2007. **177**(3): p. 822-31.
18. Li, L., et al., *DNA Methylation in Peripheral Blood: A Potential Biomarker for Cancer Molecular Epidemiology.* J Epidemiol, 2012. **22**(5): p. 384-94.
19. Kirby, M.K., et al., *Genome-wide DNA methylation measurements in prostate tissues uncovers novel prostate cancer diagnostic biomarkers and transcription factor binding patterns.* BMC Cancer, 2017. **17**(1): p. 273.
20. Dunn, G.P., L.J. Old, and R.D. Schreiber, *The immunobiology of cancer immunosurveillance and immunoediting.* Immunity, 2004. **21**(2): p. 137-48.
21. Smyth, M.J., G.P. Dunn, and R.D. Schreiber, *Cancer immunosurveillance and immunoediting: the roles of immunity in suppressing tumor development and shaping tumor immunogenicity.* Adv Immunol, 2006. **90**: p. 1-50.
22. Finn, O.J., *A Believer's Overview of Cancer Immunosurveillance and Immunotherapy.* J Immunol, 2018. **200**(2): p. 385-391.
23. Gubin, M.M., et al., *Tumor neoantigens: building a framework for personalized cancer immunotherapy.* J Clin Invest, 2015. **125**(9): p. 3413-21.
24. Parashar, S., et al., *DNA methylation signatures of breast cancer in peripheral T-cells.* BMC Cancer, 2018. **18**(1): p. 574.
25. Zhang, Y., et al., *The signature of liver cancer in immune cells DNA methylation.* Clin Epigenetics, 2018. **10**: p. 8.
26. Tost, J. and I.G. Gut, *DNA methylation analysis by pyrosequencing.* Nat Protoc, 2007. **2**(9): p. 2265-75.

27. Morris, T.J., et al., *ChAMP: 450k Chip Analysis Methylation Pipeline.* Bioinformatics, 2014. **30**(3): p. 428-30.
28. Tian, Y., et al., *ChAMP: updated methylation analysis pipeline for Illumina BeadChips.* Bioinformatics, 2017. **33**(24): p. 3982-3984.
29. Kamburov, A., et al., *ConsensusPathDB: toward a more complete picture of cell biology.* Nucleic Acids Res, 2011. **39**(Database issue): p. D712-7.
30. Institute, B. *GENE-E*. 2019 May 2019]; Available from: https://software.broadinstitute.org/GENE-E/index.html.
31. Smyth, G.K., *Limma: linear models for microarray data.*, in *Bioinformatics and Computational Biology Solutions using R and Bioconductor*, V.C. R. Gentleman, S. Dudoit, R. Irizarry, W. Huber Editor. 2005, Springer,: New York. p. 397-420.
32. Smyth, G.K., J. Michaud, and H.S. Scott, *Use of within-array replicate spots for assessing differential expression in microarray experiments.* Bioinformatics, 2005. **21**(9): p. 2067-75.
33. Thorvaldsdottir, H., J.T. Robinson, and J.P. Mesirov, *Integrative Genomics Viewer (IGV): high-performance genomics data visualization and exploration.* Brief Bioinform, 2013. **14**(2): p. 178-92.
34. Fridley, B.L., et al., *Methylation of leukocyte DNA and ovarian cancer: relationships with disease status and outcome.* BMC Med Genomics, 2014. **7**: p. 21.
35. Koestler, D.C., et al., *Peripheral blood immune cell methylation profiles are associated with nonhematopoietic cancers.* Cancer Epidemiol Biomarkers Prev, 2012. **21**(8): p. 1293-302.
36. Nosho, K., et al., *Tumour-infiltrating T-cell subsets, molecular changes in colorectal cancer, and prognosis: cohort study and literature review.* J Pathol, 2010. **222**(4): p. 350-66.
37. Kao, W.Y., et al., *Genome-wide identification of blood DNA methylation patterns associated with early-onset hepatocellular carcinoma development in hepatitis B carriers.* Mol Carcinog, 2017. **56**(2): p. 425-435.
38. Moses-Fynn, E., et al., *Correlating blood-based DNA methylation markers and prostate cancer risk in African-American men.* PLoS One, 2018. **13**(9).

39. FitzGerald, L.M., et al., *Genome-Wide Measures of Peripheral Blood Dna Methylation and Prostate Cancer Risk in a Prospective Nested Case-Control Study.* Prostate, 2017. **77**(5): p. 471-478.
40. Moran, S., C. Arribas, and M. Esteller, *Validation of a DNA methylation microarray for 850,000 CpG sites of the human genome enriched in enhancer sequences.* Epigenomics, 2016. **8**(3): p. 389-99.
41. Royo, J.L., M. Hidalgo, and A. Ruiz, *Pyrosequencing protocol using a universal biotinylated primer for mutation detection and SNP genotyping.* Nat Protoc, 2007. **2**(7): p. 1734-9.
42. Ronaghi, M., M. Uhlen, and P. Nyren, *A sequencing method based on real-time pyrophosphate.* Science, 1998. **281**(5375): p. 363, 365.
43. Teschendorff, A.E., et al., *A beta-mixture quantile normalization method for correcting probe design bias in Illumina Infinium 450 k DNA methylation data.* Bioinformatics, 2013. **29**(2): p. 189-96.
44. Wilson, L.E., et al., *Alcohol and DNA Methylation: An Epigenome-Wide Association Study in Blood and Normal Breast Tissue.* American Journal of Epidemiology, 2019. **kwz032**.
45. Varela-Rey, M., et al., *Alcohol, DNA Methylation, and Cancer.* Alcohol Res, 2013. **35**(1): p. 25-35.
46. Liu, C., et al., *A DNA methylation biomarker of alcohol consumption.* Molecular Psychiatry, 2016. **23**(2): p. 422.
47. Lee, K.W. and Z. Pausova, *Cigarette smoking and DNA methylation.* Front Genet, 2013. **4**: p. 132.
48. Li, S., et al., *Causal effect of smoking on DNA methylation in peripheral blood: a twin and family study.* Clin Epigenetics, 2018. **10**.

Supplementary Material

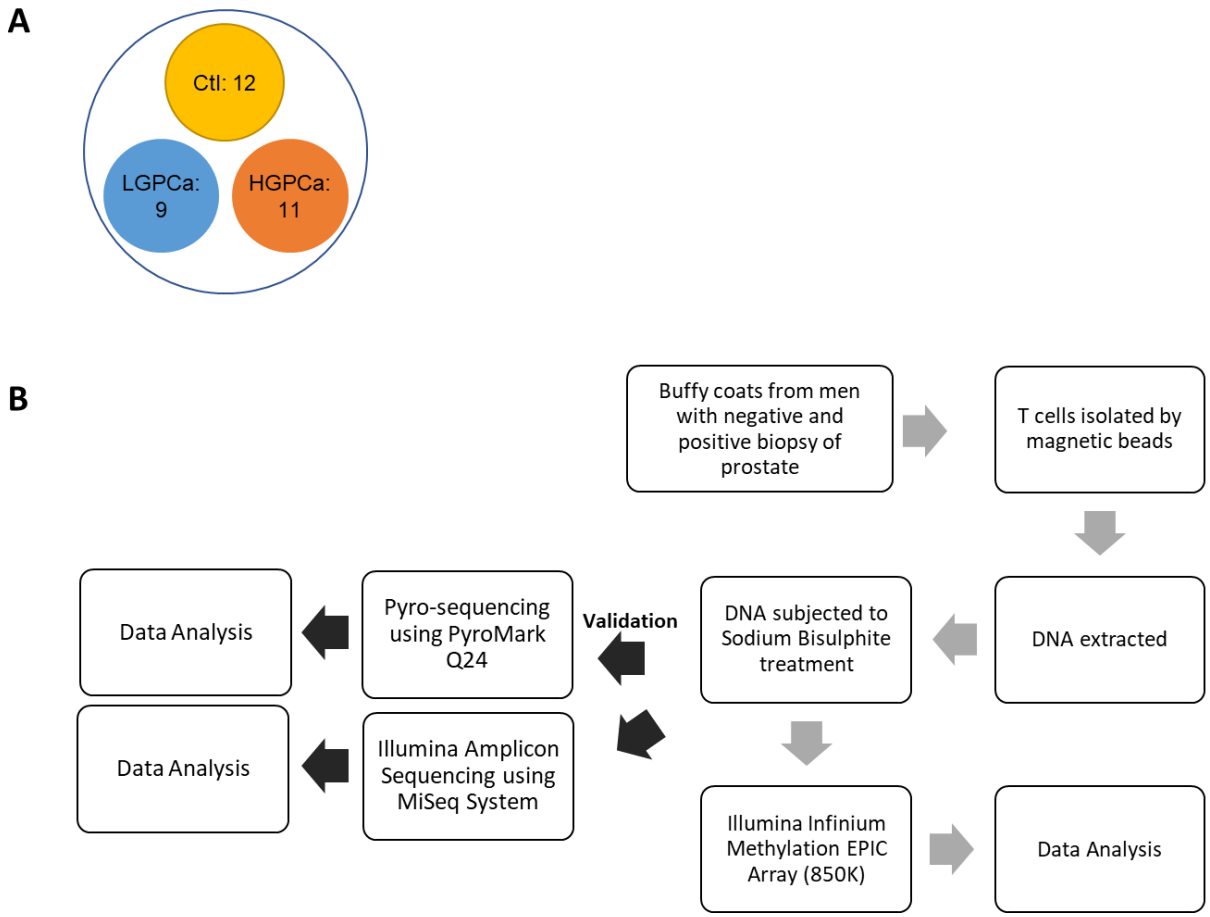

Supplementary Figure 1: (A) The number of T cell DNA samples used in the cohort 1. Ctrl, Negative-biopsy healthy control; LGPCa, Positive-biopsy low Gleason PCa; HGPCa, Positive biopsy high Gleason PCa. (B) Outline of DNA methylation signature determination in DNA of peripheral T cells in buffy coat of PCa patients and healthy controls using Illumina Infinium EPIC methylation array followed by validation with Illumina MiSeq and Pyrosequencing platforms.

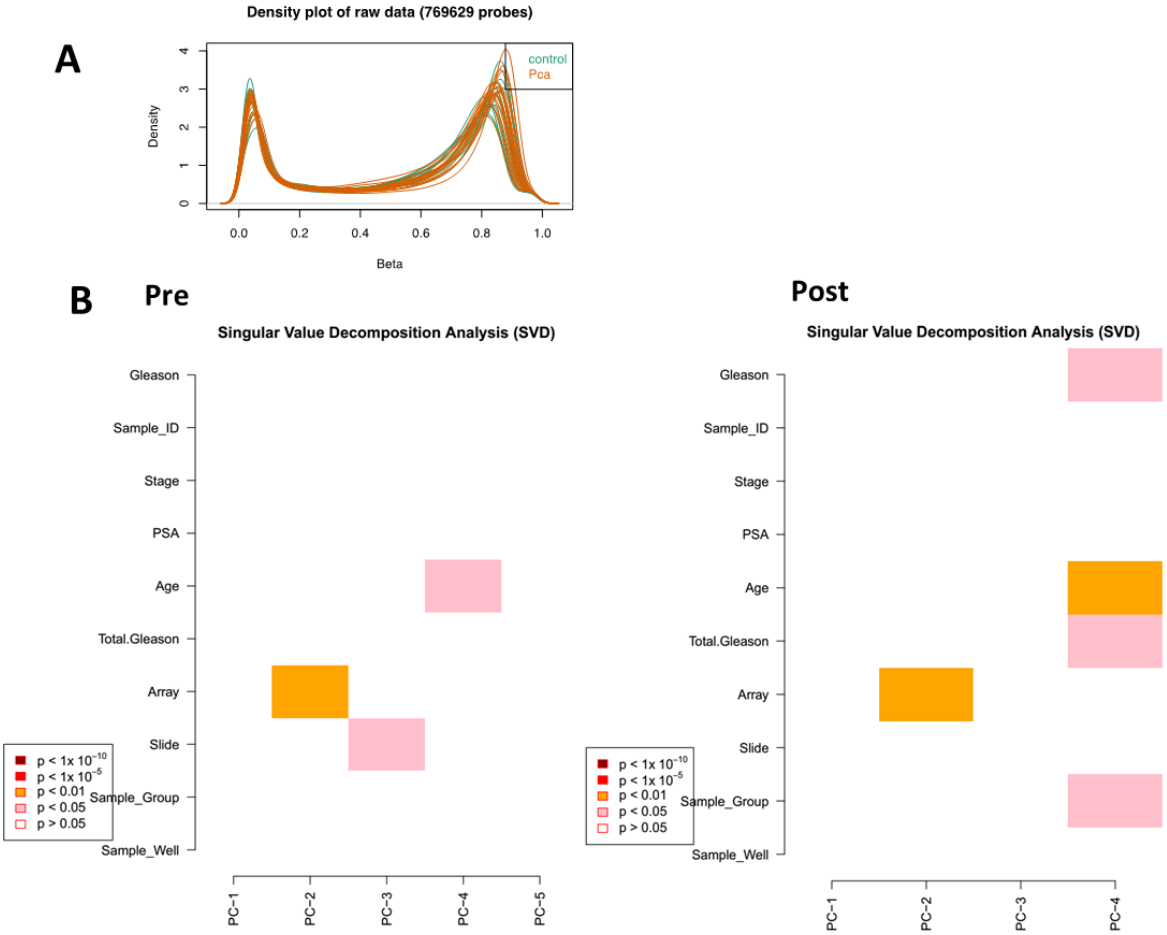

Supplementary Figure 2: Quality control (QC) of the data from Illumina Infinium EPIC methylation array using QC in ChAMP pipeline. (A) Density plot of raw data showing the beta distributions for each healthy control and PCa sample. None of the samples deviate from each other. (B) Singular value decomposition analysis (SVD) plot shows the significant components of variation in T cell DNA methylation. SVD analysis before (Pre) and after (Post) running the ComBat function in ChAMP pipeline removes the batch effects such as "Slide" variations as shown here.

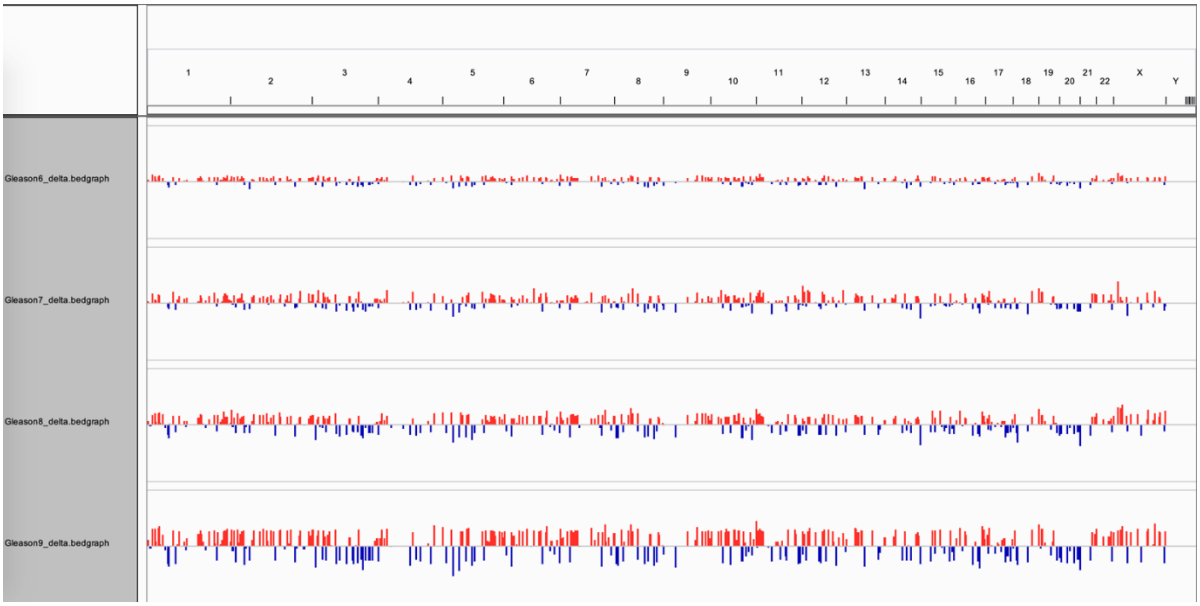

Supplementary Figure 3: Global distribution of the differentially methylated CGs that showed correlation with Gleason score in combined cohort. 1181 significant (*p <0.05*) differentially methylated CGs that had 10% methylation difference (beta value) in T cell DNA between PCa patients (with Gleason score 9) and in healthy controls were taken and input into IGV browser. Each row represents a Gleason score in a sequence of 6, 7, 8 and 9 while the first row is Chromosome numbers (1-22, X and Y). Hypomethylation (Blue) and hypermethylation (Red).

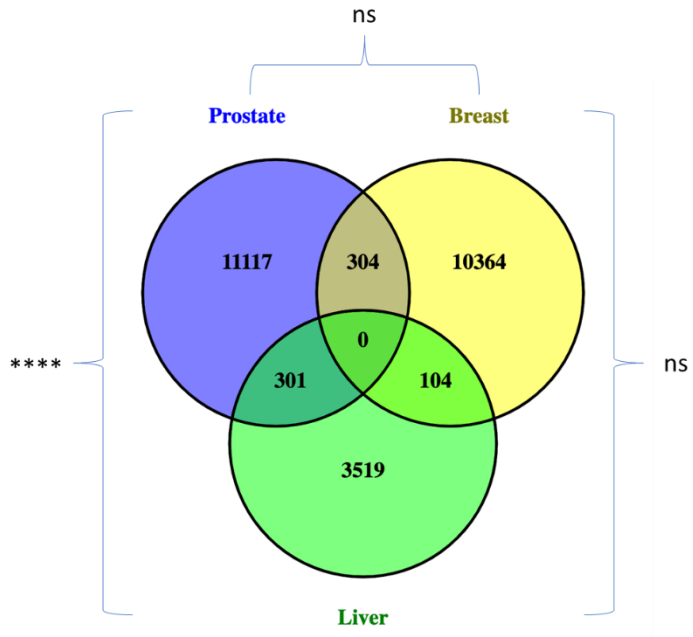

Supplementary Figure 4: Venn diagram showing the overlap of CGs between breast, liver and prostate cancer studies. Methylated CGs in T cell DNA that were correlating with Gleason score in this study were overlapped with CGs that were correlating with breast cancer and liver cancer progression in breast and liver cancer studies, respectively. ns, not significant; ****, *p <0.0001*.

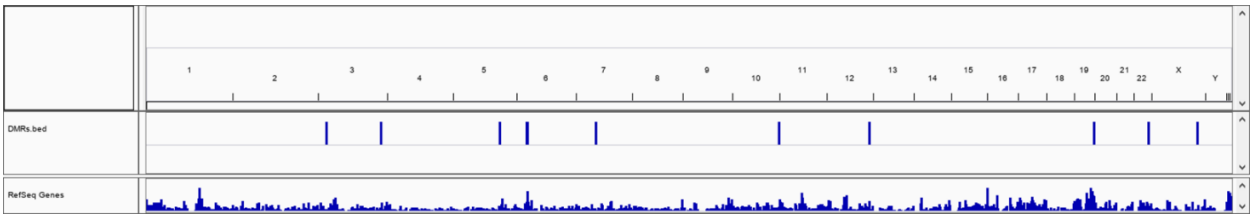

Supplementary Figure 5: Global distribution of the differentially methylated regions (DMRs). DMRs of the T cell DNA between the PCa and healthy control obtained using DMR function in the ChAMP pipeline. The data for the IGV input was obtained from Supplementary Table 3. The first row represents Chromosome numbers (1-22, X and Y), second row shows DMR positions and the last row shows the reference genome H19.

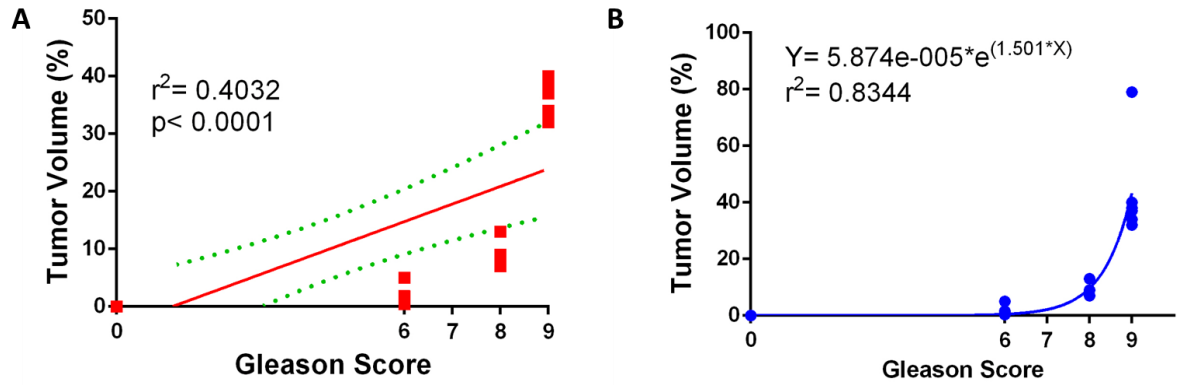

Supplementary Figure 6: Correlation analysis of percentage tumor volume and Gleason score. The percentage tumor volume was predicted from core prostate biopsies as described in Methods. Negative-biopsy healthy controls had no tumor and therefore assigned a 0% tumor volume and a Gleason score of 0. (A) Linear regression analysis of the percentage tumor volume of the PCa patients with the Gleason score. The red dotted lines show the 95% confidence band of the line of best fit. (B) Non-linear regression analysis of the percentage tumor volume of the PCa patients with Gleason score. The equation for the graph was an exponential growth curve with least square method as the fitting method.

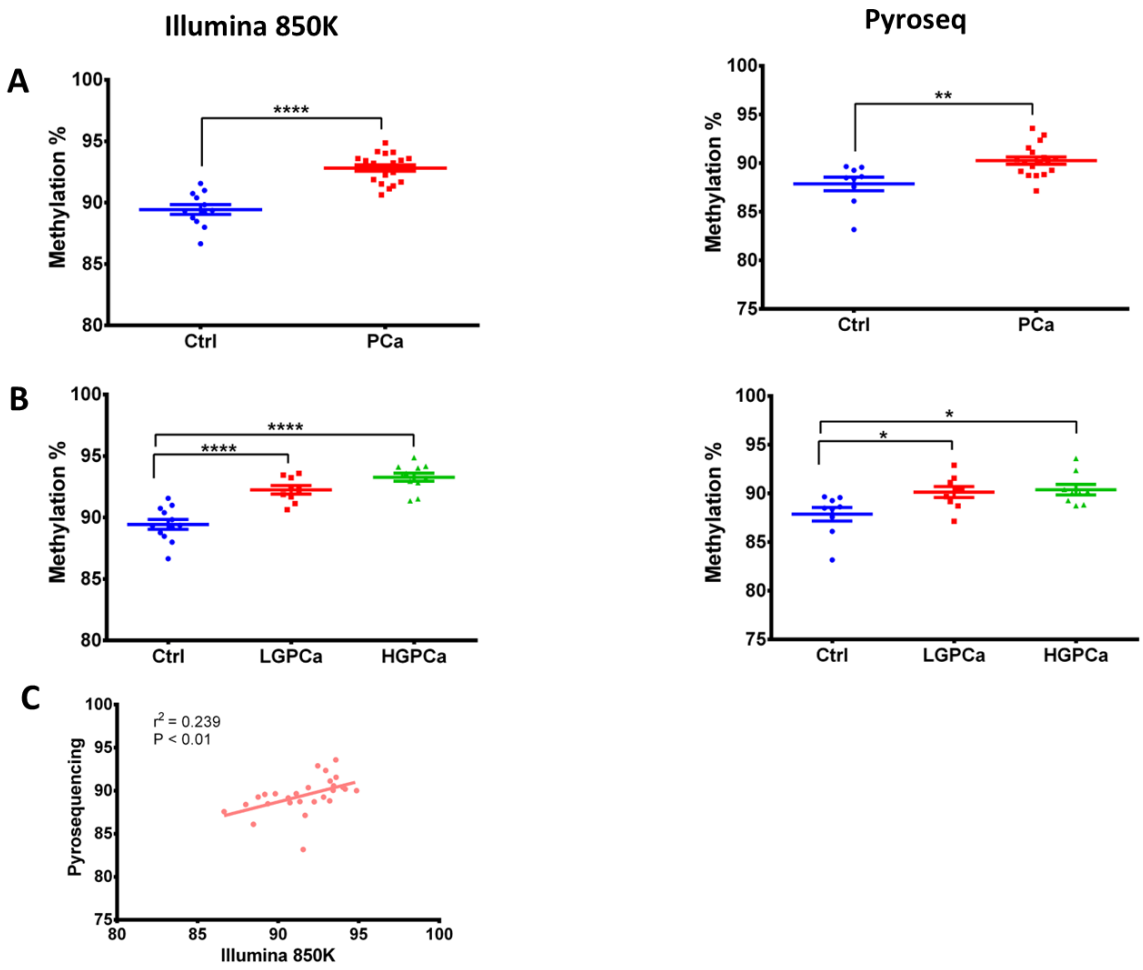

Supplementary Figure 7: Identification and validation of cg02701909 as a DNA methylation marker using Illumina EPIC (850K) and pyrosequencing. (A-B) Percentage methylation of T cell DNA at cg02701909 plotted as; (A) Ctrl (Control, Blue) and PCa (PCa, Red); (B) Ctrl (Control, Blue), LGPCa (Low Gleason PCa, Red) and HGPCa (High Gleason PCa, Green). The number of samples for pyrosequencing were; Ctrl (n = 9), LGPCa (n = 9) and HGPCa (n = 9). Statistical significance was obtained in GraphPad Prism and are represented by asterisks (*$P < 0.05$; **$P < 0.01$, ***$P < 0.001$, ****$P < 0.0001$). (C) Correlation graph between Illumina EPIC (850K) and pyrosequencing.

Supplementary Table 1: List of negative-biopsy healthy controls and positive-biopsy PCa patient sample ids with their respective Gleason score.

Cohort 1	Cohort 2	Combined

ID	Total Gleason	Age	ID	Gleason Score	Age	ID	Total Gleason	Age
Ctrl1	NA	53	Ctrl13	NA	49	Ctrl13	NA	49
Ctrl10	NA	66	Ctrl14	NA	69	Ctrl14	NA	69
Ctrl11	NA	52	Ctrl15	NA	53	Ctrl15	NA	53
Ctrl12	NA	53	Ctrl16	NA	66	Ctrl16	NA	66
Ctrl2	NA	62	Ctrl17	NA	68	Ctrl17	NA	68
Ctrl3	NA	56	Ctrl18	NA	45	Ctrl18	NA	45
Ctrl4	NA	44	Ctrl19	NA	75	Ctrl19	NA	75
Ctrl5	NA	50	Ctrl20	NA	73	Ctrl20	NA	73
Ctrl6	NA	53	Ctrl21	NA	73	Ctrl21	NA	73
Ctrl7	NA	44	Ctrl22	NA	57	Ctrl22	NA	57
Ctrl8	NA	59	Ctrl23	NA	56	Ctrl23	NA	56
Ctrl9	NA	59	LGPCa11	6	64	Ctrl1	NA	53
LGPCa1	6	70	LGPCa12	7	54	Ctrl10	NA	66
LGPCa10	6	62	LGPCa13	7	77	Ctrl11	NA	52
LGPCa2	6	46	LGPCa14	7	70	Ctrl12	NA	53
LGPCa3	6	54	LGPCa15	6	41	Ctrl2	NA	62
LGPCa4	6	63	LGPCa16	6	67	Ctrl3	NA	56
LGPCa5	6	54	LGPCa17	7	63	Ctrl4	NA	44
LGPCa7	6	49	LGPCa18	6	67	Ctrl5	NA	50
LGPCa8	6	74	LGPCa19	6	50	Ctrl6	NA	53
LGPCa9	6	64	LGPCa20	7	63	Ctrl7	NA	44
HGPCa1	8	58	LGPCa21	7	60	Ctrl8	NA	59
HGPCa11	9	68	LGPCa22	6	60	Ctrl9	NA	59
HGPCa12	9	72	LGPCa23	7	66	LGPCa1	6	70
HGPCa13	9	66				LGPCa10	6	62
HGPCa2	8	52				LGPCa2	6	46
HGPCa3	9	62				LGPCa3	6	54
HGPCa4	9	60				LGPCa4	6	63
HGPCa6	9	75				LGPCa5	6	54
HGPCa7	8	83				LGPCa7	6	49
HGPCa8	8	59				LGPCa8	6	74
HGPCa9	9	65				LGPCa9	6	64
						LGPCa11	6	64
						LGPCa15	6	41
						LGPCa16	6	67

LGPCa18	6	67
LGPCa19	6	50
LGPCa22	6	60
LGPCa12	7	54
LGPCa13	7	77
LGPCa14	7	70
LGPCa17	7	63
LGPCa20	7	63
LGPCa21	7	60
LGPCa23	7	66
HGPCa1	8	58
HGPCa2	8	52
HGPCa7	8	83
HGPCa8	8	59
HGPCa11	9	68
HGPCa12	9	72
HGPCa13	9	66
HGPCa3	9	62
HGPCa4	9	60
HGPCa6	9	75
HGPCa9	9	65

Supplementary Table 2: List of the primers used for pyrosequencing and amplicon sequencing (Illumina MiSeq system).

	CG	Primer	Id	Sequence
Pyrosequencing	**cg14713996**	PCR	Forward (biotinylated)	TAAGAAAGAATTTTGTGGTAGGTTGTAT
		PCR	Reverse	ATACCCCACAACCCACTCTAATTTTA
		Sequencing	S1	CCTAAAAATCTCACCC
	cg05133736	PCR	Forward (biotinylated)	AATGTATTTGAGTGTGGTTATG
		PCR	Reverse	CCCCTCTTTCCCTCTCATTCCTAAT
		Sequencing	S1	AACTCACAAAATAAAACACTA
	cg02701909	PCR	Forward	GGTTTGGTTTTGATTAGGTGTATT

		PCR	Reverse (biotinylated)	ACCCCAACTCACAACCTACTAACTACAA
		Sequencing	S1	ATTATGTTGGGTATTATTGTT
Amplicon Sequencing	**cg14713996**	PCR	Forward	TAAGAAAGAATTTTGTGGTAGG
		PCR	Reverse	CACAACCCACTCTAATTTTAACA
	cg05133736	PCR	Forward	TTATTGTTGAGTTGTATTGATATG
		PCR	Reverse	TTTAAAAAACACCTCAAACATAAT

Supplementary Table 3: Differentially methylated regions (DMRs) between the PCa T cell DNA and healthy control T cell DNA. The data was obtained using DMR function in the ChAMP pipeline and input into the IGV browser to identify nearby genes and location of each DMR manually. Reference genome H19 was used for alignment. TSS, Transcription start site.

DMR	BumphunterDMR.seqnames	BumphunterDMR.start	BumphunterDMR.end	BumphunterDMR.width	BumphunterDMR.value	BumphunterDMR.area	BumphunterDMR.cluster	BumphunterDMR.clusterL	BumphunterDMR.p.value	BumphunterDMR.p.valueArea	Nearby Gene	Location of DMR
1	Chr 5	135415693	135416613	920	1.24	17.41	160505	14	0.00028	0.00081	VTRNA2-1	Covering entire gene
2	Chr 6	31539539	31540750	1211	0.41	7.01	168218	17	0.00289	0.0112	LTA	From TSS to Exon 3
3	Chr 6	29648360	29649084	724	0.46	6.95	167616	21	0.00353	0.01138	ZFP57	Not in the gene
4	Chr 22	46449430	46450114	684	-0.57	5.72	131969	10	0.00716	0.01886	PRR34	From TSS till Exon 1
5	Chr 3	182817190	182817626	436	-0.51	5.56	143070	11	0.00887	0.02029	MCCC1	TSS
6	Chr 10	134600295	134600701	406	-0.42	5.06	30457	17	0.00881	0.02628	NKX6-2	Not in the gene
7	Chr 19	58220295	58220818	523	0.56	4.48	106659	9	0.01818	0.0357	ZNF154	TSS till Exon 1
8	Chr 7	56516076	56516504	428	0.53	4.27	182274	8	0.02209	0.04007	LOC650226	TSS
9	Chr 3	24536562	24537182	620	-0.47	4.20	134238	20	0.0224	0.04174	THRB	TSS
10	Chr 12	122711988	122712381	393	0.50	4.01	51965	8	0.02809	0.04617	DIABLO and NR_103497	Intergenic

Other supplementary files can be downloaded from the following link (supplementary additional files).

CHAPTER THREE: Enhanced Anticancer Effect of a Combination of S-adenosylmethionine (SAM) and Immune Checkpoint Inhibitor (ICPi) in a Syngeneic Mouse Model of Advanced Melanoma

Preface

An imbalance between carcinogenesis and cancer immunosurveillance system occurs that leads to cancer progression (Figure 4). After reassuring that DNA methylation changes occur not only in cancer cells but also in components of immunosurveillance system (Chapter 2), the next step was to target these mechanisms to shift the balance towards cancer regression and elimination. Melanoma is a devastating disease accounting for 232,100 new cases and about 55,500 deaths annually [124]. A major break through in the treatment of melanoma came from CPIs. However, about a two-third of the patients are unresponsive to CPIs due to intrinsic or acquired resistance. Accordingly, combinational approaches to complement CPIs are being investigated. Intriguingly, studies have identified aberrant methylomes that might be causing resistance to CPIs. S-adenosylmethionine (SAM), a methyl donor targeting DNA hypomethylation, has significant anti-cancer effects in several malignancies. However, an unanswered question remained; will SAM have anti-cancer effects in melanoma? We hypothesized the beneficial effect of SAM alone and in a novel combination with anti-PD-1 antibody against melanoma. We first targeted triple wild-type (WT) genetic subtype of melanoma because for triple-WT, B16-B6 syngeneic mouse model was well-established at that time. B16-B6 model is an aggressive melanoma mouse model that faithfully represent various aspects of human melanoma pathology including melanogenesis, tumorigenesis (with 100% penetrance) and metastasis. However, B16-B6 is a short-term model, is less immunogenic, and treatment of tumors is notoriously difficult. Nevertheless, B16-B6 is an immunocompetent model that has shown low to moderate response to CPIs. In this chapter, we first tested some known anti-cancer effects of SAM on B16 cells and tested if anti-PD-1/PD-L1 pathway has intrinsic signalling in B16 cells (*in vitro*). Then we optimized B16-B6 melanoma mouse model in the laboratory, and carried out anti-cancer efficacy study with SAM, anti-PD-1 antibody, and combination. We also carried out transcriptome (RNA-sequencing) analysis of the primary tumors to delineate the gene/pathways involved in providing the anti-cancer effect. Extensive tumor and lymph node immunophenotyping using flow cytometry was also carried out to determine the effect of monotherapies and combination on anti-cancer immunity and immunosurveillance system. Clinical analysis using various melanoma databases including MGDB (gene set of known melanoma driving genes), TCGA and GTEX was also performed with the help of UCSC Xena platform (a functional genomics explorer tool) and other online tools to form meaningful conclusions.

Chapter Three follows the author generated version of the manuscript referenced below.

- **Mehdi, A**., M. Attias, N. Mahmood, A. Arakelian, C. Mihalcioiu, C.A. Piccirillo, M. Szyf, and S.A. Rabbani, *Enhanced Anticancer Effect of a Combination of S-adenosylmethionine (SAM) and Immune Checkpoint Inhibitor (ICPi) in a Syngeneic Mouse Model of Advanced Melanoma.* Front Oncol, 2020. **10**: p. 1361.

Abstract

Immune checkpoint inhibitors (ICPi) targeting PD-1/PD-L1 pathway have shown marked success in patients with advanced melanoma. However, 60–70% of patients fail to respond warranting a therapeutic intervention that could increase response rates. We and others have shown that S-adenosylmethionine (SAM), a universal methyl donor, has significant anti-cancer effects in numerous cancers previously, however, its effect on melanoma progression has not been evaluated. Interestingly, SAM was reported to be essential for T cells activation and proliferation and thus could potentially cooperate with ICPi and block melanoma progression.

In this study, we examined anti-tumor effects of SAM and ICPi alone and in combination in a well-established melanoma mouse model wherein syngeneic C57BL/6 mouse were sub-cutaneously (orthotopic) injected with B16-F1 cells. Treatment of mice with either SAM or anti-PD-1 antibody alone resulted in significant reduction in tumor volumes and weights; effects which were highest in mice treated with a combination of SAM+anti-PD-1. RNA-sequencing analysis of the primary tumors showed numerous differentially expressed genes (DEGs) following treatment with SAM+anti-PD-1 which was shown to down-regulate cancer, MAPK and tyrosine kinase pathways. Indeed, SAM+anti-PD-1 reversed the aberrant expression of some known melanoma genes. Tumor immunophenotyping revealed SAM+anti-PD-1 combination was significantly more effective than either SAM or anti-PD-1 as the $CD8^+$ T cells were having higher activation, proliferation and cytokines production as compared to all other groups.

This study shows that combination of, currently approved agents, SAM and ICPi can effectively block melanoma via alteration of key genes/pathways implicated in cancer and immune response pathways, providing the rationale for the initiation of clinical trials with SAM and ICPi.

Introduction

Melanoma has one of the top ten incidence rate amongst tumor types causing high rates of mortality warranting an urgent need for the development of new innovative therapeutic strategies particularly for patients with advanced melanoma for whom treatment options are very limited (Schadendorf et al., 2018).

Epigenetic deregulation of gene transcription via DNA methylation, histone modification and noncoding RNA is a common heritable mechanism in many cancers including melanoma which can alter the expression of key genes implicated in tumor progression (Sang and Deng, 2019). The first report of 'substantial hypomethylation' of CpG dinucleotides present in human cancer cells was published in 1983 (Feinberg and Vogelstein, 1983). Since then, numerous studies have shown that typically in cancer, genome-wide global DNA hypomethylation occurs in cancer which contribute to genomic instability and activation of silenced oncogenes (Ehrlich, 2009). S-adenosylmethionine (SAM) is synthesized endogenously and acts as a methyl group donor in DNA methylation reactions and has also been approved as a nutraceutical agent (Bottiglieri, 2002;Mahmood et al., 2018). SAM treatment has significant anticancer effects on breast, osteosarcoma, prostate, hepatocellular, gastric, colon and other cancer models (Pakneshan et al., 2004;Parashar et al., 2015;Shukeir et al., 2015;Mahmood et al., 2018;Mahmood and Rabbani, 2019). SAM effectively reduces cancer proliferation and metastasis by inhibiting angiogenesis, reducing inflammation and down regulating several genes involved in promoting cell proliferation, invasion and metastasis (Bottiglieri, 2002;Pakneshan et al., 2004;Sahin et al., 2011;Li et al., 2012;Parashar et al., 2015;Shukeir et al., 2015;Mahmood et al., 2018;Mahmood and Rabbani, 2019). For instance, we reported that the anti-metastatic activity of SAM in breast and prostate cancer is likely due to downregulation of pro-metastatic genes such as urokinase plasminogen activator (*uPA)* and Matrix metallopeptidase 2 (*MMP2)* (Shukeir et al., 2015;Mahmood et al., 2018). It is unknown whether SAM has similar effects on melanoma. SAM has also been reported to be required for activation and proliferation of T cells (Tobena et al., 1996;LeGros et al., 1997;Zeng et al., 2001;Hote et al., 2008). In activated T cells, both SAM levels and the rate of its utilization increase, while inhibition of SAM synthesis results in reduced T cell proliferation (Tobena et al., 1996;LeGros et al., 1997;Zeng et al., 2001;Hote et al., 2008). However, the role of SAM in cancer immunity has not been yet examined.

An important step involved in melanoma progression is immune evasion. A major pathway through which tumors induce immunosuppression involves binding of Programmed death ligand 1 (PD-L1), expressed on the surface of melanoma cells, on to its receptor Programmed cell death 1 (PD-1), a co-inhibitory surface checkpoint receptor on T cells (Dong et al., 2002;Pardoll, 2012). PD-1 signaling results in inhibition of T cell proliferation, cytokine production, production of anti-apoptotic molecules and a metabolic shift that amounts to a state of exhaustion (Dong et al., 2002;Sheppard et al., 2004;Pardoll, 2012;Alsaab et al., 2017). Immune checkpoint inhibitors (ICPi) such as anti-PD-1 and anti-PD-L1 monoclonal antibodies reverse this immunologically tolerant state and induces tumor regression in responding patients (Pardoll, 2012;Alsaab et al., 2017;Schadendorf et al., 2018). Apart from metastatic melanoma, FDA has approved ICPi as a frontline treatment of multiple cancers including non-small cell lung cancer (NSCLC), renal cell carcinoma (RCCs), and bladder or urothelial cancer (Pardoll, 2012;Alsaab et al., 2017;Schadendorf et al., 2018). However, there is significant variability in response to ICPi therapy and 60–70% of patients fail to respond to single-agent ICPi therapy (Pardoll, 2012;Topalian et al., 2012;Alsaab et al., 2017;Larkins et al., 2017;Schadendorf et al., 2018). Thus, there is a need to develop innovative approaches to enhance the response to ICPi monotherapy.

Epigenetic drugs are a class of agents that could potentially enhance ICPi anticancer activity by altering the epigenetic programming of genes that mediate the checkpoint response in the immune system and the cellular responses in cancer cells. Both clinical studies and animal models have shown that some epigenetic drugs prime the immune system and upregulate expression of immune-response signalling pathways in cancer cells thereby improving immune recognition and immunogenicity (Chiappinelli et al., 2016;Dunn and Rao, 2017;Mahmood and Rabbani, 2019). SAM being a methylating agent could lead to alterations in the expression of immune related genes which could increase immunogenicity of the tumors. Also, SAM, known for its anticancer effects in various cancers and an immune regulator essential for T cell activation and proliferation, could thus provide a superior anticancer effect when combined with ICPi. In this report, we tested first whether SAM would have anticancer effects in melanoma, second whether a combination of SAM and ICPi would have an enhanced antitumor effect and third we delineated the molecular pathways affected by the combination in comparison to monotherapy with either ICPi or SAM.

Materials and Methods

Cell lines

The B16-F1 mouse melanoma cell line (CRL-6323™) was obtained from the American Type Culture Collection (ATCC; Manassas, Virginia). Cells were cultured in Dulbecco's modified Eagle's medium (DMEM) supplemented with 10% fetal bovine serum (FBS), 1% penicillin-streptomycin sulfate and 2 mM L-glutamine. The cells were maintained in incubators at 37°C and 5% CO_2 and were found to be mycoplasma free.

Proliferation, colony formation and invasion assays

For *in vitro* efficacy, we used 200µM of SAM (catalog # B9003S, New England Biolabs, Canada) which was found to be the optimum dose in our previous studies and following the evaluation of different doses of SAM in B16-F1 cells and 50µg/mL of anti-PD-L1 (clone 10F.9G2, catalog #BE0101, BioXcell, USA)(Pakneshan et al., 2004;Shukeir et al., 2004;Parashar et al., 2015;Shukeir et al., 2015;Black et al., 2016;Mahmood et al., 2018). B16-F1 cells ($2x10^4$ cells) were seeded in 6-well plates. The experiment had five treatment groups; No rPD-1 (control without rPD-1), rPD-1 control (Control with rPD-1), SAM, anti-PD-L1 and SAM+anti-PD-L1 and cells in these wells were treated accordingly. B16-F1 cells were stimulated with 0.2µM rPD-1 (catalog # 1021-PD-100, R&D systems, USA) on day 3 to stimulate the PD-1/PD-L1 pathway before adding 50µg anti-PD-L1 on day 4. 200µM of SAM was added on day 2, 3 and 4 and cells were harvested on day 5. Each experiment was carried out in duplicate.

For proliferation assay, cells on day 5 were trypsinized and counted using Beckman Coulter counter (Model ZF; Coulter Electronics, Hertfordshire, UK) according to manufacturer's instructions. Proliferation assay results are mean of 4 independent experiments performed in duplicates. Results are presented as the percentage of proportion to the rPD-1 Control ± SEM.

For colony formation assay, after following the proliferation assay protocol, 5000 treated cells in DMEM (13% FBS) were mixed with agar in a 3:1 ratio and poured into a well of 6-well plates until solidified followed by adding 2 mL of DMEM on top. Colonies were monitored and counted after 2 weeks. Data is presented as mean number of colonies ± SEM.

Following the proliferation assay protocol, invasion assay was performed as previously described by us using a two-compartment Boyden chamber invasion assay (Costar Transwell, Corning Corporation, Sigma-Aldrich, Oakville, ON, Canada) (Mahmood et al., 2018). The precise steps for the invasion assay is detailed in the previous paper (Mahmood et al., 2018) except that the B16-F1 cells were incubated for 24 hours instead of 18 hours. Data is presented as mean number of cells invaded per field ± SEM.

Animal studies

All *in vivo* studies were performed in accordance with McGill University Facility Animal Care Committee guidelines. Six to eight weeks old female C57BL/6 or Black B6 mice were purchased from Charles River Lab (Quebec, Canada) and housed at Animal Resource Division (ARD) of the Research Institute of the McGill University Health Center (RI-MUHC). To determine the effect of SAM (Life Science Laboratories, Lakewood, NJ, USA), anti-PD-1 (clone RMP1-14, BioXcell, USA) and SAM+anti-PD-1 combination on tumor growth, mice were injected orthotopically with $5x10^5$ B16-F1 cells via subcutaneous (s.c) route into the left flank to induce tumor formation. These mice were randomized into the four groups and then treated with either isotype matched control IgG (control), SAM, anti-PD-1 and SAM+anti-PD-1 combination (n= 8 per group). Treatment was started at day 3 wherein 80mg/kg of SAM diluted in PBS was given daily via oral gavage using feeding needles while 10mg/kg anti-PD-1 was given via intra-peritoneal (i.p.) injection twice a week with a total of 4 doses of anti-PD-1. The dose of SAM 80mg/kg was established in our previous study (Mahmood et al., 2018) while the dose of anti-PD-1, 10mg/kg, was established previously in preclinical and clinical trails (Wang et al., 2014;Naidoo et al., 2015;Moynihan et al., 2016;Alsaab et al., 2017;Bertrand et al., 2017;Triplett et al., 2018;Han et al., 2019). Tumor volumes were measured by palpation at day 12 and 14 using a calliper. On day 16, mice were sacrificed, tumor weight (T.W) and tumor volumes (T.V) were measured and calculated using the formula; $T.V = (\text{length} \times \text{width}^2)/2$. Percentage (%) tumor reduction at day 16 was calculated as ((mean T.V or T.W of (control-treatment group))/mean T.V or T.W of control) *100). The animals were weighed at the start of study and at time of tumor volume measurement. Regular examinations were carried out for any body weight loss or potential adverse effect as we have previously reported in the B16 melanoma model (Rastelli et al., 2011). Due to low viability of tumor-infiltrating cells at humane endpoint, pilot studies were performed to determine the

optimal experimental endpoint for detection of immune cell populations in the tumor microenvironment of B16-tumor inoculated B6 mice. For immunophenotyping experiments, we selected day 14 as our experimental endpoint and used the SAM treatment arms and dosage, however, mice receiving anti-PD-1 were injected with a total of 3 injections post-tumor inoculation.

RNA extraction and reverse transcriptase quantitative real-time PCR (RT-qPCR)

Total cellular and tumoral RNA was extracted using the RNeasy kit (Qiagen; Hilden, Germany, Cat# 71404) according to manufacturer's instructions. The RT-qPCR assay was performed following our previously described protocol (Mahmood et al., 2018). The primers are listed in Supplementary Table 1. Change in gene expression among various groups was analysed by using the 2-ΔΔCT method.

RNA-sequencing (RNA-seq)

Total RNA from the cells and tumors was extracted as described above. The extracted RNA was sent to Genome Quebec and Innovation Centre (McGill University) for carrying out paired-end RNA sequencing using Illumina HiSeq 4000 platform (with a depth of 50 million reads) following standard protocols. The obtained data was analyzed using DeSeq2 script in R according to writer's recommendations (Love et al., 2014).

Immunophenotyping

Mice (n=8/group from two independent experiments) were sacrificed at day 14 and primary tumors, spleens and lymph nodes (draining and contralateral) were harvested and placed in RPMI 1640 1x (Wisent, Saint-Jean-Baptiste QC, Canada; Cat# 319-015-CL). Spleens and lymph nodes were dissociated mechanically into single cell suspensions. Whole tumors were shredded thinly, before digestion with collagenase IV (Gibco) and DNAse I (Sigma-Aldrich) for 1 hour at 37°C. Cells were then passed through a 70μm cell strainer to obtain single-cell suspensions. After lymphocyte isolation, the cells were then washed in PBS, stained first with antiCD16/CD32 (clone 2.4G2, BD), then extracellular markers, fixed, and permeabilized for intracellular staining followed by flow cytometry analysis. For assessment of cytokine production, single cell

suspensions were stimulated with Phorbol 12-myristate 13-acetate (PMA), Ionomycin, and incubated in the presence of GolgiStop (BD Biosciences) for 3 hours at 37ºC before staining for flow cytometry analysis. Samples were acquired using the BD Fortessa LSR-X20 and analyzed using FlowJo v10 (TreeStar) (Cossarizza et al., 2019). The fluorescence-conjugated antibodies used for staining are listed in Supplementary Table 2.

Statistical analysis

Results were analyzed and presented as ± SEM or SD, statistical difference between different groups determined by two-tailed Student's t-test and one-way ANOVA where values of $*P < 0.05$, $**P < 0.01$, $***P < 0.001$, $****P < 0.0001$ were considered statistically significant. For gene set enrichment analysis, Consensus PathDB was used (Kamburov et al., 2011).

Results

Effect of SAM and anti PD-L1 antibody on B16 melanoma cell proliferation, colony formation and invasion *in vitro.*

SAM has been reported to have significant anti-cancer effects both *in vitro* and *in vivo* in several cancers, however the effect of SAM has not been tested on melanoma yet (Pakneshan et al., 2004;Parashar et al., 2015;Shukeir et al., 2015;Mahmood et al., 2018;Mahmood and Rabbani, 2019). We first investigated the effect of increasing doses of SAM on B16-F1 cell proliferation where 200 μM was most effective in reducing cell proliferation (Supplementary Figure 1). The maximum anti-cancer effects of SAM were seen following treatment with 200 μM and no additional increment was seen with higher dose of SAM. Although it is established that the major anti-cancer effects of blockage of PD-1/PD-L1 pathway are related to enhancing the immunity against cancer, there are various reports that PD-L1 triggers intrinsic signalling independent of the immune checkpoint, which promotes tumorigenesis (Dong et al., 2018;Escors et al., 2018). Hence, we determined the effect of SAM and anti-PD-L1 in an *in vitro* cell proliferation assay. Since PD-1 is not present in an *in vitro* system, we used recombinant PD-1 (r-PD-1) to stimulate the intracellular PD-1/PD-L1 pathway. As in other cancer cell line models, SAM treatment resulted in

a significant decrease in B16-F1 melanoma cell proliferation. Although anti-PD-L1 showed a slight decrease in cell proliferation, it was not statistically significant, however combination of SAM+anti-PD-L1 showed significantly higher reduction in cell proliferation compared to control (Figure 1A). A similar pattern was observed for B16-F1 cells in a colony formation assay where lowest number of colonies were seen following treatment with SAM+anti-PD-L1 in combination setting (Figure 1B). Number of invasive cells were significantly lower in combination of SAM+anti-PD-L1 group compared to all the other groups (Figure 1C). Collectively, these results showed that SAM, but not anti-PD-L1, decreased cell proliferation, anchorage-independent growth and invasive ability of B16-F1 melanoma cells *in vitro*. These results provide evidence that SAM is effective in blocking melanoma cell proliferation, colony formation and invasion *in vitro*, results which are similar to our and others' previous studies in several cancer cell lines (Pakneshan et al., 2004;Sahin et al., 2011;Li et al., 2012;Parashar et al., 2015;Shukeir et al., 2015;Mahmood et al., 2018;Mahmood and Rabbani, 2019).

Effect of SAM and anti-PD-1 antibody alone and their combination on tumor growth in syngeneic B16-F1 mouse melanoma model.

Next, we examined the effect of SAM and anti-PD-1 and the combination of both agents in B16-F1 melanoma-bearing mice. Using this syngeneic cell line approach, immunocompetent mice develop a failing adaptive immune response that does not stop tumor growth. This model has been widely used for preclinical assessment of anti-melanoma immunotherapies (Overwijk and Restifo, 2001;Kuzu et al., 2015). B16-F1 melanoma cells were injected via subcutaneous (s.c.) route into female C57BL/6 mice followed by treatment with either control IgG, SAM, anti-PD-1 antibody or SAM+anti-PD-1 antibody. Tumor volumes were measured at timed intervals (day 12 and 14) and at the end of this study on day 16, all control and experimental mice were sacrificed. In this model of aggressive advanced melanoma, all three treatment arms had statistically significant reduced tumor burdens compared to the controls (SAM, 646 mm^3, $p < 0.05$; anti-PD-1, 567 mm^3, $p < 0.05$ and; control 1020 mm^3) whereas the combination group of SAM+anti-PD-1 had significantly lower mean tumor volume (315 mm^3) relative to control ($p < 0.0001$) and SAM ($p < 0.05$) at end point (Figure 2A). Moreover, in the SAM+anti-PD-1 group, there was no measurable increase in mean tumor volume between day 14 and day 16 (Figure 2A). Additionally, the SAM+anti-PD-1 treated group had the highest percentage of tumor volume reduction (69%, *p*

<0.0001) relative to control as compared to SAM and anti-PD-1 alone (37% and 44%, respectively) at end point (Figure 2B). Similarly, all three treatment arms had significantly lower mean tumor weight compared to control (SAM, 0.42g, *p <0.05*; anti-PD-1, 0.37g, *p <0.01* and; control, 0.68g) while the SAM+anti-PD-1 group had significantly lower mean tumor weight (0.20g) compared to control (*p <0.0001*) and SAM (*p <0.05*) (Figure 2C). The percentage tumor weight reduction was also significantly lower for SAM+anti-PD-1 group (71%) relative to control (*p <0.0001*) and SAM (39%, *p <0.05*) (Supplementary Figure 2). Regular examinations of control and experimental groups of animals showed no significance (*p >0.05*) body weight loss following all treatments (Figure 2D). These data support the benefit of a combination of SAM+anti-PD-1 for inhibiting melanoma growth and progression as compared to SAM and anti-PD-1 as a monotherapy.

Effect of combined SAM+anti PD-1 therapy on the transcriptional landscape of B16-F1 tumors.

We next determined which molecular pathways are triggered by a combination of SAM and anti-PD-1 and are possibly involved in the enhanced anti-tumor effects. We performed RNA sequencing analysis on primary tumors isolated from the control, SAM, anti-PD-1 and combination treated mice. Differential gene expression analysis revealed numerous genes significantly (FDR< 0.05) up- or down-regulated in SAM, anti-PD-1 and the combination when compared to control as shown in Figure 3. The combination of SAM and anti-PD-1, when compared to the control group, showed high number (887 up- and 847 down-regulated) of significantly (FDR< 0.05) differentially expressed genes (DEGs) than either monotherapy. This differential regulation indicated that combination treatment simultaneously affected several pathways which resulted in blocking tumor growth as shown in Figure 2. The pathway analysis of down-regulated genes showed various pathways which were enriched in combination treatment compared to monotherapy and control (Figure 3). These repressed pathways were mainly involved in cancer, cell cycle, DNA repair and immune system (Table 1). Various MAPK and tyrosine kinases pathways that are major oncogenic pathways involved in melanoma tumorigenesis were significantly downregulated in tumors treated with the combination of SAM+anti-PD-1 but not in SAM (except one of the MAPK pathways) and anti-PD-1 alone (Table 1)(Network, 2015;Zhang

et al., 2015). In contrast, pathways that were upregulated were mainly involved in mRNA processing, translation, metabolism and transcription (Table 2).

Next, we overlapped our DEGs of tumors treated with SAM+anti-PD-1 (compared to control) with known melanoma cancer genes from The Melanoma Gene Database (MGDB) that has 422 melanoma specific protein-coding genes (Zhang et al., 2015) and The Cancer Genome Atlas (TCGA) (Figure 3D and Supplementary Figure 3)(Cerami et al., 2012;Network, 2015) . We found 28 melanoma specific genes to be common between our data and MGDB, out of which, 18 DEGs were downregulated and 10 were up-regulated with SAM+anti-PD-1 treatment. However, only one was down-regulated with SAM and two with anti-PD-1 antibody (Figure 3D). We analysed a few of the top DEGs (*NRP2, CAPN3, DMBT1, BRAF, DDIT3, PPP1R3C, NF1*) using The UCSC Xena platform (Mary Goldman, 2019) that has large number of RNA-seq data of normal tissue from healthy individuals (GTEx) and primary tumor and metastatic tissue data from melanoma patients (TCGA).

Neuropilins (NRPs) function as co-receptors of VEGF family and plexins and are involved in promoting angiogenesis and in axonal guidance, respectively (Rushing et al., 2012;Moriarty et al., 2016). NRP2 was recently found to be an oncogene involved in accelerating melanoma tumor growth and progression *in vivo* (Rushing et al., 2012;Moriarty et al., 2016). *NRP2* showed significantly high expression in the primary tumors and metastatic tissues of the melanoma patient samples while normal tissues had low expression (Figure 4A-B). In addition, *NRP2* had the highest expression in melanoma TCGA data compared to all other cancers in TCGA Pan-Cancer Atlas (Supplementary Figure 4). Interestingly, the tumor-bearing mice treated with combination of both SAM+anti-PD-1 had lowest expression of *Nrp2* compared to other groups (Figure 4C). Tumors treated with SAM+anti-PD-1 showed significant downregulation of *Nrp2* compared to control ($p< 0.05$) while *Nrp2* expression in tumors treated with SAM and anti-PD-1 alone were not found to be significantly down-regulated in RNA-seq data. Down-regulation of *Nrp2* expression in SAM+anti-PD-1 treated tumors (n =4 tumors/ group) was further validated using RT-qPCR (Supplementary Figure 5). Moreover, high expression of *NRP2* was found to have significantly low overall survival and progression-free survival rates ($p< 0.0001$) in melanoma patients (Figure 4D-E).

Deleted in malignant brain tumors 1 (*DMBT1*) has been reported to be a tumor suppressor gene (TSG) in brain (medulloblastoma, GBM), lung and gastrointestinal tumors based on homozygous deletions, lack of expression, its instability in cancer and having key roles in immune defense and epithelial differentiation (Mollenhauer et al., 2000). *DMBT1* showed significantly low expression in the primary tumors and metastatic tissues of the melanoma patient samples while normal tissue had high expression (Figure 5A-B). In addition, *DMBT1* had one of the lowest expressions in melanoma TCGA data compared to all other cancers in TCGA Pan-Cancer Atlas (Supplementary Figure 6). The tumor bearing mice which were treated with combination of both SAM+anti-PD-1 had significantly highest expression of *Dmbt1* compared to control, SAM alone and anti-PD-1 alone (Figure 5C). Tumors treated with SAM+anti-PD-1 showed significant up-regulation of *Dmbt1* compared to control ($p< 0.001$) while *Dmbt1* expression in tumors treated with SAM and anti-PD-1 alone were not found to be significantly up-regulated in RNA-seq data. Up-regulation of *Dmbt1* expression in SAM+anti-PD-1 treated tumors (n =4 tumors/ group) was further validated using RT-qPCR (Supplementary Figure 5). *DMBT1* was not found to have a good prognostic value in melanoma (Figure 5D-E) but high expression of *DMBT1* was favourable in endometrial cancer (Cerami et al., 2012). *Braf* and *Nf1*, known melanoma driver genes (Network, 2015), were found to be significantly down-regulated in tumors treated with SAM+anti-PD-1 compared to control. *BRAF* and examples of a few other genes are showed in Supplementary Figures 7-14. These data may indicate that the combination of SAM+anti-PD-1 therapy reversed the expression of some of the aberrantly expressed genes in melanoma which might be underpinning its therapeutic effect against melanoma tumors in mice.

Next, we validated the highest significantly down (*Myh2, Mybh, Sypl2, Xirp1, Mybpc1*) and up (*Fcgbp, Areg*) regulated genes including the melanoma specific genes (*Dmnt1* and *Nrp2*) identified by RNA sequencing following treatment with SAM+anti-PD-1 by RT-qPCR. These genes were similarly up/down regulated in primary tumoral RNA of mice treated with SAM+anti-PD-1 (Supplementary Figure 5).

Beneficial effect of SAM and anti-PD-1 combinatorial therapy on anti-cancer immune response

We carried out immuno-phenotyping of infiltrating cells from primary tumors of control group and mice treated with SAM, anti-PD-1 antibody and SAM+anti-PD-1 (Figure 6). Here, we opted for a suboptimal administration scheme of anti-PD-1 to parse out the additive effects of combination therapy. To confirm the immune effect of anti-PD-1 treatment, we assessed the level of expression of PD-1 on $CD8^+$ tumor infiltrating lymphocytes (TILs) at endpoint by flow cytometry. In both groups having received anti-PD-1, we observed a 20% reduction of PD-1 mean fluorescence intensity (MFI) amongst PD-1^{High} $CD8^+$ T cells (Figure 6B and 6J). In this experiment, only the SAM+anti-PD-1 arm displayed a significant reduction in tumor volume at endpoint (Figure 6A). Accordingly, the density of tumor-infiltrating T cells ($CD45^+$ $CD3^+$) and $CD8^+$ T cells, measured as number of cells/cm^3 of tumor, was significantly increased in the combination therapy group (Figure 6C-D). We observed a corresponding increase in the proportion of $CD8^+$ T cells in the tumor-draining lymph node, suggesting increased expansion and/or recruitment of $CD8^+$ cells to the tumor (Supplementary Figure 15A-B). Furthermore, the proliferation of $CD8^+$ T cells, measured by expression of the mitotic marker Ki67, was significantly increased in the SAM+anti-PD-1 group (Figure 6E), and anti-PD-1 also restored the proliferative capacity of PD-1^+ TILs (Figure 6J).

As $CD8^+$ T cells are known to be potent effectors of anti-tumor responses, we then sought to characterize their cytokine-production capabilities. Despite a high level of variability in the tumors of the control group, we observed a significant increase in the percentage of $CD8^+$ T cells secreting IFNγ after polyclonal PMA/Ionomycin stimulation in the combination group (mean=23.0 ±12.7%), compared to the control (6.88 ±6.35 %) and anti-PD-1 monotherapy group (5.33 ±5.02%) (Figure 6F and 6K). This high level of variability was explained by the heterogeneity of tumor sizes at endpoint. Indeed, there was a strong negative correlation between the frequency of $CD8^+$ T cells secreting IFNγ and tumor size at endpoint (r^2=0.436, $p<0.0001$), suggesting that IFNγ^+ $CD8^+$ cells confer protective anti-tumor immunity in our model (Figure 6G and Supplementary Figure 15C). Furthermore, despite not observing a significant difference in the proportion of $CD8^+$ T cells secreting TNFα, combination therapy readily induced a population of IFNγ^+ TNFα^+ $CD8^+$ cells that was mostly absent in all other treatment arms (Figure 6H-I). Finally, $CD8^+$ T cells from the combination group upregulated T-bet expression in $CD8^+$ cells (Supplementary Figure 15D). Notably, this overall increase in proliferation and effector functions was not observed in conventional $CD4^+$ T cells ($CD4^+Foxp3^-$) (Supplementary Figure 15E-H).

We assessed the frequency of myeloid cell subsets as well as their level of PD-L1 expression (Supplementary Figure 16-18). We did not observe any significant difference in the frequency of macrophages (CD11b+ F4/80^{High}), dendritic cells (CD11c^{+}), neutrophils & granulocytic-myeloid-derived suppressive cells (MDSCs, Ly6G^{+} Ly6C^{Int}), monocytes & monocytic MDSCs (CD11b^{+} Ly6C^{+} F480^{int}) (Supplementary Figure 16-18). However, we observed an increase in the frequency of PD-L1^{+} macrophages, monocytes and M-MDSCs and CD11b^{+} dendritic cells (Supplementary Figure 16G-L). Furthermore, the level of expression of PD-L1, measured by MFI, was increased in 3 out of 4 mice in the combination group. PD-L1 expression is known to be inducible by IFNγ, and paradoxically, high levels of PD-L1 expression has been proposed as a predictive marker of response to anti-PD-1(Schadendorf et al., 2018). Taken together, these data show that treatment with SAM potentialized the efficacy of anti-PD-1 and increased anti-tumor immunity through a specific activation and proliferation of CD8^{+} T cells, recapitulating known hallmarks of response to treatment.

Discussion

Immune checkpoint inhibitors (ICPi) have received FDA approval as early as of 2011 for the treatment of advanced melanoma (Pardoll, 2012;Alsaab et al., 2017;Schadendorf et al., 2018). However, despite melanoma being the solid tumor type most responsive to anti-PD-1 monoclonal antibody, overall response rates are estimated around 30-33%, indicating that a considerable number of patients do not experience a reduction in tumor burden, resulting in high morbidity and mortality (Pardoll, 2012;Topalian et al., 2012;Alsaab et al., 2017;Larkins et al., 2017;Schadendorf et al., 2018). The immunological basis of treatment failure is a very actively researched topic. Nevertheless, considering the tremendous clinical improvements experienced by high responder patients, there is a need for therapeutic strategies to potentialize the effect of anti-PD-1 and strengthen anti-tumor immunity. Here, we show that the combination of an approved nutraceutical, the epigenetic modulator SAM with an anti-PD-1 antibody displayed strong anti-cancer effects against B16 cells, the most commonly used preclinical syngeneic mouse model of advanced melanoma. Furthermore, using a suboptimal administration scheme of anti-PD-1 in which tumor burden is not reduced by monotherapy, we provide evidence that co-administration of SAM is sufficient to potentialize the effect of anti-PD-1 and induce a strong anti-tumor immune response.

Previous studies have demonstrated that global and target gene specific hypomethylation are present in the cancer epigenome which plays a crucial role in the initiation and progression of cancer (Ehrlich, 2009). Furthermore, there is insufficient SAM available in the tumor microenvironment (Ulanovskaya et al., 2013). SAM treatment results in significant anti-tumor effects in breast, osteosarcoma, prostate, hepatocellular, gastric, colon and other cancers (Pakneshan et al., 2004;Parashar et al., 2015;Shukeir et al., 2015;Mahmood et al., 2018;Mahmood and Rabbani, 2019). Here we show significant anti-cancer effect of SAM as monotherapy in a model of advanced melanoma that is at least as effective as anti-PD-1 treatment. The fact that an approved nutraceutical agent, SAM, with a good safety profile and shows potentiating effects on anti-PD-1 in a model resistant to immunotherapy should encourage translation of these findings to the clinic.

Human anti-PD-1 antibodies (nivolumab and pembrolizumab) are currently recommended as the first line of treatment in advanced melanoma and are FDA-approved for several other cancer indications. The PD-1/PD-L1 signaling axis dampens TCR and CD28 signalling in T cells and is hijacked by PD-L1 expressing tumor cells to deactivate anti-tumor responses (Pardoll, 2012;Alsaab et al., 2017;Schadendorf et al., 2018). However, PD-L1 has been extensively reported to have intrinsic signaling in various cancer cell types, which promotes cancer initiation, metastasis, development, resistance to therapy, enhances cancer cell survival, regulates stress responses and confer resistance toward pro-apoptotic stimuli (Dong et al., 2018;Escors et al., 2018). Hence, we investigated the consequences of blocking the PD-1/PD-L1 pathway in *in vitro* using B16-F1 cells. In order to induce PD-L1 signalling, we first added rPD-1 in the medium and then blocked the PD-1/PD-L1 pathway with anti-PD-L1 antibody (Black et al., 2016). We didn't use anti-PD-1 antibody *in vitro* as the monoclonal antibody would bind and neutralize rPD-1 directly. The anti-cancer effect of anti-PD-L1 on B16-F1 cells was low which is consistent with the previously published literature showing that the protective effect of this ICPi is mainly through the enhancement of the immune response (Dong et al., 2002;Sheppard et al., 2004;Pardoll, 2012;Alsaab et al., 2017;Schadendorf et al., 2018).

To study the impact of SAM on tumor control *in vivo*, we used a murine anti-PD-1 antibody as a comparator since it is the standard of care for human advanced melanoma patients. Having first shown that SAM had similar protection to anti-PD-1 in immunocompetent mice, we then

opted for a suboptimal anti-PD-1 administration scheme to model for treatment failure and demonstrate the superior effect of SAM with anti-PD-1. In this setting, anti-PD-1 monotherapy decreased the level of PD-1 expression on $CD4^+$ and $CD8^+$ T cells but failed to increase $CD8^+$ infiltration and effector functions in the tumor microenvironment. However, co-administration of SAM was sufficient to restore protective immunity. Mice in the combination group recapitulated known hallmarks of successive response to PD-1 blockade, namely: increased infiltration, proliferation and secretion of IFNγ and expression of T-bet by $CD8^+$ T cells. Polyfunctional $CD8^+$ T cells secreting both IFNγ and TNFα are highly active effector $CD8^+$ T cells that are associated with improved anti-tumor immunity in preclinical mouse models and in patients, and are considered to be potent mediators of anti-tumor activity (Wimmers et al., 2016). The combination therapy of SAM with anti-PD-1 antibody induced higher population of polyfunctional $CD8^+$ T cells.

Despite its efficacy in the clinic, it is well established that the protective effect of murine anti-PD-1 monotherapy is less potent in the B16-F1 model (Han et al., 2019;Wang et al., 2019). Indeed, this model is considered very aggressive and poorly immunogenic with low levels of MHC I expression in these cells (Kuzu et al., 2015). Also, early preclinical models that demonstrated the protective effect of anti-PD-1 used vaccination with irradiated B16 melanoma cells as a combinatory approach to elicit protection (Curran et al., 2010). Furthermore, other reports show no protective effect of monotherapy in models of quickly progressing B16-F1 mouse melanoma tumors, through lack of clonal expansion and effector functions of antigen-specific $CD8^+$ T cells (Black et al., 2016;Rajani et al., 2016;Ordikhani et al., 2018;D'Alterio et al., 2019;Daneshmandi et al., 2019). In clear contrast to anti-PD-1 monotherapy, treatment with SAM+anti-PD-1 showed significant reduction in tumor growth, and enhanced anti-cancer immunity, even in a setting with fewer injections of anti-PD-1 where monotherapy alone fails to induce protection. Our data also showed that SAM not only complements the anti-cancer effect by reducing oncogenic gene expression, as reported herein and previously using microarray and RNA-seq analysis, but also enhances the anti-cancer immunity alongside anti-PD-1 (Bottiglieri, 2002;Pakneshan et al., 2004;Sahin et al., 2011;Li et al., 2012;Parashar et al., 2015;Shukeir et al., 2015;Wang et al., 2017;Mahmood et al., 2018;Mahmood and Rabbani, 2019). Our immunophenotyping data is consistent with the previously published literature that show SAM could potentially increase activation and proliferation of T cells which was observed in combination with anti-PD-1 (Tobena

et al., 1996;LeGros et al., 1997;Zeng et al., 2001;Hote et al., 2008). The fact that SAM can dramatically enhance suboptimal activity of ICPi points to the possibility that it might be possible to achieve effective antitumor activity with a lower frequency of ICPi dose, thus reducing its toxicity and adverse effects.

Another objective of the current study was to determine the molecular pathways triggered by SAM, anti-PD-1 and SAM+anti-PD-1. RNA-sequencing data showed that SAM (compared to control) caused downregulation of 57 genes and up-regulation of only two genes. This is consistent with previously published literature that SAM-mediated promoter hypermethylation would result in greater gene silencing (Pakneshan et al., 2004;Li et al., 2012;Parashar et al., 2015;Shukeir et al., 2015;Mahmood et al., 2018;Mahmood and Rabbani, 2019). Compared to the effect of SAM on DEGs, SAM+anti-PD-1 had very high number of up- (887) and down- regulated (847) genes. While examining common DEGs between SAM, anti-PD-1 and SAM+anti-PD-1, it appeared that many DEGs (1438) in the combination treatment did not overlap with DEGs triggered by either SAM or anti-PD-1 monotherapy. This implies that the major reduction in tumor growth shown by the SAM+anti-PD-1 treatment is associated with a larger pool of genes that are involved in a diverse array of molecular pathways including down-regulation of key tumorigenesis pathways of melanoma, MAPK and tyrosine kinases related pathways, that could not be inhibited by the monotherapy treatment. Moreover, upon deeper analysis, it was observed that the combination treatment of SAM+anti-PD-1 acted on a group of specific genes that are aberrantly expressed in melanoma tumors which might underlie the therapeutic effects. This molecular analysis supports the conclusion that combination of SAM and anti-PD-1 is significantly more active than the monotherapy because it launches molecular pathways that could not be triggered by either agent on its own.

A limitation of preclinical models of melanoma is their high aggressiveness, with the engraftment of a large number of tumorigenic cells not recapitulating the natural course of disease progression. In untreated mice, most tumors reach a critical volume within 16 days of tumor engraftment limiting the ability to determine long-term effects of treatment regimens. However, even with this short-term aggressive melanoma model, SAM delayed tumor growth, and combination of SAM with anti-PD-1 had a superior protective effect and restored $CD8^+$ T cell proliferation and effector functions within the tumor microenvironment. Furthermore, the

combination of SAM+anti-PD-1 showed highest tumor volume and weight reduction (69% and 71%, respectively) at day 16. Thus, future studies evaluating the effect of SAM+anti-PD-1 in a less aggressive model of melanoma and other common cancers is warranted. This study did not evaluate the adverse effects of SAM and anti-PD-1 treatment on mice extensively. However, we did not observe a significant change in the mice body weight between each group. Moreover, immune-related adverse events upon PD-1 blockade such as reported in pharmacovigilance data have never been described in the B16 preclinical model of melanoma. Furthermore, SAM has an excellent safety profile that warranted its licensing as a nutraceutical agent and its anti-cancer effects have been shown to be selective of tumor cells, without affecting normal epithelial cells (Bottiglieri, 2002;Mahmood et al., 2018;Mahmood and Rabbani, 2019). Therefore, we hypothesize that combination of SAM with anti-PD-1 will have a similar safety profile to immunotherapy alone. However, preclinical toxicity studies are necessary to assess the safety of this treatment regimen.

In summary, this is the first evidence for the anti-melanoma effects of a methylating agent such as SAM. Furthermore, adjuvantation of anti-PD-1 with SAM was sufficient to reactivate an exhausted anti-tumor immune response. The major advantage of this approach is that both ICPi (such as anti-PD-1) and SAM are approved agents with long term safety profiles. This should help accelerating its clinical translation through the initiation of clinical trials in patients with melanoma and other common cancers to reduce cancer associated morbidity and mortality.

Figures (Chapter Three)

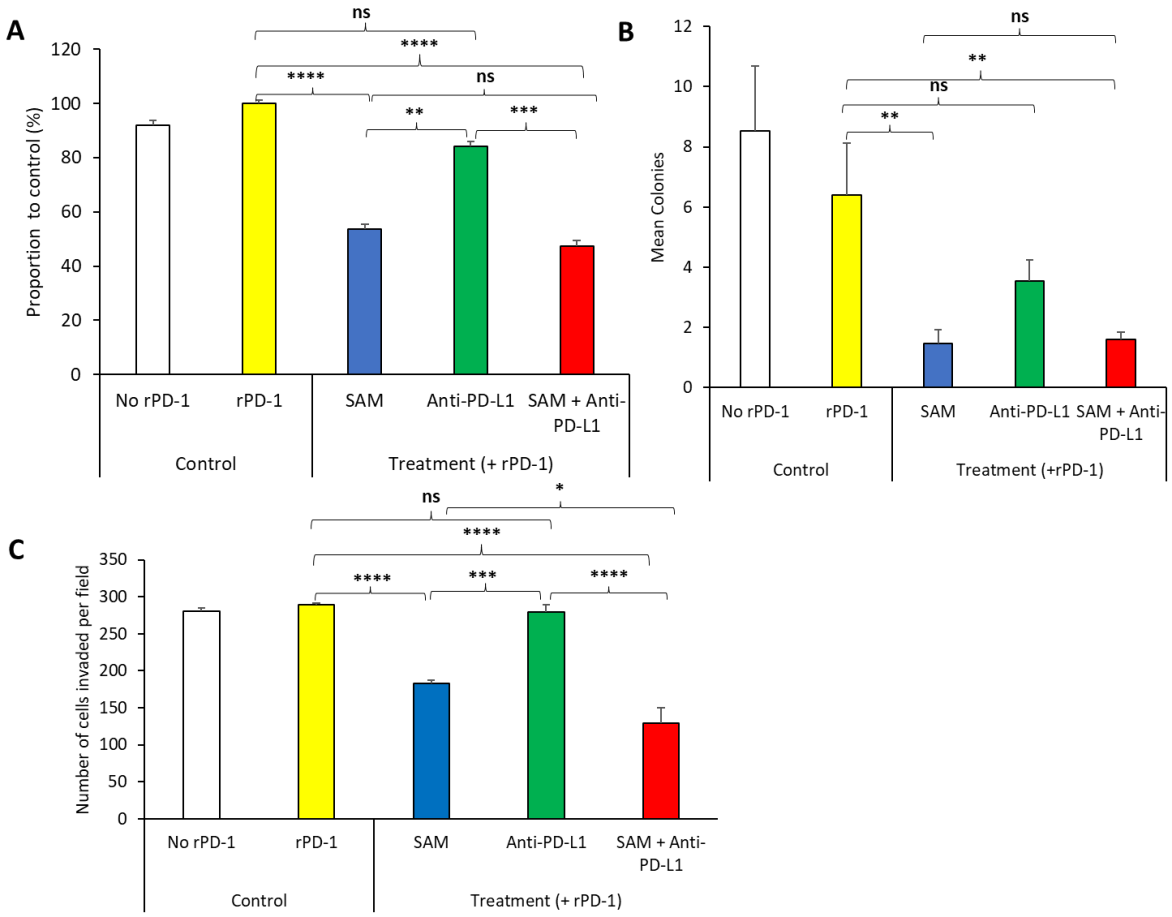

Figure 1: Effect of SAM and anti-PD-L1 antibody on B16-F1 melanoma cell proliferation, colony formation and invasion *in vitro*. B16-F1 cells ($2x10^4$ cells) were seeded in 6-well plates and were stimulated with rPD-1. The experiment had five treatment groups; No rPD-1 added (control no rPD-1); 0.2µM rPD-1 control (Control with rPD-1); treated with 0.2µM rPD-1 followed by treatment with 200µM SAM (SAM), 50µg/mL of anti-PD-L1 or combination of SAM+anti-PD-L1 and cells were subjected to proliferation, colony formation and invasion assay as described in "Materials and Methods". **(A)** Proliferation is presented as the percentage of rPD-1 Control ± SEM. **(B)** Colony formation is presented as mean ± SEM. **(C)** Invasion assay is presented as mean number of cells invaded per field ± SEM. Results are mean of at least 2 independent experiments. Statistical significance was determined by ANOVA in GraphPad prism and are represented by asterisks (ns, not significant, $*P < 0.05$; $**P < 0.01$, $***P < 0.001$ and $****P < 0.0001$).

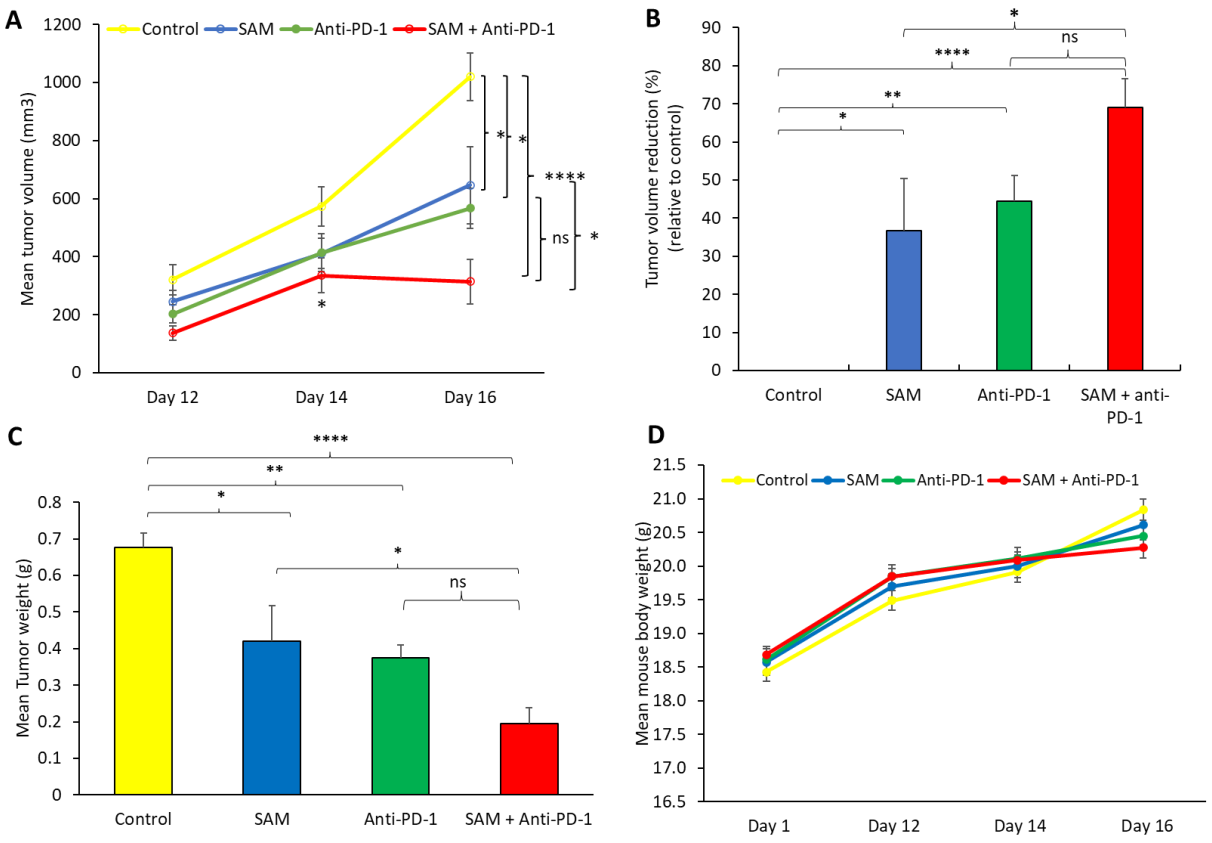

Figure 2: Anti-tumor effect of SAM and anti-PD-1 antibody in a syngeneic mouse B16-F1 melanoma model *in vivo*. 5x10^5 B16-F1 mouse melanoma cells were injected via sub-cutaneous route into the right flank of C57BL/6 mouse (n=8/group). From day 3 post tumor cells inoculation mice were treated with control IgG alone (control), 80mg/kg SAM (SAM), 10mg/kg anti-PD-1 antibody and SAM+anti-PD-1 antibody as described in "Materials and Methods". **(A)** Tumor volume was measured at day 12, 14 and 16. All control and experimental mice were sacrificed on day 16. **(B)** Percentage (%) of tumor volume reduction in each group relative to control at day 16. **(C)** Tumor weight was measured after sacrificed on day 16. **(D)** Mean mouse body weights measured at different time intervals (Day 1, 12, 14 and 16) for each group. **(A-D)** Results are representative of mean ± SEM of at least 8 mice per group. Statistical significance was obtained by ANOVA in GraphPad prism and are represented by asterisks *(*ns, not significant*, **P < 0.05, **P < 0.01, ***P < 0.001* and *****P < 0.0001*).

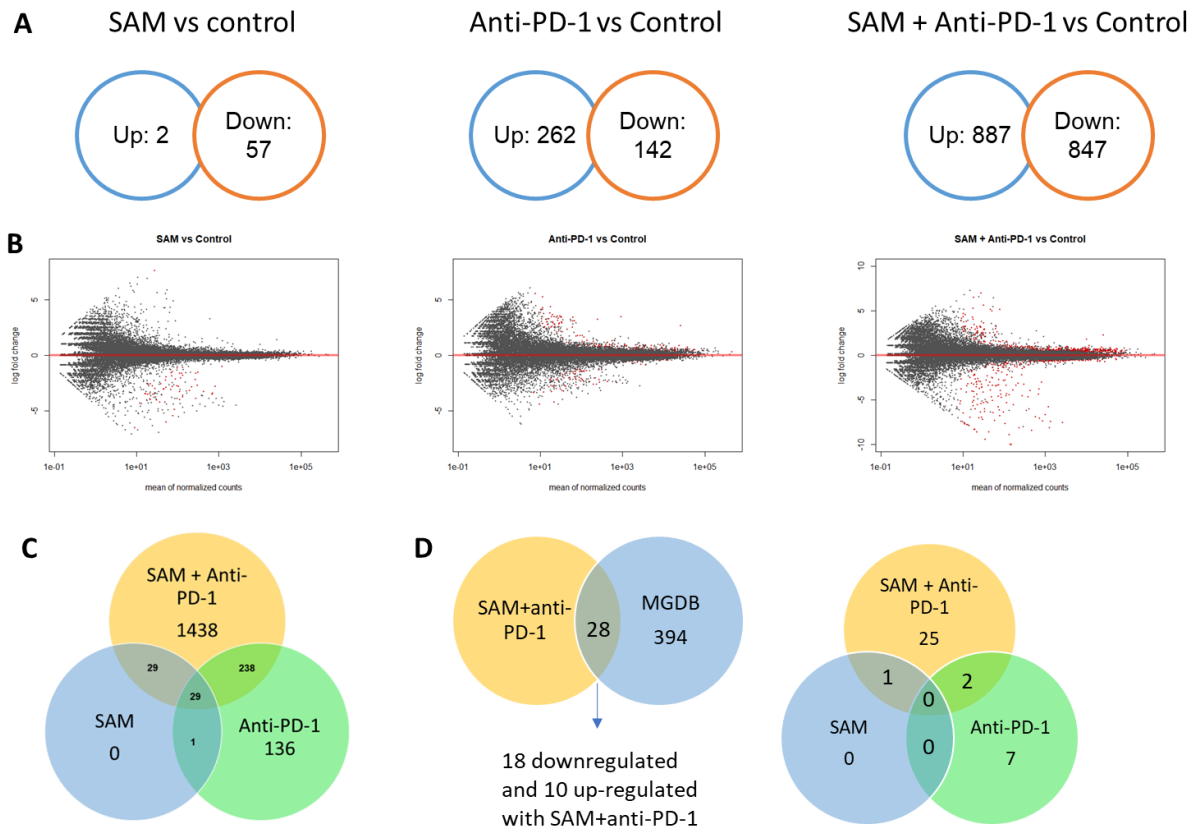

Figure 3: Transcriptome analysis of control and experimental B16-F1 mouse melanoma tumors. Numerous genes differentially regulated as revealed from RNA-sequencing analysis on primary B16-F1 tumors from syngeneic mice after treatment with control IgG alone, SAM, anti-PD-1 and SAM-anti-PD-1. **(A)** Venn Diagrams showing significant differentially regulated genes (FDR<0.05) in; SAM versus control group; anti-PD-1 versus control group; and SAM+anti-PD-1 versus control group. **(B)** MA plots of all genes differentially regulated in; SAM versus control group; anti-PD-1 versus control group; and SAM+anti-PD-1 versus control group. The red dots describe genes that were significantly up- or down- regulated while the black dots represent non-significant genes. **(C)** Venn Diagram representing significant (FDR<0.05) genes differentially regulated in all three groups and overlapping genes between groups. **(D)** The differentially expressed genes (DEGs) obtained from RNA-seq data were overlapped with The Melanoma Gene Database (MGDB). MGDB is a database of 422 known melanoma protein-coding genes (Zhang et al., 2015). Left panel; DEGs obtained from SAM+anti-PD-1 group overlapped with MGDB

genes; right panel; common DEGs from each group SAM, anti-PD-1 and SAM+anti-PD-1 group and the MGDB were plotted to show common and unique genes between each treatment group.

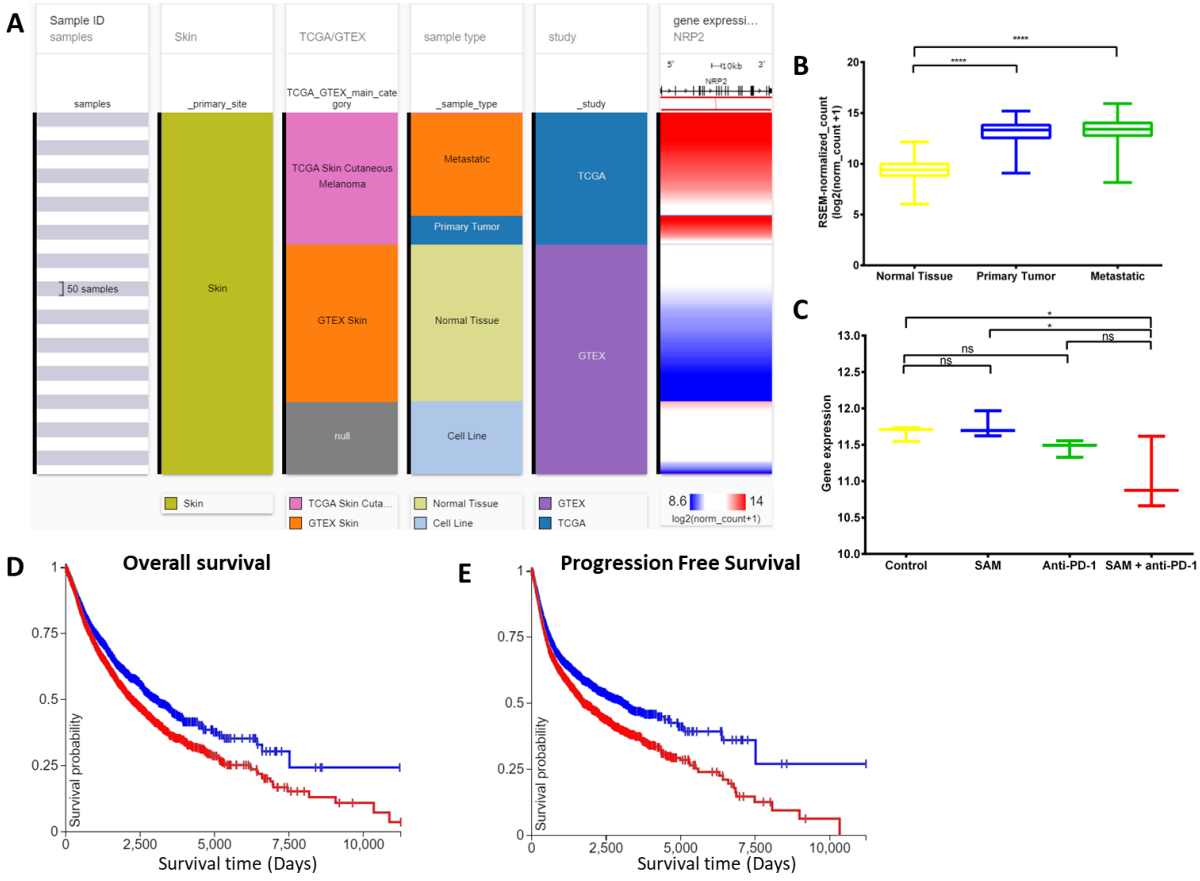

Figure 4: Analysis of *NRP2* gene expression in clinical public data. **(A)** Expression of *NRP2* gene in human healthy and skin cutaneous melanoma patients of GTEx and TCGA databases respectively. The columns show various phenotypic categories applied in order to stratify samples according to Sample Id, Skin (true), TCGA/GTEX, sample type (normal tissue, primary tumor, metastatic tissue or cell line) and study. The last column shows gene expression of *NRP2* of samples stratified according to the previous columns. Each row contains data from a single sample. **(B)** The expression data of *NRP2* in the normal tissue, primary tumor, metastatic tissue samples in **(A)** has been plotted in a Box-plot graph (n=1024 samples). Expression values are in RSEM (RNA-Seq by Expectation Maximization). **(C)** The expression data of *Nrp2* from RNA-sequencing of the primary B16 tumors after treatment with SAM, Anti-PD-1 and combination in this study (n =12; 3/group). Expression values are DeSEq2 normalized counts. **(D-E)** Overall survival and progression-free survival Kaplan Meier curves of *NRP2* from RNA-seq of GTEx and

TCGA databases; X-axis: survival time (days); Y-axis: survival probability. **(D)** Low (blue) n= 4504; High (red) n = 5930; *P* = ****. **(E)** Low (blue) n= 4346; High (red) n = 5926; *P* = ****. Statistical significance was obtained by ANOVA in GraphPad prism and are represented by asterisks (ns, not significant; *$P < 0.05$; **$P < 0.01$, ***$P < 0.001$ and ****$P < 0.0001$). All the data and Figures, except **(C)**, were generated using The UCSC Xena platform (Mary Goldman, 2019).

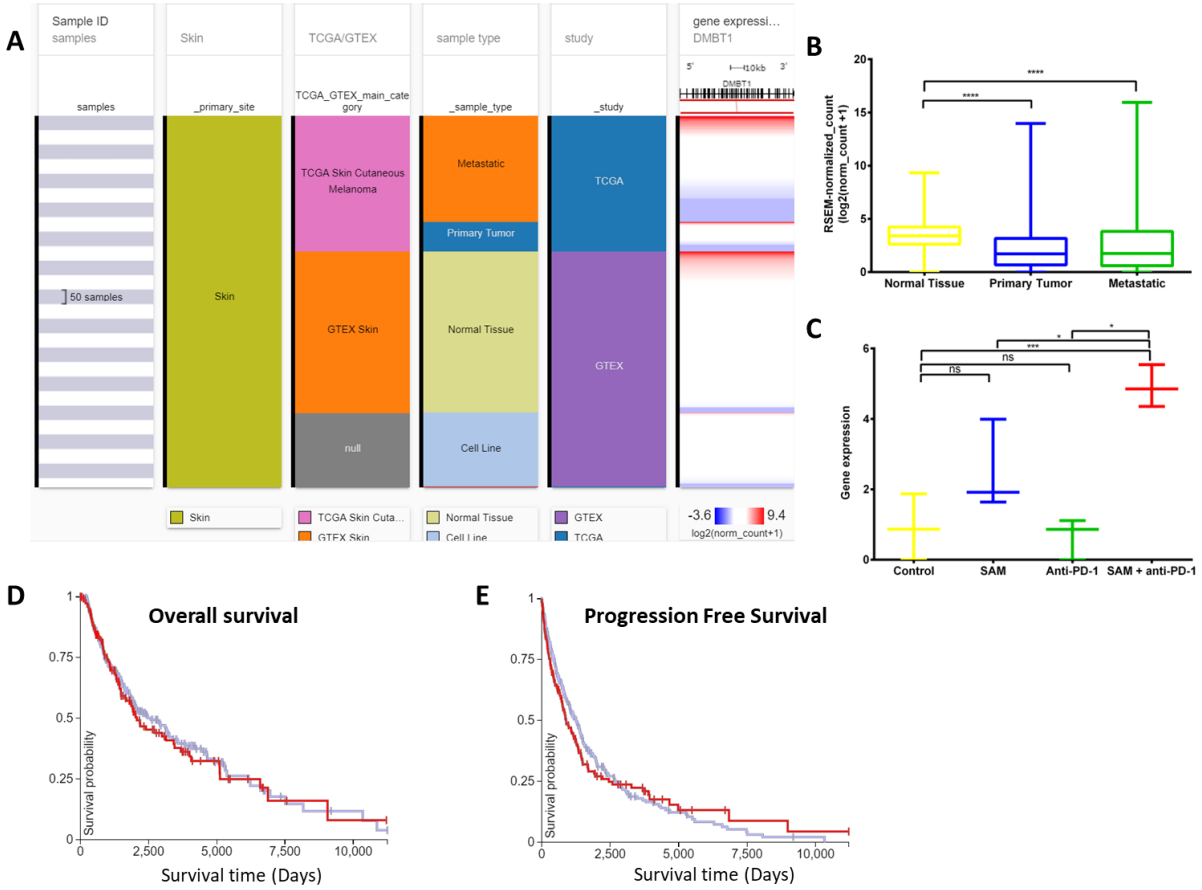

Figure 5: Analysis of *DMBT1* gene expression in clinical public data. (A) Expression of *DMBT1* gene in human healthy and skin cutaneous melanoma patients of GTEx and TCGA databases respectively. The columns show various phenotypic categories applied in order to stratify samples according to Sample Id, Skin (true), TCGA/GTEX, sample type (normal tissue, primary tumor, metastatic tissue or cell line) and study. The last column shows gene expression of *DMBT1* of samples stratified according to the previous columns. Each row contains data from a

single sample. **(B)** The expression data of *DMBT1* in the normal tissue, primary tumor, metastatic tissue samples in (A) has been plotted in a Box-plot graph (n=1024 samples). Expression values are in RSEM (RNA-Seq by Expectation Maximization). **(C)** The expression data of *Dmbt1* from RNA-sequencing of the primary B16 tumors after treatment with SAM, Anti-PD-1 and combination in this study (n =12; 3/group). Expression values are DeSEq2 normalized counts. **(D-E)** Overall survival and progression-free survival Kaplan Meier curves of *DMBT1* from RNA-seq of GTEx and TCGA databases; X-axis: survival time (days); Y-axis: survival probability. **(D)** Low (blue) n= 302; High (red) n = 153; *P* = ns **(E)** Low (blue) n= 302; High (red) n = 154; *P* = ns. Statistical significance was obtained by ANOVA in GraphPad prism and are represented by asterisks (ns, not significant; **P < 0.05; **P < 0.01, ***P < 0.001 and ****P < 0.0001*). All the data and Figures, except (C), were generated using The UCSC Xena platform (Mary Goldman, 2019).

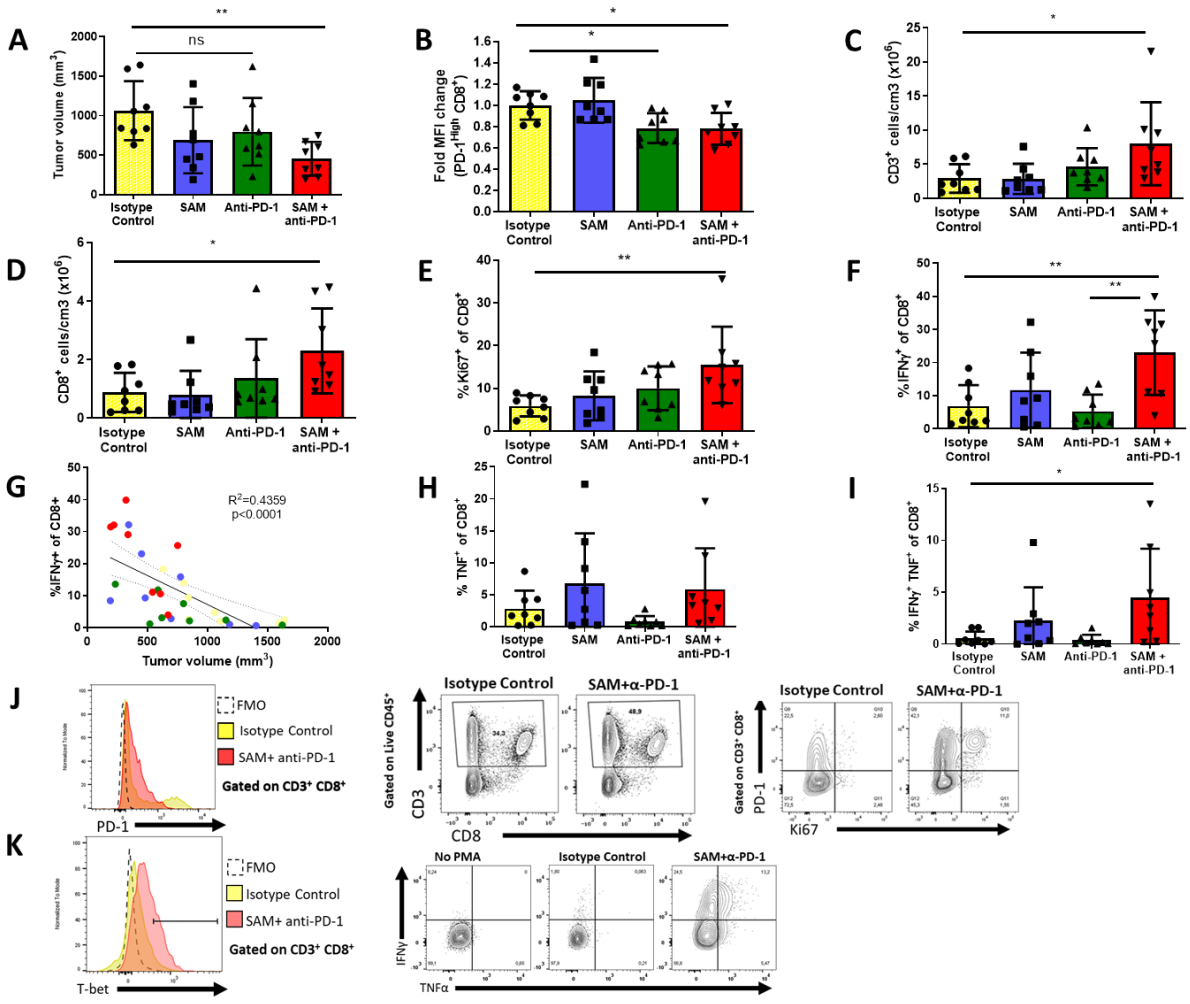

Figure 6: Effect of SAM, anti-PD-1 and SAM+anti-PD-1 on immune responses in the tumor micro-environment as determined by tumor immune-phenotyping using flow cytometry. B16-F1 tumor-inoculated mice were treated with control IgG alone (control), SAM (SAM), anti-PD-1 antibody and SAM+anti-PD-1 antibody and mice were sacrificed at day 14 and subjected to immune-phenotyping as described in "Materials and Methods". **(A)** Tumor volume was measured at day 14 and results are representative of mean ± SEM (n=8 mice per group from 2 independent experiments). **(B)** Fold change mean fluorescence intensity (MFI) of CD8+ T cells expressing high levels of PD-1. **(C and D)** Number of $CD3^+$ and $CD8^+$ cells per cm^3 of tumor tissue, respectively. (**E-F, H-I**) Percentage of $Ki67^+$, IFN-γ^+, $TNF\alpha^+$, and IFN-γ^+ and $TNF\alpha^+$ T cells, respectively, in all the groups tested. **(G)** Correlation analysis of percentage (%) of IFN-γ^+ $CD8^+$ T cells against tumor volume (mm^3) of all the mouse in the 4 groups tested. **(J)** Representative flow plots for expression of CD3, CD8 (middle), PD-1 (left) and Ki67 (right) in tumor-infiltrating lymphocytes.

Fluorescence Minus One (FMO) was used as technical control to determine gates. **(K)** Representative flow plots for expression of T-bet, IFNγ and TNFα after PMA/Ionomycin stimulation. No PMA stimulation is shown as a biological control. Statistical significance was obtained by ANOVA in GraphPad prism and are represented by asterisks (*$P < 0.05$; **$P < 0.01$, and ***$P < 0.001$).

Tables (Chapter Three)

Table 1: Representative key pathways down-regulated as revealed from gene enrichment analysis using Consensus PathDB on down-regulated genes from RNA-sequencing analysis of primary B16-F1 tumors treated with SAM+anti-PD-1 compared to Control.

	Pathway name	**p-value**
Cancer	NRAGE signals death through JNK	3.49E-08
	Cell death signalling via NRAGE, NRIF and NADE	3.17E-07
	PTEN Regulation	1.54E-05
	Death Receptor Signalling	2.80E-05
	Regulation of TP53 Activity through Acetylation	3.30E-05
	mTOR signaling pathway - Mus musculus (mouse)	0.000778
	ErbB signaling pathway - Mus musculus (mouse)	0.00285
	Endometrial cancer - Mus musculus (mouse)	0.011
	Colorectal cancer - Mus musculus (mouse)	0.0121
	Androgen Receptor Signaling Pathway	0.0194
	Breast cancer - Mus musculus (mouse)	0.0225
	Hepatocellular carcinoma - Mus musculus (mouse)	0.0302
	Glioma - Mus musculus (mouse)	0.0304
	Beta-catenin phosphorylation cascade	0.0385
	Wnt Signaling Pathway	0.041
	Pathways in cancer - Mus musculus (mouse)	0.0435
Cell Cycle	Cell Cycle	9.37E-06

	Cell Cycle, Mitotic	0.000257
	Mitotic Prometaphase	0.000265
	M Phase	0.000639
	Cell Cycle Checkpoints	0.0113
	G2/M Checkpoints	0.0378
	G2/M Transition	0.0181
	Mitotic G2-G2/M phases	0.0201
DNA repair	SUMOylation of DNA damage response and repair proteins	0.00163
	Homology Directed Repair	0.00217
	DNA Double-Strand Break Repair	0.00652
	DNA Repair	0.00793
	HDR through Single Strand Annealing (SSA)	0.0135
	HDR through Homologous Recombination (HR) or Single Strand Annealing (SSA)	0.0138
	HDR through Homologous Recombination (HRR)	0.0183
	Homologous DNA Pairing and Strand Exchange	0.0287
Other Cancer related pathways	Regulation of PTEN stability and activity	0.00123
	PIP3 activates AKT signaling	0.00179
	Signaling by TGF-beta Receptor Complex	0.00327
	Wnt Signaling Pathway NetPath	0.00604
	Regulation of TP53 Activity	0.00654
	MAPK1/MAPK3 signaling	0.00847
	Phosphatidylinositol signaling system - Mus musculus (mouse)	0.00854
	Transcriptional Regulation by E2F6	0.00902
	Regulation of PTEN gene transcription	0.00908
	Neurophilin interactions with VEGF and VEGFR	0.0102
	MAPK family signaling cascades	0.0115
	Antigen processing: Ubiquitination & Proteasome degradation	0.0115
	Proteoglycans in cancer - Mus musculus (mouse)	0.0133
	Transcriptional Regulation by TP53	0.0139
	RAF/MAP kinase cascade	0.014

	EGFR1 Signaling Pathway	0.0177
	AMPK signaling pathway - Mus musculus (mouse)	0.0181
	RAF activation	0.0228
	3-phosphoinositide biosynthesis	0.0228
	Signaling by EGFR	0.0236
	Signaling by TGF-beta family members	0.0329
	Regulation of PTEN localization	0.0424
	EGFR Transactivation by Gastrin	0.0424
	MAPK signaling pathway - Mus musculus (mouse)	0.0451
	Signaling by Receptor Tyrosine Kinases	0.0488

Table 2: Representative key pathways up-regulated as revealed from gene enrichment analysis using Consensus PathDB on up-regulated genes from RNA-sequencing analysis of primary B16-F1 tumors treated with SAM+anti-PD-1 group compared to Control.

	Pathway name	**p-value**
mRNA processing	mRNA Capping	7.37E-05
	mRNA processing	7.72E-15
	mRNA Splicing	5.75E-13
	mRNA Splicing - Major Pathway	2.69E-11
	mRNA Splicing - Minor Pathway	2.82E-09
	Metabolism of RNA	5.73E-09
	Spliceosome - Mus musculus (mouse)	2.02E-14
Translation	Ribosome - Mus musculus (mouse)	6.14E-93
	Eukaryotic Translation Initiation	9.34E-33
	Translation initiation complex formation	1.58E-32
	Metabolism of proteins	2.54E-11
	Proteasome - Mus musculus (mouse)	1.19E-07
	Proteasome Degradation	3.82E-06
	Protein export - Mus musculus (mouse)	7.37E-05

	Targeted protein degradation	1.38E-05
Metabolism	Oxidative phosphorylation - Mus musculus (mouse)	6.80E-44
	Electron Transport Chain	5.74E-43
	Translation	5.58E-42
	aerobic respiration -- electron donor II	6.63E-39
	Respiratory electron transport, ATP synthesis by chemiosmotic coupling, and heat production by uncoupling proteins.	3.88E-31
	NADH to cytochrome bo oxidase electron transfer	5.26E-29
	NADH to cytochrome bd oxidase electron transfer	5.26E-29
	Oxidative phosphorylation	2.89E-26
	Respiratory electron transport	1.18E-24
	The citric acid (TCA) cycle and respiratory electron transport	2.20E-23
	Oxidative Stress	0.000601
Transcription	RNA polymerase - Mus musculus (mouse)	7.58E-06
	RNA Polymerase I Chain Elongation	9.40E-05
	RNA Polymerase I Promoter Escape	0.000119
	RNA Polymerase I Transcription Termination	0.000148
	RNA Polymerase II Promoter Escape	0.000294
	RNA Polymerase II Transcription Initiation And Promoter Clearance	0.000344
	RNA Polymerase II Transcription Pre-Initiation And Promoter Opening	0.000344
	RNA Polymerase II Transcription Initiation	0.000344
	RNA Polymerase III Transcription Initiation From Type 1 Promoter	0.000601
	RNA Polymerase III Transcription Initiation From Type 3 Promoter	0.000601
	Eukaryotic Transcription Initiation	0.000776
	RNA transport - Mus musculus (mouse)	0.000779
	RNA Polymerase II Transcription Elongation	0.00134
	Formation of RNA Pol II elongation complex	0.00134

RNA Polymerase I Transcription Initiation	0.0016
RNA Polymerase III Transcription Initiation	0.00239
RNA Polymerase III Transcription	0.00239
RNA Polymerase II Pre-transcription Events	0.00341
RNA Polymerase I Promoter Clearance	0.00857
RNA Polymerase I Transcription	0.00913
Gene Silencing by RNA	0.0131
RNA Polymerase II Transcription Termination	0.0137
mRNA 3,-end processing	0.0262
RNA degradation - Mus musculus (mouse)	0.0419

Declarations and other statements

Conflict of interests

MS is the founder of HKG Epitherapeutics and Montreal EpiTerapia. All other authors declare no potential conflicts of interest.

Authors' contributions

SAR, MS and AM conceived the study and experimental design. AM and AA carried out various experimental procedures and immunophenotyping was done by AM, AA, NM, MA and data analysis was carried out by AM and MA. Manuscript was written by AM, SAR, MS, MA and CP. All authors read and approved the final manuscript.

Data availability

All relevant data generated or analyzed are available within the main article and the supplementary files. The raw data of this study can be provided upon request. The RNA-seq raw data has been deposited in Sequence Read Archive (SRA) database with the accession number, PRJNA613336.

Funding and Acknowledgements

This work was supported by a grant from the Canadian Institutes for Health Research (MOP 130410) to SAR. and MS. AM is the recipient of Queen Elizabeth II scholarship.

Contribution to the Field

Melanoma causes one of the highest morbidity and mortality rates amongst other cancers especially in advanced stages where treatment options are very limited. A major pathway through which melanoma tumors grow and progress involves binding of Programmed death ligand 1 (PD-L1), expressed on the surface of melanoma cells, on to its receptor Programmed cell death 1 (PD-1), a co-inhibitory surface checkpoint receptor on T cells making T cells non-functional. Immune checkpoint inhibitors (ICPi) such as anti-PD-1 that target the PD-1/PD-L1 pathway have been approved for advanced melanoma, however, around one-third of patients fail to respond to ICPi. This study provides first evidence of S-adenosylmethionine (SAM) and SAM's combination with anti-PD-1 that lead to enhanced anti-melanoma effects through alterations of key cancer genes/pathways, and a greater immune response in an aggressive advanced stage mouse melanoma model. Both anti-PD-1 and SAM are approved agents with long term safety profiles accelerating their clinical translation potentially benefiting patients with melanoma.

List of abbreviations

SAM/SAMe: s-adenosylmethionine
PD-1: Programmed cell death 1
PD-L1: Programmed death ligand 1
ICPi: Immune checkpoint inhibitors
r-PD-1: Recombinant PD-1
DEGs: Differentially expressed genes
MAPK: Mitogen-activated protein kinase
CD: Cluster of differentiation
RT-qPCR: reverse transcriptase quantitative real-time PCR
PMA: Phorbol 12-myristate 13-acetate
MFI: Mean fluorescence intensity
FMO: Fluorescence Minus One

DMBT1: Deleted in malignant brain tumors 1

NRP2: Neuropilin 2

TSG: Tumor suppressor gene

TILs: Tumor infiltrating lymphocytes

IFNγ: Interferon-gamma

TNFα: Tumor necrosis factor alpha

TCR: T cell receptor

MHC I: Major histocompatibility complex

References

Alsaab, H.O., Sau, S., Alzhrani, R., Tatiparti, K., Bhise, K., Kashaw, S.K., and Iyer, A.K. (2017). PD-1 and PD-L1 Checkpoint Signaling Inhibition for Cancer Immunotherapy: Mechanism, Combinations, and Clinical Outcome. *Front Pharmacol* 8**,** 561.

Bertrand, F., Montfort, A., Marcheteau, E., Imbert, C., Gilhodes, J., Filleron, T., Rochaix, P., Andrieu-Abadie, N., Levade, T., Meyer, N., Colacios, C., and Segui, B. (2017). TNFalpha blockade overcomes resistance to anti-PD-1 in experimental melanoma. *Nat Commun* 8**,** 2256.

Black, M., Barsoum, I.B., Truesdell, P., Cotechini, T., Macdonald-Goodfellow, S.K., Petroff, M., Siemens, D.R., Koti, M., Craig, A.W., and Graham, C.H. (2016). Activation of the PD-1/PD-L1 immune checkpoint confers tumor cell chemoresistance associated with increased metastasis. *Oncotarget* 7**,** 10557-10567.

Bottiglieri, T. (2002). S-Adenosyl-L-methionine (SAMe): from the bench to the bedside--molecular basis of a pleiotrophic molecule. *Am J Clin Nutr* 76**,** 1151s-1157s.

Cerami, E., Gao, J., Dogrusoz, U., Gross, B.E., Sumer, S.O., Aksoy, B.A., Jacobsen, A., Byrne, C.J., Heuer, M.L., Larsson, E., Antipin, Y., Reva, B., Goldberg, A.P., Sander, C., and Schultz, N. (2012). The cBio cancer genomics portal: an open platform for exploring multidimensional cancer genomics data. *Cancer Discov* 2**,** 401-404.

Chiappinelli, K.B., Zahnow, C.A., Ahuja, N., and Baylin, S.B. (2016). Combining Epigenetic and Immunotherapy to Combat Cancer. *Cancer Res* 76**,** 1683-1689.

Cossarizza, A., Chang, H.D., Radbruch, A., Acs, A., Adam, D., Adam-Klages, S., Agace, W.W., Aghaeepour, N., Akdis, M., Allez, M., Almeida, L.N., Alvisi, G., Anderson, G., Andra, I., Annunziato, F., Anselmo, A., Bacher, P., Baldari, C.T., Bari, S., Barnaba, V., Barros-Martins, J., Battistini, L., Bauer, W., Baumgart, S., Baumgarth, N., Baumjohann, D., Baying, B., Bebawy, M., Becher, B., Beisker, W., Benes, V., Beyaert, R., Blanco, A., Boardman, D.A., Bogdan, C., Borger, J.G., Borsellino, G., Boulais, P.E., Bradford, J.A., Brenner, D., Brinkman, R.R., Brooks, A.E.S., Busch, D.H., Buscher, M., Bushnell, T.P., Calzetti, F., Cameron, G., Cammarata, I., Cao, X., Cardell, S.L., Casola, S., Cassatella, M.A., Cavani, A., Celada, A., Chatenoud, L., Chattopadhyay, P.K., Chow, S., Christakou, E., Cicin-Sain, L., Clerici, M., Colombo, F.S., Cook, L., Cooke, A., Cooper, A.M., Corbett, A.J., Cosma, A., Cosmi, L., Coulie, P.G., Cumano, A., Cvetkovic, L., Dang, V.D., Dang-Heine, C., Davey, M.S., Davies, D., De Biasi, S., Del Zotto, G., Dela Cruz, G.V., Delacher, M., Della Bella, S., Dellabona, P., Deniz, G., Dessing, M., Di Santo, J.P., Diefenbach, A., Dieli, F., Dolf, A., Dorner, T., Dress, R.J., Dudziak, D., Dustin, M., Dutertre, C.A., Ebner, F., Eckle, S.B.G., Edinger, M., Eede, P., Ehrhardt, G.R.A., Eich, M., Engel, P., Engelhardt, B., Erdei, A., et al. (2019). Guidelines for the use of flow cytometry and cell sorting in immunological studies (second edition). *Eur J Immunol* 49**,** 1457-1973.

Curran, M.A., Montalvo, W., Yagita, H., and Allison, J.P. (2010). PD-1 and CTLA-4 combination blockade expands infiltrating T cells and reduces regulatory T and myeloid cells within B16 melanoma tumors. *Proc Natl Acad Sci U S A* 107**,** 4275-4280.

D'alterio, C., Buoncervello, M., Ierano, C., Napolitano, M., Portella, L., Rea, G., Barbieri, A., Luciano, A., Scognamiglio, G., Tatangelo, F., Anniciello, A.M., Monaco, M., Cavalcanti, E., Maiolino, P., Romagnoli, G., Arra, C., Botti, G., Gabriele, L., and Scala, S. (2019). Targeting CXCR4 potentiates anti-PD-1 efficacy modifying the tumor microenvironment and inhibiting neoplastic PD-1. *J Exp Clin Cancer Res* 38**,** 432.

Daneshmandi, S., Wegiel, B., and Seth, P. (2019). Blockade of Lactate Dehydrogenase-A (LDH-A) Improves Efficacy of Anti-Programmed Cell Death-1 (PD-1) Therapy in Melanoma. *Cancers (Basel)* 11.

Dong, H., Strome, S.E., Salomao, D.R., Tamura, H., Hirano, F., Flies, D.B., Roche, P.C., Lu, J., Zhu, G., Tamada, K., Lennon, V.A., Celis, E., and Chen, L. (2002). Tumor-associated B7-

H1 promotes T-cell apoptosis: a potential mechanism of immune evasion. *Nat Med* 8**,** 793-800.

Dong, P., Xiong, Y., Yue, J., Hanley, S.J.B., and Watari, H. (2018). Tumor-Intrinsic PD-L1 Signaling in Cancer Initiation, Development and Treatment: Beyond Immune Evasion. *Front Oncol* 8.

Dunn, J., and Rao, S. (2017). Epigenetics and immunotherapy: The current state of play. *Mol Immunol* 87**,** 227-239.

Ehrlich, M. (2009). DNA hypomethylation in cancer cells. *Epigenomics* 1**,** 239-259.

Escors, D., Gato-Cañas, M., Zuazo, M., Arasanz, H., García-Granda, M.J., Vera, R., and Kochan, G. (2018). The intracellular signalosome of PD-L1 in cancer cells. *Signal Transduct Target Ther* 3.

Feinberg, A.P., and Vogelstein, B. (1983). Hypomethylation distinguishes genes of some human cancers from their normal counterparts. *Nature* 301**,** 89-92.

Han, X., Wang, Y., Sun, J., Tan, T., Cai, X., Lin, P., Tan, Y., Zheng, B., Wang, B., Wang, J., Xu, L., Yu, Z., Xu, Q., Wu, X., and Gu, Y. (2019). Role of CXCR3 signaling in response to anti-PD-1 therapy. *EBioMedicine* 48**,** 169-177.

Hote, P.T., Sahoo, R., Jani, T.S., Ghare, S.S., Chen, T., Joshi-Barve, S., Mcclain, C.J., and Barve, S.S. (2008). Ethanol inhibits methionine adenosyltransferase II activity and S-adenosylmethionine biosynthesis and enhances caspase-3-dependent cell death in T lymphocytes: relevance to alcohol-induced immunosuppression. *J Nutr Biochem* 19**,** 384-391.

Kamburov, A., Pentchev, K., Galicka, H., Wierling, C., Lehrach, H., and Herwig, R. (2011). ConsensusPathDB: toward a more complete picture of cell biology. *Nucleic Acids Res* 39**,** D712-717.

Kuzu, O.F., Nguyen, F.D., Noory, M.A., and Sharma, A. (2015). Current State of Animal (Mouse) Modeling in Melanoma Research. *Cancer Growth Metastasis* 8**,** 81-94.

Larkins, E., Blumenthal, G.M., Yuan, W., He, K., Sridhara, R., Subramaniam, S., Zhao, H., Liu, C., Yu, J., Goldberg, K.B., Mckee, A.E., Keegan, P., and Pazdur, R. (2017). FDA Approval Summary: Pembrolizumab for the Treatment of Recurrent or Metastatic Head and Neck Squamous Cell Carcinoma with Disease Progression on or After Platinum-Containing Chemotherapy. *Oncologist* 22**,** 873-878.

Legros, H.L., Jr., Geller, A.M., and Kotb, M. (1997). Differential regulation of methionine adenosyltransferase in superantigen and mitogen stimulated human T lymphocytes. *J Biol Chem* 272**,** 16040-16047.

Li, T.W., Yang, H., Peng, H., Xia, M., Mato, J.M., and Lu, S.C. (2012). Effects of S-adenosylmethionine and methylthioadenosine on inflammation-induced colon cancer in mice. *Carcinogenesis* 33**,** 427-435.

Love, M.I., Huber, W., and Anders, S. (2014). Moderated estimation of fold change and dispersion for RNA-seq data with DESeq2. *Genome Biol* 15**,** 550.

Mahmood, N., Cheishvili, D., Arakelian, A., Tanvir, I., Khan, H.A., Pepin, A.S., Szyf, M., and Rabbani, S.A. (2018). Methyl donor S-adenosylmethionine (SAM) supplementation attenuates breast cancer growth, invasion, and metastasis in vivo; therapeutic and chemopreventive applications. *Oncotarget* 9**,** 5169-5183.

Mahmood, N., and Rabbani, S.A. (2019). Targeting DNA Hypomethylation in Malignancy by Epigenetic Therapies. *Adv Exp Med Biol* 1164**,** 179-196.

Mary Goldman, B.C., Mim Hastie, Kristupas Repečka, Akhil Kamath, Fran Mcdade, Dave Rogers, Angela N Brooks, Jingchun Zhu, David Haussler (2019). The UCSC Xena platform for public and private cancer genomics data visualization and interpretation. *bioRxiv* 326470.

Mollenhauer, J., Herbertz, S., Holmskov, U., Tolnay, M., Krebs, I., Merlo, A., Schroder, H.D., Maier, D., Breitling, F., Wiemann, S., Grone, H.J., and Poustka, A. (2000). DMBT1 encodes a protein involved in the immune defense and in epithelial differentiation and is highly unstable in cancer. *Cancer Res* 60**,** 1704-1710.

Moriarty, W.F., Kim, E., Gerber, S.A., Hammers, H., and Alani, R.M. (2016). Neuropilin-2 promotes melanoma growth and progression in vivo. *Melanoma Res* 26**,** 321-328.

Moynihan, K.D., Opel, C.F., Szeto, G.L., Tzeng, A., Zhu, E.F., Engreitz, J.M., Williams, R.T., Rakhra, K., Zhang, M.H., Rothschilds, A.M., Kumari, S., Kelly, R.L., Kwan, B.H., Abraham, W., Hu, K., Mehta, N.K., Kauke, M.J., Suh, H., Cochran, J.R., Lauffenburger, D.A., Wittrup, K.D., and Irvine, D.J. (2016). Eradication of large established tumors in mice by combination immunotherapy that engages innate and adaptive immune responses. *Nat Med* 22**,** 1402-1410.

Naidoo, J., Page, D.B., Li, B.T., Connell, L.C., Schindler, K., Lacouture, M.E., Postow, M.A., and Wolchok, J.D. (2015). Toxicities of the anti-PD-1 and anti-PD-L1 immune checkpoint antibodies. *Ann Oncol* 26**,** 2375-2391.

Network, T.C.G.A. (2015). Genomic Classification of Cutaneous Melanoma. *Cell* 161**,** 1681-1696.

Ordikhani, F., Uehara, M., Kasinath, V., Dai, L., Eskandari, S.K., Bahmani, B., Yonar, M., Azzi, J.R., Haik, Y., Sage, P.T., Murphy, G.F., Annabi, N., Schatton, T., Guleria, I., and Abdi, R. (2018). Targeting antigen-presenting cells by anti-PD-1 nanoparticles augments antitumor immunity. *JCI Insight* 3.

Overwijk, W.W., and Restifo, N.P. (2001). B16 as a mouse model for human melanoma. *Curr Protoc Immunol* Chapter 20**,** Unit 20.21.

Pakneshan, P., Szyf, M., Farias-Eisner, R., and Rabbani, S.A. (2004). Reversal of the hypomethylation status of urokinase (uPA) promoter blocks breast cancer growth and metastasis. *J Biol Chem* 279**,** 31735-31744.

Parashar, S., Cheishvili, D., Arakelian, A., Hussain, Z., Tanvir, I., Khan, H.A., Szyf, M., and Rabbani, S.A. (2015). S-adenosylmethionine blocks osteosarcoma cells proliferation and invasion in vitro and tumor metastasis in vivo: therapeutic and diagnostic clinical applications. *Cancer Med* 4**,** 732-744.

Pardoll, D.M. (2012). The blockade of immune checkpoints in cancer immunotherapy. *Nature Reviews Cancer* 12**,** 252.

Rajani, K., Parrish, C., Kottke, T., Thompson, J., Zaidi, S., Ilett, L., Shim, K.G., Diaz, R.M., Pandha, H., Harrington, K., Coffey, M., Melcher, A., and Vile, R. (2016). Combination Therapy With Reovirus and Anti-PD-1 Blockade Controls Tumor Growth Through Innate and Adaptive Immune Responses. *Mol Ther* 24**,** 166-174.

Rastelli, L., Valentino, M.L., Minderman, M.C., Landin, J., Malyankar, U.M., Lescoe, M.K., Kitson, R., Brunson, K., Souan, L., Forenza, S., Goldfarb, R.H., and Rabbani, S.A. (2011). A KDR-binding peptide (ST100,059) can block angiogenesis, melanoma tumor growth and metastasis in vitro and in vivo. *Int J Oncol* 39**,** 401-408.

Rushing, E.C., Stine, M.J., Hahn, S.J., Shea, S., Eller, M.S., Naif, A., Khanna, S., Westra, W.H., Jungbluth, A.A., Busam, K.J., Mahalingam, M., and Alani, R.M. (2012). Neuropilin-2: a novel biomarker for malignant melanoma? *Hum Pathol* 43**,** 381-389.

Sahin, M., Sahin, E., Gumuslu, S., Erdogan, A., and Gultekin, M. (2011). Inhibition of angiogenesis by S-adenosylmethionine. *Biochem Biophys Res Commun* 408**,** 145-148.

Sang, Y., and Deng, Y. (2019). Current insights into the epigenetic mechanisms of skin cancer. *Dermatol Ther* 32**,** e12964.

Schadendorf, D., Van Akkooi, A.C.J., Berking, C., Griewank, K.G., Gutzmer, R., Hauschild, A., Stang, A., Roesch, A., and Ugurel, S. (2018). Melanoma. *Lancet* 392**,** 971-984.

Sheppard, K.A., Fitz, L.J., Lee, J.M., Benander, C., George, J.A., Wooters, J., Qiu, Y., Jussif, J.M., Carter, L.L., Wood, C.R., and Chaudhary, D. (2004). PD-1 inhibits T-cell receptor induced phosphorylation of the ZAP70/CD3zeta signalosome and downstream signaling to PKCtheta. *FEBS Lett* 574**,** 37-41.

Shukeir, N., Arakelian, A., Chen, G., Garde, S., Ruiz, M., Panchal, C., and Rabbani, S.A. (2004). A synthetic 15-mer peptide (PCK3145) derived from prostate secretory protein can reduce tumor growth, experimental skeletal metastases, and malignancy-associated hypercalcemia. *Cancer Res* 64**,** 5370-5377.

Shukeir, N., Stefanska, B., Parashar, S., Chik, F., Arakelian, A., Szyf, M., and Rabbani, S.A. (2015). Pharmacological methyl group donors block skeletal metastasis in vitro and in vivo. *Br J Pharmacol* 172**,** 2769-2781.

Tobena, R., Horikawa, S., Calvo, V., and Alemany, S. (1996). Interleukin-2 induces gamma-S-adenosyl-L-methionine synthetase gene expression during T-lymphocyte activation. *Biochem J* 319 (Pt 3)**,** 929-933.

Topalian, S.L., Hodi, F.S., Brahmer, J.R., Gettinger, S.N., Smith, D.C., Mcdermott, D.F., Powderly, J.D., Carvajal, R.D., Sosman, J.A., Atkins, M.B., Leming, P.D., Spigel, D.R., Antonia, S.J., Horn, L., Drake, C.G., Pardoll, D.M., Chen, L., Sharfman, W.H., Anders, R.A., Taube, J.M., Mcmiller, T.L., Xu, H., Korman, A.J., Jure-Kunkel, M., Agrawal, S., Mcdonald, D., Kollia, G.D., Gupta, A., Wigginton, J.M., and Sznol, M. (2012). Safety, activity, and immune correlates of anti-PD-1 antibody in cancer. *N Engl J Med* 366**,** 2443-2454.

Triplett, T.A., Garrison, K.C., Marshall, N., Donkor, M., Blazeck, J., Lamb, C., Qerqez, A., Dekker, J.D., Tanno, Y., Lu, W.C., Karamitros, C.S., Ford, K., Tan, B., Zhang, X.M., Mcgovern, K., Coma, S., Kumada, Y., Yamany, M.S., Sentandreu, E., Fromm, G., Tiziani, S., Schreiber, T.H., Manfredi, M., Ehrlich, L.I.R., Stone, E., and Georgiou, G. (2018).

Reversal of indoleamine 2,3-dioxygenase-mediated cancer immune suppression by systemic kynurenine depletion with a therapeutic enzyme. *Nat Biotechnol* 36**,** 758-764.

Ulanovskaya, O.A., Zuhl, A.M., and Cravatt, B.F. (2013). NNMT promotes epigenetic remodeling in cancer by creating a metabolic methylation sink. *Nat Chem Biol* 9**,** 300-306.

Wang, C., Thudium, K.B., Han, M., Wang, X.T., Huang, H., Feingersh, D., Garcia, C., Wu, Y., Kuhne, M., Srinivasan, M., Singh, S., Wong, S., Garner, N., Leblanc, H., Bunch, R.T., Blanset, D., Selby, M.J., and Korman, A.J. (2014). In vitro characterization of the anti-PD-1 antibody nivolumab, BMS-936558, and in vivo toxicology in non-human primates. *Cancer Immunol Res* 2**,** 846-856.

Wang, Y., Li, J.J., Ba, H.J., Wang, K.F., Wen, X.Z., Li, D.D., Zhu, X.F., and Zhang, X.S. (2019). Down Regulation of c-FLIPL Enhance PD-1 Blockade Efficacy in B16 Melanoma. *Front Oncol* 9**,** 857.

Wang, Y., Sun, Z., and Szyf, M. (2017). S-adenosyl-methionine (SAM) alters the transcriptome and methylome and specifically blocks growth and invasiveness of liver cancer cells. *Oncotarget* 8**,** 111866-111881.

Wimmers, F., Aarntzen, E.H., Duiveman-Deboer, T., Figdor, C.G., Jacobs, J.F., Tel, J., and De Vries, I.J. (2016). Long-lasting multifunctional CD8(+) T cell responses in end-stage melanoma patients can be induced by dendritic cell vaccination. *Oncoimmunology* 5**,** e1067745.

Zeng, Z., Yang, H., Huang, Z.Z., Chen, C., Wang, J., and Lu, S.C. (2001). The role of c-Myb in the up-regulation of methionine adenosyltransferase 2A expression in activated Jurkat cells. *Biochem J* 353**,** 163-168.

Zhang, D., Zhu, R., Zhang, H., Zheng, C.H., and Xia, J. (2015). MGDB: a comprehensive database of genes involved in melanoma. *Database (Oxford)* 2015.

Supplementary Material

Supplementary Figures

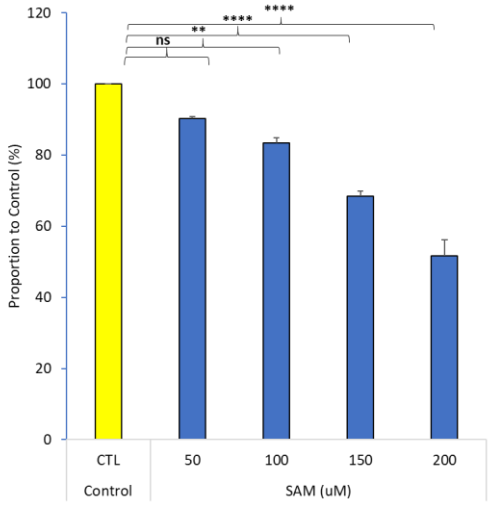

Supplementary Figure 1: SAM dose-dependent effect on B16 cells proliferation. B16 cells ($2x10^4$ cells) were seeded in 6-well plates. Proliferation is presented as the percentage of proportion to the Control ± SEM. Statistical significance was obtained by two-tailed T-test in Excel and are represented by asterisks (**P < 0.05; **P < 0.01, ***P < 0.001 and ****P < 0.0001*).

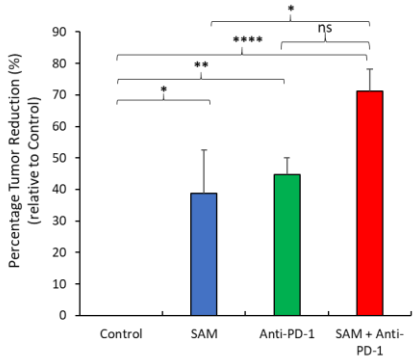

Supplementary Figure 2: Anti-tumor effect of SAM and anti-PD-1 antibody in a syngeneic mouse B16-F1 melanoma model *in vivo*. Percentage (%) of tumor weight reduction in each group relative to control at day 16. Results are representative of mean ± SEM of at least 8 mice

per group. Statistical significance was obtained by ANOVA in GraphPad prism and are represented by asterisks (*$P < 0.05$; **$P < 0.01$, ***$P < 0.001$ and ****$P < 0.0001$).

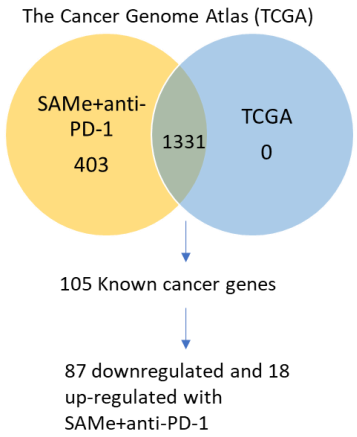

Supplementary Figure 3: The differentially expressed genes (DEGs) obtained from RNA-seq data of SAMe+anti-PD-1 group were overlapped with TCGA database of melanoma genes.

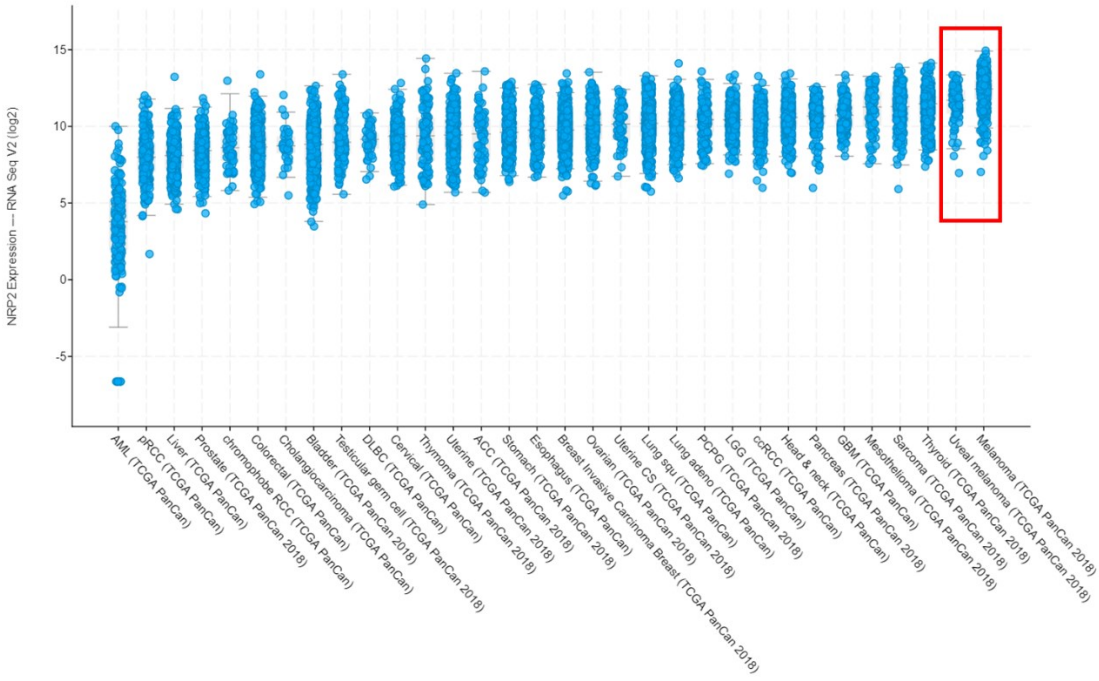

Supplementary Figure 4: Expression of *NRP2* in the TCGA Pan-Cancer Atlas. RNA Seq V2 (log2) median expression is plotted against each tumor type. The red box shows melanoma. Total number of samples are 10967 samples.

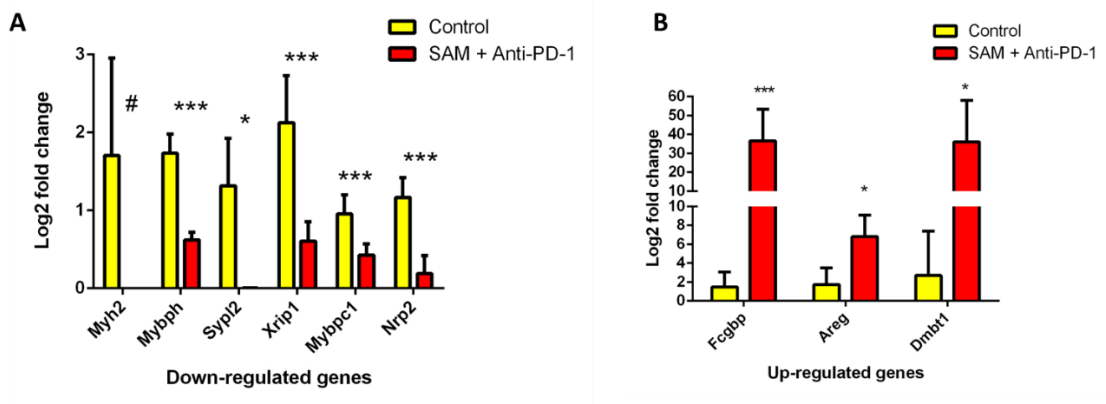

Supplementary Figure 5: Validation of top up and down regulated genes obtained from RNA-sequencing data of control and experimental B16-F1 mouse melanoma tumors. Top up- and down- regulated genes obtained from RNA sequencing analysis of SAMe+anti-PD-1 compared to control animals were validated by RT-qPCR. Results are mean of at least 2 independent experiments. Significant differences were determined using T-test and are represented by asterisks (*$P < 0.05$; **$P < 0.01$, and ***$P < 0.001$). # shows *Myh2* gene expression in the tumors of SAMe+anti-PD-1 group was undetectable.

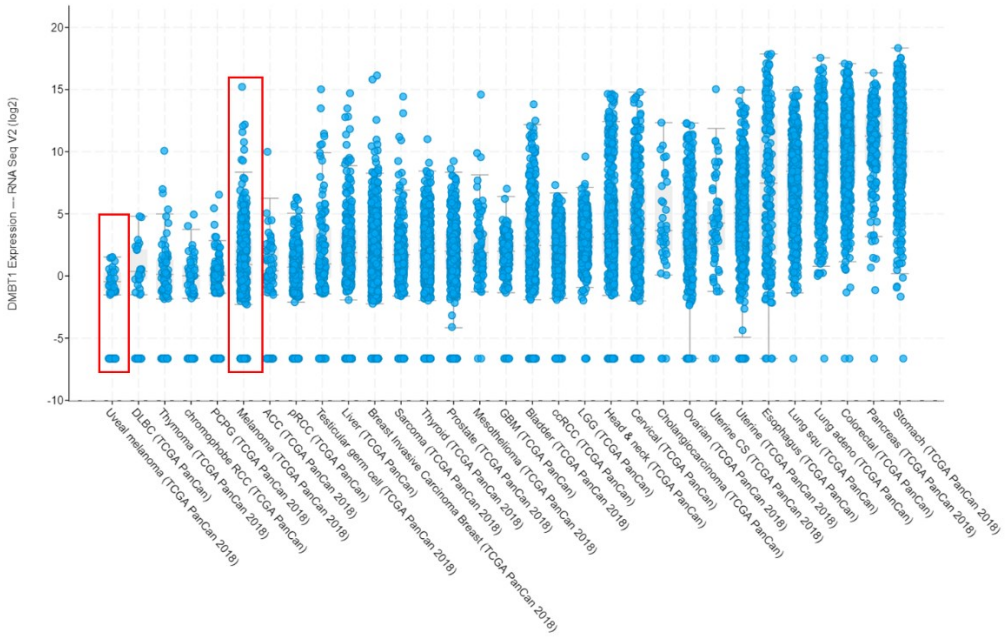

Supplementary Figure 6: Expression of *DMBT1* in the TCGA Pan-Cancer Atlas. RNA Seq V2 (log2) median expression is plotted against each tumor type. The red box shows melanoma. Total number of samples are 10967 samples.

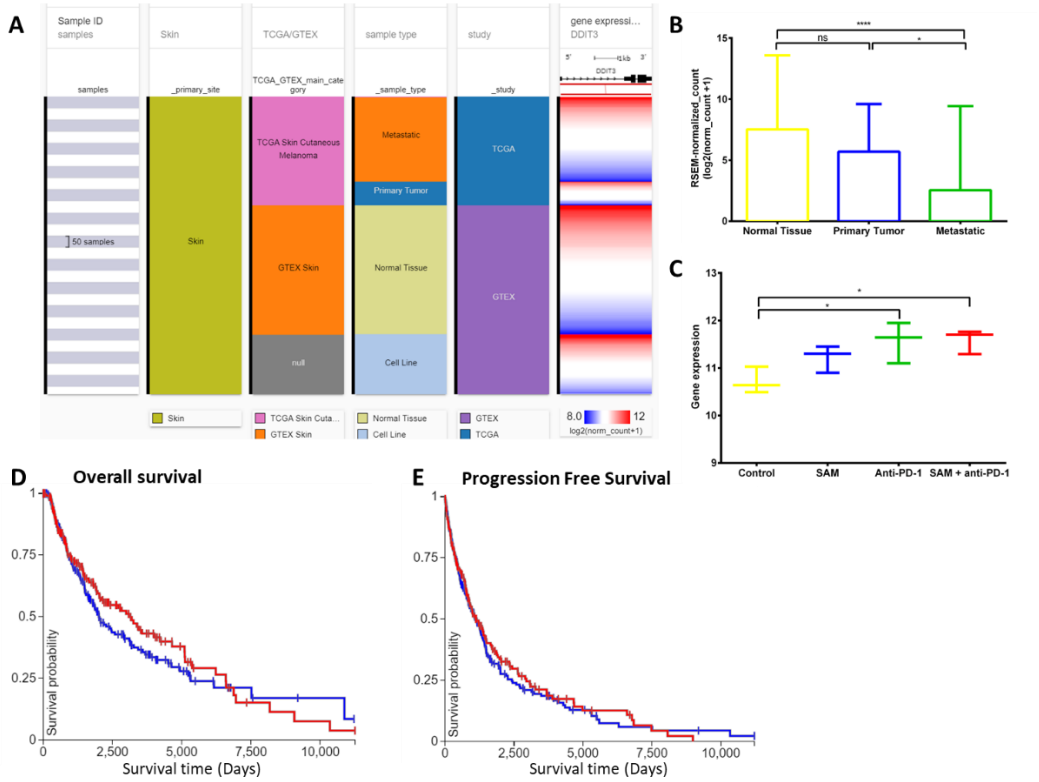

Supplementary Figure 7: Clinical data analysis of *DDIT3* gene identified from overlapping MGDB with RNA-seq data. (A) Expression of *DDIT3* gene in human healthy and skin cutaneous melanoma patients of GTEx and TCGA databases respectively. The columns show various phenotypic categories applied in order to stratify samples according to Sample Id, Skin (true), TCGA/GTEX, sample type (normal tissue, primary tumor, metastatic tissue or cell line) and study. The last column shows gene expression of *DDIT3* of samples stratified according to the previous columns. Each row contains data from a single sample. (B) The expression data of *DDIT3* in the normal tissue, primary tumor, metastatic tissue samples in (A) has been plotted in a Box-plot graph (n=1024 samples). Expression values are in RSEM (RNA-Seq by Expectation Maximization). (C) The expression data of *Ddit3* from RNA-sequencing of the primary B16 tumors after treatment with SAM, Anti-PD-1 and combination in this study (n =12; 3/group). Expression values are DeSEq2 normalized counts; X-axis: survival time (days); Y-axis: survival probability. (D-E) Overall survival and progression-free survival Kaplan Meier curves of *DDIT3* from RNA-seq of GTEx and TCGA databases. (D) Low (blue) n= 247; High (red) n = 208. (E) Low (blue) n= 248; High (red) n = 208. Statistical significance was obtained by ANOVA in GraphPad prism and are

represented by asterisks (**P < 0.05; **P < 0.01, ***P < 0.001 and ****P < 0.0001*). All the data and Supplementary Figure s, except (C), were generated using The UCSC Xena platform.

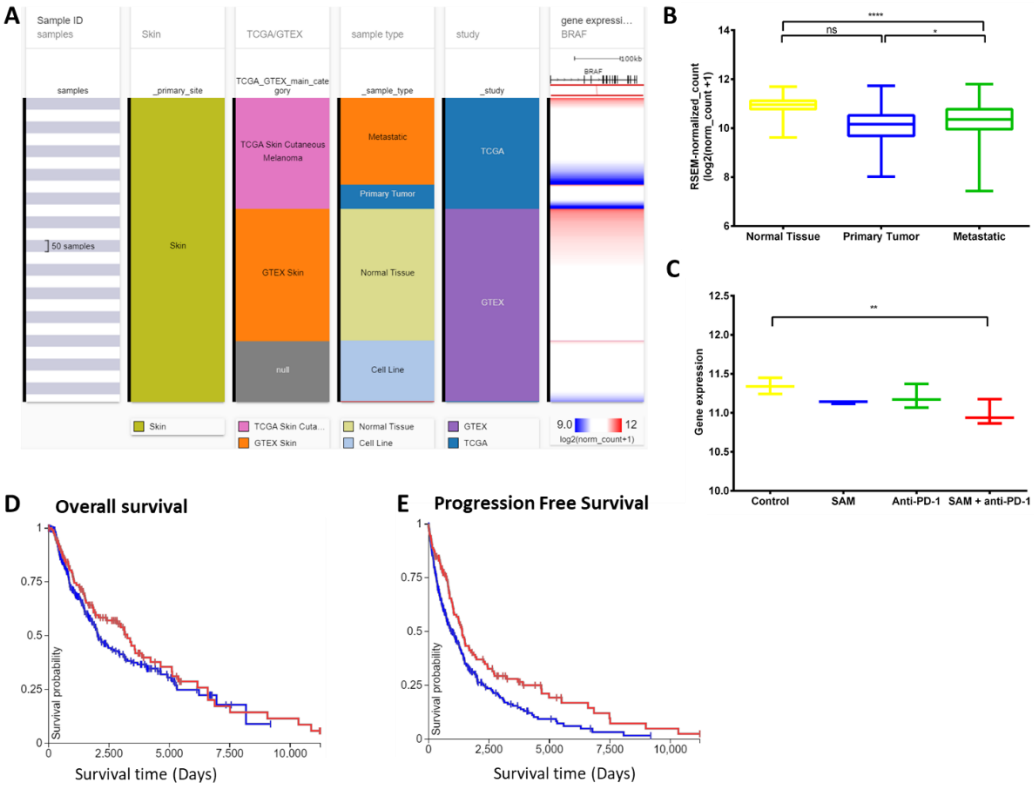

Supplementary Figure 8: Clinical data analysis of *BRAF* gene identified from overlapping MGDB with RNA-seq data. (A) Expression of *BRAF* gene in human healthy and skin cutaneous melanoma patients of GTEx and TCGA databases respectively. The columns show various phenotypic categories applied in order to stratify samples according to Sample Id, Skin (true), TCGA/GTEX, sample type (normal tissue, primary tumor, metastatic tissue or cell line) and study. The last column shows gene expression of *BRAF* of samples stratified according to the previous columns. Each row contains data from a single sample. (B) The expression data of *BRAF* in the normal tissue, primary tumor, metastatic tissue samples in (A) has been plotted in a Box-plot graph (n=1024 samples). Expression values are in RSEM (RNA-Seq by Expectation Maximization). (C) The expression data of *Braf* from RNA-sequencing of the primary B16 tumors after treatment with SAM, Anti-PD-1 and combination in this study (n =12; 3/group). Expression values are DeSEq2 normalized counts. (D-E) Overall survival and progression-free survival Kaplan Meier curves of *BRAF* from RNA-seq of GTEx and TCGA databases; X-axis: survival time (days); Y-axis:

survival probability. (D) Low (blue) n= 327; High (red) n = 128. (E) Low (blue) n= 328; High (red) n = 128; P = **. Statistical significance was obtained by ANOVA in GraphPad prism and are represented by asterisks (**P < 0.05; **P < 0.01, ***P < 0.001 and ****P < 0.0001*). All the data and Supplementary Figure s, except (C), were generated using The UCSC Xena platform.

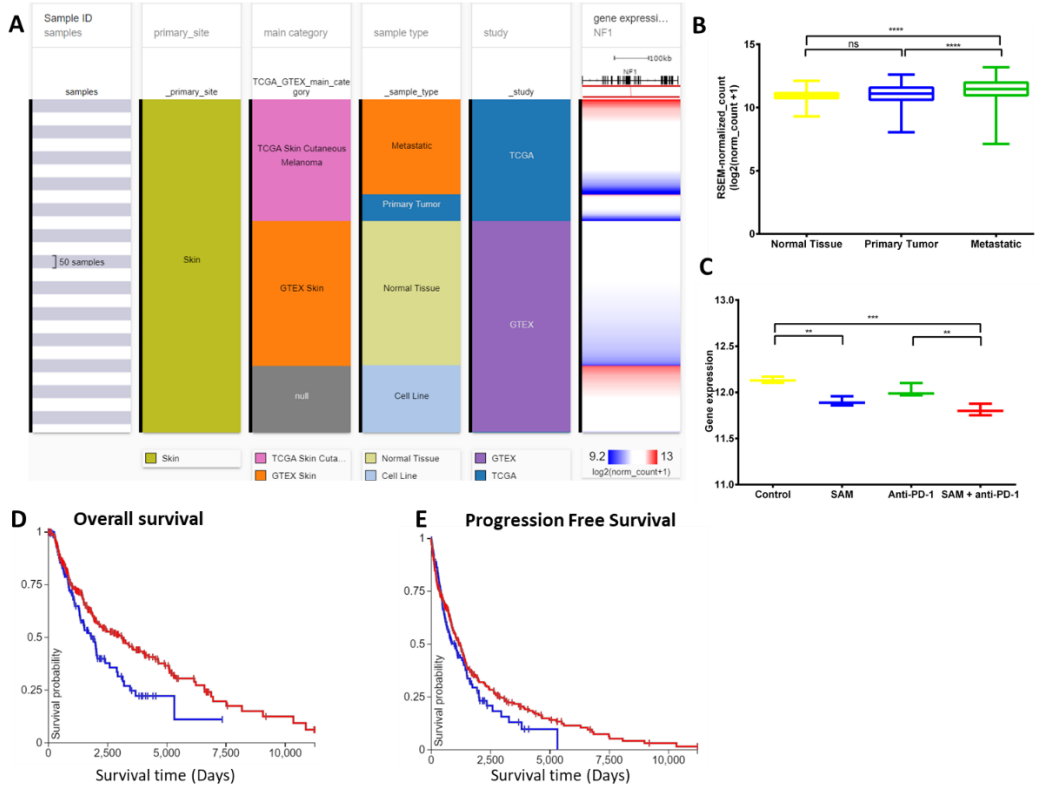

Supplementary Figure 9: Clinical data analysis of *NF1* gene identified from overlapping MGDB with RNA-seq data. (A) Expression of *NF1* gene in human healthy and skin cutaneous melanoma patients of GTEx and TCGA databases respectively. The columns show various phenotypic categories applied in order to stratify samples according to Sample Id, Skin (true), TCGA/GTEX, sample type (normal tissue, primary tumor, metastatic tissue or cell line) and study. The last column shows gene expression of *NF1* of samples stratified according to the previous columns. Each row contains data from a single sample. (B) The expression data of *NF1* in the normal tissue, primary tumor, metastatic tissue samples in (A) has been plotted in a Box-plot graph (n=1024 samples). Expression values are in RSEM (RNA-Seq by Expectation Maximization). (C) The expression data of *Nf1* from RNA-sequencing of the primary B16 tumors after treatment with SAM, Anti-PD-1 and combination in this study (n =12; 3/group). Expression values are DeSEq2

normalized counts. (D-E) Overall survival and progression-free survival Kaplan Meier curves of *NF1* from RNA-seq of GTEx and TCGA databases; X-axis: survival time (days); Y-axis: survival probability. (D) Low (blue) n= 164; High (red) n = 291; P = ****. (E) Low (blue) n= 165; High (red) n = 291. Statistical significance was obtained by ANOVA in GraphPad prism and are represented by asterisks (**P < 0.05; **P < 0.01, ***P < 0.001 and ****P < 0.0001*). All the data and Supplementary Figure s, except (C), were generated using The UCSC Xena platform.

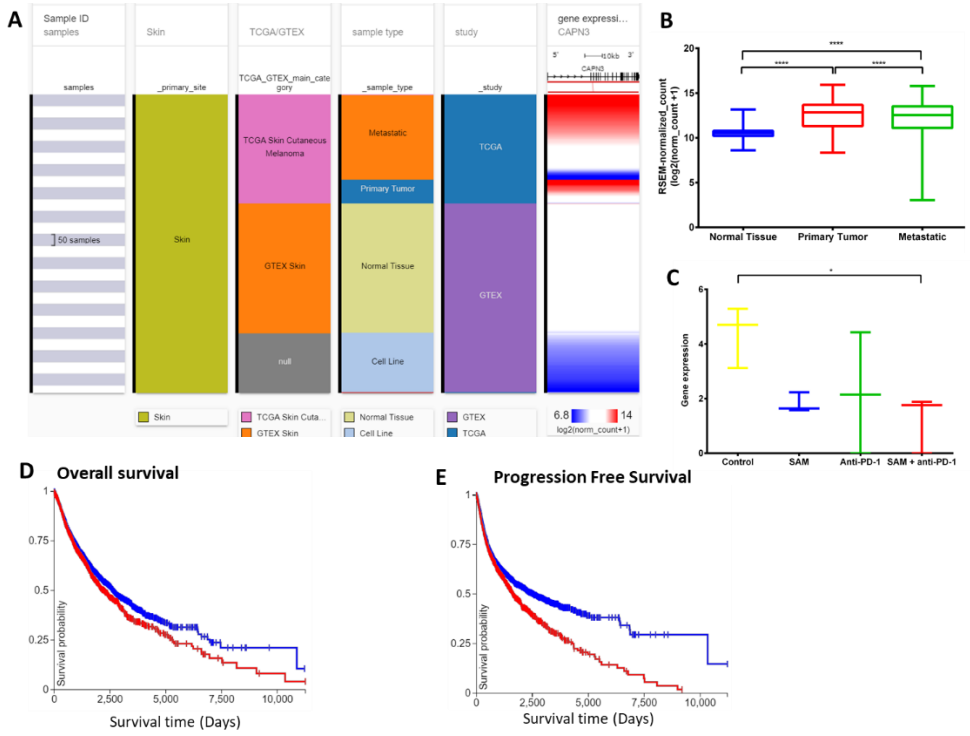

Supplementary Figure 10: Analysis of *CAPN3* gene expression in clinical public data. (A) Expression of *CAPN3* gene in human healthy and skin cutaneous melanoma patients of GTEx and TCGA databases respectively. The columns show various phenotypic categories applied in order to stratify samples according to Sample Id, Skin (true), TCGA/GTEX, sample type (normal tissue, primary tumor, metastatic tissue or cell line) and study. The last column shows gene expression of *CAPN3* of samples stratified according to the previous columns. Each row contains data from a single sample. **(B)** The expression data of *CAPN3* in the normal tissue, primary tumor, metastatic tissue samples in (A) has been plotted in a Box-plot graph (n=1024 samples). Expression values are in RSEM (RNA-Seq by Expectation Maximization). **(C)** The expression data of *Capn3* from RNA-sequencing of the primary B16 tumors after treatment with SAM, Anti-PD-1 and

combination in this study (n =12; 3/group). Expression values are DeSEq2 normalized counts. (D-E) Overall survival and progression-free survival Kaplan Meier curves of CAPN3 from RNA-seq of GTEx and TCGA databases; X-axis: survival time (days); Y-axis: survival probability. **(D)** P=****; Log-rank test statistics = 8.356; Low (blue) n= 8098; High (red) n = 2336. (E) P = ****; Log-rank test statistics = 29.36; Low (blue) n= 8054; High (red) n = 2218. Statistical significance was obtained by ANOVA in GraphPad prism and are represented by asterisks (**P < 0.05; **P < 0.01, ***P < 0.001 and ****P < 0.0001*). All the data and Supplementary Figure s, except (C), were generated using The UCSC Xena platform.

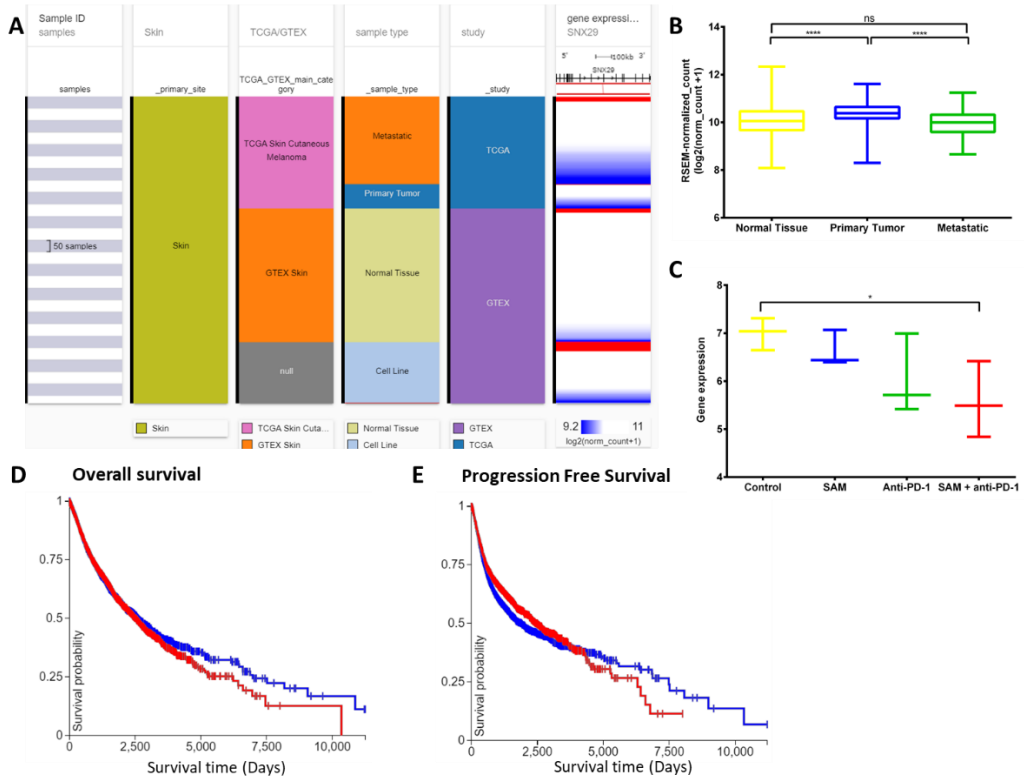

Supplementary Figure 11: Clinical data analysis of *SNX29* gene identified from overlapping TCGA with RNA-seq data. (A) Expression of *SNX29* gene in human healthy and skin cutaneous melanoma patients of GTEx and TCGA databases respectively. The columns show various phenotypic categories applied in order to stratify samples according to Sample Id, Skin (true), TCGA/GTEX, sample type (normal tissue, primary tumor, metastatic tissue or cell line) and study. The last column shows gene expression of *SNX29* of samples stratified according to the previous

columns. Each row contains data from a single sample. (B) The expression data of *SNX29* in the normal tissue, primary tumor, metastatic tissue samples in (A) has been plotted in a Box-plot graph (n=1024 samples). Expression values are in RSEM (RNA-Seq by Expectation Maximization). (C) The expression data of *Snx29* from RNA-sequencing of the primary B16 tumors after treatment with SAM, Anti-PD-1 and combination in this study (n =12; 3/group). Expression values are DeSEq2 normalized counts. (D-E) Overall survival and progression-free survival Kaplan Meier curves of *SNX29* from RNA-seq of GTEx and TCGA databases; X-axis: survival time (days); Y-axis: survival probability. (D) Low (blue) n= 5156; High (red) n = 5278. (E) Low (blue) n= 5155; High (red) n = 5117; P = ****. Statistical significance was obtained by ANOVA in GraphPad prism and are represented by asterisks (*$P < 0.05$; **$P < 0.01$, ***$P < 0.001$ and ****$P < 0.0001$). All the data and Supplementary Figure s, except (C), were generated using The UCSC Xena platform.

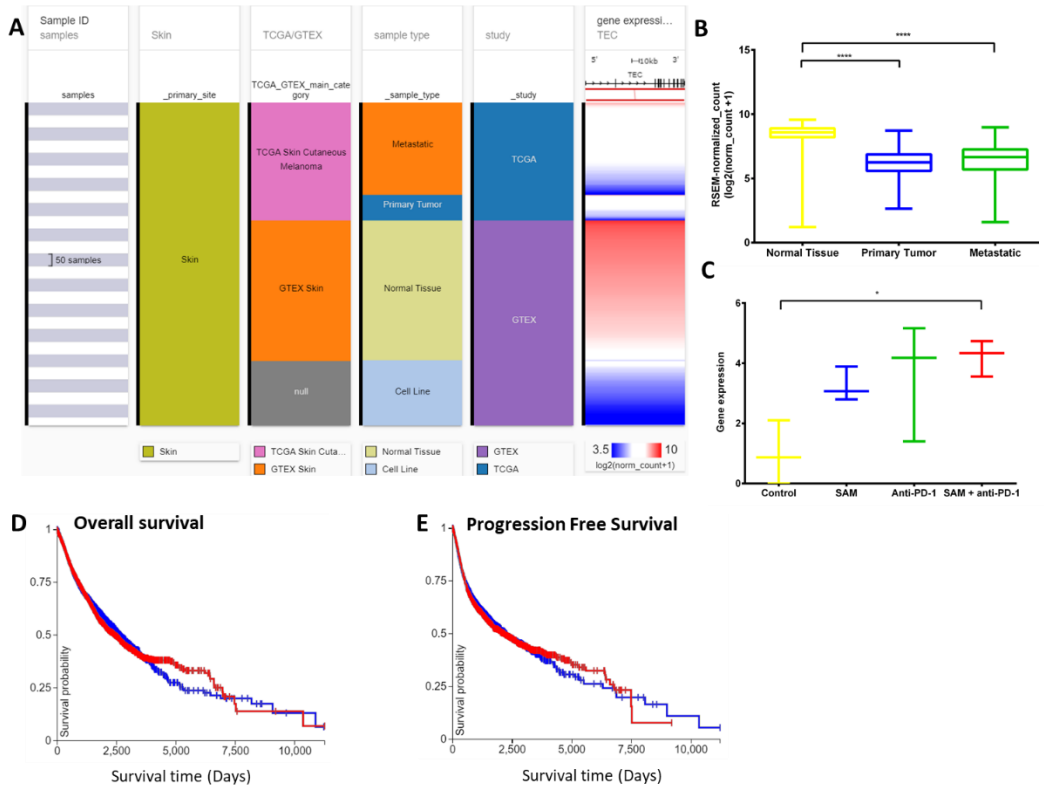

Supplementary Figure 12: Clinical data analysis of *TEC* gene identified from overlapping TCGA with RNA-seq data. (A) Expression of *TEC* gene in human healthy and skin cutaneous melanoma patients of GTEx and TCGA databases respectively. The columns show various

phenotypic categories applied in order to stratify samples according to Sample Id, Skin (true), TCGA/GTEX, sample type (normal tissue, primary tumor, metastatic tissue or cell line) and study. The last column shows gene expression of *TEC* of samples stratified according to the previous columns. Each row contains data from a single sample. (B) The expression data of *TEC* in the normal tissue, primary tumor, metastatic tissue samples in (A) has been plotted in a Box-plot graph (n=1024 samples). Expression values are in RSEM (RNA-Seq by Expectation Maximization). (C) The expression data of mouse *TEC* from RNA-sequencing of the primary B16 tumors after treatment with SAM, Anti-PD-1 and combination in this study (n =12; 3/group). Expression values are DeSEq2 normalized counts. (D-E) Overall survival and progression-free survival Kaplan Meier curves of *TEC* from RNA-seq of GTEx and TCGA databases; X-axis: survival time (days); Y-axis: survival probability. (D) Low (blue) n= 5180; High (red) n = 5254. (E) Low (blue) n= 5179; High (red) n = 5093. Statistical significance was obtained by ANOVA in GraphPad prism and are represented by asterisks (*$*P < 0.05; **P < 0.01, ***P < 0.001 and ****P < 0.0001$*). All the data and Supplementary Figure s, except (C), were generated using The UCSC Xena platform.

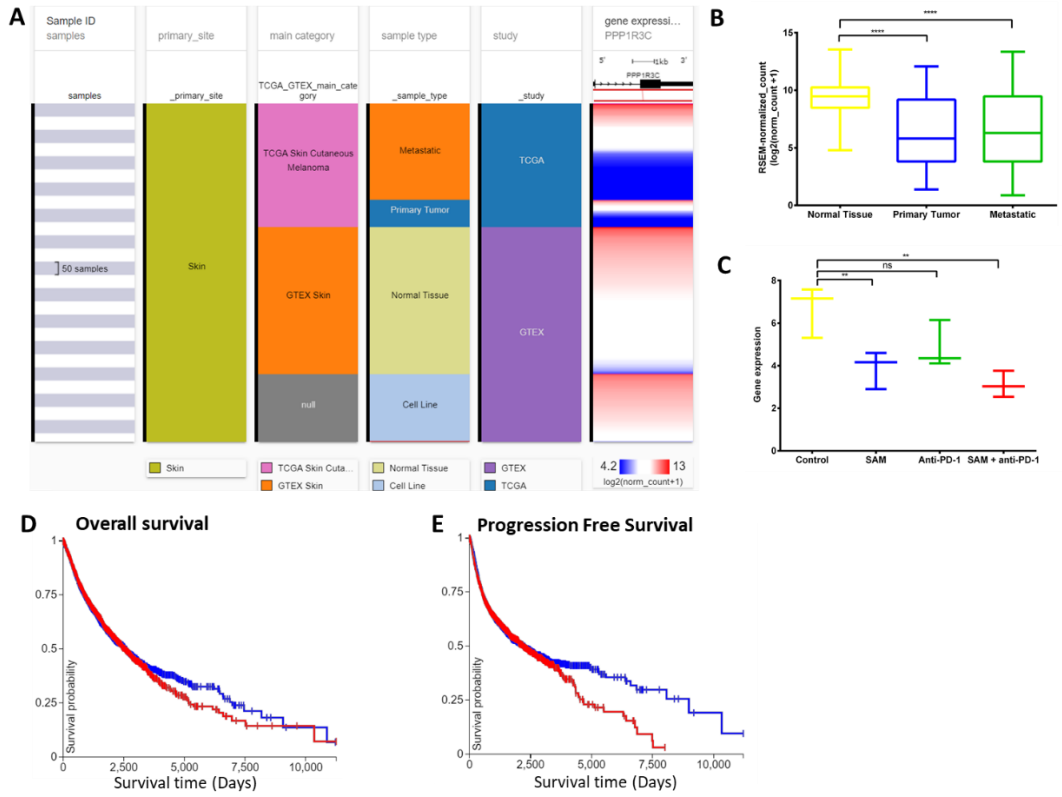

Supplementary Figure 13: Clinical data analysis of *PPP1R3C* gene identified from overlapping MGDB with RNA-seq data. (A) Expression of *PPP1R3C* gene in human healthy and skin cutaneous melanoma patients of GTEx and TCGA databases respectively. The columns show various phenotypic categories applied in order to stratify samples according to Sample Id, Skin (true), TCGA/GTEX, sample type (normal tissue, primary tumor, metastatic tissue or cell line) and study. The last column shows gene expression of *PPP1R3C* of samples stratified according to the previous columns. Each row contains data from a single sample. (B) The expression data of *PPP1R3C* in the normal tissue, primary tumor, metastatic tissue samples in (A) has been plotted in a Box-plot graph (n=1024 samples). Expression values are in RSEM (RNA-Seq by Expectation Maximization). (C) The expression data of *Ppp1r3c* from RNA-sequencing of the primary B16 tumors after treatment with SAM, Anti-PD-1 and combination in this study (n =12; 3/group). Expression values are DeSEq2 normalized counts. (D-E) Overall survival and progression-free survival Kaplan Meier curves of *PPP1R3C* from RNA-seq of GTEx and TCGA databases; X-axis: survival time (days); Y-axis: survival probability. (D) Low (blue) n= 6269; High (red) n = 4165. (E) Low (blue) n= 6108; High (red) n = 4164. Statistical significance was obtained by ANOVA in GraphPad prism and are represented by asterisks (*$P < 0.05$; **$P < 0.01$,

****P < 0.001 and ****P < 0.0001*). All the data and Supplementary Figure s, except (C), were generated using The UCSC Xena platform.

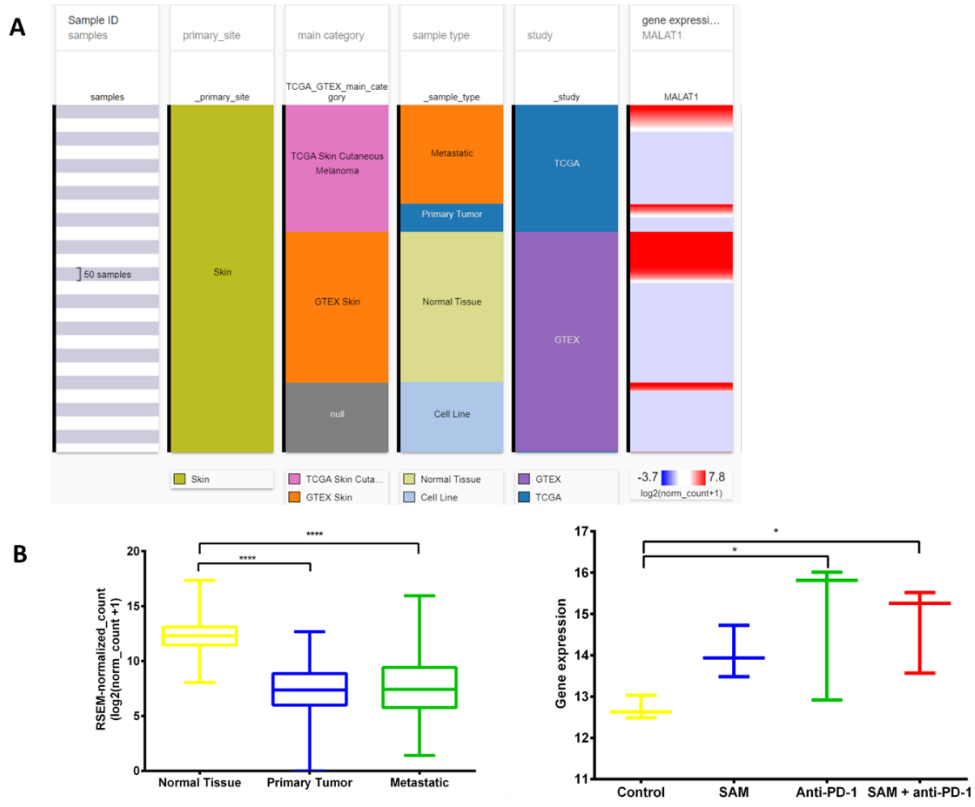

Supplementary Figure 14: Clinical data analysis of a non-coding *MALAT1* gene identified from overlapping MGDB with RNA-seq data. (A) Expression of *MALAT1* gene in human healthy and skin cutaneous melanoma patients of GTEx and TCGA databases respectively. The columns show various phenotypic categories applied in order to stratify samples according to Sample Id, Skin (true), TCGA/GTEX, sample type (normal tissue, primary tumor, metastatic tissue or cell line) and study. The last column shows gene expression of *MALAT1*of samples stratified according to the previous columns. Each row contains data from a single sample. (B) The expression data of *MALAT1* in the normal tissue, primary tumor, metastatic tissue samples in (A) has been plotted in a Box-plot graph. Expression values are in RSEM (RNA-Seq by Expectation Maximization). (C) The expression data of *Malat1* from RNA-sequencing of the primary B16 tumors after treatment with SAM, Anti-PD-1 and combination in this study (n =12; 3/group). Expression values are DeSEq2 normalized counts. Statistical significance was obtained by ANOVA in GraphPad prism and are represented by asterisks (**P < 0.05; **P < 0.01, ***P <*

*0.001 and ****P < 0.0001*). All the data and Supplementary Figure s, except (C), were generated using The UCSC Xena platform.

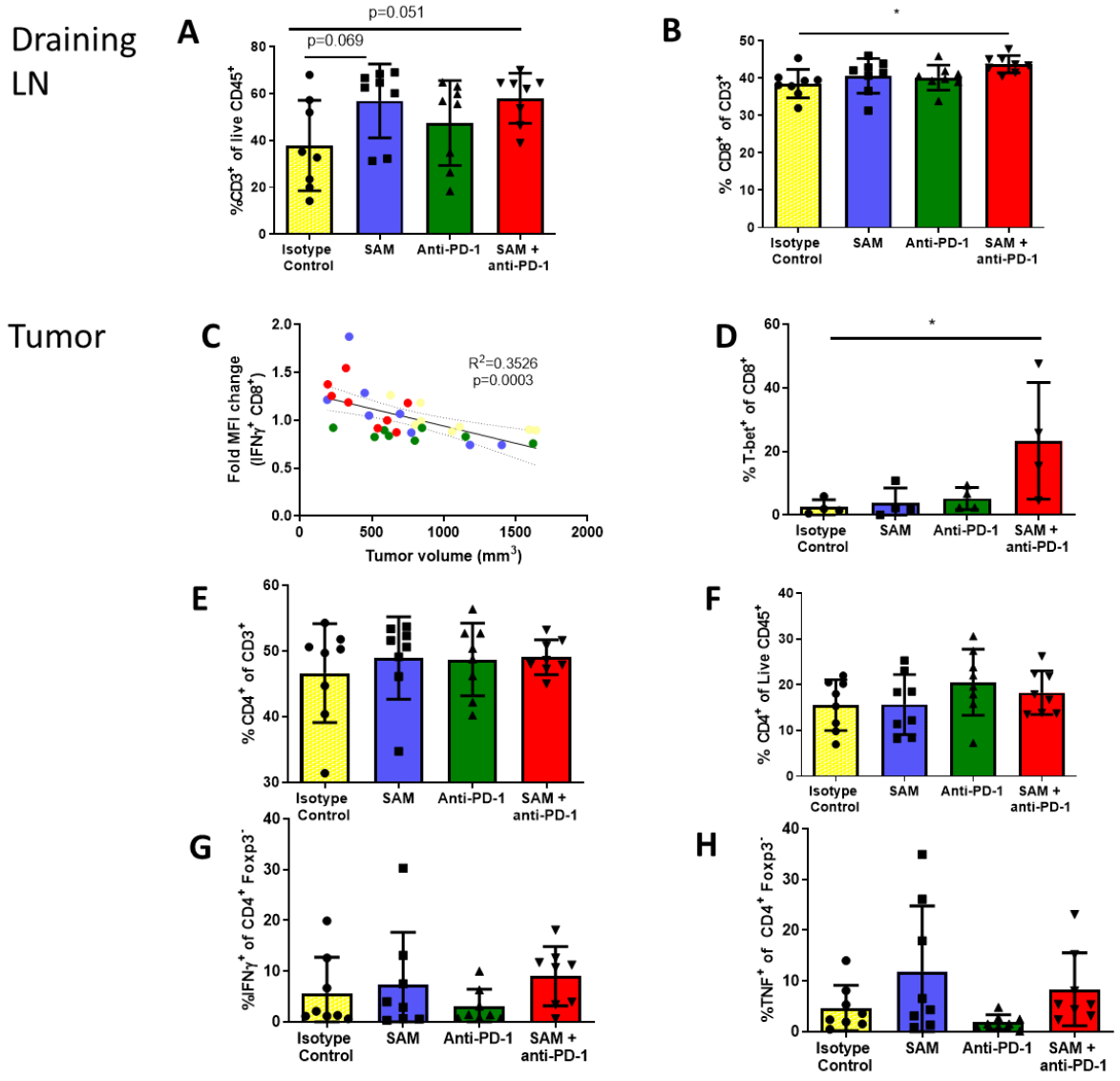

Supplementary Figure 15: Effect of SAM, anti-PD-1 and SAM+anti-PD-1 on immune system in tumor micro-environment and draining lymph nodes (LN) as determined by tumor immuno-phenotyping using flow cytometry. Treatment experiment had 4 groups; isotype IgG

control, SAMe, anti-PD-1 and SAMe+anti-PD-1. (**A and B**) Percentage (%) of CD3+ cells in live CD45+ cells (checked from viability dye) and % of CD8+ of CD3+ T cells in the draining LN of mice treated with SAMe, anti-PD-1 and SAMe+anti-PD-1. (**C**) Correlation analysis of mean fluorescence intensity (MFI) of IFN-γ+ CD8+ T cells against tumor volume (mm3) of all the mouse in the 4 groups tested. (**D**) Percentage of T-bet+ CD8+ T cells in all the groups tested. (**E-F**) Percentage (%) of CD4+ T cells in CD3+ and in live CD45+ cells (checked from viability dye), respectively, in the primary tumors of mice in the 4 treatment groups. (**G-H**) Percentage of IFNγ+ and TNFα+ analysed in CD4+ Foxp3- T cells in all 4 groups. Statistical analysis was performed by ANOVA in GraphPad prism are represented by asterisks *(*P < 0.05*; ***P < 0.01*, and ****P < 0.001*).

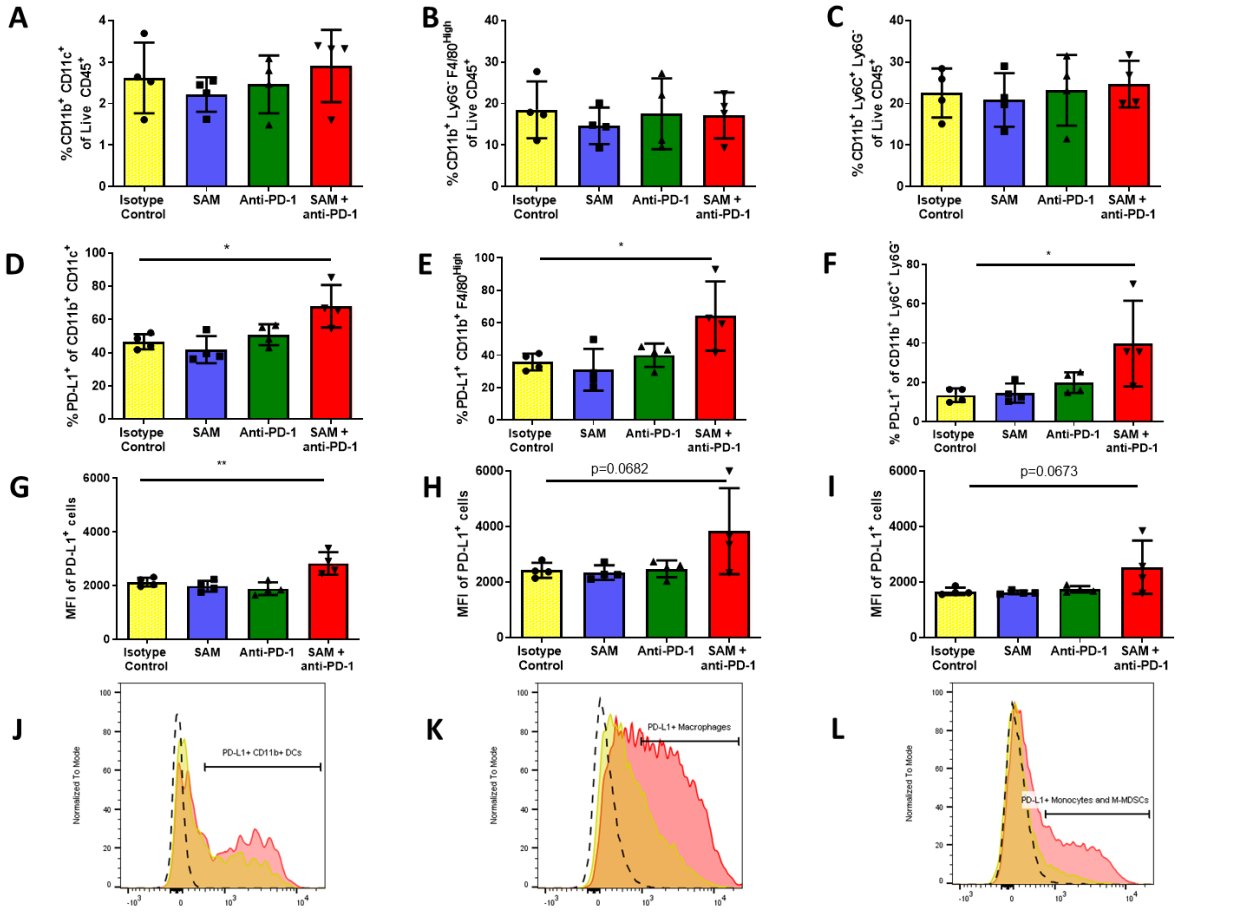

Supplementary Figure 16: Effect of SAM, anti-PD-1 and SAM+anti-PD-1 on myeloid cells of the immune system in tumor micro-environment as determined by tumor immuno-phenotyping using flow cytometry.

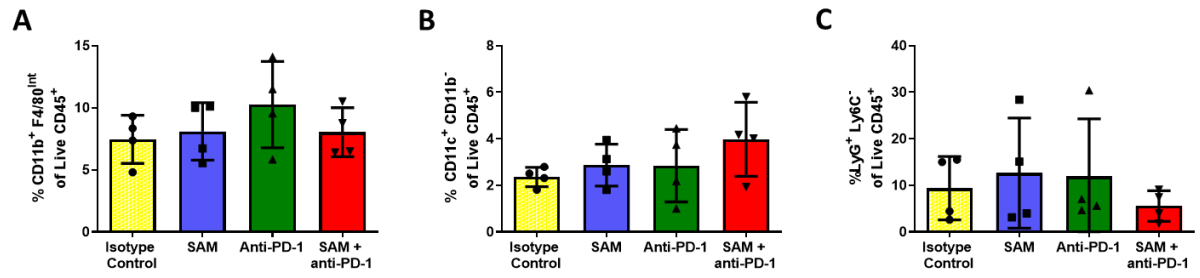

Supplementary Figure 17: Effect of SAM, anti-PD-1 and SAM+anti-PD-1 on myeloid cells of the immune system in tumor micro-environment as determined by tumor immuno-phenotyping using flow cytometry.

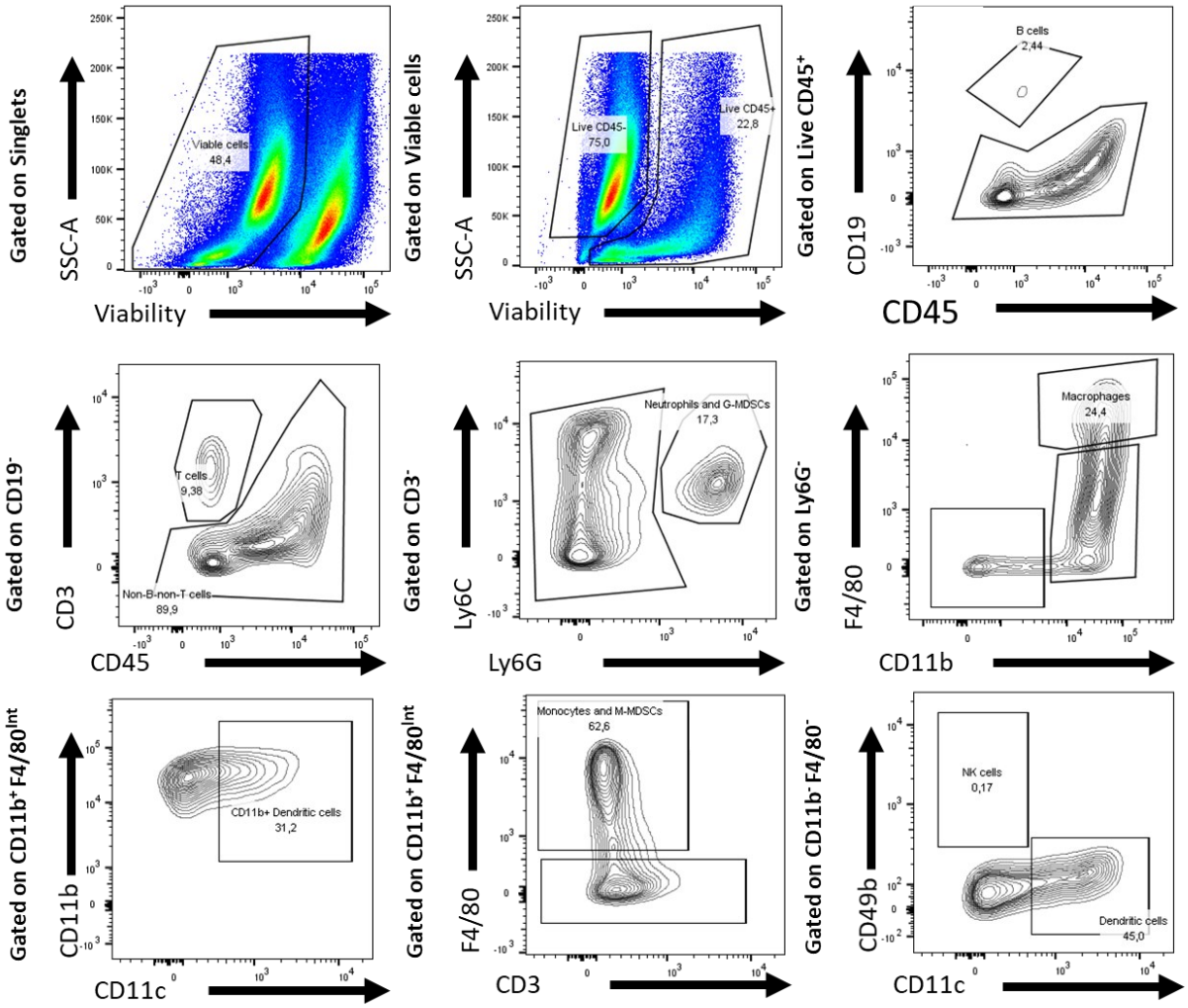

Supplementary Figure 18: Representative gating strategy utilized for examining cell surface markers of myeloid cells in primary tumor of mice using flow cytometry. Example used here is for tumor of isotype control group.

Supplementary Tables

Supplementary Table 1: List of primers used for this study.

Gene Name	Forward	Reverse
Areg	GGTCTTAGGCTCAGGCCATTA	CGCTTATGGTGGAAACCTCTC
Fcgbp	AGTGGAAGGTCAAGGTGAACG	CAGGCCAAAGTCGGTTTCAAT
Myh2	AAGTGACTGTGAAAACAGAAGCA	GCAGCCATTTGTAAGGGTTGAC
Xirp1	GCTCCGGCGTCTCTACAAAC	CCAGCGCATACACTGAACATC
Mybpc1	ATGGAATGGTTCACCGTCATTG	TAGTTGCATCCTCGCTAAGGC
Mybph	CAGCCACTAAGCCTGAACCTC	TCCAACACATAGCCTTGAAGC
Sypl2	CGCACCTCGGACAAGTCTC	CCCGAAGGCGAAAATAGCAAA
Dmbt1	TCAGCACAAGTCCTCCATCAT	TCCACAGGTGAGACTCATACC
Nrp2	GCTGGCTACATCACTTCCCC	CAATCCACTCACAGTTCTGGTG

Supplementary Table 2: List of antibodies used for immunophenotyping along with their fluorophores.

T cell panels	Cytokine panel	Myeloid panel
Fixable Viability Dye eFluor 780 (eBioscience)	V450 – Ki67 (clone B56, BD)	BUV395 – CD45.2 (clone104, eBioscience)
BUV737 – CD3 (clone 17A2, BD)	PE-Cy7 IFNγ (clone XMG1.2, BD)	FITC – CD3 (clone 17A2, BD)
Alexa Fluor 700 – CD4 (clone GK1.5, ThermoFisher)	BUV737 – IFNγ (clone XMG1.2, BD)	BUV737 – CD19 (clone 1D3, BD)
BV510 – CD8b (clone H35-17.2, BD)	PE-Cy7 – T-bet (clone 4B10, ThermoFisher)	Fixable Viability Dye eFluor 506 (eBioscience)

PE – PD-1 (clone J43, BD)	APC – IL-2 (BD)	PE-Cy7 – F4/80 (clone BM8, eBioscience)
PE-Cy7 – CD25 (clone PC61, BD)	PerCP-Cy5.5 – TNF (clone MP6-XT22, BD)	PerCP-Cy5.5 – CD11c (clone HL3, BD)
PerCP-Cy5.5 – CD25 (clone PC61.5, BD)	AntiCD16/CD32 (clone 2.4G2, BD)	Pacific Blue – CD11b (clone M1/70, eBioscience)
APC- ICOS (clone C396.4A, Thermofisher)		PE- CD49b (clone DX5, BD)
PE-Cy7 – CTLA-4 (clone UC-4B9, Biolegend)		Alexa Fluor 700 – Ly6G (clone 1A8, BioLegend)
APC – PD-L1 (clone MIH5, BD)		APC-780 – Ly6C (clone AL21, BD)
FITC – Foxp3 (clone FJK16s, eBioscience)		AntiCD16/CD32 (clone 2.4G2, BD)
BUV395 – CD45 (clone 104, BD)		

Other supplementary files can be downloaded from the following link (supplementary additional files).

CHAPTER FOUR: S-adenosylmethionine blocks tumorigenesis and with immune checkpoint inhibitor enhances anti-cancer efficacy against BRAF mutant and wildtype melanomas

Preface

In the next part of the thesis, we targeted the most prevalent subtype, BRAF mutant melanoma, that represents ~50% of the melanoma patients [126]. However, we were initially limited by availability of a syngeneic mouse model that can faithfully recapitulate the human melanoma pathology such as high burden of somatic mutations and tumorigenesis driven by BRAFV600E driver mutation along with passenger CDKN2A and PTEN mutations. Nevertheless, a YUMMER1.7 cell line and respective syngeneic mouse model was developed by Dr. Marcus Bosenberg's laboratory which allowed us to study BRAF mutant melanoma [247]. In addition to this, we were intrigued by the superior anti-cancer effects of SAM alone and in combination with anti-PD-1 antibody even in a less immunogenic short-term aggressive B16-B6 mouse model, and therefore we further investigated the molecular pathways affected by SAM in both BRAF mutant and WT melanoma. However, since SAM is a pleiotropic molecule and affects diverse genes and pathways, we focused on major driving forces of melanoma tumorigenesis including cell proliferation, phenotype switching, and immunoregulatory pathways. In this chapter, we also carried out transcriptome analysis of the melanoma cells to delineate the effect of SAM on various genes and pathways involved in the aforementioned pathways. After optimizing the YUMMER1.7-B6 mouse model in the laboratory, we carried out anti-cancer efficacy studies of SAM, anti-PD-1 antibody, and combination. Moreover, mouse survival studies were carried out to determine the long-term beneficial effect and effect on survival of tumor-bearing mice. Furthermore, extensive tumor immunophenotyping studies using flow cytometry were performed to delineate the effect of monotherapies and combination on anti-cancer immunity in the TME of YUMMER1.7 tumors. Lastly, since metastasis is the most important factor in tumor progression that results in high mortality rates of melanoma patients, we evaluated the effect of SAM, anti-PD-1 antibody, and combination on lung metastasis.

Chapter Four follows the paper published in *Neoplasia* which is part of Elsevier journals and is referenced below.

- Mehdi, A., M. Attias, A. Arakelian, M. Szyf, C.A. Piccirillo, and S.A. Rabbani, *S-adenosylmethionine blocks tumorigenesis and with immune checkpoint inhibitor enhances anti-cancer efficacy against BRAF mutant and wildtype melanomas.* Neoplasia, 2023. **36**: p. 100874.

Abstract

Despite marked success in treatment with immune checkpoint inhibitor (CPI), only a third of patients are responsive. Thus, melanoma still has one of the highest prevalence and mortality rates; which has led to a search for novel combination therapies that might complement CPI. Aberrant methylomes are one of the mechanisms of resistance to CPI therapy. S-adenosylmethionine (SAM), methyl donor of important epigenetic processes, has significant anti-cancer effects in several malignancies; however, SAM's effect has never been extensively investigated in melanoma. We demonstrate that SAM modulates phenotype switching of melanoma cells and directs the cells towards differentiation indicated by increased melanogenesis (melanin and melanosome synthesis), melanocyte-like morphology, elevated Mitf and Mitf activators' expression, increased antigen expression, reduced proliferation, and reduced stemness genes' expression. Consistently, providing SAM orally, reduced tumor growth and progression, and metastasis of syngeneic BRAF mutant and wild-type (WT) melanoma mouse models. Of note, SAM and anti-PD-1 antibody combination treatment had enhanced anti-cancer efficacy compared to monotherapies, showed significant reduction in tumor growth and progression, and increased survival. Furthermore, SAM and anti-PD-1 antibody combination triggered significantly higher immune cell infiltration, higher $CD8^+$ T cells infiltration and effector functions, and polyfunctionality of $CD8^+$ T cells in YUMMER1.7 tumors. Therefore, SAM combined with CPI provides a novel therapeutic strategy against BRAF mutant and WT melanomas and provides potential to be translated into clinic.

Keywords: S-adenosylmethionine, immune checkpoint inhibitors, anti-PD-1 antibody, phenotype switching, MITF, melanoma, YUMMER1.7, B16, melanin.

Introduction

There are 232,100 new cases of melanoma diagnosed and about 55,500 cancer deaths from melanoma annually [1]. Melanoma can be genetically stratified into four major subgroups; (1) activating BRAFV600 mutations (~50%); (2) N/H/K-RAS mutations (15–20%), (3) inactivating mutations of NF-1 (~10%), and (4) triple wild-type (WT)- WT BRAF, N/H/K-RAS and NF-1 (30–35 %) [2]. CPI therapy has shown long lasting responses in a group of patients and has led to a paradigm shift in treating all melanoma genotypes [3, 4]. However, 60–70% of melanoma patients do not respond to CPI therapy due to mechanisms such as tumor-intrinsic lack of immunogenicity, immunosuppressive tumor microenvironment (TME) as well as innate and acquired resistance [5, 6]. Therefore, there is an urgent need to develop novel combinational therapies that could complement CPI and improve melanoma related morbidity and mortality.

The resistance to CPI can stem from the heterogeneous nature of melanoma cells that switch between differentiated, highly proliferative, and invasive stem-cell like states [7-10]. While acting as a rheostat, microphthalmia-associated transcription factor (MITF), a master transcription factor, primarily controls phenotype switching of melanoma cells [7-10]. Increased MITF expression leads to low-proliferative terminally differentiated cells called melanocytes which produce melanin via melanogenesis [11]. Transcription factors, cAMP-response element binding protein (CREB) and SRY-box transcription factor 10 (SOX10), are activators that increase MITF expression and are also involved in melanogenesis [11, 12]. MITF also increases transcription of tyrosinase (TYR) and tyrosinase related enzymes, TYRP-1, and TYRP-2, that convert tyrosine to melanin [11-13]. Moreover, premelanosome protein (PMEL or GP100) and Melanocyte antigen recognized by T cells (MART-1 or MELAN-A), genes required for melanogenesis and melanosome generation, are also regulated by MITF [11-14]. Reduction of MITF expression results in dedifferentiated melanomas that are resistant to therapies, highly invasive and metastatic, and causes reduced overall survival of patients [10, 15, 16]. Therefore, directing phenotype switching by modulating MITF levels has been suggested as an effective anti-melanoma therapy [7, 9].

Melanocyte differentiation antigens (MDAs) are peptides generated from genes involved in melanogenesis and melanosome generation including TYR, TYRP-1, TYRP-2, MART-1 and PMEL [14]. Although MDAs are self-antigens, autologous cytotoxic T lymphocytes directed against MDAs, can mediate tumor regression, break tolerance to the tumor, and therefore are being

evaluated as targets for anti-melanoma immunotherapy and in melanoma vaccines [14]. A major immune evasive mechanism is low intrinsic immunogenicity where tumor cells display reduced levels of immunogenic tumor antigens (or neoepitopes) [17]. Therefore, increasing expression of antigens such as MDAs and melanoma associated antigens (MAAs) can enhance immunogenicity of the tumor cells resulting in greater response in general and to CPIs [18, 19].

The resistance to CPI has been associated with alterations in the methylome of cancer cells [20, 21]. To distinguish CPI responders from non-responders, DNA hypomethylation was proposed as an essential biomarker for predicting tumor response to host immunity, and DNA hypomethylation could also provide a possible mechanism for immune escape and resistance to CPI [21]. Moreover, global hypomethylation levels were strongly associated with immune evasion signatures independently of aneuploidy and tumor mutational burden [21]. S-adenosylmethionine (SAM), a methyl donor of numerous epigenetic methyl transferases, was shown to counteract DNA hypomethylation and block DNA demethylation [22-24]. SAM has significant anti-cancer effects in various malignancies; however, SAM's effect has not been extensively investigated in melanoma. Interestingly, SAM is also crucial for activation, proliferation, and survival of T cells [25-29]. Furthermore, SAM levels are reduced by cancer cells via several mechanisms in TME [30, 31]. Consistently, the depletion of methionine (the pre-cursor of SAM) in TME results in $CD8^+$ T cells becoming dysfunctional and $CD8^+$ T cells become unresponsive to CPI [30]. This is another essential immune evasive mechanism used by tumor cells [30].

We have previously tested the effect of SAM and anti-PD-1 antibody combination on tumor growth of a syngeneic BRAF WT mouse model and found enhanced anti-cancer efficacy of the combination treatment. However, the effect of SAM alone and in combination with anti-PD-1 antibody along with molecular pathways involved were not extensively investigated in melanoma, in general, and in the BRAF mutant melanoma which represents 50% of patients. Hence, we tested the hypothesis that SAM elevates anti-cancer immune responses, in addition to having anticancer effects, and that an effective novel therapeutic strategy for both BRAF mutant and WT melanoma would be to combine SAM and CPI. We show here using cancer cell lines and mouse models that SAM has significant anti-cancer effects on BRAF mutated and WT melanomas. The anti-cancer effect of SAM involves marked inhibition of cell proliferation and directing phenotype switching of invasive and proliferative melanoma cells into differentiated state. We also show that SAM and anti-PD-1 antibody combination has enhanced anti-cancer efficacy in reducing tumor growth and

metastasis, and increasing survival in melanoma mouse models. The combination also markedly elevated adaptive immune responses indicated by a higher immune cell infiltration, higher $CD8^+$ T cells infiltration, activation, and effector functions, and higher polyfunctional $CD8^+$ T cells in TME of YUMMER1.7 tumors. The combination also enhanced the frequency and functionality of $CD4^+$ T_h1 cells and reduced immunosuppressive $CD4^+$ $FoxP3^+$ T_{regs} in TME of YUMMER1.7 tumors.

Results

SAM has marked anti-proliferative effects on melanoma cells

Uncontrolled cellular proliferation is a major hallmark of cancer [32]. Firstly, to determine the anti-cancer effect of SAM, we tested the effect of SAM on proliferation in human (A375) and murine (YUMM1.7, B16 and YUMMER1.7) melanoma cell lines. B16 is a BRAF WT while YUMM1.7, YUMMER1.7 and A375 are BRAF mutant cell lines. While SAM decreased cell proliferation in all cell lines in a dose-dependent manner relative to control, the effect was greatest on YUMMER1.7 cell line at both SAM 200μM and 500μM doses, followed by YUMM1.7, B16, and A375, respectively (Figure 1A).

Next, to determine the key players that regulate cell cycle progression in melanoma, we analyzed major cell cycle regulators that are differentially expressed in human melanoma primary tumor, metastatic and normal skin tissues using the Xena platform [33]. Key cell cycle regulators including inhibitors such as p21 had low expression in primary tumors and metastatic tissue compared to normal skin tissue (Figure 1B). In contrast, cell cycle dependent kinases and cyclins that drive cell cycle forward such as CDK1, CDK2 and CCNB1/2 had higher expression in primary tumors and metastatic tissues compared to normal skin tissue (Figure 1C). Importantly, treatment of YUMMER1.7 and B16 cells with SAM reversed the expression of most of the cell cycle regulators tested (Figure 1D and Supplementary Figure 1). For instance, p21 which was highly expressed in the human primary tumors and metastatic tissue was significantly upregulated by SAM in YUMMER1.7 cells and vice versa for CDK1, CDK2 and CCNB1/2 expression (Figure 1D).

RNA-sequencing of YUMMER1.7 cells treated with SAM (200μM and 500μM) revealed many differentially expressed genes (DEGs) upon SAM treatment at 200μM (up, 3715; and down,

3557 genes) and 500μM (up, 4235; and down, 3935 genes) (Supplementary Figure 2A). We carried out pathway analysis of DEGs using GSEA (Supplementary Figure 2B-C, 3 and 4 and Supplementary Table 3 and 4). Importantly, key cell cycle pathways and pathways involved in translation and related processes were significantly downregulated upon SAM (500μM) treatment in YUMMER1.7 cells indicating marked cell cycle inhibition (Supplementary Figure 2B and 3, and Supplementary Table 5).

Next, we overlapped the DEGs obtained from SAM treatment with the known melanoma driving genes (n= 422) of Melanoma Gene Database (MGDB) and found 47% of genes to be common between the MGDB and DEGs obtained after treatment with SAM (500μM) (Supplementary Figure 2D)[34]. Expectedly, pathway analysis of common genes revealed Melanoma and core cancer pathways enrichment (Supplementary file 1). Together, these results indicate that SAM regulates core genes/pathways in melanoma tumorigenesis and inhibits cell cycle pathways thereby reducing cellular proliferation of melanoma cells.

SAM increases melanin and melanosome synthesis of melanoma cells

Upon treatment of B16 cells with SAM, we noticed that B16 cells appear darker suggesting increased melanin synthesis. Since melanin pigmentation was reported to affect melanoma behaviour, we investigated the effect of SAM on melanogenesis and melanosome formation [11, 35, 36]. B16 cells produce melanin and phenotypically recapitulates clinical features of human melanoma [37]. The ability to produce melanin is lost upon subsequent cycles during *in vitro* cell culturing. We took advantage of this and treated non-pigmented B16 cells with varying concentrations of SAM (200-500μM). Increase in SAM concentration induced melanogenesis as B16 cells had increased black pigmentation in a dose-dependent manner (Figure 2A-B). Furthermore, the number of melanosomes and melanin synthesizing B16 cells were elevated as well (Figure 2A). To measure the amount of intracellular melanin, we extracted the melanin from cells and measured absorbance. Treatment with SAM showed a gradual increase in endogenous (intracellular) melanin production in a dose dependent manner (Figure 2B). We also observed slight increase in exogeneous (extracellular) melanin that changed the medium color from red to reddish black in wells treated with SAM (data not shown).

SAM regulates phenotype switching of melanoma cells through modulating Mitf expression

Melanocytes are thin, elongated cells with branched structures, consisting of a central body and dendrites, and contain numerous melanin-containing melanosomes [12, 38, 39]. Whereas B16 cells are a mixture of short spindle-shaped and epithelial-like cells lacking dendrites, and loose pigmentation (Control group, Figure 2C). Treatment with SAM resulted in differentiation of B16 cells into melanocyte-like cells (Figure 2C). These differentiated cells were thin, dark black stained, and had more melanosomes and dendrites (Figure 2C). Furthermore, in heterogeneous B16 cell population, a higher number of B16 cells appeared melanocyte-like cells in increasing SAM dose from 200μM to 500μM (Figure 2A). Moreover, the differentiated cells also had reduced proliferative ability (Figure 1A and Figure 2A).

MITF loss or low expression can lead to dedifferentiated melanomas that are resistant to therapies, are highly invasive and metastatic, and results in reduced overall survival of patients [10, 15, 16]. In addition to its clinical significance, MITF is also the master regulator of melanogenesis and hence we investigated its expression. SAM elevated *Mitf* expression by several folds in all the melanoma cell lines that we tested in a dose-dependent manner (Figure 2D). *Mitf* was also found to be significantly upregulated upon SAM treatment in RNA-seq data and was a common gene between DEGs upon SAM treatment and the MGDB database. Interestingly, 126 MITF target genes were also differentially expressed in response to SAM treatment (Supplementary Figure 2E) [40]. Moreover, the transcriptional activators *Sox10* and *Creb1*, which induce *Mitf* expression, melanogenesis, and differentiation phenotype, were also increased several folds by SAM (Figure 2D).

Cancer stem cells (CSCs) or melanoma initiating cells (MICs) have high expression of stemness marker genes including *NANOG*, *WNT*, *SOX2*, and in some studies, *BRN2* (*Pou3f2*) and *SLUG* (*Snai2*) [9, 41, 42]. We found that SAM caused significant reduction in essential MICs marker genes including *Nanog* and *Wnt* expression in both B16 and YUMMER1.7 cells, and significant downregulation of *Sox2* expression in B16 cells (Figure 2E). *Brn2* was also significantly downregulated in B16 and YUMMER1.7 cells, and *Slug* in B16 cells (Supplementary Figure 5). This indicates that SAM reduces the proportion of MICs in heterogeneous melanoma cell population and redirects MICs from dedifferentiated state towards a differentiated phenotype.

SAM increases immunogenicity and sensitivity of melanoma cells to CPIs

Since melanogenesis involves expression of melanocyte differentiation antigens (MDAs) and recognition of antigens including MDAs is central to immune response and immunotherapy against melanoma, we next determined the effect of SAM on expression of MDAs. Expectedly, SAM increased expression of most MDAs (*Tyr, Tyrp1, Tyrp2/Dct, Mart-1/Melan-A, Pmel/Gp100*) directly involved in melanogenesis by several folds in B16 and YUMMER1.7 cells (Figure 3A). As expected, YUMMER1.7 and YUMM1.7 cell lines that do not produce melanin had no/undetectable expression of *Tyr* (Figure 3A). Expression of *Tyrp1* and *Mart-1* was also upregulated by SAM while *Tryp2* expression was undetectable in YUMM1.7 cells (Figure 3A).

In addition to MDAs expression, SAM (200μM and 500μM) also increased the expression of melanoma associated antigens (MAAs) including chondroitin sulfate proteoglycan 5 (*Cspg5*), melanoma inhibitory activity (*Mia*), somatostatin receptor 2 (*Sstr2*), melanoma cell adhesion molecule (*Mcam*), proteoglycan 4 (*Prg4*) and melanoregulin (*Mreg*) in YUMMER1.7 cells (Figure 3B) except *Cspg5* at SAM 200μM [14]. In addition, tumor associated antigens (TAAs), such as the cadherins, adhesions and S100 family genes were also upregulated by SAM in YUMMER1.7 cells (Supplementary Figure 6). Consistently, pathways that generate high neoepitopes such as oxidative stress, ROS, NRF2, UV response and other related pathways were found to be the top significantly upregulated pathways upon SAM treatment (Supplementary Figure 2C and 4, and Supplementary Table 6).

Since immune checkpoints play a key role in anti-cancer or pro-cancer immune responses, we tested the expression of several immune checkpoint molecules including PD-L1 (*Cd274*), PD-L2 (*Cd273*), *Cd47*, cytotoxic T-lymphocyte-associated protein 4 (*Ctla4)*, galectin-9 (*Lgals9*), Nectin2/3 (*Cd112/113*), T Cell Immunoreceptor with Ig and ITIM Domains (*Tigit*), herpes virus entry mediator (*HVEM* or *Tnfrsf14*), and T cell immunoglobulin and mucin-domain containing-3 (*Tim-3* or *Havcr2*). We found that immune inhibitory molecules including PD-L1, galectin-9 and HVEM were significantly downregulated in SAM-treated (200μM and 500μM) YUMMER1.7 cells compared to control (Figure 3C).

Both FAS death receptor (FAS/Apo1) and its ligand (FASL/Apo1L), and TRAIL death receptors (TNFRSF10-A/B/C/D or TRAIL-R1/2/3/4) and its ligand (TNFSF10/Apo2L), are major apoptosis pathway that causes instant cell death [43-45]. The lack of expression of FAS and TRAIL receptors in tumors can result in immune evasion and is correlated with poor prognosis of malignant melanomas, whereas increased FAS and TRAIL receptor expression in tumors can

result in killing by cytotoxic $CD8^+$ T and NK cells [45-48]. Importantly, we found significantly lower expression of *FAS* receptor in primary tumors and metastatic tissues of melanoma patients as compared to normal skin tissue samples, and this was associated with lower overall survival, progression-free interval, and disease-specific survival (Figure 3D-E). Interestingly, we found SAM significantly increased expression of *Fas* receptor in YUMMER1.7 cells (Figure 3F). Additionally, SAM lowered expression of genes *Il18* and *Il18bp* in YUMMER1.7 cells which were previously shown to have a crucial role in survival of B16 melanoma cells and inhibit Fas/FasL pathway and NK mediated killing (Figure 3G) [49]. Furthermore, SAM resulted in significant upregulation of major TRAIL receptors including TRAIL-R2 (*Tnfrsf10b*), TRAIL-R1/3 (*Tnfrsf26* or *Tnfrsf1/3*) whereas downregulation of TRAIL ligand (*Tnfsf10*) expression in YUMMER1.7 cells (Figure H-I). In addition, SAM also increased TWEAKR receptor (*Tnfrsf12a*) and *Tnfrsf18* expression (Supplementary Figure 7). Consistently, FAS, apoptosis, TNF pathways and immune stimulating pathways (including T cell TCR signalling) were upregulated in YUMMER1.7 cells treated with SAM (Supplementary Table 7).

Intercellular adhesion molecule 1 (ICAM-1) is an essential antigen present on antigen presenting cells (APCs) or tumor cells that interacts with lymphocyte function associated antigen 1 (LFA-1) which is a major co-stimulatory molecule present on T cells. LFA-1/ICAM-1 interactions are essential for trans-endothelial migration of $CD8^+$ T cells into TME, and $CD8^+$ T cells initial activation and lytic functions [50-52]. Moreover, ICAM-1 overexpression on tumor cells have been reported to cause reduction in tumor growth [53, 54]. Parallel to the increase in Fas, TRAIL receptors and immunostimulatory antigens' expression, *Icam1* (200µM and 500µM) and *Icam2* (500µM only) were also significantly upregulated by several folds upon SAM treatment (Figure 3J).

Collectively, these data show that SAM alters melanoma transcriptome that is consistent with increased immunogenicity and sensitivity of melanoma cells to CPIs.

SAM modulates Mitf expression that further regulates phenotype switching

Next, to elucidate a potential mechanism for upregulation of antigens upon SAM treatment, we examined a direct involvement of the *Mitf* transcription factor. Therefore, we knocked down (KD) *Mitf* using siRNA targeting the *Mitf* gene (siMitf) at 3 sites simultaneously and confirmed that *Mitf* expression was markedly downregulated (Figure 4A). Most of the MDAs' expression

was downregulated upon siMitf KD indicating that Mitf is an important transcription factor controlling the expression of these MDAs (Figure 4A). Parallel to the effect of SAM elevating *Mitf* levels, KD of *Mitf* expression significantly increased expression of stemness genes including *Nanog*, *Wnt* and *Sox2* in B16 and YUMMER1.7 cells (Figure 4B). Hence, showing that *Mitf* induction is critical for its effect on melanogenesis and differentiation.

Collectively, these data suggest that SAM modulates the phenotype switching of melanoma cells. Treating melanoma cells with SAM switches proliferative and invasive stem-cell phenotype towards more differentiated state indicated by low proliferative ability, melanocyte-like cell morphology, elevated melanogenesis, decreased stemness ability and increased immunogenicity (Figure 4C).

SAM reduces tumor growth, progression, and metastasis of melanoma tumors

To determine effect of SAM *in vivo,* we established either YUMMER1.7 or B16 tumors in immunocompetent B6 mice and treated them with either control (PBS) or SAM (80mg/kg/day) via oral gavage. SAM treatment significantly reduced tumor growth and progression in both mouse models compared to control (Figure 5A).

Expression of nuclear protein Ki67 (Ki67) is strongly associated with various tumor parameters including growth, progression, clinical tumor stage, metastasis, and is the most extensively used proliferation marker [55]. Consistent with SAM reducing proliferation and causing cell cycle inhibition, SAM had a significant decrease in Ki67-positive stained tumor cells indicating marked reduction in proliferation, growth, and progression of YUMMER1.7 and B16 tumors (Figure 5B). Moreover, parallel to *in vitro* results, SAM also showed a significant elevation in *Mitf* and MDAs (such as *Mart-1* and *Pmel*) expression in both YUMMER1.7 and B16 tumors (Figure 5C).

Both melanosomes and melanin pigmentation have shown to significantly inhibit melanoma metastasis (*in vivo*) [35, 36]. SAM increased melanin and melanosome production, increased *Mitf* expression and reduced the pool of invasive MICs in B16 heterogenous population. Considering this, we investigated the effect of SAM in a model of B16 melanoma lung metastasis through intravenous administration of B16 cells. The mice treated with SAM had significant decrease in proportion of lung metastatic nodules compared to control lungs (Figure 5D). Moreover, treatment of SAM decreased cell migration of YUMMER1.7 and A375 cells in a

wound-healing assay (*in vitro*) (Supplementary Figure 8). Additionally, SAM reduced invasiveness of B16 cells as shown by us previously [22]. Taken together, these results suggest that SAM can significantly reduce the metastatic potential of melanoma.

SAM and anti-PD-1 antibody combination has superior anti-cancer efficacy against melanoma tumors

Based on our data above, we further hypothesized that treatment with SAM would complement with CPI therapy. We treated YUMMER1.7 tumor bearing mice with control (IgG and oral PBS), SAM, anti-PD-1 antibody, and combination of both. Both SAM and anti-PD-1 antibody alone had significant effect in reducing tumor growth and progression as indicated by lower mean tumor volume and high tumor growth inhibition (TGI) (74.4% and 72.0% at day 22), compared to control (0%), respectively (Figure 6A-B). However, SAM+anti-PD-1 combination had significantly high efficacy in blocking tumor growth and progression compared to all other groups indicated by lowest mean tumor volume and maximum TGI (88.6%) at day 22 (Figure 6A-B).

Moreover, mice treated with SAM+anti-PD-1 combination had significantly highest survival probability (100% (10/10) at day 34 and median survival of 62 days), followed by anti-PD-1 antibody (60% (6/10) at day 34 and median survival of 46 days), SAM (50% (4/8) at day 34 and median survival of 35.5 days) and control (0% (0/8) at day 30 and median survival of 23 days) (Figure 6C). Intriguingly, 20.0% (2/10) of the combination group mice had complete tumor elimination by the end of the study compared to anti-PD-1 antibody (10.0%, (1/10)), SAM (0.0%, 0/8), and control (0.0%, 0/8) (Figure 6D).

We also tested SAM+anti-PD-1 antibody combination effect on lung metastasis (Figure 6E). We found that SAM+anti-PD-1 had a larger effect on reducing lung metastasis as compared to all other groups (Figure 6E). Taken together, these data suggest that SAM and anti-PD-1 antibody combination can significantly reduce tumor growth, progression, and metastasis of melanoma.

SAM and anti-PD-1 antibody combination elevates the infiltration, effector functions and polyfunctionality of $CD8^+$ T cells in the TME

To further understand the significant reduction in tumor growth and progression by SAM, anti-PD-1 antibody, and the combination, immunophenotyping of the tumors from YUMMER1.7-tumor bearing mice was carried out. Despite considerable inter-individual variability within each group, there were significantly higher levels of immune infiltration in the tumors treated with either SAM, anti-PD-1 antibody, or SAM+anti-PD-1 combination compared to control tumors (Supplementary Figure 9). Similarly, the density of $CD3^+$ T cells was increased in all treatment groups (Figure 7A). Furthermore, their proportion amongst tumor-infiltrating immune cells was increased and correlated inversely with tumor weight (Figure 7A and Supplementary Figure 10).

Cytotoxic $CD8^+$ T cells are the most powerful effectors in the adaptive anti-cancer immune response and increased $CD8^+$ T cell activation and function are hallmarks of response to PD-1 blockade [56]. Hence, we investigated the effect of the treatments on $CD8^+$ T cells' tumor infiltration, activation, and effector functions. Significantly higher densities and frequency of $CD8^+$ T cells infiltrated tumors of mice treated with SAM+anti-PD-1 antibody combination compared to control (Figure 7B). The infiltrated $CD8^+$ T cells had higher activation levels in the SAM+anti-PD-1 antibody combination group as indicated by increased expression of the stimulatory checkpoint molecule ICOS both in terms of frequency and level of expression. Furthermore, this phenotype was inversely correlated with tumor weight ($r^2 = 0.34$) (Figure 7C). Expression of the transcription factor T-bet, which is an indicator of $CD8^+$ T cells activation and effector functions, was increased in the combination group compared to control as well (Figure 7D).

CPIs were designed to counteract the exhaustion of tumor-infiltrating T cells, a state caused by chronic activation and characterized by high levels of PD-1 signaling and loss of effector functions such as cytokine-secreting capacity [56]. This feature was recapitulated in the control tumors, with high proportions of PD-1 expressing cells (Supplementary Figure 11) and absence of polyfunctional cells secreting both IFNγ and TNFα (Figure 7E), a subset of $CD8^+$ cells considered as the most cytotoxic and the most potent effector of anti-tumor immunity [57]. Accordingly, the $CD8^+$ T cells in the TME of combination group produced significantly higher levels of T-bet (Figure 7D), which promotes CD8 effector function such as the expression of IFNγ, and cytokines including IFNγ and TNFα compared to control group (Figure 7E). Moreover, polyfunctional $CD8^+$ cells were observed in higher frequency and density in the combination group and represented up to 60% of $CD8^+$ cells in the mice with lowest tumor burden (Figure 7E).

In general, SAM group had a higher density of infiltrating $CD8^+$ T cells (Figure 7A, B, $p<0.05$), activation (MFI of $ICOS^+$ and T-bet^+ density; $p<0.05$; Figure 7C-D), and a non-significant trend towards higher cytokine expression (IFNγ and TNFα; Figure 7E; $p>0.05$;) and polyfunctionality (Figure E; $p>0.05$) compared to control. This is in line with SAM increasing the immunogenicity (antigen expression) of melanoma cells and tumors (Figure 3 and 5) which would ultimately lead to higher activation and effector functions of antigen-specific $CD8^+$ T cells. Indeed, loss of MDAs (MART-1, TYR) due to mutation or KD results in increased tumor volume in immunocompetent mice [16, 58].

SAM-mediated protection correlates with augmented $CD4^+$ T helper responses in melanoma tumors

Consistently, all treatment groups had a significantly higher density and frequency of infiltrating $CD4^+$ T cells compared to the control group (Figure 8A, $p<0.05$), in the TME. In the combination group, there was a significant shift in the composition of the $CD4^+$ T cell pool with reduced accumulation of $Foxp3^+$ T_{reg} cells and an increase in the frequency of T-bet^+ T_h1 cells (Figure 8B-C). Furthermore, the functionality of these T_h1 cells was increased in the combination group, as shown by the increased frequency of IFNγ and TNFα which correlated inversely with tumor volume (Figure 8C).

Surprisingly, we observed the presence of a subset of $CD4^+$ $IL17^+$ T cells in groups treated with SAM (SAM and SAM+anti-PD-1) which was absent in the control and anti-PD-1 antibody group (Figure 8D). These cells were confirmed as bona fide Th17 cells through RORγt co-expression and absence of T-bet and IFNγ expression (Figure 8 C, D). Furthermore, expression of *IL-6,* a cytokine known to promote Th17 polarization in the presence of TGFβ [59], was markedly increased in YUMMER1.7 cells cultured with SAM *in vitro* (Supplementary Figure 12). IL-17 responses have not been associated with response to checkpoint blockade in melanoma, and the frequency of Th17 did not correlate with tumor volume in the groups that received SAM (Figure 8D). However, in other tumor types, Th17 cells contribute to the recruitment of $CD4^+$ and $CD8^+$ T cells into TME, and activation of tumor-specific $CD8^+$ T cells [60]. In accordance with this data, the expression of *Icam1* which is essential for trans-endothelial migration and lytic functions of

$CD8^+$ T cells, was upregulated by several folds by SAM in YUMMER1.7 cells (Figure 3H) [70-72].

Taken together, these data indicate that combining SAM with anti-PD-1 antibody treatment provides no additional benefit in terms of recruitment of $CD8^+$ and $CD4^+$ T cells in the TME, however, the difference was in higher activation and effector functions of both $CD4^+$ and $CD8^+$ T cells.

Discussion

Melanoma is one of the most prevalent cancers and has high mortality rates especially after the cancer has metastasized. A high tumor mutational burden (TMB) is strongly correlated with high response and has emerged as a clinically relevant biomarker of CPI efficacy [18, 19], however DNA hypomethylation (and demethylation) was strongly correlated with immune evasive and CPI therapy resistant signatures in melanoma, independent of TMB and aneuploidy [21]. In fact, global DNA hypomethylation had a higher predictive power than TMB. Furthermore, recent studies have suggested low SAM levels within TME, and deprivation of $CD8^+$ T cells of the precursor of SAM, methionine, makes them non-functional and unresponsive to CPI therapy in melanoma. Thus, we hypothesized that targeting DNA hypomethylation with SAM would be highly beneficial and complement CPI therapy. Here we propose a novel therapeutic strategy by combining SAM with anti-PD-1 antibody to overcome the development of treatment resistance in highly aggressive BRAF mutant and WT melanomas.

During melanogenesis, melanoma cells become less aggressive as genes that repress invasion are upregulated [35, 61, 62]. In addition, melanosomes were shown to inhibit transmigration ability of melanoma cells mechanistically while melanin pigmentation inhibited metastasis [35, 36]. SAM increased the number of cells synthesizing melanin and melanosomes in a dose-dependant manner (Figure 2). Increase in melanosomes is also indicated by increased expression of *Mitf* which regulates melanosome biogenesis, and genes such as *Tyr* and *Pmel* which are melanosomal structural proteins required for early melanogenesis and melanosome biogenesis (Figure 3A) [11-14, 63]. Indeed, when SAM was tested for metastasis in *in vitro* assays (migration, invasion) and *in vivo* experiments (lung metastasis model), it significantly decreased metastasis of melanoma cells and tumors (Figure 5D, 6E, Supplementary Figure 8, and [22]).

MITF regulates expression of many pigmentation, MICs marker, and cell cycle regulatory genes. In a previous study, *MITF* amplification was found to be present in 5-20% of melanomas and *MITF* was defined as a lineage-addiction oncogene [64]. However, targeted-capture deep sequencing has shown no changes in copy number of *MITF* in clinical melanoma samples [65, 66]. Furthermore, MITF has demonstrated to suppress melanoma invasion and metastasis, and knock-out/KD of *MITF* increases tumor growth and progression, and metastasis in various melanoma mouse models [9, 10, 65-69]. MITF acts as a rheostat and dynamically controls phenotype switching and this model is extensively discussed and established [8-10, 67, 69]. Various studies have indicated that cells expressing low MITF are intrinsically resistant to MAPK pathway inhibitors (such as BRAFi/ MEKi) and immunotherapies (anti-PD-1 and anti-CTLA-4 antibodies), often persist, and have the highest ability to form tumors and metastasize [8, 9, 67, 69-72]. Importantly, dedifferentiated melanomas characterized by low MITF and low MDAs are resistant to immunotherapy as well [15, 16, 73, 74]. Consistently, differentiated dark stained tumors are also infiltrated with higher density of immune cells (immunologically hot) [69]. In addition, tumors with low MITF expression have a pro-inflammatory secretome which ultimately affects recruitment of T cells and function within TME [63]. Interestingly, inhibition of BRAFV600E activity specifically upregulates MITF levels thereby increasing the expression of MDAs which in turn increases immunogenicity of the cancer/tumor cells [75, 76]. Indeed, peripheral engineered T cells directed against MDAs led to tumor regression in tumors of human melanoma patients [77]. Recently, a directed phenotype switching was proposed as an effective anti-melanoma strategy by elevating MITF levels and switching the highly proliferative cells and highly invasive cells towards differentiation and cell death [7, 9]. Interestingly, SAM causes a similar effect by increasing *Mitf* expression and directing heterogenous proliferative and invasive melanoma cells towards differentiation as indicated by the low proliferation rates, low metastatic ability, melanocyte-like morphology, high melanin and melanosome production, and high MDAs and MAAs expression (Figures 1-5). Parallel to this, upon examining the TCGA melanoma cohort data, MITF expression strongly mirrored the expression of pigmentation genes that are MITF targets [2]. Hence, low-MITF tumors had low expression of pigmentation genes and vice versa. In line with this, melanosomes contain acidic proteases that degrades proteins into antigenic peptides in the endolysosomal pathways [63]. Since SAM increased number of melanosomes in B16 cells (Figure 2), this further supports the finding of increased antigen expression of melanoma cells by

SAM. Accordingly, SAM treatment had a significant anti-cancer efficacy and reduced tumor growth and progression, and metastasis in immunocompetent models (Figure 5, 6). Compared to control, SAM treated tumors were also more inflamed (hot) as indicated by an increased T cells infiltration (including $CD8^+$ T cells density, $CD4^+$ T cells density and frequency, and Th17 cells frequency), and higher activation of $CD8^+$ T cells ($CD8^+$ T-bet^+/g of tumor and MFI $ICOS^+$) in TME (Figure 7 and 8).

IL6 cytokine production is upregulated by endothelial cells and fibroblasts upon IL17D stimulation [78]. Additionally, IL17D is highly induced by Nrf2 and other stress pathways and can lead to tumor rejection and enhanced anti-cancer immune response [79, 80]. Our top significantly upregulated pathways with SAM were Nrf2 and oxidative stress (Supplementary Figure 2C and 4, and Supplementary Table 6), and SAM increased expression of IL17D (and its receptors) and IL6 (Supplementary Figure 12). IL17D itself was shown to elevate anti-cancer immune response via NK recruitment [79]. Therefore, Nrf2 pathway inducing IL17D expression and IL6 expression which may then lead to high Th17 cells could be another pathway enhancing immune responses against tumor cells that is induced by SAM. The intriguing effect of SAM on frequency of $IL17^+$ cells in melanoma TME and expression of IL6 and IL17D in melanoma cells will need to be further investigated.

IFNγ is one of the most powerful cytokines that can cause anti-tumor activity, determines the success of CPIs and is a characteristic feature of cytotoxic T cells that produce perforin and granzymes [81-83]. IFNγ has marked anti-tumor pleiotropic effects including inhibition of immunosuppressive T_{regs}, M1 macrophage and $CD4^+$ T_h1 polarization, DCs maturation and MHCI and II upregulation, increased cytotoxic (killing) activity, proliferation, and motility of $CD8^+$ T cells, apoptosis of cancer cells, and inhibition of angiogenesis [81-83]. T-bet regulates the transcription of IFNγ [81]. Similar to IFNγ, TNFα can also cause tumor cell death by apoptosis and inhibit angiogenesis in tumors [83]. Indeed, the greatest reduction in tumor volumes were in the SAM+anti-PD-1 combination group, which is in line with significant upregulation of IFNγ, T-bet and TNFα of cytotoxic $CD8^+$ T cells in these tumors, compared to control. In parallel, there was a trend in increase of IFNγ, T-bet and TNFα by $CD8^+$ T cells with monotherapies which is in line with significant tumor reduction compared to control. Consistently, polyfunctional $CD8^+$ T cells which are the most potent cytotoxic $CD8^+$ T cells and can cause effective tumor lysis, were

not present in the control tumors, but were significantly highest in the combination group with a trend in increase in monotherapies (Figure 7).

A high percentage (>80%) of melanoma patients relapse on the BRAFi/ MEKi cocktail, which is due to, as mentioned above, slow-growing low-MITF-expressing stem-cell like cells [1, 2, 8, 9, 67, 69-72, 84]. Hence, therapies that upregulate MITF can have distinct advantage [7]. Another challenge is that 60–70% of melanoma patients do not respond to CPI therapy [1, 5, 6, 84]. The SAM+anti-PD-1 combination proposed in this study has several advantages: (a) SAM upregulates MITF levels thereby decreasing the pool of slow-growing low-MITF-expressing stem-cell like cells that have high probability of initiating tumors, metastasis, and tumor relapse after treatment. Additionally, SAM increases the immunogenicity, in part by elevating MITF levels, of the melanoma cells. In line with this, we have not found development of pharmacological resistance to long-term treatment of SAM in this study or any other cancer model (*in vitro* and *in vivo*) [22, 23, 85-87]. (b) While anti-PD-1 antibody has some immune-related adverse effects, SAM being an approved supplement has shown no severe adverse effects in pre-clinical and clinical studies except a transient adverse behavioral effect in an individual [22, 23, 85-88]. (c) The SAM+anti-PD-1 antibody therapy is effective against both models of BRAF WT and mutant melanoma subtypes which are representative of 80-85% of the melanoma patients. Additionally, we have also observed beneficial effect of the combination in breast cancer [89]. (d) The current study along with our previous published study [22] was conducted using syngeneic melanoma cell lines and immunocompetent mouse tumor models, instead of xenograft models that are severely immune-deficient. Accordingly, these models avoid interspecies immune responses but have a complete immune system against melanoma tumors, therefore, faithfully represent the human pathophysiology that occurs in tumors of human melanoma patients [9, 90]. Along these lines, we have used only one CPI (anti-PD-1 antibody) with SAM. This also has advantages compared to the use of drug cocktails such as BRAFi and MEKi with anti-PD-1 and anti-CTLA-4 antibodies currently employed in the clinic which, for example, could have a higher risk of adverse events and more complicated therapeutic regimes. (e) Lastly, SAM+anti-PD-1 antibody combination led to complete tumor elimination in 20% of YUMMER1.7-tumor bearing mice. This is a promising finding which would need further investigation.

Although SAM and anti-PD-1 antibody combination shows significant potential against BRAF mutant and WT melanomas, the current study had some limitations. For instance, since we

observed SAM incremented immunogenicity and sensitivity of the melanoma cells *in vitro*, we had started SAM treatment of the tumor-bearing mice at 2-4 days post-tumor inoculation. The rationale behind this was to investigate the effect of SAM on priming the melanoma cells for anti-PD-1 antibody which has been carried out with other epigenetic therapies like DNA methyltransferase inhibitors (DNMTi) and histone deacetylase inhibitors (HDACi) [91, 92]. Also, SAM had to be given daily during the treatment period because of low bioavailability of orally taken SAM reported in the past [23, 85, 88].

Future studies could implement other CPIs with SAM. One promising candidate is anti-CTLA-4 antibody. This is because anti-CTLA-4 antibody elevates the expansion of tumor-infiltrating T_h1 ($PD\text{-}1^+$, $ICOS^+$, $Tbet^+$) cells and $CD8^+$ T cells, and there is some evidence that SAM is required for T cells activation and proliferation [25-29]. Moreover, triple combination of SAM+anti-PD-1+anti-CTLA-4 antibodies could also serve as a potential therapeutic strategy. However, for triple combination therapy, CPI dose would have to be reduced to avoid immune related adverse effects by CPI therapies.

To the best of our knowledge, the current study together with our previous study [22] is the first potential evidence of the beneficial anti-cancer efficacy of SAM against BRAF WT and BRAF mutant melanomas which represent 80-85% of the melanoma patients. Moreover, our studies also to demonstrate the unique anti-cancer therapeutic effects of the novel SAM and anti-PD-1 antibody combination against melanomas. The particularly attractive nature of these studies is that both SAM and anti-PD-1 antibody are approved agents and therefore can be easily translated into the clinic. Of note, a safe and relatively cheap nutritional supplement, SAM, exhibits anti-cancer/anti-metastatic and immune-stimulatory activity which are similar to the effects seen by potentially toxic and more expensive therapies. Our study points out to the potential of this agent in repurposing it for cancer therapy to reduce morbidity and mortality rates of melanoma patients.

Materials and Methods

Cell lines

Murine melanoma BRAF mutant YUMM1.7 (RRID:CVCL_JK16) and YUMMER1.7 (RRID:CVCL_A2AX) cell lines were kindly gifted by Dr. Ian Watson (Goodman Cancer Research Centre, McGill University, Montreal, QC, Canada) and Dr. Marcus Bosenberg (Yale University

School of Medicine, New Haven, CT, USA), respectively. Human melanoma A375 cell line (RRID:CVCL_0132) was gifted by Dr. Watson as well. Murine B16-F1 (B16) BRAF wild-type (RRID:CVCL_F936) melanoma cell line was obtained from ATCC (Manassas, Virginia). Apart from YUMMER1.7, all cell lines were cultured in DMEM media supplemented with 1% penicillin-streptomycin sulfate and 10% fetal bovine serum (FBS), and 1% non-essential amino acids (NEAA) was also added for YUMM1.7 cells. YUMMER1.7 was cultured in DMEM/F12 media supplemented with 10% FBS, 1%P/S, 1% NEAA. Only early passage cell lines were utilized unless indicated. All cell lines were maintained in incubators at 37°C and 5% CO_2 and found to be mycoplasma-free.

Proliferation and wound-healing assays

For proliferation assays, YUMMER1.7 ($1x10^4$ cells), YUMM1.7 ($0.5x10^4$ cells), B16 ($1.5x10^4$ cells) and A375 ($2.5x10^4$ cells) were seeded in 6-well plates. The cells were treated with two different concentrations, 200µM and 500µM, of SAM (cat# B9003S, NEB, Canada) on day 2, 4 and 6 after seeding. On day 7, the cells were collected by trypsinization, neutralized by complete media, and counted with Beckman Coulter counter (Hertfordshire, UK). The cell pellets were either frozen or used for downstream applications. Proliferation assay data is the mean of two independent experiments. Percentage proliferation (%) is calculated as: [(Mean number of cells in (treatment group/ Control group)) x100]. Migration assay followed the regular proliferation assay protocol and then YUMMER1.7 ($5x10^4$ cells) and A375 ($1x10^5$ cells) were seeded in a 6-well plate and were confluent on the next day. Next day, the confluent cell layer was scratched in the form of a cross using a 1mL pipette tip. The 6-well plates were kept in IncuCyte® Live-Cell Analysis System and programmed to take images at timed intervals. Confluency tool of the IncuCyte® was used to analyze the closure of width-gap percentage (compared to T= 0 hr) by the migrating cells and plotted using GraphPad Prism.

Analysis of public clinical and molecular data bases

RNA expression data of normal tissue, primary tumors and metastatic tissues of the healthy participants and melanoma patients samples from GTEx and TCGA databases was downloaded using the Xena platform [33] and the data were imported into GraphPad Prism for graph plotting.

Xena platform was also used for Kaplan Meier survival plots of human gene expression data (e.g. *FAS* gene).

Melanogenesis experiments

For determining effect of SAM on melanin synthesis, melanin-producing B16 ($1.5x10^4$) cells were seeded in 6-well plate and followed the regular proliferation assay protocol. On day 7, images were taken at different magnifications using bright-field Olympus microscope (IX51) with DPController software. For intracellular melanin determination, the cells on day 7 were trypsinized, centrifuged, washed with PBS and centrifuged again. Then melanin was extracted from cell pellets by following a slight modification of previously published protocol [93]. Essentially, the cell pellets were treated with 1 N NaOH containing 10% DMSO, vortexed and boiled at 80ºC for 90 minutes, with vortex after every 15 minutes. The cells were then centrifuged, and supernatant was measured at 490nm using Tecan microplate reader. Percentage relative absorbance (relative to control) was calculated and plotted using GraphPad Prism.

RNA extraction, reverse transcription, and quantitative real-time PCR (RT-qPCR)

Total RNA from cells and tumors was extracted using column extraction method utilizing the RNeasy mini kit (cat# 71404, Qiagen, Germany) and following company's guidelines. The RNA was quantified using BioDrop analyzer according to manufacturer's instructions. For reverse transcription of RNA into cDNA standard thermal cycler was utilized with M-MLV Reverse Transcriptase (cat# 28025013, ThermoFisher Scientific, Canada) enzyme following standard company's guidelines. Then, quantitative real-time qPCR system (AB StepOnePlus) with PowerUp™ SYBR™ Green Master Mix (cat# A25742, ThermoFisher Scientific, Canada) was used to obtain Ct values according to the manufacturer's instructions [22, 85]. Analysis of gene expression was carried out using the 2-ΔΔCT method. Primers are tabulated in Supplementary Table 1.

RNA Sequencing and Bioinformatics analysis

Total RNA was extracted from cells and checked for quality control (QC) by Bioanalyzer (Agilent) and NanoDrop where only RNA Integrity Number (RIN) >6.5 and an absorbance A260/280 ratio of >2.0 was used for RNA-seq. Paired-end RNA sequencing using Illumina NovaSeq 6000 platform (with a depth of 25 million reads) following standard protocols was carried out. The obtained data was checked for QC, normalized, converted into HT-seq count files, and differential gene expression analysis carried out using DESeq2 (RRID:SCR_015687) in Galaxy (www.usegalaxy.org) according to writer's recommendations [94]. The final gene list was annotated using the Annotation tool ("Annotate DESeq2/DEXSeq output tables"). Pathway analysis was carried out using SeqGSEA software (RRID:SCR_005724) [95, 96].

siRNA Knock-down (KD) experiments

siRNAs for Mitf (cat# sc-35935, Santa Cruz Biotechnology, US) containing 3 different siMitf targeting different exons of Mitf were utilized to KD the Mitf mRNA expression. KD of Mitf mouse gene was carried out using Lipofectamine™ 2000 Transfection Reagent and Opti-MEM™ (ThermoFisher Scientific, Canada) using manufacturer's standard protocol. SiScr (siRNA-A, cat# sc-37007, Santa Cruz Biotechnology, US) was used as a negative control. For Mitf KD confirmation, cells were trypsinized and total RNA was isolated after 48hrs of transfection.

Mouse studies

Male C57BL/6 mice (RRID:IMSR_CRL:027), six to eight weeks of age, were purchased from Charles River Lab (QC, Canada) and housed at ARD division of the RI-MUHC (Montreal, QC, Canada). To generate tumors, $5x10^5$ YUMMER1.7 (in 20% Matrigel and 80% saline), and $5x10^5$ B16 cells (in saline), were subcutaneously injected into the shaved right flank of mice. Mice were randomized into four groups; control (IgG and PBS); SAM; anti-PD-1 antibody; and SAM+anti-PD-1 antibody combination. When tumor became palpable (2-4 days), treatments were started wherein SAM (Life Science Laboratories, NJ, US) at 80mg/kg dose was diluted in PBS and given daily via oral gavage using feeding needles [22, 85]. Anti-PD-1 antibody (clone RMP1-14, BioXCell cat# BE0146, RRID:AB_10949053) and isotype matched control IgG (IgG2a, clone 2A3, BioXcell, cat# BE0089, RRID:AB_1107769) was given at 10mg/kg via intra-peritoneal (i.p.)

injection twice a week and diluted in *InVivo*Pure pH 7.0 Dilution Buffer (BioXcell, US) [22, 85]. The control mice were also given PBS via oral gavage. Measurement of tumor volume (T.V) was carried out by palpation using a digital calliper at timed intervals and determined using the formula; T.V = (length × width^2)/2. Tumor growth inhibition percentage (%) was calculated as ((1 – [changes of T.V in treatment group/changes of T.V in control group] × 100) [97]. For survival studies, the YUMMER1.7 tumor bearing mice (n≥ 8/group) were treated with anti-PD-1 antibody until day 22 and continued SAM treatment until the end of the study (day 65). The mice were euthanized as their tumors reached humane endpoint (a T.V of ≥2000mm^3). The data for survival studies was plotted with Kaplan Meier curve using GraphPad Prism. For generating pulmonary metastasis mouse model of melanoma, B16 (5x10^5) cells were intravenously injected (I.V) into the tail vein of the C57BL/6 mice (n= 7/group) and treated with either control (IgG and PBS), SAM, anti-PD-1 antibody, or SAM+anti-PD-1 antibody combination. The mice were euthanized at day 15 post tumor injection, lungs harvested and fixed with formalin solution, and metastatic lung nodules counted. Percentage proportion of metastatic nodules (%) was calculated relative to control as ([total lung nodules in treatment group/ mean lung nodules in control group] × 100). Mice were regularly examined physically, measuring body weight, and for other potential adverse effects [98]. All mouse studies were carried out under standard conditions and in accordance with McGill University Facility Animal Care Committee guidelines.

Immunophenotyping

Immunophenotyping was carried out to study the effect that SAM and anti-PD-1 antibody has on immune cells within TME. Briefly, YUMMER1.7-tumor bearing mice (n=8/group) were treated with either control (isotype matched IgG and PBS), SAM, anti-PD-1 antibody, or combination. The mice were sacrificed, primary tumors were harvested, processed into single cell suspensions, and stained with extracellular and intracellular markers and cytokines as previously detailed by us [22]. Samples were then acquired using the BD Fortessa LSR-X20 and analysis was performed using FlowJo (RRID:SCR_008520) [22, 99]. All fluorescence-conjugated antibodies utilized for flow cytometry are tabulated in Supplementary Table 2.

Immunohistochemistry (IHC)

Tumors treated with control and SAM were harvested at endpoint (n=4/group). Tumors were fixed with formalin for 3-5 days and washed with 70% ethanol. An automated IHC was performed on Ventana Discovery Ultra Instrument (Roche, US). Slides were deparaffinized and rehydrated, treated with EDTA buffer for antigen retrieval and then incubated with mouse anti-Ki67 antibody (Abcam cat# ab15580, RRID:AB_443209) at 1:300 dilution. Then, anti-rabbit horseradish peroxidase (HRP)-conjugated secondary antibody was added, and signal detected using DAB chromogen kit (Biocare Medical). Slides were counter stained with Haemotoxylin and Eosin (H&E). Slides were scanned with Aperio AT Turbo digital. Images (at 40x magnification) of the ki67 stained slides were taken (n=5 images/sample) randomly using ImageScope (RRID:SCR_014311) and analyzed using Fiji (RRID:SCR_002285). In Fiji, a colour deconvolution tool was utilized to separate H&E (total cell stain) and DAB ($ki67^+$ stain) sections, and then using analyze particles tool, optimal total area of H&E and DAB staining was carried out. Then a macro was created that automatically carried out the above for one image. Then the images were input one by one for each sample into the macro. Percentage of ki67 staining was calculated as [total area of ((DAB/H&E) staining) x100%)] and was plotted using GraphPad Prism (RRID:SCR_002798).

Statistical analysis

Significance testing was determined by two-tailed Student's t-test or one-way/two-way ANOVA using GraphPad Prism (RRID:SCR_002798). Significance values are represented by asterisks *(*$p < 0.05$*; **$p < 0.01$, ***$p < 0.001$* and ****$p < 0.0001$*).

Figures (Chapter Four)

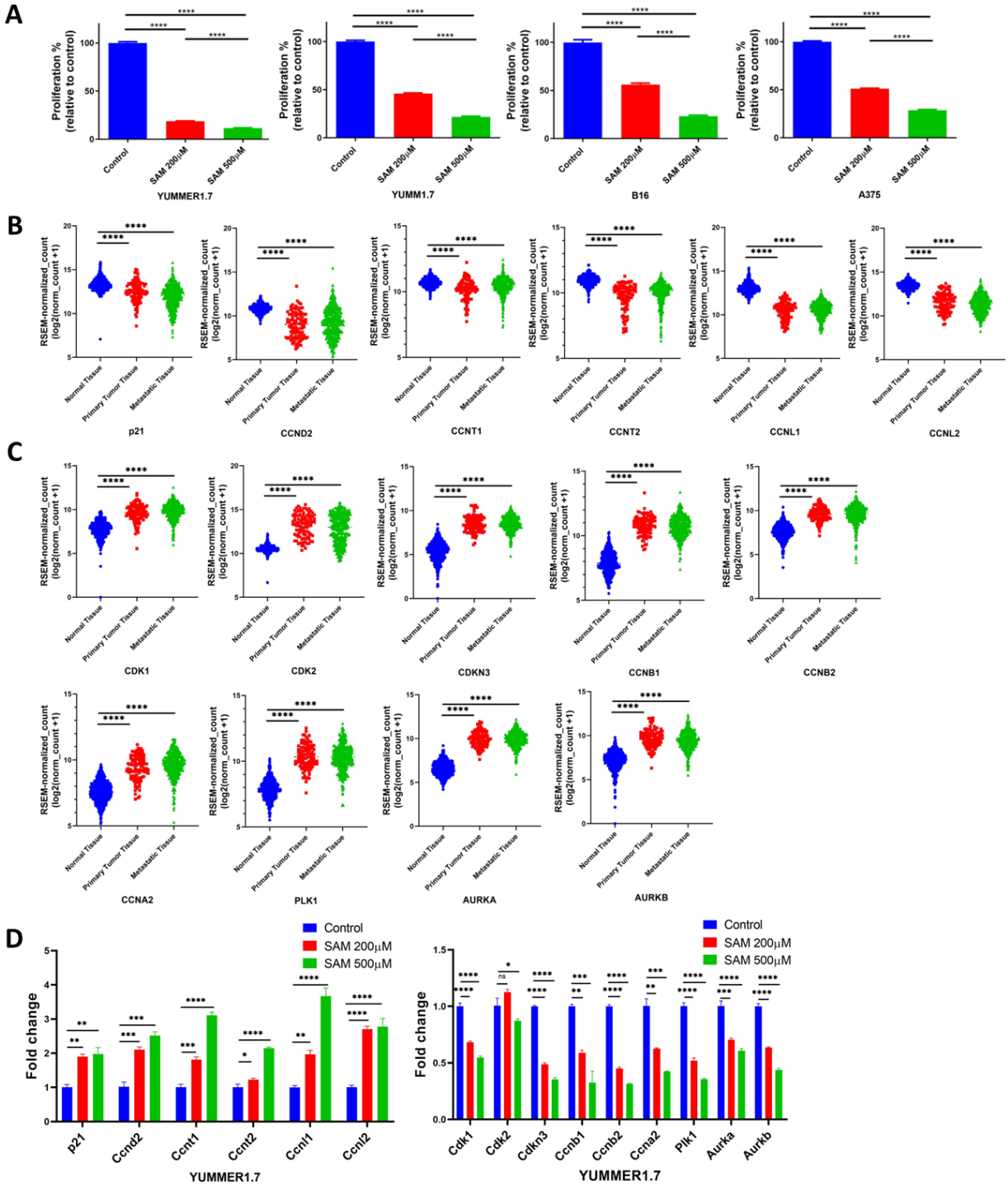

Figure 1: **SAM decreases cell proliferation of human and murine melanoma cell lines via modulating expression of key cell cycle regulators.** (A) Effect of SAM on cell proliferation of

melanoma cell lines. YUMMER1.7 (1x10^4 cells), YUMM1.7 (0.5x10^4 cells), B16 (1.5x10^4 cells) and A375 (2.5x10^4 cells) were seeded in 6-well plates and treated with two doses of SAM, 200µM and 500µM. Proliferation is represented as the percentage of proportion to Control (± SEM). (B-C) Expression of key cell cycle regulators in normal skin, primary tumor and metastatic tissue of human melanoma patients and normal healthy individuals extracted from TCGA and GTEx databases using Xena platform [33]. The expression data of genes has been plotted in a scatter-plot graph (1024 samples). (D) Expression of cell cycle regulators in YUMMER1.7 cells after treatment with two doses of SAM, 200µM and 500µM as determined using RT-qPCR. Expression is depicted as fold change (± SEM) relative to control. Statistical significance was calculated using (A-D) one-way ANOVA test.

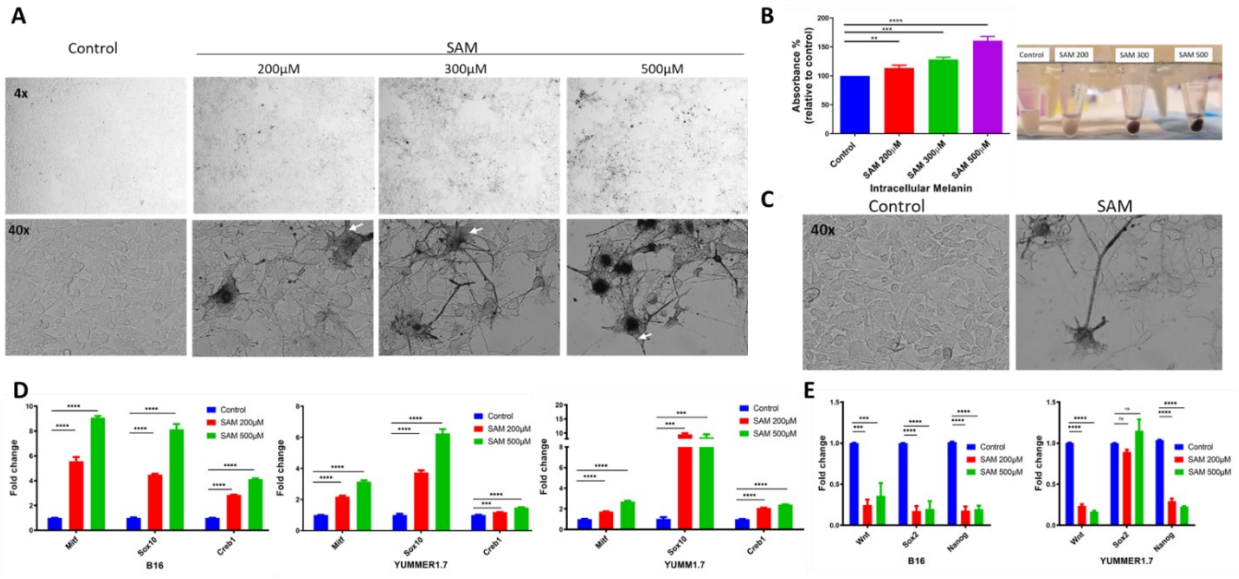

Figure 2: **SAM increases melanogenesis and drives phenotype switching of melanoma cells.** (A) Microscope images (top; lens, 4x, magnification, 40x; and bottom; lens, 40x, magnification, 400x) showing effect of SAM on melanin and melanosome synthesis of B16 cells. B16 (1.5x10^4) cells were seeded in 6-well plates and treated with vehicle or SAM (200µM, 300µM and 500µM). Melanosomes can be viewed as dots (indicated by white arrows). (B, left) Percentage absorbance (relative to Control) of intracellular melanin extracted from B16 cell pellets treated with varying doses of SAM (200-500µM). Absorbance (± SEM) was measured at 490nm which is optimal wavelength for measuring melanin pigment. (B, right) Cell pellets showing SAM increases

melanin of B16 cells in a dose dependent manner. (C) Images (lens, 40x, magnification, 400x) of B16 cells treated with control and SAM (200µM) showing morphological changes upon SAM treatment. (D-E) Expression of (D) melanocyte transcription factors (TFs) and; (E) master CSC marker genes (*Wnt*, *Sox2* and *Nanog*); in melanoma cell lines upon treatment with SAM (200 and 500 µM) analyzed with RT-qPCR. Expression is depicted as fold change (± SEM) relative to control. Statistical significance was calculated using (B, D, E) one-way ANOVA test.

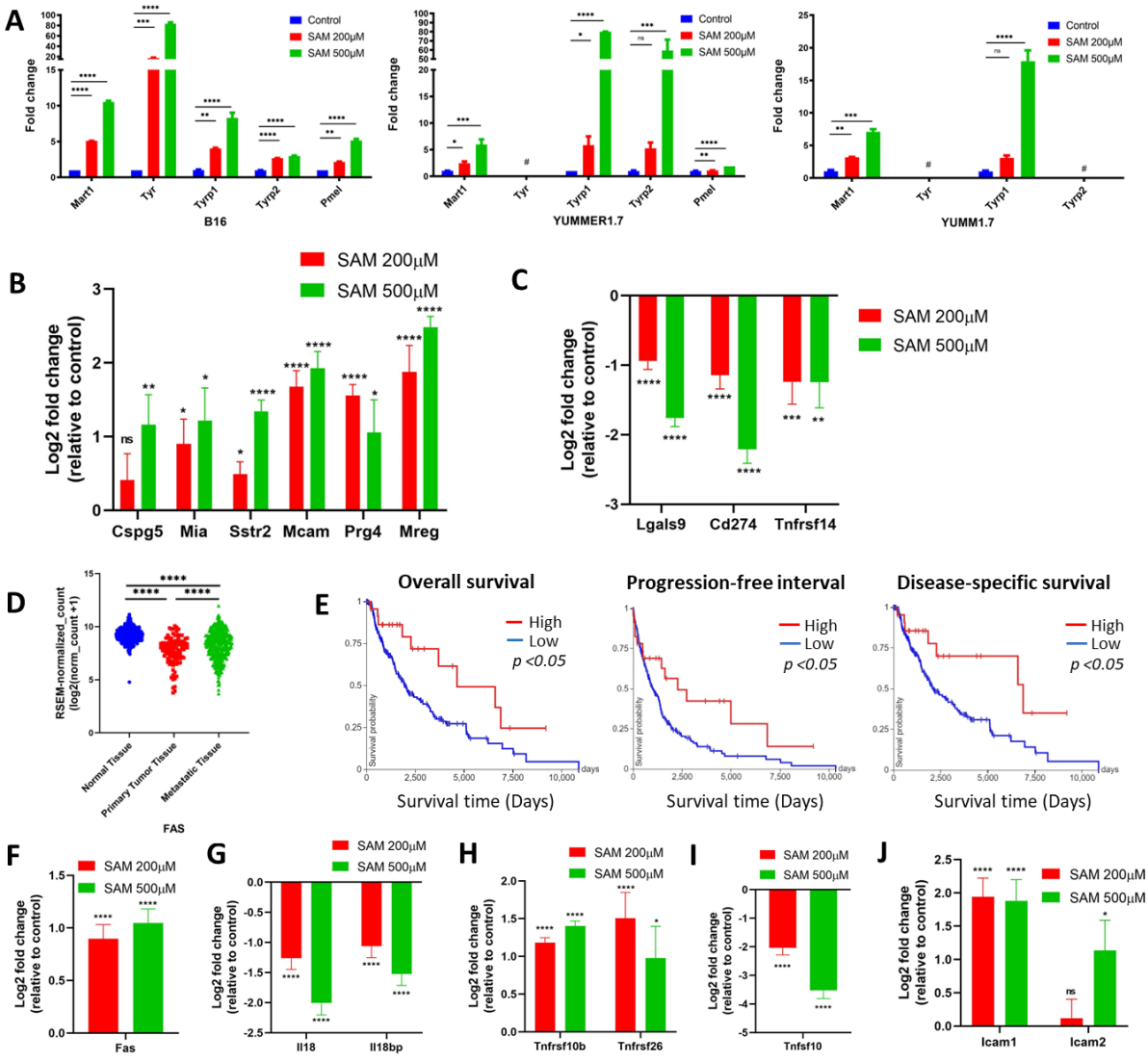

Figure 3: **SAM increases immunogenicity of murine melanoma cell lines.** (A) Expression of melanocyte differentiation antigens (MDAs) in B16, YUMMER1.7 and YUMM1.7 cells upon treatment with SAM (200 and 500µM) analyzed with RT-qPCR. # *Tyr* had no/undetectable

expression in non-pigmented YUMMER1.7 and YUMM1.7 cells while *Tryp2* expression was also undetectable in YUMM1.7 cells. Expression is depicted as fold change (± SEM) relative to control. Statistical significance was calculated using one-way ANOVA for each gene. (B-C) Expression of (B) melanoma associated antigens (MAAs); and (C) immune inhibitory molecules in YUMMER1.7 cells upon treatment with SAM (200 and 500μM) extracted from RNA-seq data. The log2 fold change is relative to Control where value of control is 0. The FDR values are placed on top of each bar and are relative to control. (D) Expression of *FAS* in the normal skin tissue, primary tumor and metastatic tissue samples of healthy and melanoma patients (n=1024 samples) extracted from GTEx and TCGA databases, respectively, and produced using Xena [33]. RSEM (RNA-Seq by Expectation Maximization) represents expression values. (E) Overall survival, progression-free interval and disease specific survival Kaplan Meier curves of *FAS*; X-axis: survival time (days); Y-axis: probability of survival. (E, left) Low (blue) n= 248; High (red) n = 23; *P* = *. (E, middle) Low (blue) n= 249; High (red) n = 23; *P* = *. (E, right) Low (blue) n= 244; High (red) n = 22; *P* = *. Survival plots were produced using Xena. (F-J) Expression of (F) *Fas* receptor;(G) *Il18* and *Il18bp*; (H) TRAIL receptors (*Tnfrsf10b, Tnfrsf26*); (I) TRAIL ligand (*Tnfsf10*); and (J) *Icam1* and *Icam2* genes in YUMMER1.7 cells upon treatment with SAM (200 and 500 μM) extracted from RNA-seq data. The log2 fold change is relative to Control where value of control is 0. The FDR values are placed on top of each bar and are relative to control. Statistical significance was calculated using (A, D) one-way ANOVA test; (B, C, F-J) Wald test with BH FDR.

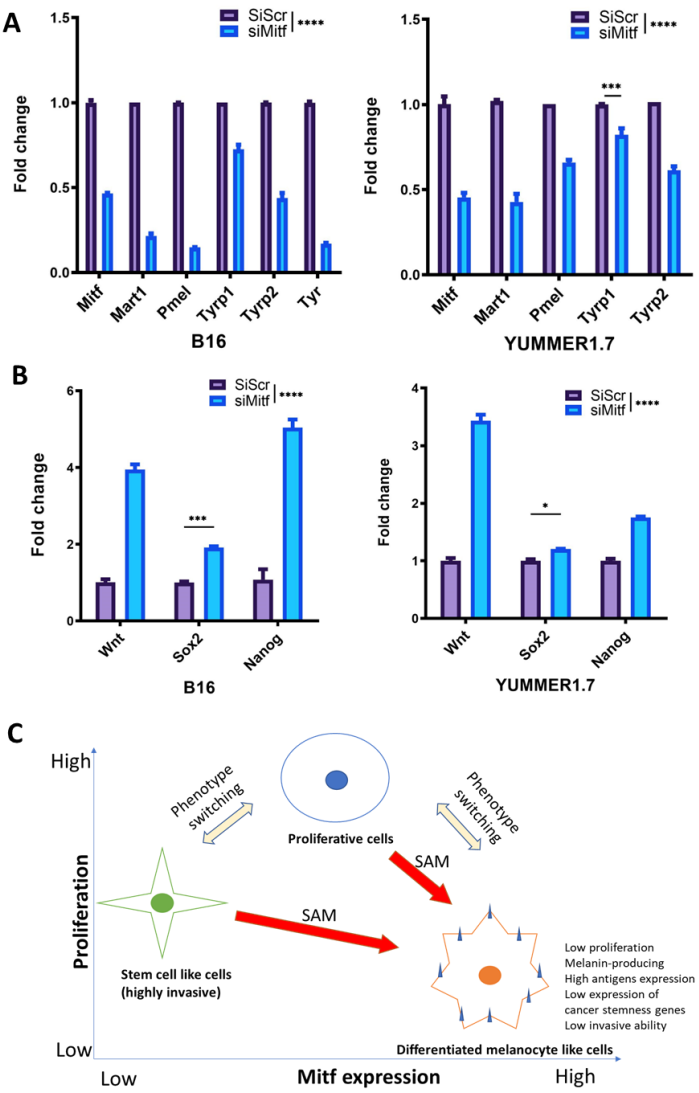

Figure 4: *Mitf* is responsible for phenotype switching and controls the expression of MDAs and stemness genes in melanoma cells. (A-B) Expression (±SEM) of (A) *Mitf* and MDAs; and (B) master CSC marker genes (*Wnt*, *Sox2* and *Nanog*); in B16 and YUMMER1.7 cells upon siMitf (35nM) treatment analysed using RT-qPCR. The fold change is relative to scramble control (siScr) where value of control is 1. Statistical significance was calculated using (A-B) two-way ANOVA test and are **** unless indicated. (C) Model figure summarizing the effect of SAM on phenotype switching of melanoma cells from invasive and proliferative to differentiated state which could be due to elevation in Mitf levels.

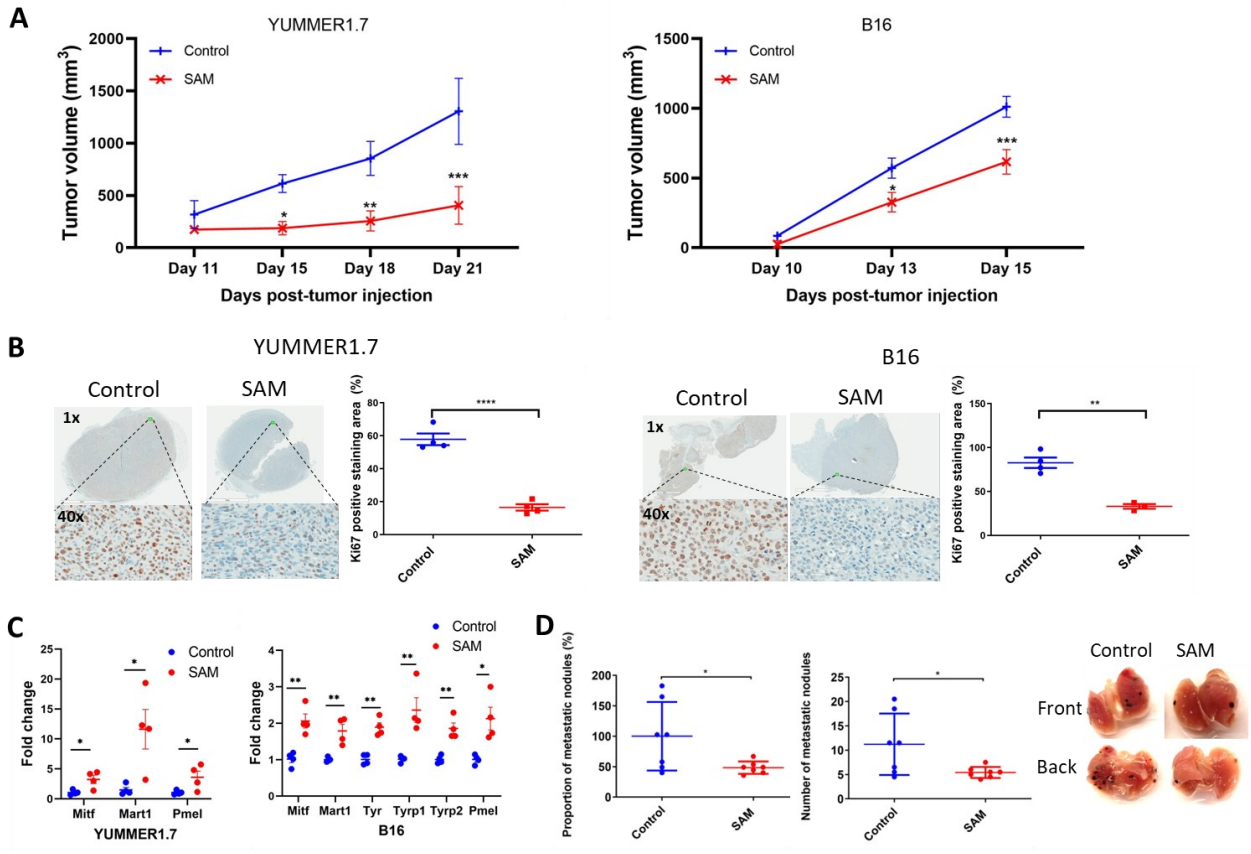

Figure 5: **SAM reduces tumor growth and progression, and metastasis of melanoma mouse models.** (A) Tumor volume (mm^3) of control (PBS) and SAM treated YUMMER1.7 (n≥7/group) and B16 (n≥10/group) tumor bearing mice plotted against days post tumor injection. Data pooled from two independent repeats. Essentially, YUMMER1.7 ($5x10^5$) and B16 ($5x10^5$) cells were subcutaneously injected in C57BL/6 mice, and once the tumors were palpable treatment was initiated with either control (PBS) or SAM via oral gavage. Tumor volumes were measured at timed intervals. (B, left) Immunohistochemical images (top; lens, 1x, magnification, 10x; and bottom; lens, 40x, magnification, 400x) of the primary YUMMER1.7 (n=4 samples/group) and B16 (n≥3 samples/group) tumors stained with murine antibody against Ki67 proliferation marker (brown) from control and SAM treated group showing proliferative ability of tumor cells. The nucleus is stained blue. (B, right) Ki67 positive staining area percentage (n= 5 images/sample ±SEM). (C) Expression (±SEM) of *Mitf* and MDAs in YUMMER1.7 and B16 tumors from control and SAM treated group (n=4 samples/group) determined with RT-qPCR. (D) Percentage proportion of metastatic nodules (relative to control, ±SEM) and number of metastatic nodules (±SEM) on lungs of control and SAM treated mice. Representative lung images showing front and

back. Essentially, B16 ($2.5x10^5$) cells were intravenously injected in C57BL/6 mice (n≥ 7/group) and treated with PBS (control) or SAM. Statistical significance was calculated using (A) two-way ANOVA test; (B-D) two-tailed t-test.

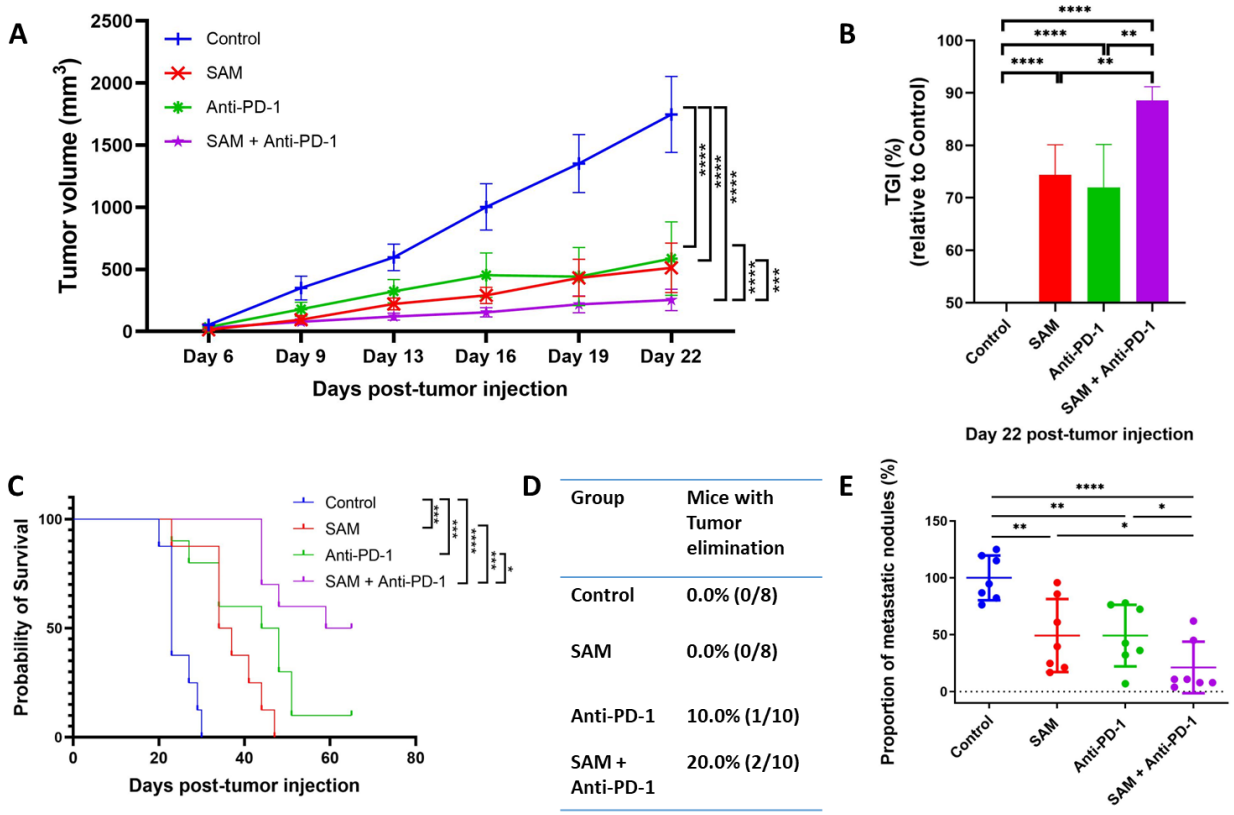

Figure 6: **Combination of SAM with anti-PD-1 antibody results in significant higher anti-cancer efficacy in melanoma mouse models.** (A) Tumor volume (mm^3) of control (IgG and PBS), SAM, anti-PD-1 antibody and combination treated YUMMER1.7 (n≥20/group) tumor bearing mice plotted against days post tumor injection. Data pooled from three independent experiments. Essentially, YUMMER1.7 ($5x10^5$) cells in 20% Matrigel were subcutaneously injected in C57BL/6 mice. When tumors were palpable (day 2-4), treatment was initiated with either control (IgG and PBS), SAM, anti-PD-1 antibody or combination of SAM+anti-PD-1. Tumor volumes (±95% CI) were measured at timed intervals. (B) Percentage tumor growth inhibition (%) (±SEM) of SAM, anti-PD-1 and combination group (n≥20/group) relative to control at Day 22. (C) Kaplan-Meier curve showing the probability of survival of YUMMER1.7 tumor bearing mice in the treated groups (n≥8/group) against days elapsed (or days post-tumor injection). The mice were sacrificed as they reached humane end point (T.V ≥ $2000mm^3$). (D) Table showing

the percentage of mice with complete tumor elimination at the end of the study (day 65). (E) Percentage proportion of metastatic nodules (relative to control, ±SEM) on lungs of treated mice at day 15 post-tumor injection. Essentially, B16 ($5x10^5$) cells were intravenously injected in C57BL/6 mice (n≥ 7/group) and treated with either Control (IgG and PBS), SAM, anti-PD-1 antibody or combination of SAM+anti-PD-1. Statistical significance was calculated using (A) two-way ANOVA test; (C) log-rank test; and (B,E) one-way ANOVA test.

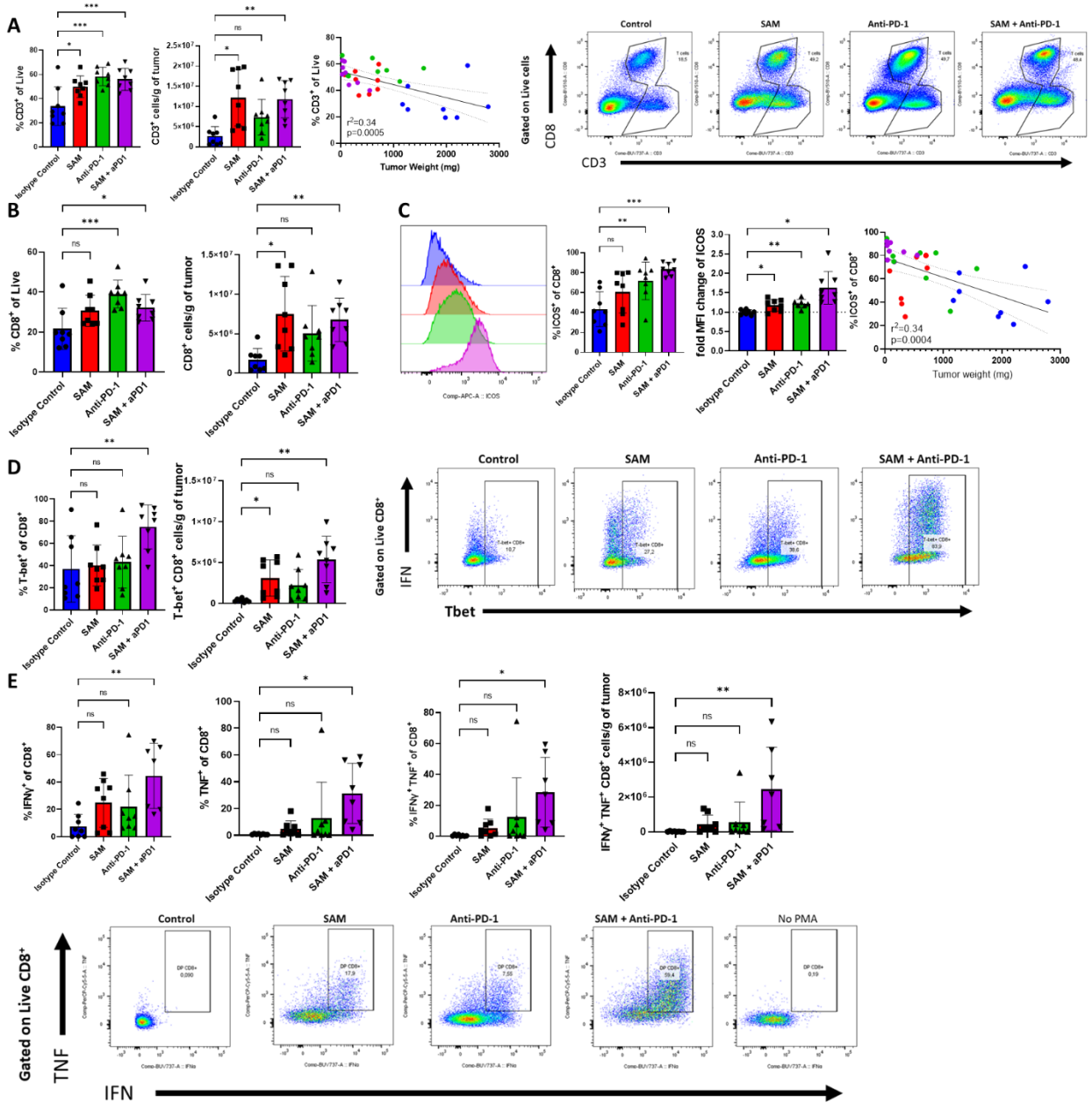

Figure 7: SAM in combination with anti-PD-1 antibody enhances $CD8^+$ T cells' tumor infiltration, activation, cytokine production and polyfunctionality in the TME. Briefly, YUMMER1.7 tumor-bearing mice were treated with control (isotype matched IgG and PBS), SAM, anti-PD-1 antibody, and combination. At day 22, mice were euthanized, tumors harvested and immunophenotyping by flow cytometry was carried out. (A) Flow cytometry analysis of CD3 and CD8 expression. Representative flow plots gated on live cells. (B) $CD8^+$ T cells frequency ($CD8^+$ $CD3^+$ cell of Live cells) and density (cells per gram of tumor). (C) Flow cytometry analysis of ICOS expression on $CD8^+$ T cells. Representative flow plots of ICOS. Mean fluorescence Intensity (gated on Live $CD3^+$ $CD8^+$ cells). (D) Flow cytometry analysis of T-bet expression. Representative flow plots gated on live $CD45^+$ $CD8^+$ cells. (E) Flow cytometry analysis of IFNγ and TNFα expression (top). Representative flow plots gated on live $CD45^+$ $CD8^+$ cells (bottom). Cells were stimulated for 3h with a cocktail of PMA/Ionomycin/GolgiStop® or cRPMI as control. All histograms are represented as mean ± SD. Statistical significance was calculated using one-way ANOVA test. Data points from all groups were pooled to calculate linear correlations with tumor weight. Treatment groups are indicated by color-coding. The slope's deviation from zero was evaluated using Fisher's test.

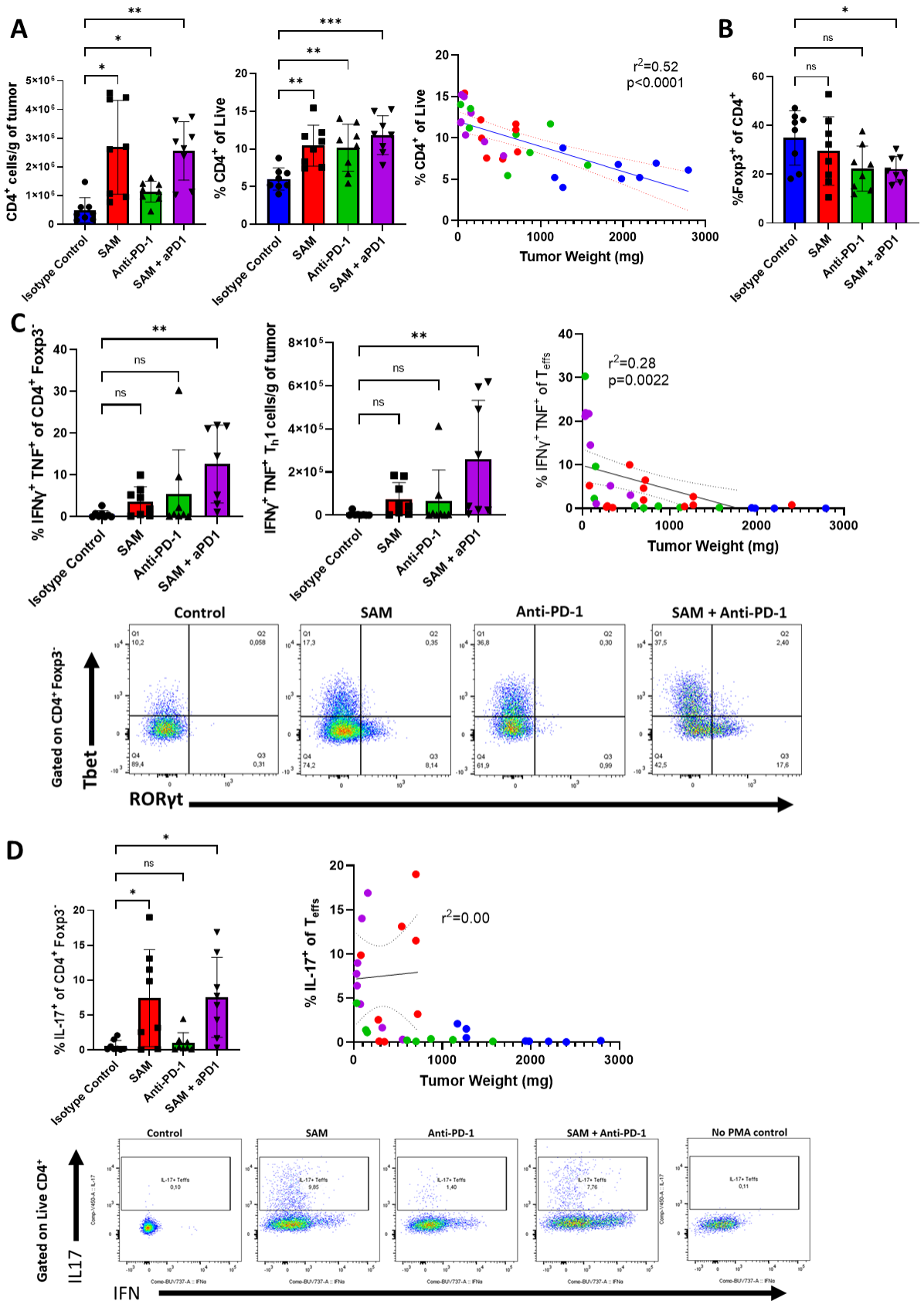
A
B
C
D
CD4+ cells/g of tumor
% CD4+ of Live
%Foxp3+ of CD4+
r2=0.52
p<0.0001
Tumor Weight (mg)
Isotype Control
SAM
Anti-PD-1
SAM + aPD1
% IFNγ+ TNF+ of CD4+ Foxp3-
IFNγ+ TNF+ Th1 cells/g of tumor
% IFNγ+ TNF+ of Teffs
r2=0.28
p=0.0022
Control
SAM
Anti-PD-1
SAM + Anti-PD-1
Gated on CD4+Foxp3-
Tbet
RORγt
% IL-17+ of CD4+ Foxp3-
% IL-17+ of Teffs
r2=0.00
No PMA control
Gated on Live CD4+
IL17
IFN

Figure 8: SAM elevates $CD4^+$ T helper cell responses in the TME. Briefly, YUMMER1.7 tumor-bearing mice were treated with control (isotype matched IgG and PBS), SAM, anti-PD-1 antibody, and combination. At day 22, mice were euthanized, tumors harvested and immunophenotyping by flow cytometry was carried out. (A) Flow cytometry analysis of $CD4^+$ T cells in the TME. Density (cells per g of tumor) of $CD4^+$ T cells; frequency (% $CD3^+$ $CD4^+$ of live cells) of $CD4^+$ T cells; and correlation of $CD4^+$ T cells with tumor weight is presented. (B) Percentage of $Foxp3^+$ of $CD4^+$ T cells. (C) Flow cytometry analysis of T-bet and RORγT expression. Representative flow plots gated on Live $CD45^+$ $CD4^+$ $Foxp3^-$ cells. (D) Flow cytometry analysis of IFNγ and IL-17 expression. Representative flow plots gated on Live $CD45^+$ $CD4^+$ $Foxp3^-$ cells. Cells were stimulated for 3h with a cocktail of PMA/Ionomycin/GolgiStop® or cRPMI as control. All histograms are represented as mean ± SD. Statistical significance was calculated using one-way ANOVA test. Data points from all groups were pooled to calculate linear correlations with tumor weight. Treatment groups are indicated by color-coding. The slope's deviation from zero was evaluated using Fisher's test.

Declarations and other statements

Contribution of authors: Conceptualization, Ali Mehdi and Shafaat Rabbani; Data curation, Ali Mehdi, Ciriaco Piccirillo, Mikhael Attias; Formal analysis, Ali Mehdi, Mikhael Attias; Funding acquisition, Shafaat Rabbani, Ciriaco Piccirillo; Investigation, Ali Mehdi, Mikhael Attias and Ani Arakelian; Methodology, Ali Mehdi; Resources, Shafaat Rabbani; Software, Ali Mehdi; Supervision, Ciriaco Piccirillo, Moshe Szyf and Shafaat Rabbani; Validation, Ali Mehdi and Ani Arakelian; Visualization, Ali Mehdi, Mikhael Attias; Writing – original draft, Ali Mehdi; Writing – review & editing, Ali Mehdi, Mikhael Attias, Ciriaco Piccirillo, Moshe Szyf and Shafaat Rabbani.

Conflict of interest statement: The authors declare no potential conflicts of interest.

Acknowledgements and Funding: The study was supported by the Canadian Institutes of Health Research (CIHR) grants, PJT-156225 and PJT-148821, awarded to Shafaat A. Rabbani and Ciriaco A. Piccirillo, respectively. Ali Mehdi is recipient of Fonds de recherche du Québec – Santé (FRQ-S) scholarship.

Data availability statement: The data analyzed or generated is available within the main file and in the supplementary files.

Ethics statement: Guidelines of the Facility Animal Care Committee (FACC) of McGill University were followed for all animal studies.

References

1. Schadendorf, D., et al., *Melanoma.* Lancet, 2018. **392**(10151): p. 971-984.
2. Network, T.C.G.A., *Genomic Classification of Cutaneous Melanoma.* Cell, 2015. **161**(7): p. 1681-96.
3. Rogiers, A., et al., *Long-Term Survival, Quality of Life, and Psychosocial Outcomes in Advanced Melanoma Patients Treated with Immune Checkpoint Inhibitors.* J Oncol, 2019. **2019**: p. 5269062.
4. Asmar, R., J. Yang, and R.D. Carvajal, *Clinical utility of nivolumab in the treatment of advanced melanoma.* Ther Clin Risk Manag, 2016. **12**: p. 313-25.
5. Kalbasi, A. and A. Ribas, *Tumour-intrinsic resistance to immune checkpoint blockade.* Nat Rev Immunol, 2020. **20**(1): p. 25-39.
6. Barrueto, L., et al., *Resistance to Checkpoint Inhibition in Cancer Immunotherapy.* Transl Oncol, 2020. **13**(3): p. 100738.
7. Saez-Ayala, M., et al., *Directed phenotype switching as an effective antimelanoma strategy.* Cancer Cell, 2013. **24**(1): p. 105-19.
8. Rambow, F., J.C. Marine, and C.R. Goding, *Melanoma plasticity and phenotypic diversity: therapeutic barriers and opportunities.* Genes Dev, 2019. **33**(19-20): p. 1295-1318.
9. Cheli, Y., et al., *Mitf is the key molecular switch between mouse or human melanoma initiating cells and their differentiated progeny.* Oncogene, 2011. **30**(20): p. 2307-18.
10. Hoek, K.S., et al., *In vivo switching of human melanoma cells between proliferative and invasive states.* Cancer Res, 2008. **68**(3): p. 650-6.
11. D'Mello, S.A., et al., *Signaling Pathways in Melanogenesis.* Int J Mol Sci, 2016. **17**(7).

12. Page, S., V. Chandhoke, and A. Baranova, *Melanin and melanogenesis in adipose tissue: possible mechanisms for abating oxidative stress and inflammation?* Obes Rev, 2011. **12**(5): p. e21-31.
13. Levy, C., M. Khaled, and D.E. Fisher, *MITF: master regulator of melanocyte development and melanoma oncogene.* Trends Mol Med, 2006. **12**(9): p. 406-14.
14. Pitcovski, J., et al., *Melanoma antigens and related immunological markers.* Crit Rev Oncol Hematol, 2017. **115**: p. 36-49.
15. Landsberg, J., et al., *Melanomas resist T-cell therapy through inflammation-induced reversible dedifferentiation.* Nature, 2012. **490**(7420): p. 412-6.
16. Huang, F., et al., *Inhibiting the MNK1/2-eIF4E axis impairs melanoma phenotype switching and potentiates antitumor immune responses.* J Clin Invest, 2021. **131**(8).
17. Beatty, G.L. and W.L. Gladney, *Immune escape mechanisms as a guide for cancer immunotherapy.* Clin Cancer Res, 2015. **21**(4): p. 687-92.
18. Alexandrov, L.B., et al., *Signatures of mutational processes in human cancer.* Nature, 2013. **500**(7463): p. 415-21.
19. Yarchoan, M., A. Hopkins, and E.M. Jaffee, *Tumor Mutational Burden and Response Rate to PD-1 Inhibition.* N Engl J Med, 2017. **377**(25): p. 2500-2501.
20. Romero-Garcia, S., H. Prado-Garcia, and A. Carlos-Reyes, *Role of DNA Methylation in the Resistance to Therapy in Solid Tumors.* Front Oncol, 2020. **10**: p. 1152.
21. Jung, H., et al., *DNA methylation loss promotes immune evasion of tumours with high mutation and copy number load.* Nat Commun, 2019. **10**(1): p. 4278.
22. Mehdi, A., et al., *Enhanced Anticancer Effect of a Combination of S-adenosylmethionine (SAM) and Immune Checkpoint Inhibitor (ICPi) in a Syngeneic Mouse Model of Advanced Melanoma.* Front Oncol, 2020. **10**: p. 1361.
23. Mahmood, N., et al., *An enhanced chemopreventive effect of methyl donor S-adenosylmethionine in combination with 25-hydroxyvitamin D in blocking mammary tumor growth and metastasis.* Bone Res, 2020. **8**: p. 28.
24. Bottiglieri, T., *S-Adenosyl-L-methionine (SAMe): from the bench to the bedside--molecular basis of a pleiotrophic molecule.* Am J Clin Nutr, 2002. **76**(5): p. 1151S-7S.
25. Hote, P.T., et al., *Ethanol inhibits methionine adenosyltransferase II activity and S-adenosylmethionine biosynthesis and enhances caspase-3-dependent cell death in T*

lymphocytes: relevance to alcohol-induced immunosuppression. J Nutr Biochem, 2008. **19**(6): p. 384-91.

26. Tobena, R., et al., *Interleukin-2 induces gamma-S-adenosyl-L-methionine synthetase gene expression during T-lymphocyte activation.* Biochem J, 1996. **319 (Pt 3)**: p. 929-33.
27. LeGros, H.L., Jr., A.M. Geller, and M. Kotb, *Differential regulation of methionine adenosyltransferase in superantigen and mitogen stimulated human T lymphocytes.* J Biol Chem, 1997. **272**(25): p. 16040-7.
28. Kotb, M., J.B. Dale, and E.H. Beachey, *Stimulation of S-adenosylmethionine synthetase in human lymphocytes by streptococcal M protein.* J Immunol, 1987. **139**(1): p. 202-6.
29. De La Rosa, J., et al., *Induction of interleukin 2 production but not methionine adenosyltransferase activity or S-adenosylmethionine turnover in Jurkat T-cells.* Cancer Res, 1992. **52**(12): p. 3361-6.
30. Bian, Y., et al., *Cancer SLC43A2 alters T cell methionine metabolism and histone methylation.* Nature, 2020.
31. Ulanovskaya, O.A., A.M. Zuhl, and B.F. Cravatt, *NNMT promotes epigenetic remodeling in cancer by creating a metabolic methylation sink.* Nat Chem Biol, 2013. **9**(5): p. 300-6.
32. Hanahan, D. and R.A. Weinberg, *Hallmarks of cancer: the next generation.* Cell, 2011. **144**(5): p. 646-74.
33. Goldman, M.J., et al., *Visualizing and interpreting cancer genomics data via the Xena platform.* Nat Biotechnol, 2020. **38**(6): p. 675-678.
34. Zhang, D., et al., *MGDB: a comprehensive database of genes involved in melanoma.* Database (Oxford), 2015. **2015**.
35. Sarna, M., et al., *Melanin presence inhibits melanoma cell spread in mice in a unique mechanical fashion.* Sci Rep, 2019. **9**(1): p. 9280.
36. Sarna, M., et al., *Cell elasticity is an important indicator of the metastatic phenotype of melanoma cells.* Exp Dermatol, 2014. **23**(11): p. 813-8.
37. Overwijk, W.W. and N.P. Restifo, *B16 as a mouse model for human melanoma.* Curr Protoc Immunol, 2001. **Chapter 20**: p. Unit 20.1.
38. Hirobe, T., et al., *Effects of fibroblast-derived factors on the proliferation and differentiation of human melanocytes in culture.* J Dermatol Sci, 2013. **71**(1): p. 45-57.

39. Cichorek, M., et al., *Skin melanocytes: biology and development.* Postepy Dermatol Alergol, 2013. **30**(1): p. 30-41.
40. Hoek, K.S., et al., *Novel MITF targets identified using a two-step DNA microarray strategy.* Pigment Cell Melanoma Res, 2008. **21**(6): p. 665-76.
41. Perego, M., et al., *Heterogeneous phenotype of human melanoma cells with in vitro and in vivo features of tumor-initiating cells.* J Invest Dermatol, 2010. **130**(7): p. 1877-86.
42. Parmiani, G., *Melanoma Cancer Stem Cells: Markers and Functions.* Cancers (Basel), 2016. **8**(3).
43. Friesen, C., et al., *Involvement of the CD95 (APO-1/FAS) receptor/ligand system in drug-induced apoptosis in leukemia cells.* Nat Med, 1996. **2**(5): p. 574-7.
44. Hahne, M., et al., *Melanoma cell expression of Fas(Apo-1/CD95) ligand: implications for tumor immune escape.* Science, 1996. **274**(5291): p. 1363-6.
45. Dostert, C., et al., *The TNF Family of Ligands and Receptors: Communication Modules in the Immune System and Beyond.* Physiol Rev, 2019. **99**(1): p. 115-160.
46. Helmbach, H., et al., *Drug-resistance in human melanoma.* Int J Cancer, 2001. **93**(5): p. 617-22.
47. Cai, L., et al., *Role of inhibitor of growth 4 in the suppression of human melanoma cells through the Fas/FasL-mediated apoptosis pathway.* Int J Mol Med, 2018. **41**(2): p. 1055-1061.
48. Upadhyay, R., et al., *A Critical Role for Fas-Mediated Off-Target Tumor Killing in T-cell Immunotherapy.* Cancer Discov, 2021. **11**(3): p. 599-613.
49. Cho, D., et al., *Endogenous interleukin-18 modulates immune escape of murine melanoma cells by regulating the expression of Fas ligand and reactive oxygen intermediates.* Cancer Res, 2000. **60**(10): p. 2703-9.
50. Deeths, M.J. and M.F. Mescher, *ICAM-1 and B7-1 provide similar but distinct costimulation for CD8+ T cells, while CD4+ T cells are poorly costimulated by ICAM-1.* Eur J Immunol, 1999. **29**(1): p. 45-53.
51. Shier, P., K. Ngo, and W.P. Fung-Leung, *Defective CD8+ T cell activation and cytolytic function in the absence of LFA-1 cannot be restored by increased TCR signaling.* J Immunol, 1999. **163**(9): p. 4826-32.

52. Blank, C., et al., *ICAM-1 contributes to but is not essential for tumor antigen cross-priming and CD8+ T cell-mediated tumor rejection in vivo.* J Immunol, 2005. **174**(6): p. 3416-20.
53. Lefor, A.T. and D.F. Fabian, *Enhanced cytolytic activity of tumor infiltrating lymphocytes (TILs) derived from an ICAM-1 transfected tumor in a murine model.* J Surg Res, 1998. **75**(1): p. 49-53.
54. Sartor, W.M., et al., *Enhanced expression of ICAM-1 in a murine fibrosarcoma reduces tumor growth rate.* J Surg Res, 1995. **59**(1): p. 66-74.
55. Li, L.T., et al., *Ki67 is a promising molecular target in the diagnosis of cancer (review).* Mol Med Rep, 2015. **11**(3): p. 1566-72.
56. Pardoll, D.M., *The blockade of immune checkpoints in cancer immunotherapy.* Nature Reviews Cancer, 2012. **12**(4): p. 252.
57. Wimmers, F., et al., *Long-lasting multifunctional CD8(+) T cell responses in end-stage melanoma patients can be induced by dendritic cell vaccination.* Oncoimmunology, 2016. **5**(1): p. e1067745.
58. Saran, A., et al., *Loss of tyrosinase activity confers increased skin tumor susceptibility in mice.* Oncogene, 2004. **23**(23): p. 4130-5.
59. Prud'homme, G.J., *Pathobiology of transforming growth factor beta in cancer, fibrosis and immunologic disease, and therapeutic considerations.* Lab Invest, 2007. **87**(11): p. 1077-91.
60. Martin-Orozco, N., et al., *T helper 17 cells promote cytotoxic T cell activation in tumor immunity.* Immunity, 2009. **31**(5): p. 787-98.
61. Hoek, K.S., et al., *Metastatic potential of melanomas defined by specific gene expression profiles with no BRAF signature.* Pigment Cell Res, 2006. **19**(4): p. 290-302.
62. Carreira, S., et al., *Mitf regulation of Dia1 controls melanoma proliferation and invasiveness.* Genes Dev, 2006. **20**(24): p. 3426-39.
63. Ballotti, R., Y. Cheli, and C. Bertolotto, *The complex relationship between MITF and the immune system: a Melanoma ImmunoTherapy (response) Factor?* Mol Cancer, 2020. **19**(1): p. 170.
64. Garraway, L.A., et al., *Integrative genomic analyses identify MITF as a lineage survival oncogene amplified in malignant melanoma.* Nature, 2005. **436**(7047): p. 117-22.

65. Hartman, M.L. and M. Czyz, *Pro-survival role of MITF in melanoma.* J Invest Dermatol, 2015. **135**(2): p. 352-358.
66. Harbst, K., et al., *Molecular and genetic diversity in the metastatic process of melanoma.* J Pathol, 2014. **233**(1): p. 39-50.
67. Cheli, Y., et al., *Hypoxia and MITF control metastatic behaviour in mouse and human melanoma cells.* Oncogene, 2012. **31**(19): p. 2461-70.
68. Bell, R.E., et al., *Transcription factor/microRNA axis blocks melanoma invasion program by miR-211 targeting NUAK1.* J Invest Dermatol, 2014. **134**(2): p. 441-451.
69. Wiedemann, G.M., et al., *Microphthalmia-Associated Transcription Factor (MITF) Regulates Immune Cell Migration into Melanoma.* Transl Oncol, 2019. **12**(2): p. 350-360.
70. Dilshat, R., et al., *MITF reprograms the extracellular matrix and focal adhesion in melanoma.* Elife, 2021. **10**.
71. Rambow, F., et al., *Toward Minimal Residual Disease-Directed Therapy in Melanoma.* Cell, 2018. **174**(4): p. 843-855 e19.
72. Travnickova, J., et al., *Zebrafish MITF-Low Melanoma Subtype Models Reveal Transcriptional Subclusters and MITF-Independent Residual Disease.* Cancer Res, 2019. **79**(22): p. 5769-5784.
73. Mehta, A., et al., *Immunotherapy Resistance by Inflammation-Induced Dedifferentiation.* Cancer Discov, 2018. **8**(8): p. 935-943.
74. Srour, N., et al., *PRMT7 ablation stimulates anti-tumor immunity and sensitizes melanoma to immune checkpoint blockade.* Cell Rep, 2022. **38**(13): p. 110582.
75. Hsiao, J.J. and D.E. Fisher, *The roles of microphthalmia-associated transcription factor and pigmentation in melanoma.* Arch Biochem Biophys, 2014. **563**: p. 28-34.
76. Boni, A., et al., *Selective BRAFV600E inhibition enhances T-cell recognition of melanoma without affecting lymphocyte function.* Cancer Res, 2010. **70**(13): p. 5213-9.
77. Johnson, L.A., et al., *Gene therapy with human and mouse T-cell receptors mediates cancer regression and targets normal tissues expressing cognate antigen.* Blood, 2009. **114**(3): p. 535-46.
78. Starnes, T., et al., *Cutting edge: IL-17D, a novel member of the IL-17 family, stimulates cytokine production and inhibits hemopoiesis.* J Immunol, 2002. **169**(2): p. 642-6.

79. O'Sullivan, T., et al., *Interleukin-17D mediates tumor rejection through recruitment of natural killer cells.* Cell Rep, 2014. **7**(4): p. 989-98.
80. Saddawi-Konefka, R., et al., *Nrf2 Induces IL-17D to Mediate Tumor and Virus Surveillance.* Cell Rep, 2016. **16**(9): p. 2348-58.
81. Jorgovanovic, D., et al., *Roles of IFN-gamma in tumor progression and regression: a review.* Biomark Res, 2020. **8**: p. 49.
82. Bhat, P., et al., *Interferon-gamma derived from cytotoxic lymphocytes directly enhances their motility and cytotoxicity.* Cell Death Dis, 2017. **8**(6): p. e2836.
83. Shen, J., et al., *Anti-cancer therapy with TNFalpha and IFNgamma: A comprehensive review.* Cell Prolif, 2018. **51**(4): p. e12441.
84. Rebecca, V.W., R. Somasundaram, and M. Herlyn, *Pre-clinical modeling of cutaneous melanoma.* Nat Commun, 2020. **11**(1): p. 2858.
85. Mahmood, N., et al., *Methyl donor S-adenosylmethionine (SAM) supplementation attenuates breast cancer growth, invasion, and metastasis in vivo; therapeutic and chemopreventive applications.* Oncotarget, 2018. **9**(4): p. 5169-5183.
86. Mahmood, N. and S.A. Rabbani, *Targeting DNA Hypomethylation in Malignancy by Epigenetic Therapies.* Adv Exp Med Biol, 2019. **1164**: p. 179-196.
87. Parashar, S., et al., *S-adenosylmethionine blocks osteosarcoma cells proliferation and invasion in vitro and tumor metastasis in vivo: therapeutic and diagnostic clinical applications.* Cancer Med, 2015. **4**(5): p. 732-44.
88. Goren, J.L., et al., *Bioavailability and lack of toxicity of S-adenosyl-L-methionine (SAMe) in humans.* Pharmacotherapy, 2004. **24**(11): p. 1501-7.
89. Mehdi, A., et al., *Co-Targeting Luminal B Breast Cancer with S-Adenosylmethionine and Immune Checkpoint Inhibitor Reduces Primary Tumor Growth and Progression, and Metastasis to Lungs and Bone.* Cancers, 2023. **15**(1): p. 48.
90. Bertolotto, C., et al., *Microphthalmia gene product as a signal transducer in cAMP-induced differentiation of melanocytes.* J Cell Biol, 1998. **142**(3): p. 827-35.
91. Mehdi, A. and S.A. Rabbani, *Role of Methylation in Pro- and Anti-Cancer Immunity.* Cancers (Basel), 2021. **13**(3).
92. Dunn, J. and S. Rao, *Epigenetics and immunotherapy: The current state of play.* Mol Immunol, 2017. **87**: p. 227-239.

93. Chung, S., G.J. Lim, and J.Y. Lee, *Quantitative analysis of melanin content in a three-dimensional melanoma cell culture.* Sci Rep, 2019. **9**(1): p. 780.

94. Love, M.I., W. Huber, and S. Anders, *Moderated estimation of fold change and dispersion for RNA-seq data with DESeq2.* Genome Biol, 2014. **15**(12): p. 550.

95. Mootha, V.K., et al., *PGC-1alpha-responsive genes involved in oxidative phosphorylation are coordinately downregulated in human diabetes.* Nat Genet, 2003. **34**(3): p. 267-73.

96. Subramanian, A., et al., *Gene set enrichment analysis: a knowledge-based approach for interpreting genome-wide expression profiles.* Proc Natl Acad Sci U S A, 2005. **102**(43): p. 15545-50.

97. Ubezio, P., *Beyond The T/C Ratio: Old And New Anticancer Activity Scores In Vivo.* Cancer Manag Res, 2019. **11**: p. 8529-8538.

98. Rastelli, L., et al., *A KDR-binding peptide (ST100,059) can block angiogenesis, melanoma tumor growth and metastasis in vitro and in vivo.* Int J Oncol, 2011. **39**(2): p. 401-8.

99. Cossarizza, A., et al., *Guidelines for the use of flow cytometry and cell sorting in immunological studies (second edition).* Eur J Immunol, 2019. **49**(10): p. 1457-1973.

Supplementary Material

Supplementary Figures and Tables

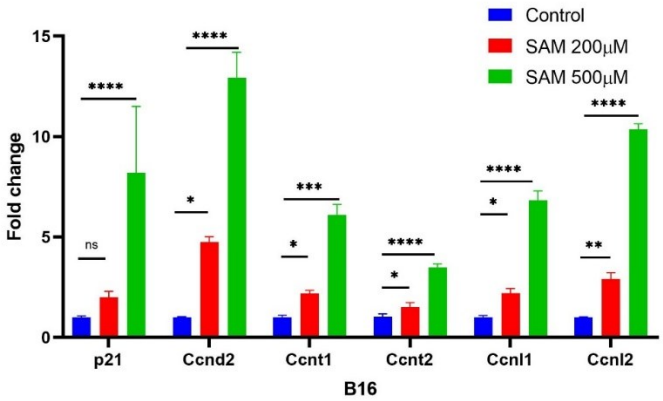

Supplementary Figure 1: Expression of cell cycle regulators in B16 cells after treatment with two doses of SAM, 200μM and 500μM as determined using RT-qPCR. Expression is depicted as fold change (± SEM) relative to control. Significant differences were determined using one-way ANOVA test.

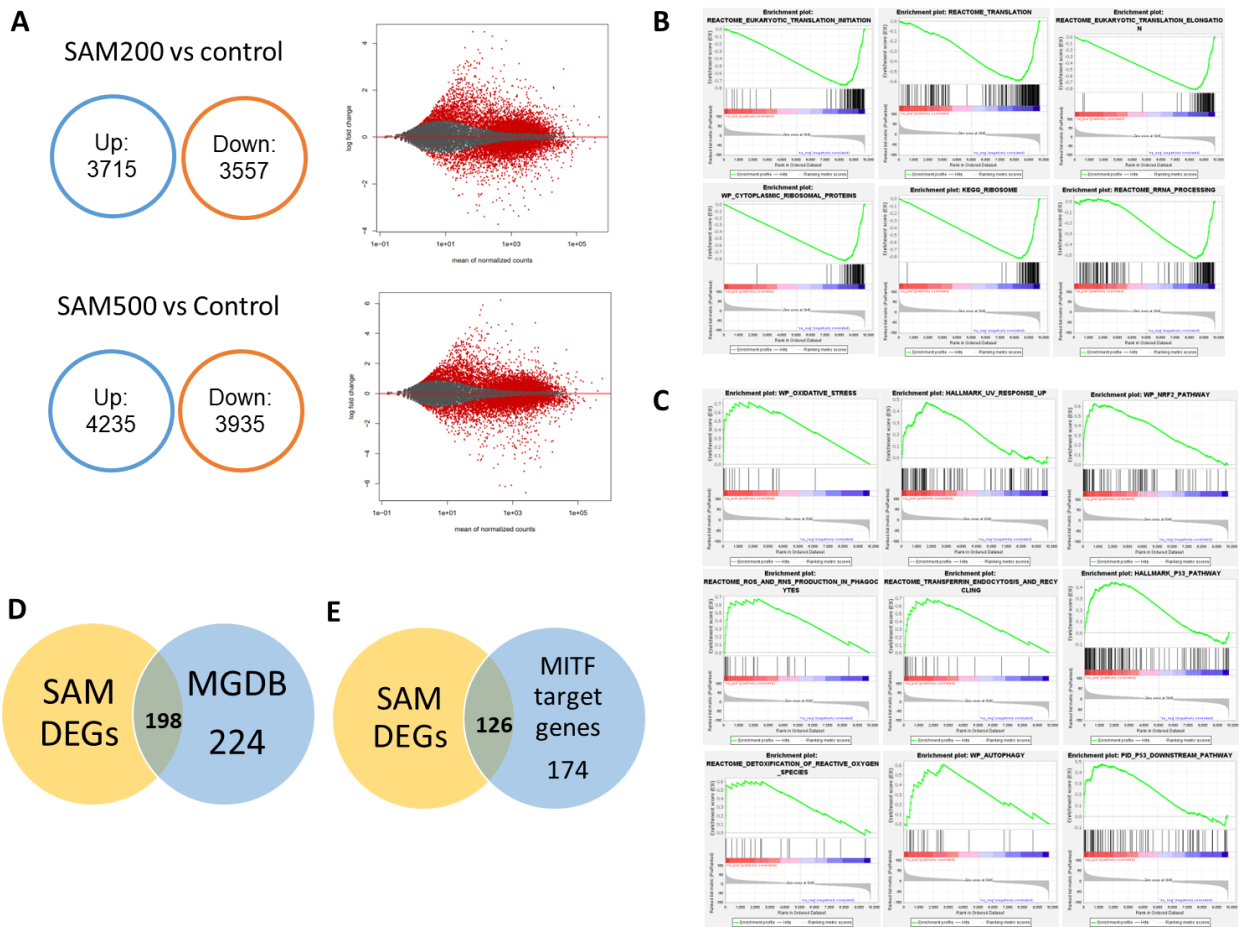

Supplementary Figure 2: Transcriptome analysis of BRAF mutant YUMMER1.7 cells treated with SAM. Large number of differentially expressed genes (DEGs) revealed from RNA-sequencing analysis on YUMMER1.7 cells treated with SAM two different SAM concentrations, 200µM and 500µM. (A) Venn Diagrams (left) and MA plot (right) showing significant DEGs (FDR<0.05) in SAM 200µM (top) and SAM 500µM (bottom) versus control groups. The red dots in MA plots represent significant DEGs while the black dots represent non-significant DEGs. (B-C) Top significantly downregulated (B) and upregulated (C) pathways derived from significantly DEGs obtained from RNA-seq of YUMMER1.7 cells treated with SAM (500µM) and analyzed using GSEA pathway analysis. (D) DEGs obtained upon SAM treatment (500µM) were overlapped with The Melanoma Gene Database (MGDB) which represent 422 known core melanoma protein-coding genes [1]. © DEGs obtained upon SAM treatment (500µM) were overlapped with MITF target genes [2].

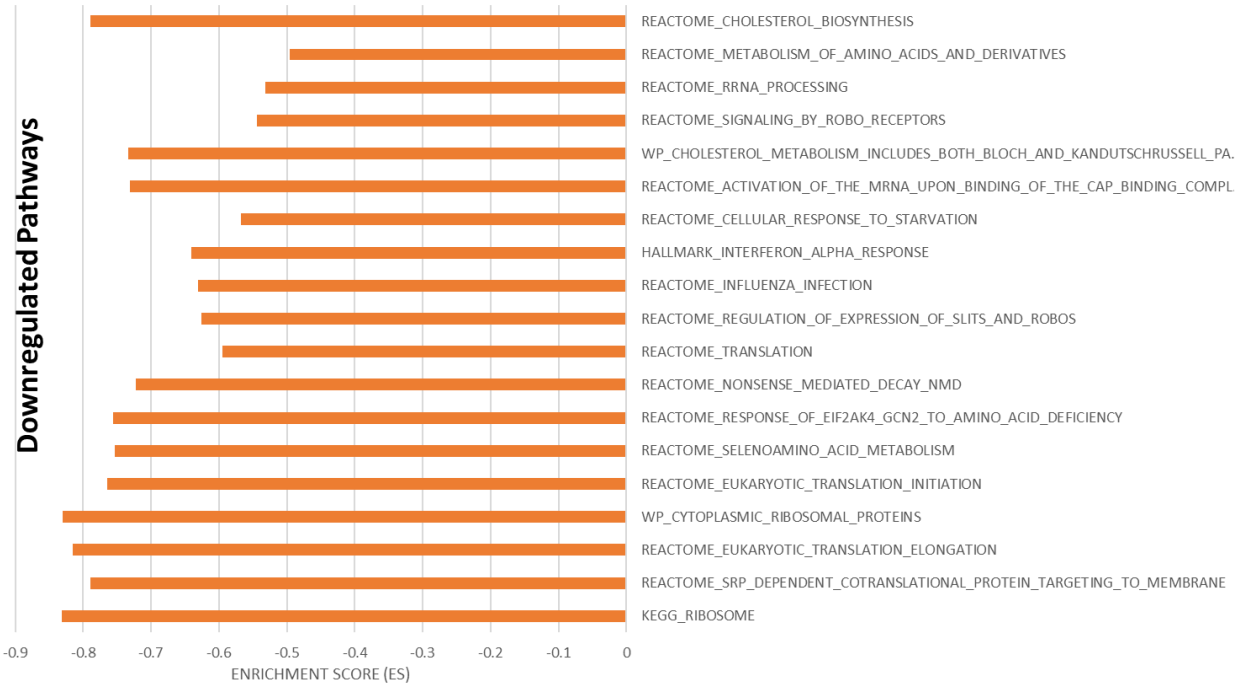

Supplementary Figure 3: Pathway analysis of BRAF mutant YUMMER1.7 cells treated with SAM. Top significantly downregulated pathways derived from significantly downregulated genes obtained from RNA-seq of YUMMER1.7 cells treated with SAM (500µM) and analyzed using GSEA pathway analysis.

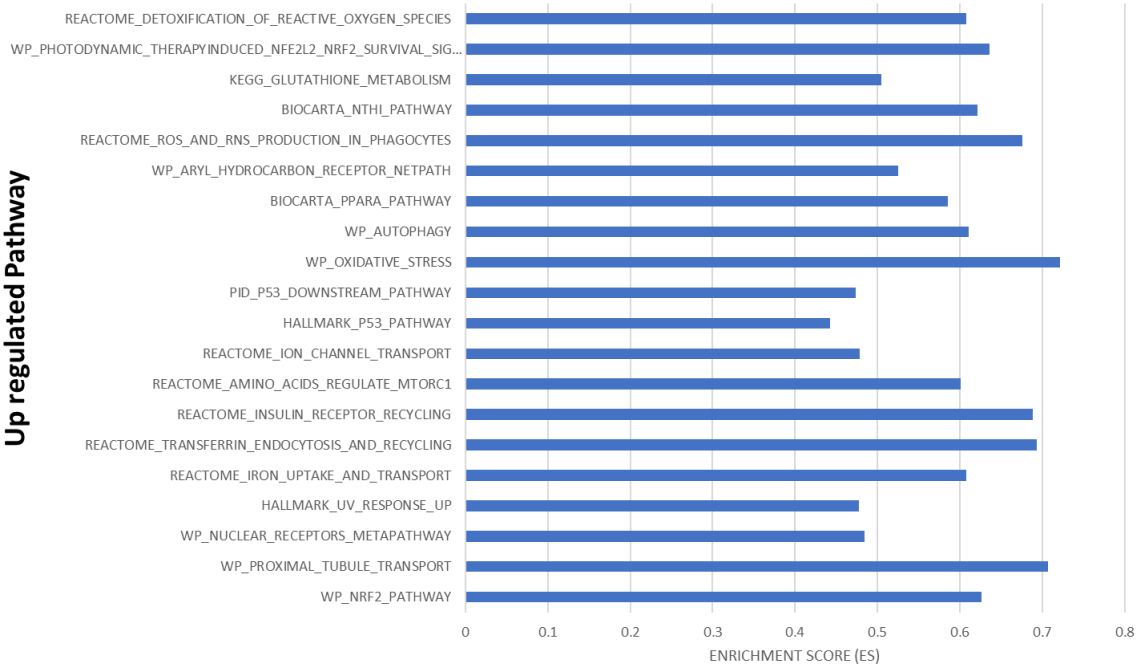

Supplementary Figure 4: Pathway analysis of BRAF mutant YUMMER1.7 cells treated with SAM. Top significantly upregulated pathways derived from significantly upregulated genes obtained from RNA-seq of YUMMER1.7 cells treated with SAM (500µM) and analyzed using GSEA pathway analysis.

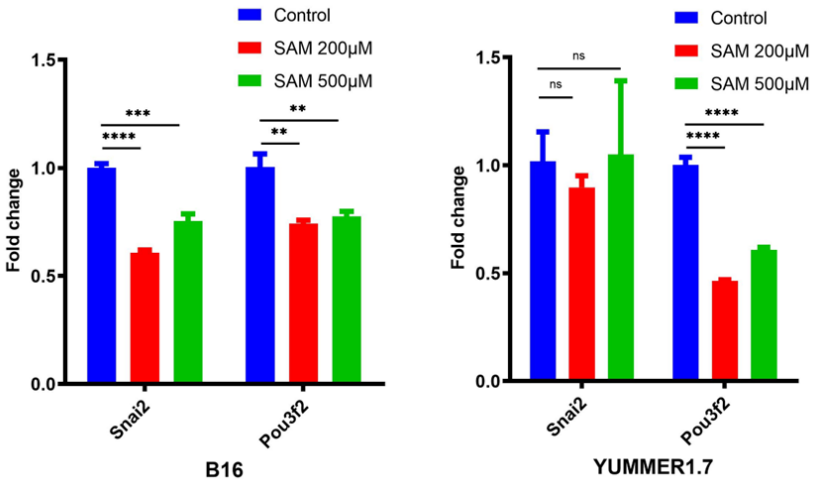

Supplementary Figure 5: Expression of master CSC marker genes, Slug (Sani2) and Brn2 (Pou3f2) in YUMMER1.7 and B16 upon treatment with SAM (200 and 500 µM) analyzed with RT-qPCR. Expression is depicted as fold change (± SEM) relative to control. Significant differences were determined using one-way ANOVA test.

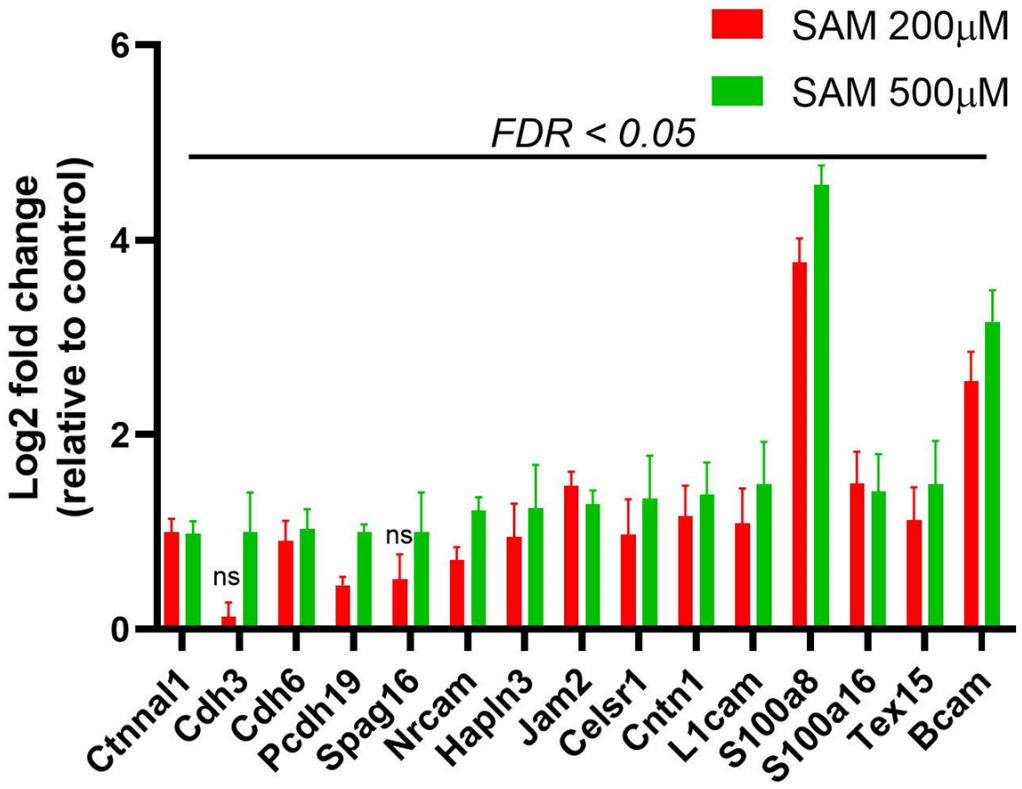

Supplementary Figure 6: Expression of tumor associated antigens (TAAs) including cadherins, adhesions and S100 family genes (FDR<0.05) in YUMMER1.7 upon treatment with SAM (200 and 500 μM) extracted from RNA-seq data. The log2 fold change is relative to Control where value of control is 0. Significant differences were determined using Wald test with BH FDR. Ns indicates not significant.

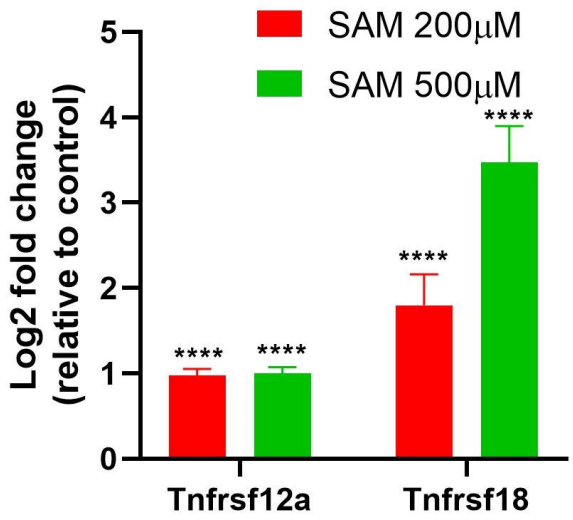

Supplementary Figure 7: Expression of TWEAKR receptor (*Tnfrsf12a*) and *Tnfrsf18* genes (FDR<0.05) in YUMMER1.7 upon treatment with SAM (200 and 500 μM) extracted from RNA-seq data. The log2 fold change is relative to Control where value of control is 0. Significant differences were determined using Wald test with BH FDR.

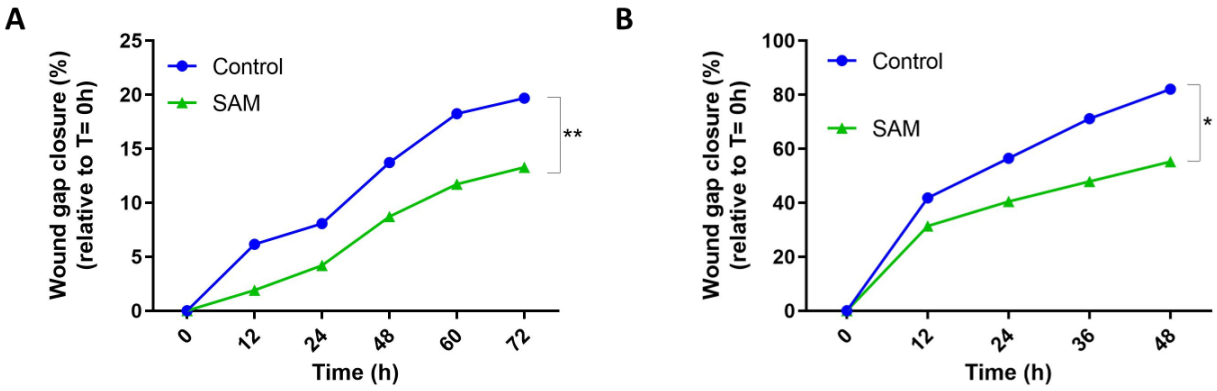

Supplementary Figure 8: Effect of SAM (500 μM) on migration of A375 (A) and YUMMER1.7 (B) cells in wound healing (scratch) assay. The graph shows the closure of width-gap percentage compared to wound gap at time, T= 0 hr. Significant differences were determined using two-way ANOVA test in GraphPad prism.

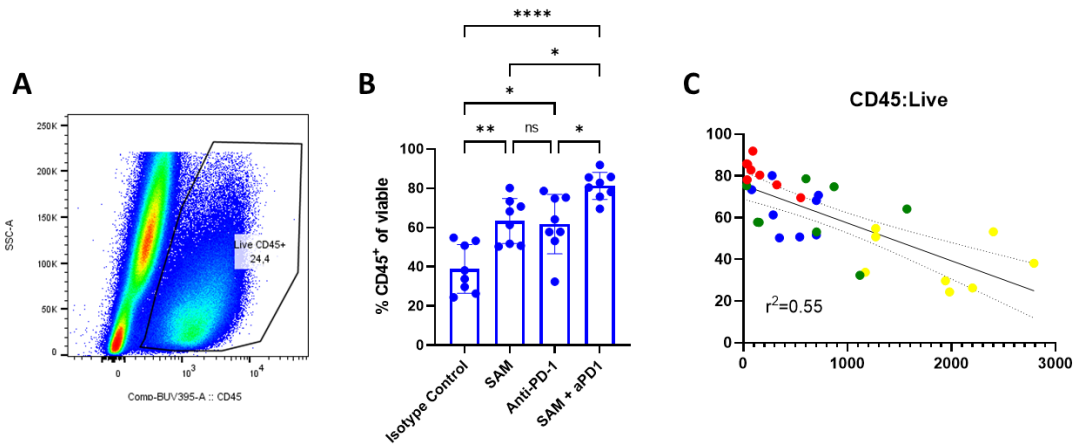

Supplementary Figure 9: SAM, anti-PD-1 antibody and combination enhances CD45$^+$ cells tumor infiltration into the TME of YUMMER1.7 tumors. (A) Gating strategy of live CD45$^+$ cells. (B) Percentage live CD45$^+$ cells of viable total cells infiltrating in the TME. (C) Correlation of CD45$^+$ T cells with tumor weight.

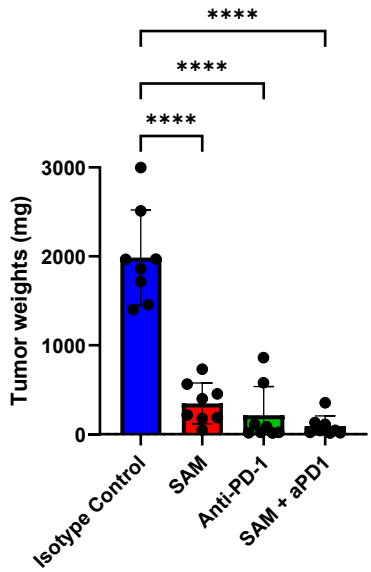

Supplementary Figure 10: SAM, anti-PD-1 antibody and combination decreases tumor weight of YUMMER1.7 tumors. Tumor weight (mg) of control (IgG and PBS), SAM, anti-PD-1 antibody and combination treated YUMMER1.7 (n=8/group) mice at day 22 post tumor injection.

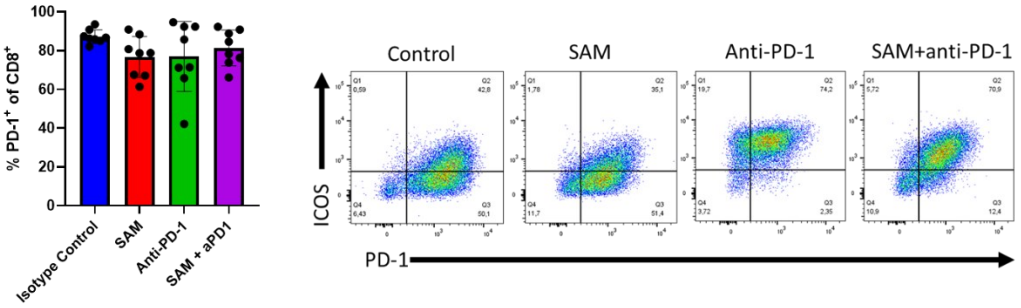

Supplementary Figure 11: Flow cytometry analysis of PD-1 expressing CD8+ T cells in YUMMER1.7 tumors. Representative flow plots gated on $CD8^+$ T cells.

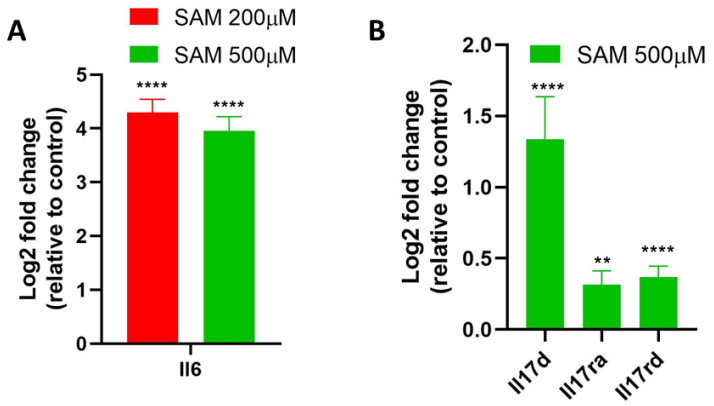

Supplementary Figure 12: Expression of Th17 polarization cytokines. (A) Expression of *Il6* (FDR<0.0001) in YUMMER1.7 cells upon treatment with SAM (200 and 500 μM) extracted from RNA-seq data. (B) Expression of *Il17d*, *Il17ra* and *Il17rd* (FDR<0.001) in YUMMER1.7 cells upon treatment with SAM (500 μM) extracted from RNA-seq data The log2 fold change is relative to Control where value of control is 0. Significant differences were determined Wald test with BH FDR.

Supplementary Table 1: List of RT-qPCR primers used in this study.

Gene	**Forward**	**Reverse**
Tyr	TCTTCTCCTCCTGGCAGATCA	CCTCAGGTGTTCCATCGCAT
Tyrp1	TGAGCAGCTCTGTGCTGTATT	GCTAGGGGGAGGACGTTGTA
Tyrp2/Dct	TTTGCAACCGGGAAGAACGA	GTAGTCATCCAAGCTGTCGCA
Mitf	CCAGGCCTTACCATCAGCAA	TGGGGAAAATACACGCTGTGA
Creb1	GAGCAGACAACCAGCAGAGT	TGGCATGGATACCTGGGCTA
Pmel/Gp100	GCCTGATGATGCCTGTGTCT	TGCCAGTATTTTCCCCAGGTC
Sox10	GCAGAAAGCTAGCCGACCA	CTTTCGTTCAGCAACCTCCA
Mart1/Mlana	TGTTCCTCGGGGAAGGTGTC	CAGCAGTGACATAGGAGCGT
Nanog	AAGGATGAAGTGCAAGCGGT	GGTGCTGAGCCCTTCTGAAT
Cdkn3	GCGATGAAGCCGCCCAT	GCGACAGAGGTAGCCATGAA
Ccnb2	AGCCAAGAGCCATGTGACTA	GTGTTCTGAGGTTTCTTCGCC
Ccnb1	ACCTACCGTGTTTACTTGCTCT	TCGACAACTTCCGTTAGCCT
Ccna2	GTCCTAACGCTCCCATCTCC	TTCGGAAAGAGTGTCAGCCTC
Cdk1	GGTCCGTCGTAACCTGTTGA	CCACACCGTAAGTACCTTCTCC
Plk1	GGTTTTCAATCGCTCCCAGC	AGGGGGTTCTCCACACCTTT
Aurkb	CCGTTTCATCGTGGCACTCA	AGGATGTTGGGATGTTTCAGGT
Aurka	GCTGAGCTACCGGGATCG	TACATCTGTCCATGTCACAGGC
Cdk2	AGAAGATTGGAGAGGGCACG	ACACCTTCAGTCTCAGTGTCG
Cdkn1a/p21	CCAGGCCAAGATGGTGTCTT	TGCTTTGACACCCACGGTAT
Ccnd2	CTGTGCGCTACCGACTTCAA	ATCATCCTGCTGAAGCCCAC
Ccnt2	CCACGGTTACCCTAGAGCTG	TCTTAGCCATAGCCCTCCAGT
Ccnt1	ACTCCAAGCAGGCTGAAACG	TTGTCTGCTCCGACGTGTTT
Ccnl1	ATTCGGAATTGGAGGGCGTA	ATTGTCTGCTCCGACGTGTT
Ccnl2	CTCCCAAGCTGGAATCCCC	TTTCCGTTTGGCGCTCTTTC
Sox2	GATCAGCATGTACCTCCCCG	CTGGGCCATGTGCAGTCTAC
Snai2	GAACTGGACACACACACAGTTAT	ATAGGGCTGTATGCTCCCGA
Pou3f2	GTCCAGTGAACTCAAGCGGG	CCCAGGAAAGACTGTGGACC
Wnt	GAACCCTTTTGCCATCCTGA	CACCTTCAAGAGTTGACCTC

Supplementary Table 2: List of antibodies used for immunophenotyping along with their fluorophores.

T cell phenotype	T cell cytokines	Myeloid Panel
Fixable Viability Dye eFluor 506 (eBioscience)	Fixable Viability Dye eFluor 780 (eBioscience)	Fixable Viability Dye eFluor 506 (eBioscience)
BUV737 – CD3 (clone 17A2, BD)	BUV395 – CD45.2 (clone104,eBioscience)	BUV395 – CD45.2 (clone 104, BD)
Alexa Fluor 700/APC-eFluor 780 – CD4 (clone RM4-5, Biolegend)	Alexa Fluor 700 – CD4 (clone RM4-5, Biolegend)	BUV737 – CD19 (clone 1D3,BD)
BV510/R718 – CD8b (cloneH35-17.2, BD)	BV510 – CD8b (clone H35-17.2,BD)	PE-Cy7 – F4/80 (clone BM8, eBioscience)
APC- ICOS (clone C396.4A, Thermofisher)	APC – CXCR3 (clone CXCR3-173, ThermoFisher)	PE-Cy7 CD8a (clone53-6.7, eBioscience)
PE-Cy7 – PD-1 (clone J43, BD)	PE/BUV737 – IFNγ (clone XMG1.2, BD)	PerCP-Cy5.5 – CD11c (clone HL3, BD)
BUV395 – KLRG1 (clone 2F1, BD)	PE-Cy7 – T-bet (clone 4B10, ThermoFisher)	AntiCD16/CD32 (clone 2.4G2, BD)
PE/V450 – Ki67 (clone B56,BD)	PerCP-Cy5.5 – TNF (clone MP6-XT22, BD)	Pacific Blue – CD11b (clone M1/70, eBioscience)
PerCP-Cy5.5 – CTLA-4 (clone UC- 4B9, Biolegend)	PE – IL2 (BD)	FITC: I-A[b] (clone AF6-120.1, BD)
V450/PE – Helios (clone 22F6, Biolegend)	eFluor450 – IL-17A (clone eBio17B7, eBioscience)	PE- CD103 (clone 2E7, BD)
FITC – Foxp3 (clone FJK16s, eBioscience)	FITC – Foxp3 (clone FJK16s, eBioscience)	Alexa Fluor 700 – Ly6G (clone 1A8, BioLegend)
AntiCD16/CD32 (clone 2.4G2, BD)	BV786 -RORgT (clone Q31-378, BD)	Alexa Fluor 700 – CD4 (clone GK1.5, Thermofisher)
	AntiCD16/CD32 (clone 2.4G2, BD)	APC – PD-L1 (clone MIH5, BD)
		APC-780 – Ly6C (clone AL21, BD)

Supplementary Table 3: Top significantly downregulated pathways derived from significantly downregulated genes obtained from RNA-seq of YUMMER1.7 cells treated with SAM (500µM) and analyzed using GSEA pathway analysis.

PATHWAY NAME	SIZE	ES	NOM p-val	FDR q-val
KEGG_RIBOSOME	81	-0.83159	0	0
REACTOME_SRP_DEPENDENT_COTRANSLATIONAL_PROTEIN_TARGETING_TO_MEMBRANE	98	-0.78976	0	0
REACTOME_EUKARYOTIC_TRANSLATION_ELONGATION	87	-0.81592	0	0
WP_CYTOPLASMIC_RIBOSOMAL_PROTEINS	81	-0.8303	0	0
REACTOME_EUKARYOTIC_TRANSLATION_INITIATION	100	-0.76453	0	0
REACTOME_SELENOAMINO_ACID_METABOLISM	96	-0.75401	0	0
REACTOME_RESPONSE_OF_EIF2AK4_GCN2_TO_AMINO_ACID_DEFICIENCY	90	-0.75566	0	0
REACTOME_NONSENSE_MEDIATED_DECAY_NMD	101	-0.72301	0	0
REACTOME_TRANSLATION	198	-0.59435	0	0
REACTOME_REGULATION_OF_EXPRESSION_OF_SLITS_AND_ROBOS	132	-0.62566	0	0
REACTOME_INFLUENZA_INFECTION	121	-0.63066	0	0
HALLMARK_INTERFERON_ALPHA_RESPONSE	79	-0.64109	0	0
REACTOME_CELLULAR_RESPONSE_TO_STARVATION	124	-0.56713	0	0
REACTOME_ACTIVATION_OF_THE_MRNA_UPON_BINDING_OF_THE_CAP_BINDING_COMPLEX_AND_EIFS_AND_SUBSEQUENT_BINDING_TO_43S	47	-0.73168	0	0
WP_CHOLESTEROL_METABOLISM_INCLUDES_BOTH_BLOCH_AND_KANDUTSCHRUSSELL_PATHWAYS	33	-0.73379	0	0
REACTOME_SIGNALING_BY_ROBO_RECEPTORS	160	-0.54405	0	0
REACTOME_RRNA_PROCESSING	151	-0.53154	0	0
REACTOME_METABOLISM_OF_AMINO_ACIDS_AND_DERIVATIVES	225	-0.49591	0	0
REACTOME_CHOLESTEROL_BIOSYNTHESIS	22	-0.78979	0	0

Supplementary Table 4: Top significantly upregulated pathways derived from significantly upregulated genes obtained from RNA-seq of YUMMER1.7 cells treated with SAM (500µM) and analyzed using GSEA pathway analysis.

PATHWAY NAME	SIZE	ES	NOM p-val	FDR q-val
WP_NRF2_PATHWAY	75	0.625775	0	0
WP_PROXIMAL_TUBULE_TRANSPORT	23	0.706754	0	0
WP_NUCLEAR_RECEPTORS_METAPATHWAY	159	0.483923	0	0
HALLMARK_UV_RESPONSE_UP	92	0.477468	0	0.002652
REACTOME_IRON_UPTAKE_AND_TRANSPORT	34	0.608186	0	0.002122
REACTOME_TRANSFERRIN_ENDOCYTOSIS_AND_RECYCLING	20	0.693396	0	0.001768
REACTOME_INSULIN_RECEPTOR_RECYCLING	17	0.688314	0	0.003062
REACTOME_AMINO_ACIDS_REGULATE_MTORC1	34	0.601245	0	0.002679
REACTOME_ION_CHANNEL_TRANSPORT	81	0.47853	0	0.003668
HALLMARK_P53_PATHWAY	132	0.442129	0	0.006733
PID_P53_DOWNSTREAM_PATHWAY	84	0.473795	0	0.006121
WP_OXIDATIVE_STRESS	17	0.72137	0	0.008498
WP_AUTOPHAGY	20	0.610554	0	0.008752
BIOCARTA_PPARA_PATHWAY	28	0.585093	0	0.008945
WP_ARYL_HYDROCARBON_RECEPTOR_NETPATH	29	0.524708	0	0.015138
REACTOME_ROS_AND_RNS_PRODUCTION_IN_PHAGOCYTES	20	0.675938	0	0.014192
BIOCARTA_NTHI_PATHWAY	17	0.621186	0	0.018019
KEGG_GLUTATHIONE_METABOLISM	34	0.504635	0	0.030215
WP_PHOTODYNAMIC_THERAPYINDUCED_NFE2L2_NRF2_SURVIVAL_SIGNALING	17	0.635614	0	0.028625
REACTOME_DETOXIFICATION_OF_REACTIVE_OXYGEN_SPECIES	19	0.608149	0	0.033395

Supplementary Table 5: Representative cell cycle pathways within top 100 significantly downregulated pathways in BRAF mutant YUMMER1.7 cells treated with SAM (500µM).

PATHWAY NAME	SIZE	ES	NOM p-val	FDR q-val
PID_AURORA_B_PATHWAY	26	-0.67507	0	0
PID_PLK1_PATHWAY	34	-0.61752	0	0
HALLMARK_E2F_TARGETS	130	-0.42135	0	0.004535
REACTOME_APC_C_MEDIATED_DEGRADATION_OF_CELL_CYCLE_PROTEINS	56	-0.49215	0	0.005892
HALLMARK_G2M_CHECKPOINT	140	-0.4072	0	0.012338
REACTOME_MITOTIC_METAPHASE_AND_ANAPHASE	151	-0.37299	0	0.022424
REACTOME_SEPARATION_OF_SISTER_CHROMATIDS	120	-0.37615	0	0.024461
REACTOME_DEPOSITION_OF_NEW_CENPA_CONTAINING_NUCLEOSOMES_AT_THE_CENTROMERE	21	-0.56123	0	0.026791
REACTOME_CELL_CYCLE_MITOTIC	325	-0.32042	0	0.026784
REACTOME_RESOLUTION_OF_SISTER_CHROMATID_COHESION	82	-0.41581	0	0.031394
REACTOME_MITOTIC_PROMETAPHASE	133	-0.37192	0	0.032184
REACTOME_CHROMOSOME_MAINTENANCE	56	-0.42145	0	0.041931
REACTOME_M_PHASE	228	-0.33519	0	0.058118
REACTOME_CELL_CYCLE	395	-0.30554	0	0.066203
REACTOME_CYCLIN_A_B1_B2_ASSOCIATED_EVENTS_DURING_G2_M_TRANSITION	15	-0.58672	0	0.069692
REACTOME_GROWTH_HORMONE_RECEPTOR_SIGNALING	15	-0.57107	0	0.075702
REACTOME_THE_ROLE_OF_GTSE1_IN_G2_M_PROGRESSION_AFTER_G2_CHECKPOINT	45	-0.42436	0	0.082372
REACTOME_MITOTIC_SPINDLE_CHECKPOINT	77	-0.38308	0	0.083835
HALLMARK_MITOTIC_SPINDLE	133	-0.34505	0.018519	0.099165

Supplementary Table 6: Representative stress induced pathways within top 100 significantly upregulated pathways in BRAF mutant YUMMER1.7 cells treated with SAM (500µM).

PATHWAY NAME	SIZE	ES	NOM p-val	FDR q-val
WP_NRF2_PATHWAY	75	0.625775	0	0
HALLMARK_UV_RESPONSE_UP	92	0.477468	0	0.002652
REACTOME_TRANSFERRIN_ENDOCYTOSIS_AND_RECYCLING	20	0.693396	0	0.001768
REACTOME_AMINO_ACIDS_REGULATE_MTORC1	34	0.601245	0	0.002679
HALLMARK_P53_PATHWAY	132	0.442129	0	0.006733
PID_P53_DOWNSTREAM_PATHWAY	84	0.473795	0	0.006121
WP_OXIDATIVE_STRESS	17	0.72137	0	0.008498
WP_AUTOPHAGY	20	0.610554	0	0.008752
BIOCARTA_PPARA_PATHWAY	28	0.585093	0	0.008945
REACTOME_ROS_AND_RNS_PRODUCTION_IN_PHAGOCYTES	20	0.675938	0	0.014192
WP_PHOTODYNAMIC_THERAPYINDUCED_NFE2L2_NRF2_SURVIVAL_SIGNALING	17	0.635614	0	0.028625
REACTOME_DETOXIFICATION_OF_REACTIVE_OXYGEN_SPECIES	19	0.608149	0	0.033395
REACTOME_TP53_REGULATES_METABOLIC_GENES	57	0.436909	0	0.039312
REACTOME_BIOLOGICAL_OXIDATIONS	84	0.386459	0	0.057654
BIOCARTA_STRESS_PATHWAY	16	0.599733	0	0.062347
WP_NRF2ARE_REGULATION	17	0.577772	0	0.078046
WP_APOPTOSISRELATED_NETWORK_DUE_TO_ALTERED_NOTCH3_IN_OVARIAN_CANCER	38	0.448567	0	0.092355
HALLMARK_REACTIVE_OXYGEN_SPECIES_PATHWAY	32	0.465603	0	0.110354
REACTOME_CELLULAR_RESPONSE_TO_CHEMICAL_STRESS	89	0.362985	0	0.112147
REACTOME_ENERGY_DEPENDENT_REGULATION_OF_MTOR_BY_LKB1_AMPK	23	0.502013	0	0.116151
REACTOME_TP53_REGULATES_TRANSCRIPTION_OF_CELL_DEATH_GENES	23	0.494952	0.018868	0.149021

Supplementary Table 7: Representative apoptosis and immune induced pathways within top 100 significantly upregulated pathways in BRAF mutant YUMMER1.7 cells treated with SAM (500μM).

PATHWAY NAME	SIZE	ES	NOM p-val	FDR q-val
HALLMARK_TNFA_SIGNALING_VIA_NFKB	139	0.402443	0	0.039805
PID_TNF_PATHWAY	30	0.512727	0	0.05794
KEGG_LYSOSOME	77	0.397526	0	0.072577
WP_APOPTOSISRELATED_NETWORK_DUE_TO_ALTERED_NOTCH3_IN_OVARIAN_CANCER	38	0.448567	0	0.092355
HALLMARK_IL2_STAT5_SIGNALING	98	0.343669	0	0.140626
WP_TNF_ALPHA_SIGNALING_PATHWAY	64	0.358566	0	0.149085
BIOCARTA_IL1R_PATHWAY	19	0.474112	0.043478	0.147041
PID_IL1_PATHWAY	19	0.518983	0.039216	0.148216
WP_TGFBETA_RECEPTOR_SIGNALING	33	0.425725	0.042553	0.162822
REACTOME_INTERLEUKIN_10_SIGNALING	24	0.465288	0	0.164624
WP_APOPTOSIS	53	0.391863	0.040816	0.167352
PID_FAS_PATHWAY	27	0.423453	0.036364	0.168111
HALLMARK_APOPTOSIS	107	0.330175	0	0.17623
WP_TCELL_ANTIGEN_RECEPTOR_TCR_SIGNALING_PATHWAY	45	0.373339	0	0.19447

1. Zhang, D., et al., *MGDB: a comprehensive database of genes involved in melanoma.* Database (Oxford), 2015. **2015**.
2. Hoek, K.S., et al., *Novel MITF targets identified using a two-step DNA microarray strategy.* Pigment Cell Melanoma Res, 2008. **21**(6): p. 665-76.

Other supplementary files can be downloaded from the following link (supplementary additional files).

CHAPTER FIVE: Co-Targeting Luminal B Breast Cancer with S-Adenosylmethionine and Immune Checkpoint Inhibitor Reduces Primary Tumor Growth and Progression, and Metastasis to Lungs and Bone

Preface

Breast cancer (BCa) is a devastating disease which has a high prevalence in women accounting for 11.7% of all cancers [131,132]. Metastasis is a major cause of mortality and estimated to be as high as 90% of all cancer-associated deaths [134,135]. Skeletal metastasis is another complication of BCa patients that result in skeletal related events (SREs) and account for majority of BCa associated deaths. Luminal B subtype of BCa is low immunogenic and/or unresponsive to CPIs and for which CPI has not been yet approved. This subtype of BCa also has the highest propensity to form bone metastasis compared to other BCa subtypes. Hence, our next unaddressed approach was to evaluate the efficacy of the combination treatment in luminal B subtype of BCa. We first carried out *in vitro* assays using luminal B Eo771 and PyMT-R221A BCa cell lines to determine the effect of SAM on cell proliferation and invasion which are the major hallmarks of cancer progression and metastasis. We also tested for PD-L1 intrinsic signalling (*in vitro*). For *in vivo* studies, we utilized the luminal B Eo771 orthotopic mouse model, which is syngeneic, immunocompetent, tumorigenic (with 100% penetrance), and can metastasize to lungs and bones. However, we were limited by a therapeutic window of only 20 days as Eo771 primary tumors form ulcerations after 20-22 days and the mice need to be euthanized. After optimizing the Eo771 mouse model in the laboratory, we tested for anti-cancer efficacy using SAM, anti-PD-1 antibody, and the combination on tumor growth and progression, and lung metastasis. We also established Eo771 intra-tibial mouse model to study the effect of monotherapies and combination on bone metastasis. For studying various aspects of bone metastasis in-depth, we carried out digital radiography and immunohistochemistry (IHC) of decalcified tumor-inoculated tibia of the mice. Finally, transcriptome analysis (RNA-sequencing) of the primary Eo771 tumors together with IHC was performed to delineate the effect of the combination on key genes/pathways involved in anti-cancer and immunostimulatory effects in luminal B BCa model.

Chapter Five follows the manuscript published in *Cancers* which is part of MDPI journals and is referenced below.

- **Mehdi, A**., M. Attias, A. Arakelian, C.A. Piccirillo, M. Szyf, and S.A. Rabbani, *Co-Targeting Luminal B Breast Cancer with S-Adenosylmethionine and Immune Checkpoint*

Inhibitor Reduces Primary Tumor Growth and Progression, and Metastasis to Lungs and Bone. Cancers, 2023. **15**(1): p. 48.

Abstract

Breast cancer (BCa) is the most prevalent cancer in females and has a high rate of mortality, especially due to increased metastasis to skeletal and non-skeletal sites. Despite the marked clinical accomplishment of immune checkpoint inhibitor (CPI) therapy in patients with several cancers, it has had limited success in luminal subtypes of BCa. Accordingly, recent efforts have focused on combination therapy with CPI, including epigenetic modulators, to increase response rates of CPI in luminal BCa. We have previously shown that S-adenosylmethionine (SAM), the ubiquitous methyl donor, has strong anti-cancer effects in various cancers, including all subtypes of BCa. In the current study, we took a novel approach and examined the effect of CPI alone and in combination with SAM on tumor growth and metastasis in a syngeneic mouse model of luminal B BCa. We showed that SAM decreases cell proliferation, colony-formation (survival), and invasion of luminal B BCa cell lines (Eo771, R221A) *in vitro*. In *in vivo* studies, in Eo771 tumor-bearing mice, either SAM or anti-PD-1 antibody treatment alone significantly reduced tumor growth and progression, while the SAM+anti-PD-1 combination treatment had the highest anti-cancer efficacy of all groups. The SAM+anti-PD-1 combination reduced the percentage of animals with lung metastasis, as well as total metastatic lesion area, compared to control. Additionally, the SAM+anti-PD-1 combination significantly reduced the skeletal lesion area and protected tibial integrity to a greater extent than the monotherapies in an Eo771 bone metastasis model. Transcriptome analysis of Eo771 primary tumors revealed significant downregulation of pro-metastatic genes, including Matrix metalloproteinases (MMPs) and related pathways. On the other hand, $CD8^+$ T cell infiltration, $CD8^+$ T cell cytotoxicity (elevated granzymes), and immunostimulatory genes and pathways were significantly upregulated by the combination treatment. The results presented point to a combination of SAM with CPI as a possible treatment for luminal B BCa that should be tested in clinical studies.

Keywords: S-adenosylmethionine, luminal B, breast cancer, anti-PD-1 antibody, Eo771, bone metastasis.

Introduction

Breast cancer (BCa) is now the primary cause of cancer incidence worldwide in females, with approximately 2.3 million new cases, or 11.7% of all cancers, in 2020 [1,2]. It has become the fifth leading cause of cancer-related death globally, accounting for more than half a million deaths annually [1,2]. High rates of morbidity and mortality are primarily due to increased metastasis to the lungs, brain, and especially to the skeleton [3]. The 10-year survival rate is reduced from 88% in stage I/II BCa to between 10 and 40% in stage III patients, with less than 10% for stage IV BCa [3]. In fact, metastasis accounts for approximately 90% of cancer-related deaths [4,5]. Therefore, there is an urgent need to reduce the morbidity and mortality, and the increase survival, of patients, especially those with metastatic BCa [3].

BCa is a heterogeneous cancer that has four major molecular subtypes: Luminal A (estrogen receptor $(ER)^{high}$, progesterone receptor $(PR)^{high/low}$, human epidermal growth factor receptor 2 $(HER2)^{low}$); Luminal B (ER^{high}, $PR^{high/low}$, $HER2^{high/low}$ki-67^{high}); HER2 enriched (ER^{low}, PR^{low}, $Her2^{high}$); Triple-negative BCa (ER^{low}, PR^{low} and $HER2^{low}$) [6]. Luminal A and B account for 70% of invasive BCa cases [2]. Compared to luminal A, luminal B tumors show higher proliferation and are associated with a higher cumulative incidence of distant metastasis [7,8]. Importantly, patients with the luminal B BCa subtype have the highest probability of forming bone metastasis, leading to skeletal-related events (SREs) that include hypercalcemia, intractable bone pain, nerve compression, and increased bone fragility, which collectively increase cancer-associated morbidity and mortality [9-12].

Immune checkpoint inhibitors (CPIs) increase $CD8^+$ T cell anti-tumor activity and reverse the immune tolerant state [13-15]. Although the approval of CPI has led to a paradigm shift in cancer therapy, a significant proportion of patients do not respond and are resistant to CPI therapy, especially BCa patients [16,17]. The objective response rate to CPI is highly correlated to mutational burden ($p < 0.001$) [18,19]. BCa is generally considered to be less immunogenic due to a low mutational load (around 1/Mb) compared to melanoma and lung cancer (10/Mb) [19,20]. Moreover, BCa cases usually have high immunosuppressive regulatory T cell (Tregs) infiltration in the tumor microenvironment (TME) [21].

Luminal A and B are considered immunologically low; hence, the role of CPI therapy has been least investigated in these subtypes [22]. However, the luminal B BCa subtype may have certain immunological features that could increase sensitivity to CPI, including the expression of

immune checkpoints, higher mutational load, and immune infiltration in TME, compared to luminal A [23]. In addition, the luminal B subtype was classified as an immune benefit subtype of BCa using breast tumor expression profiles and associated clinical data [24]. Furthermore, therapies including radiotherapy and chemotherapy that increase tumor mutational burden and immune infiltration into TME have the potential to enhance effectiveness of CPI against luminal B subtype BCa [22,23].

To distinguish CPI responders from non-responders, DNA hypomethylation has been identified as an essential biomarker that predicts low tumor response to host immunity and can also provide a mechanism for immune evasion and resistance to CPI [25]. These data are consistent with the idea that increased genomic methylation might restore CPI responsiveness. We have previously shown that S-adenosylmethionine (SAM), a ubiquitous methyl donor, targets DNA hypomethylation and blocks DNA demethylation, resulting in the downregulation of several essential oncogenes and pro-metastatic genes, including urokinase plasminogen activator (uPA) and matrix metalloproteinase-2 and 9 (MMP-2/9) [26,27]. SAM blocks BCa growth and metastasis in transgenic (MMTV-PyMT) and xenograft (MDA-MB-231) mouse models in a therapeutic setting [28-31]. Interestingly, SAM is also essential for T cell activation, proliferation, and survival [32-40]. SAM was also demonstrated to methylate the *FOXP3* gene, reducing *FOXP3* expression, hence, reducing the immunosuppressive capacity of Tregs [41]. In fact, a unique tumor immune escape mechanism that tumor cells use is depriving $CD8^+$ T cells of methionine (a pre-cursor of SAM) in TME, which renders $CD8^+$ T cells unable to produce cytokines and respond to CPI [42]. Lastly, SAM levels are reduced from the TME by tumor cells via various metabolic mechanisms [42,43].

Since cancer progression and metastasis involve a combination of multiple essential oncogenic and immune-suppressive pathways, CPI can be combined with other therapeutic agents, especially those targeting low immunogenic BCa subtypes [13,14,44]. Here, we used a novel therapeutic strategy by combining the methyl donor, SAM, with CPI and tested the anti-cancer efficacy on the luminal B BCa subtype that is immunogenically low and has a low response to CPI.

Results

SAM decreases proliferation, colony formation, and invasion of BCa cell lines

One of the hallmarks of cancer is uncontrolled cellular proliferation [45]. Hence, first, we tested the anti-proliferative effects of SAM on two luminal B BCa cell lines, Eo771 and PyMT-R221A (R221A), using a well-established cell proliferation assay. SAM significantly decreased cell proliferation of both Eo771 and R221A cell lines compared to the untreated control (Figure 1A). The proliferation, relative to the control, was 62%, 43%, and 29% for Eo771 cells, and 73%, 56%, and 37% for R221A cells at day 1, 2, and 3 after the SAM treatment, respectively (Figure 1A). Next, we tested the effect of SAM on anchorage-independent growth of BCa cells using a soft agar colony formation (survival) assay. SAM significantly reduced the colony-forming potential of both Eo771 and R221A BCa cells, as the survival fraction for SAM-treated cells was 51% and 53%, relative to the control (100%), respectively (Figure 1B). Cancer metastasis processes require invasion and migration of the cancer cells through the extracellular matrix (ECM), and degradation and intravasation into the blood vessels. Thus, we tested the anti-metastatic effect of SAM using a robust cell invasion assay. Eo771 and R221A cells treated with SAM showed a significant reduction in cell invasive potential, as the invasion was 55% and 62% relative to the control (100%), respectively (Figure 1C). This data indicated that SAM reduces the proliferative, colony-forming (survival), and invasive ability of luminal B BCa cells.

Blocking Programmed death ligand 1 (PD-L1) intrinsic signalling has no effect on cell proliferation of BCa cell lines

First, we established that PD-L1 is expressed in murine (Eo771, R221A, and EMT6) BCa cell lines, which are, therefore, candidates for CPI, wherein Eo771 cells showed the highest PD-L1 expression (Figure 2A). Although the major anti-cancer effects of blocking programmed cell death 1 (PD-1) and PD-L1 interactions *in vivo* are driven by the marked upregulation of anti-cancer adaptive immune responses, several studies have reported that PD-L1 also triggers intrinsic carcinogenic signaling independent of the immune checkpoint pathway [46,47]. We, therefore, tested the effects of SAM anti-PD-L1 antibody treatments and their combination on cellular proliferation. EMT6 is not a luminal B BCa cell line, but it has a moderate response to anti-PD-

1/anti-PD-L1 antibodies *in vivo* and, thus, we tested for PD-L1 intrinsic signaling in EMT6 as well. The anti-PD-L1 antibody alone did not decrease cell proliferation in Eo771, R221A, and EMT6 cells (Figure 2B–D). The failure to decrease cell proliferation is consistent with previous reports indicating that the major effect of PD-1/PD-L1 blockade is through the rejuvenation of effector functions of $CD8^+$ T cells and its tumor lytic activity [14,48]. Our results showed that PD-L1 intrinsic signaling does not affect cell proliferation. The decrease in cellular proliferation in the SAM+anti PD-L1 combination group was probably only due to SAM in the luminal B BCa cell lines.

The SAM and anti-PD-1 antibody combination has superior effect in reducing primary breast tumor growth compared to monotherapies

The luminal B subtype of BCa has the highest propensity to metastasize to the lungs and skeletal system amongst the BCa subtypes [9-12]. Eo771 BCa cells show a molecular pattern of $ER\alpha^-$, $ER\beta^+$, PR^+, and $ErbB2^+$, and have recently been characterized as the luminal B subtype [49,50]. Eo771 tumor-bearing syngeneic mice can be established by inoculating Eo771 cells in immunocompetent C57BL/6 mice. Furthermore, this model offers the advantage of studying lung metastasis naturally derived from primary tumors. We first established the tumor growth kinetics of Eo771 tumor-bearing mice by injecting varying numbers of Eo771 cells orthotopically into female C57BL/6 mice at the 4th mammary fat pad (m.f.p). We found that the tumors started to ulcerate from day 22–24 post-inoculation, and we, therefore, set the timeline of our experiments for 20 days post-inoculation.

Treatment with either SAM or anti-PD-1 antibody significantly reduced tumor growth and progression in Eo771 tumor-bearing animals compared to the control at day 20 post-tumor injection. However, the SAM+anti-PD-1 antibody combination had the highest efficacy in controlling tumor growth and progression at day 20 post-tumor injection compared to all groups, as indicated by the least mean tumor volume and tumor weights (Figure 3A,C). The combination treatment also had the maximum percentage of tumor growth inhibition (TGI) at 82% compared to the control (0%), SAM (58%), and anti-PD-1 antibody (66%), although the TGI difference between the combination treatment and anti-PD-1 antibody alone was barely significant (Figure 3B). We found no difference in the mouse body weights between the control and treatment groups (Figure 3D).

The SAM and anti-PD-1 antibody combination decreases lung metastasis

Lung metastasis is a common feature of luminal B BCa [9-12]. Accordingly, we investigated the effect of SAM and anti-PD-1 antibody on lung metastasis using the Eo771 BCa mouse model. The Eo771 primary tumor cells followed the progressive steps of metastasis and formed metastatic lesions in the lungs. At the end of these studies, on day 20 post-Eo771 tumor cells inoculation, the animals were euthanized, and the lungs were harvested, fixed, permeabilized, and stained with Hematoxylin and Eosin (H&E). Lungs of animals treated with SAM and anti-PD-1 antibody alone showed a significant decrease in the total metastatic lesion area compared to the lungs of the control animals (Figure 4A, B). Furthermore, lungs of animals that were treated with the SAM and anti-PD-1 combination showed the smallest total metastatic lesion area compared to all groups, though the difference did not reach statistical significance compared to either monotherapy (Figure 4A, B). Additionally, the combination treatment had the lowest percentage (1/4 mice; 25%) of mice with lung metastasis compared to SAM (2/4 mice; 50%), anti-PD-1 antibody (2/4 mice; 50%), and control (4/4 mice; 100%) (Figure 4C).

The SAM and anti-PD-1 antibody combination blocks bone metastasis and protects bone from tumor osteolytic damage

Bone metastasis is a common feature of BCa, wherein tumor osteolytic lesions are formed, which leads to SREs and a poorer prognosis for BCa patients. Moreover, luminal B BCa has the highest propensity to metastasize to skeletal sites [9-12]. Therefore, we evaluated the effect of the SAM+anti-PD-1 combination on skeletal metastasis. We first established a syngeneic luminal B bone metastasis model by injecting several doses of Eo771 cells into the tibia of black B6 mice intra-tibially (i.t). Ten thousand Eo771 cells were determined to be optimal for forming bone lesions and provided a sufficient therapeutic window of 21 days.

After establishing the bone metastasis model, we investigated the impact of SAM, anti-PD-1 antibody, and the combination on metastasis of Eo771 BCa cells within the bone microenvironment and treated these animals for 21 days. Skeletal lesions were calculated using a bone lesion score (BLS) as described in the Materials and Methods section. Digital radiography showed the highest BLS for the control animals, followed by significantly lower BLS for anti-PD-1 antibody and SAM alone (Figure 5A, B). Moreover, the tibias of animals treated with the

SAM+anti-PD-1 combination scored significantly lower for BLS as compared to the other groups (Figure 5A, B).

To confirm the X-ray results, we harvested the tibias of the animals, fixed and decalcified the bones, and carried out H&E staining. The tumor lesions in the tibias of the control group digested the cortical bone outside the tibia, as well as through the growth plate into the epiphysis upwards, and metaphysis and diaphysis downwards (Figure 5C). For all control group tibias, most of the cortical bone was broken and the tumor had grown into the whole bone marrow. To be consistent, we measured the tumor lesion area only within the tibia. SAM and anti-PD-1 antibody alone had a significant effect on controlling tumor lesion growth within the tibia compared to the control, as the tumor lesions were smaller (Figure 5C, D). However, the combination of SAM and anti-PD-1 antibody significantly reduced tumor lesion growth compared to monotherapies, as indicated by the smallest lesion area compared to all groups (Figure 5C, D). The combination treatment also protected the bone as the cortical bones were thicker, and the tissues, including bone marrow, epiphysis, growth plate, metaphysis, and diaphysis, were intact, mirroring the histology of a normal mouse tibia (Figure 5C). Lastly, the combination treatment had the lowest percentage (20%) of mice with bone metastasis compared to SAM (60%), anti-PD-1 (80%), and control (100%) (Figure 5E).

The SAM and anti-PD-1 antibody combination reduces expression of oncogenes while elevating expression of immunostimulatory genes as well as $CD8^+$ T cells infiltration and activity

To determine the reason for the significant reduction in tumor growth and progression and metastasis due to the combination treatment, we carried out RNA-sequencing analysis of the Eo771 tumors treated with the combination treatment and the control. RNA-seq revealed that 128 protein coding genes were differentially expressed in the combination group as compared to the control (Figure 6A, Supplementary file 1).

Matrix metalloproteinases (MMPs) are endopeptidases that are involved in tumor growth, progression, and metastasis [51,52]. The significantly top downregulated genes were enriched in pathways related to the organization of extracellular matrix (ECM), activation of MMPs, and degradation of the ECM (Figure 6B and Supplementary Figure S1). Specifically, *Mmp9*, *Mmp10, Adamts4,* and *Ctsk,* which are involved in degradation of the ECM, were downregulated in the

combination treatment group (Figure 6B). We also validated the downregulation of *Mmp9* and *Mmp10* using RT-qPCR (Figure 6B). We carried out clinical database analysis of the TCGA and GTEx databases using the Xena platform [53]. We found that both *Mmp9* and *Mmp10* genes are upregulated in primary tumors of human breast cancer patients compared to normal solid tissue (Figure 6C).

$CD8^+$ T cells control tumor growth by killing tumor cells directly using proteases, including granzymes, upon activation, and becoming cytotoxic effector cells [54-56]. We found that the top significantly upregulated genes were involved in antigen processing and presentation, immunostimulatory molecules, granzymes, and genes that provide a high response to CPI therapy (Figure 6D). Firstly, the number of $CD8^+$ T cells was increased in the TME of combination-treated tumors, as indicated by increased *Cd8a* expression. Secondly, different genes (including *Cd74*, *H2-Aa*, *H2-Ab1*, *H2-Eb1*) of antigen processing and presentation machinery (APM) were increased in combination-treated tumors. Thirdly, the granzymes (*Gzma* and *Gzmc*) that are released by $CD8^+$ and NK cells to kill tumor cells had a higher expression in combination-treated tumors compared to control. Fourthly, a key immunostimulatory gene, *Nkg7*, whose elevation has been associated with good response to CPI therapy in multiple studies [57,58], was also upregulated in the combination treatment group. Moreover, other immune-stimulating genes, including *Cma1,* were upregulated as well. We also validated the upregulation of key genes, including *Cd8a, Gzma*, *Gzmc,* and *Nkg7,* using RT-qPCR (Figure 6D). Lastly, we found that the top significantly upregulated pathways were involved in elevating anti-cancer immune responses, such as antigen processing and presentation, Th1, Th2, and Th17 differentiation, Allograft rejection, and other immune stimulating pathways (Supplementary Figure S2).

We also carried out immunohistochemistry (IHC) of the Eo771 tumors from groups treated with the combination and controls. We performed H&E staining and staining for the $CD8^+$ T cell marker in order to determine the extent of $CD8^+$ T cell infiltration in either the Eo771 tumors treated with the combination or the control group. We found a higher number of $CD8^+$ T cells in the tumors that were treated with the combination treatment compared to the control (Figure 6E). The higher $CD8^+$ T cell infiltration together with higher granzymes expression data could indicate higher activation and function of $CD8^+$ T cells.

Taken together, these data indicate that treatment with the SAM and anti-PD-1 antibody combination reduces tumor growth and progression by downregulating oncogenes, elevating immune responses, and upregulating immunostimulatory genes.

Discussion

Although CPIs are considered a breakthrough in cancer treatment, they have limited therapeutic effect in less immunogenic cancer types such as luminal B BCa [22,23]. Furthermore, CPI therapy causes adverse effects. Hence, current therapies have evolved to combine CPI therapy with other agents to enhance the CPI response and reduce the toxicity of CPI. In the current study, we examined a new approach that involves combining a methyl donor, SAM, with CPI to enhance responses to immunotherapy in the luminal B BCa subtype. The luminal B subtype was studied here since it has the lowest response rates to CPI and highest propensity to form bone metastasis compared to other subtypes of BCa [9,10,22,23]. In *in vitro* studies, SAM was effective in inhibiting several cancer growth and invasion parameters in luminal B BCa cell lines. The reduction in proliferation by SAM was reported to be due to the downregulation of cyclins, upregulation of cell cycle inhibitors, and/or downregulation of Jak/Stat pathways in prostate cancer, osteosarcoma, gall bladder carcinoma, and pancreatic cancer [59-64]. We believe the mechanism of repressed proliferation by SAM could be similar in luminal B BCa. In *in vivo* studies, either SAM or anti-PD-1 antibody on their own reduced primary tumor growth of a syngeneic Eo771-tumor bearing mouse model compared to control mice. However, the combination treatment had the highest reduction in tumor growth and progression, and reduced metastasis to the lungs and bones.

We chose the Eo771 model for our *in vivo* studies for the following reasons. Firstly, Eo771 cells have the highest expression of PD-L1 amongst the luminal B cell lines (Figure 2A) [49,50]. Secondly, we found that Eo771-tumor bearing mice show immune infiltration in the TME. Thirdly, the Eo771 cell line is one of the few syngeneic luminal B BCa subtypes that can form primary tumors as well as metastasize to skeletal and non-skeletal sites with characteristics similar to the human disease [65]. Fourthly, Eo771 cell inoculation has a consistent (100%) tumor uptake/penetrance [66]. However, Eo771 tumor-bearing mice form ulcers at from around 22–25 days following tumor inoculation at the m.f.p, therefore, the animals were sacrificed on day 20 in accordance with McGill University guidelines. Due to the short experimental therapeutic window

of this model, we could not assess the long-term effects of SAM and anti-PD-1 antibody. Nevertheless, based on the established efficacy of SAM and anti-PD-1 antibody in several cancers, including melanoma, we anticipate continued benefit and effectiveness of SAM+anti-PD-1 in a luminal B BCa model, which could be translated to a clinical setting [28,30].

In patients with luminal B BCa, skeletal metastasis is a major complication that ultimately leads to SREs [9-12]. However, limited therapeutic options are available and most of the therapies are palliative, targeting bone pain reduction and reversing bone resorption [67]. We, therefore, examined whether the combination therapy might address this challenge. We first established a bone metastasis model by injecting Eo771 cells via the intra-tibial route [68,69]. Then, we evaluated the effect of SAM, anti-PD-1 antibody, and the combination of both on the formation of bone metastatic lesions. We found that SAM and anti-PD-1 antibody alone could significantly reduce the ability of Eo771 cells to form metastatic lesions. Importantly, SAM in combination with anti-PD-1 antibody had the highest effect in reducing tumor cells in the tibia and resulted in a reduced lesion area. Following histological analysis, animals treated with the combination therapy showed higher integrity and the tibia was similar to a normal mouse tibia, suggesting rapid clearance of tumor cells from the bone microenvironment by the combination treatment.

MMPs are endopeptidases that function as proteolytic enzymes. High expression of MMPs in tumors allow them to degrade ECM proteins and the basement membrane to invade and metastasize to nearby tissues and distant organs [51,52]. Apart from being key players in the metastasis of cancer cells, MMPs are also linked to tumorigenesis due to their functions in proliferation, apoptosis, and angiogenesis [51,52]. A meta-analysis comprised of 41 studies and 6517 breast cancer patients demonstrated that a higher expression of *Mmp2* and *Mmp9* in tumor cells of patients was strongly associated with larger tumors and metastasis to lymph nodes and distant organs [52]. Higher expression of *Mmp2* and *Mmp9* was also associated with histological grade, higher clinical stage, and predicted poor survival of breast cancer patients [52]. The SAM and anti-PD-1 antibody combination-treated tumors had significant downregulation of the *Mmp9* gene (and other MMP-related genes) and pathways involved in ECM degradation and activation of MMPs. Our lab also demonstrated that SAM reduces the expression of pro-metastatic genes, including MMPs in BCa, prostate cancer, and osteosarcoma [27,31,62,70]. The results reported herein and previously published together are consistent with the idea that the reduction in tumor

growth and progression, and metastasis to skeletal and non-skeletal sites, could be attributed to the effects on these well-established oncogenic and metastatic pathways.

$CD8^+$ T cell activation depends upon engagement of the CD8 receptor with antigens presented by MHC class I. MHC I and II complexes are mutated or downregulated in several cancers, and this is a major tumor immune evasion mechanism used by tumor cells to avoid immune destruction [71]. Therefore, elevated antigen processing and presentation (by MHC class I/II), increased immunostimulatory molecules, and increased production of granzymes are major anti-cancer immune mechanisms and factors that determine the success of CPIs [72]. Upregulation of anti-cancer immunity, especially $CD8^+$ T cell infiltration, activation, and effector functions by the SAM and anti-PD-1 antibody combination, has been reported by us in a melanoma mouse model [48]. This observation was also true in the current study, where $CD8^+$ T cell infiltration and effector functions, such as higher granzyme production, were elevated upon SAM and anti-PD-1 antibody combination treatment. Parallel to this, methionine (pre-cursor of SAM) supplementation restored $CD8^+$ T cell immunity in melanoma and ovarian murine tumors [42]. However, the enhancing effect of SAM on anti-cancer immunity was not observed in hepatocellular carcinoma, where SAM led to T cell exhaustion [73]. The effect of SAM on anti-cancer immunity could be cancer-type- or TME-dependent. To address this question, future studies could examine the effect of SAM alone and with anti-PD-1 antibody in combination on $CD8^+$ T cells and other immune cells in TME through single-cell RNA sequencing analysis.

Although SAM has been delivered via different routes in other studies, we found that delivery of SAM via oral gavage has several advantages. Firstly, oral gavage provides the ability to accurately control the actual amount of SAM given to each mouse, as compared to adding SAM into drinking water, in which case the precise amount for each mouse cannot be controlled. Secondly, in previous studies, we found that the oral route resulted in elevated levels of SAM in the mice serum [28,30]. Thirdly, this method avoids eliciting an immune response and effectively avoids injection of SAM into different tissues/organs, a potential risk associated with i.p. injections. Lastly, SAM is non-toxic, is already an approved nutraceutical agent, and treatment with SAM has not been shown to trigger adverse effects in pre-clinical and clinical studies [28,30,31,48,74]. Therefore, SAM can be given in a combination setting and continued thereafter in a non-hospital setting following the successful completion of CPI in BCa patients to block tumor progression, metastasis, and BCa-associated morbidity, which remain our ultimate goal..

Conclusions

Overall, our results showed that while both SAM and anti-PD-1 antibody are effective, the combination of SAM and anti-PD-1 antibody has the greatest effect in reducing tumor growth, progression, and metastasis of a luminal B BCa syngeneic mouse model. Since CPI is already approved for several cancers, including metastatic BCa, and SAM has been extensively shown to block tumor growth and metastasis in several models, including BCa, we propose the potential use of SAM+CPI in patients with luminal BCa. Collectively, results from these studies provide a possible therapeutic strategy combining SAM and CPI (anti-PD-1 antibody) to reduce cancer-associated morbidity and mortality.

Materials and Methods

Cell lines

Murine BCa Eo771 and PyMT-R221A (R221A) cell lines were generously provided by Dr. Conor C. Lynch (H. Lee Moffitt Cancer Center and Research Institute, Tampa, FL, USA) and Dr. Jean S. Marshall (Dalhousie University, Halifax, Nova Scotia, Canada), respectively. The EMT6 mouse BCa cell line was obtained from ATCC (Manassas, Virginia). Eo771. R221A and EMT6 cells were cultured in DMEM supplemented with 10% FBS, 1% penicillin-streptomycin sulfate, HEPES, and 2 mM L-glutamine. All the cell lines used were of early passage, were found to be mycoplasma free, and were maintained in incubators at 37 °C and 5% CO_2.

Proliferation, soft agar colony formation, and invasion assays

For *in vitro* studies, we used 200 μM of SAM (cat# B9003S, NEB, Mississauga, Canada) and 50 μg/mL of anti-PD-L1 antibody (clone 10F.9G2, cat# BE0101, BioXcell, Lebanon, NH, USA), as these concentrations were found to be optimal in our previous dose response studies [26,28,48,62,63,75,76].

For the proliferation assay, Eo771 (4×10^4), EMT6 (4×10^4) and R221A (2.5×10^4) were seeded in 6-well plates. Cells were treated with SAM (200 μM) on day 2, 3, and 4 and were

collected on day 5. On day 5, the treated cells were trypsinized, mixed with complete DMEM, and counted using Beckman Coulter (Hertfordshire, UK). Percentage proliferation (%) was calculated as (mean number of cells in treatment group/mean number of cells in control group) × 100. To determine the effect of intracellular signaling of PD-L1 on cellular proliferation, the Eo771 (4×10^4), EMT6 (4×10^4), and R221A (2.5×10^4) cells were seeded and treated with recombinant PD-1 (rPD-1, Control), SAM, anti-PD-L1 antibody, and SAM+anti-PD-L1. Eo771, EMT6, and R221A cells were supplemented with 0.2 µM rPD-1 (cat# 1021-PD-100, R&D systems, Minneapolis, MN, USA) on day 3, which was followed with 50 µg anti-PD-L1 on day 4. The treated cells were counted on day 5.

Soft agar colony formation assay followed the regular proliferation protocol for SAM treatment and was carried out as previously described [28,30]. Briefly, Eo771 (5×10^3) and R221A (5×10^3) SAM- and control-treated cells in complete DMEM media supplemented with 13% FBS were mixed with 0.6% agar. This cell–agar mixture was seeded and allowed to solidify on top of another 2% agar solidified layer in a 6-well plate. Media was added on top and replenished every 4–5 days. After 3 weeks, the colonies were counted under a light microscope. A group of at least 50 cells that were not overlapping was considered a colony and the percentage survival fraction calculated as previously described [28,30]. Invasion assay followed the regular proliferation protocol for SAM treatment and was run precisely as detailed by us previously, using a two-compartment Boyden chamber coated with Matrigel (Sigma-Aldrich, Oakville, ON, Canada) [28,48]. The Eo771 and R221A cells were allowed to invade for 18 h. Percentage invasion (%) was calculated as (mean number of cells invading per field in SAM or control group/mean number of cells invading per field in control group) × 100. All assays are presented as the average of at least three independent repeats..

Animal studies

Female C57BL/6 mice (six to eight weeks old) were obtained from Charles River Lab (Quebec, Canada) and kept at an ARD facility of the RI-MUHC. Mice were injected orthotopically with 2×10^5 Eo771 cells at m.f.p to form tumors. The animals were randomized into the four treatment groups, including control (isotype matched IgG2a and PBS), SAM (Life Science Laboratories, Lakewood, NJ, USA), anti-PD-1 antibody (clone RMP1-14, BioXcell, Lebanon, NH, USA), and SAM+anti-PD-1 combination. SAM (80 mg/kg) was diluted in PBS (1×) and was

given daily using feeding needles via oral gavage once the tumors became palpable, and anti-PD-1 antibody (5 mg/kg) and isotype matched IgG2a antibody (5 mg/kg) were administered via intra-peritoneal (i.p.) injection twice a week. The dose of SAM and anti-PD-1 antibody was established previously [13,28,48,77-79]. Tumor volume (T.V) was measured by palpation at timed intervals using a digital caliper. On day 20, the mice were sacrificed and tumor weight and T.V were measured. T.V was calculated using the formula T.V = (length × width^2)/2. Percentage (%) tumor growth inhibition was calculated as ((1–[changes of T.V in treatment group/changes of T.V in control group] × 100). The mice were observed regularly for weight loss or potential adverse effects [80].

RNA extraction and reverse transcriptase quantitative real-time PCR (RT-qPCR)

Total RNA was isolated using the RNeasy kit (cat# 71404, Qiagen, Hilden, Germany). The RT-qPCR assay was run as previously described by us [28,48]. Gene expression changes were analyzed by following the 2-ΔΔCT method. The primer list has been tabulated in Supplementary Table S1.

RNA-sequencing (RNA-seq) and analysis

The total RNA was extracted from Eo771 breast tumors and subjected to quality control (QC) using Bioanalyzer and NanoDrop. An A260/280 absorbance ratio of >2.0 and RIN of >6.5 qualified the samples for RNA-seq. After QC, paired-end RNA-seq was carried out using the Illumina NovaSeq 6000 platform (with a depth of 25 million reads) following the standard methodology by Genome Quebec (McGill University). The raw sequencing data was checked for QC, normalized, and used to generate HT-seq count files. The HT-seq files were then input into the DeSeq2 tool (RRID:SCR_015687) to carry out the differential gene expression (DEGs) analysis (*FDR ≤ 0.2*) in Galaxy (www.usegalaxy.org). Pathway enrichment analysis of DEGs was performed by ConsensusPathDB (RRID:SCR_002231).

Intratibial model for skeletal metastasis

Firstly, a murine luminal B BCa bone metastasis model was established by implanting varying doses of Eo771 cells (2×10^5, 1×10^5, 0.5×10^5, 0.2×10^5,0.1×10^5) into the tibia of

female C57BL/6 mice (six to eight weeks old) using 27G surgical needles. Briefly, the needles were inserted intra-tibially into the tibial region of the mice via the knee joint in a clockwise rotation. Once the needles were completely inserted into the bone, the cells were slowly released into the bone microenvironment. After detailed assessment, we found that 0.1×10^5 Eo771 cells were optimal for our experiments, as this provided a decent therapeutic window; this concentration was bearable for the mice as the bones were not fragile upon harvest and the knee joints were intact upon harvest for most mice. Then, we assessed whether SAM, anti-PD-1 antibody, and their combination can reduce tumor cell growth within the bone microenvironment of these models. Briefly, Eo771 (0.1×10^5) cells were injected via intra-tibial route and the mice were randomized two days post-tumor implantation. The mice were treated with either vehicle (IgG2a via i.p. injection twice a week and PBS), SAM (via oral gavage daily), anti-PD-1 antibody (via i.p. injection two times a week), or the combination until sacrifice on day 21 ($n = 10$/group). Digital radiography of hind limbs was performed at day 21 using Bruker In-Vivo Xtreme, according to standard protocol at the RI-MUHC. Skeletal lesions were analyzed and given a BLS as previously described by us and others [81-83]. The BLS was averaged from two separate histologist scorings. Briefly, the BLS was determined from 0–4 as follows: 0 represents no tumor lesions with highest bone integrity (no breaks in the peripheral margin); 1 represents minor lesions; 2 represents small lesions; 3 represents considerable tumor lesions with minor breaks in peripheral margin; 4 represents the maximum tumor lesion area with lowest bone integrity and with major breaks in the peripheral margin [81-83].

Immunohistochemistry

The lungs of animals treated with the control (IgG2a and PBS), SAM, anti-PD-1 antibody, and the combination were harvested at the endpoint. The lungs were fixed with formalin for between 3 and 5 days, washed with 70% ethanol, embedded in paraffin, sectioned, and stained with H&E staining. Following the intratibial model of bone metastasis, tibias were harvested at the endpoint (day 21), fixed with Periodate–Lysine–Paraformaldehyde (PLP) reagent, washed with 5% glycerol, 10% glycerol, and 15% glycerol, and decalcified with EDTA-G for 3 weeks for further tumor tibial lesion histological assessment, as detailed in our previous study [30]. The decalcified tibias were washed with PBS, dehydrated, fixed in paraffin, sectioned, and stained with H&E staining. The tumor lesion area from the stained lung and bone sections was measured with

the annotation tool of the ImageScope software (RRID:SCR_014311). For CD8a T cell staining, tumors were harvested from mice (n = 4/group) and IHC was carried out using an automated Ventana Discovery Ultra Instrument (Roche, Basel, Switzerland). The slides were deparaffinized and rehydrated. For antigen retrieval, the slides were treated with EDTA buffer and then incubated with primary mouse anti-CD8a antibody (cell signaling, cat# #98941S) at a dilution of 1:70 for 24 min. This was followed by incubation with secondary anti-rabbit antibody conjugated to horseradish peroxidase (HRP). The signal was detected using a DAB chromogen kit. Slides were scanned with Aperio AT Turbo digital. The brown staining indicated CD8a positive staining. Microscopy images (at 400× magnification) were captured randomly using ImageScope and analyzed using Fiji (RRID:SCR_002285). For each sample, five images were captured. Then, in Fiji, images were input and the color deconvolution tool was utilized to separate H&E (total cell stain) and DAB ($Cd8a^+$ stain) sections. Next, the analyze particles tool was used to measure the optimal total area of H&E and DAB staining. To calculate the $Cd8a^+$ staining area automatically for each image, a macro was created, and images were input one-by-one. $Cd8a^+$ staining of T cells percentage was calculated relative to the total cells as [total area of ((DAB/H&E) staining) × 100%)].

Statistical analysis

Statistical significance was analyzed by two-tailed Student's T-test and one-way/two-way ANOVA using GraphPad Prism 8 (RRID:SCR_002798).

Figures (Chapter Five)

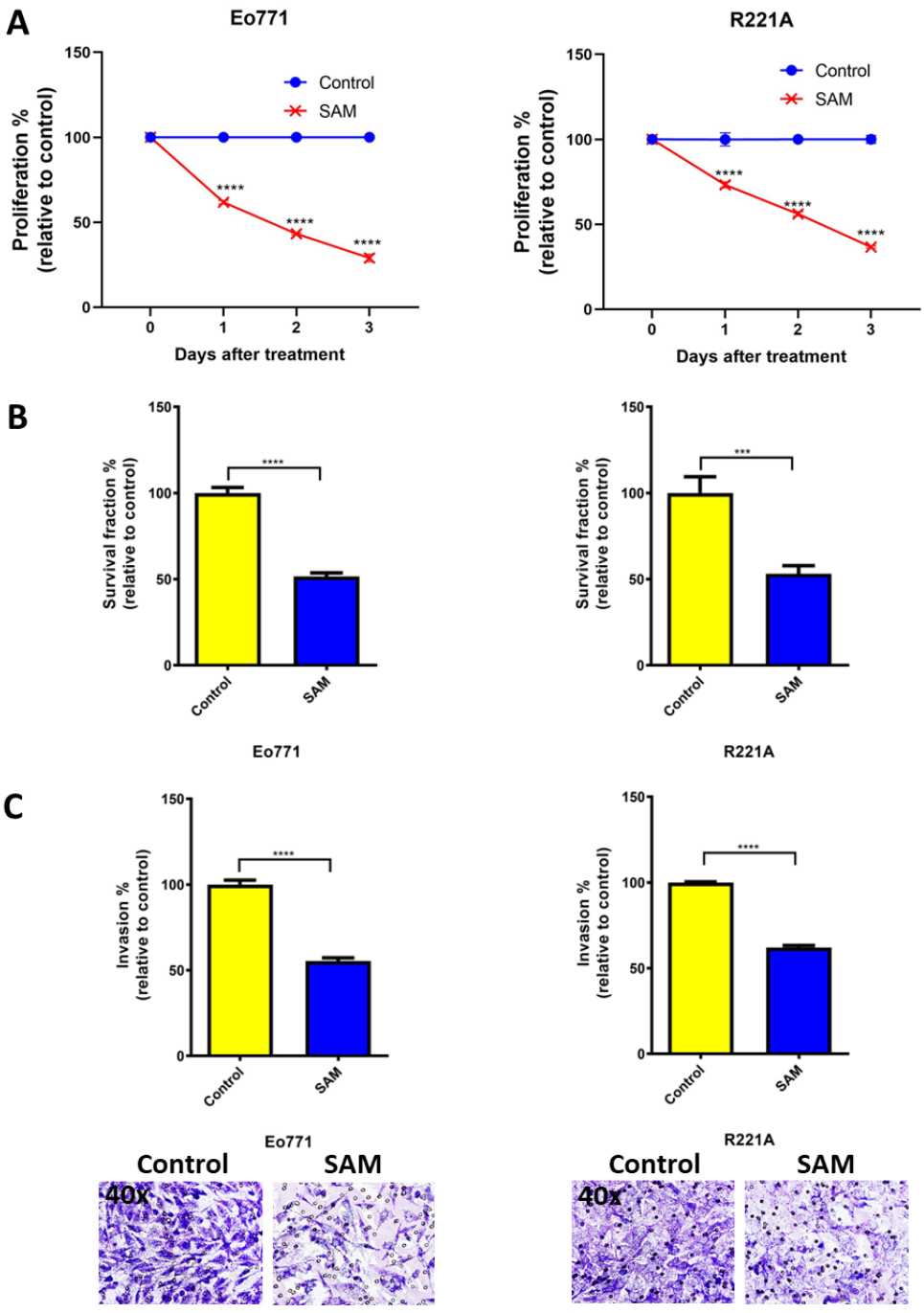

Figure 1. Effect of SAM on proliferation, colony-formation (survival), and invasion of luminal B BCa cell lines. (**A**) Percentage proliferation (± SEM) relative to control at 1, 2, and 3 days after SAM treatment. Briefly, Eo771 (4×10^4) and R221A (1×10^4) cells were seeded in 6-well plates, treatment with SAM (200 µM) started 2 days after seeding, and they were treated every day for 3

days. Cells were trypsinized and counted 1, 2, and 3 days after SAM treatment. (**B**) Percentage survival fraction (± SEM) relative to control obtained from soft agar colony formation assay. The colony formation assay was performed after the regular proliferation assay, and then the treated Eo771 (5×10^3) and R221A (5×10^3) cells were plated. Media was replenished every 4–5 days and colonies were counted after 3 weeks. (**C**) Invasion assay was performed after performing the regular proliferation assay and then incubating the treated cells (1.25×10^5) for 18 h in two-compartment Boyden chambers coated with Matrigel. Top: Percentage invasion (± SEM) relative to control. Bottom: Representative images (lens, 40×; magnification, 400×) of invaded cells. Results are the mean of at least three independent experiments. Statistical significance was determined by (**A**) two-way ANOVA and (**B**, **C**) T-test in GraphPad prism. Significance values are represented by asterisks (*** $p < 0.001$; **** $p < 0.0001$).

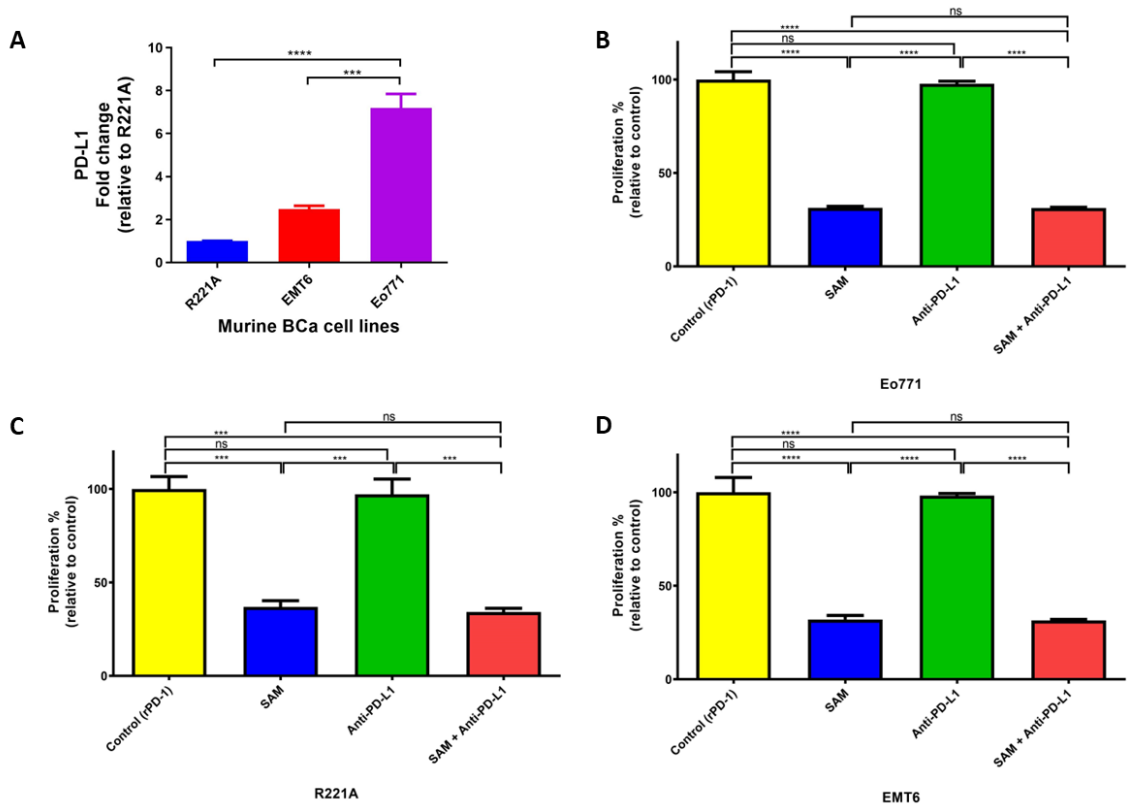

Figure 2. PD-L1 expression and effect of PD-L1 intracellular signaling on cell proliferation of murine BCa cells. (**A**) Expression of PD-L1 in murine BCa cell lines analyzed by RT-qPCR. The fold change was relative to the expression of R221A. (**B**–**D**) Effect of SAM and anti-PD-L1 antibody on proliferation of murine BCa cells. (**B**) Eo771 (4×10^4), (**C**) R221A (1×10^4), and (**D**)

EMT6 (4×10^4) cells were seeded in 6-well plates and were added to rPD-1 (0.2 µg/mL, day 3). The cells were treated with either control (only rPD-1), SAM (200 µM, day 2, 3, 4), anti-PD-L1 antibody (50 µg/mL, day 4), or SAM and anti-PD-L1 in combination. The results are the mean of at least three independent experiments. Proliferation is represented as the percentage proportional to the control (± SEM). Statistical significance was determined by one-way ANOVA in GraphPad prism. Significance values are represented by asterisks (ns; not significant; *** $p < 0.001$; **** $p < 0.0001$).

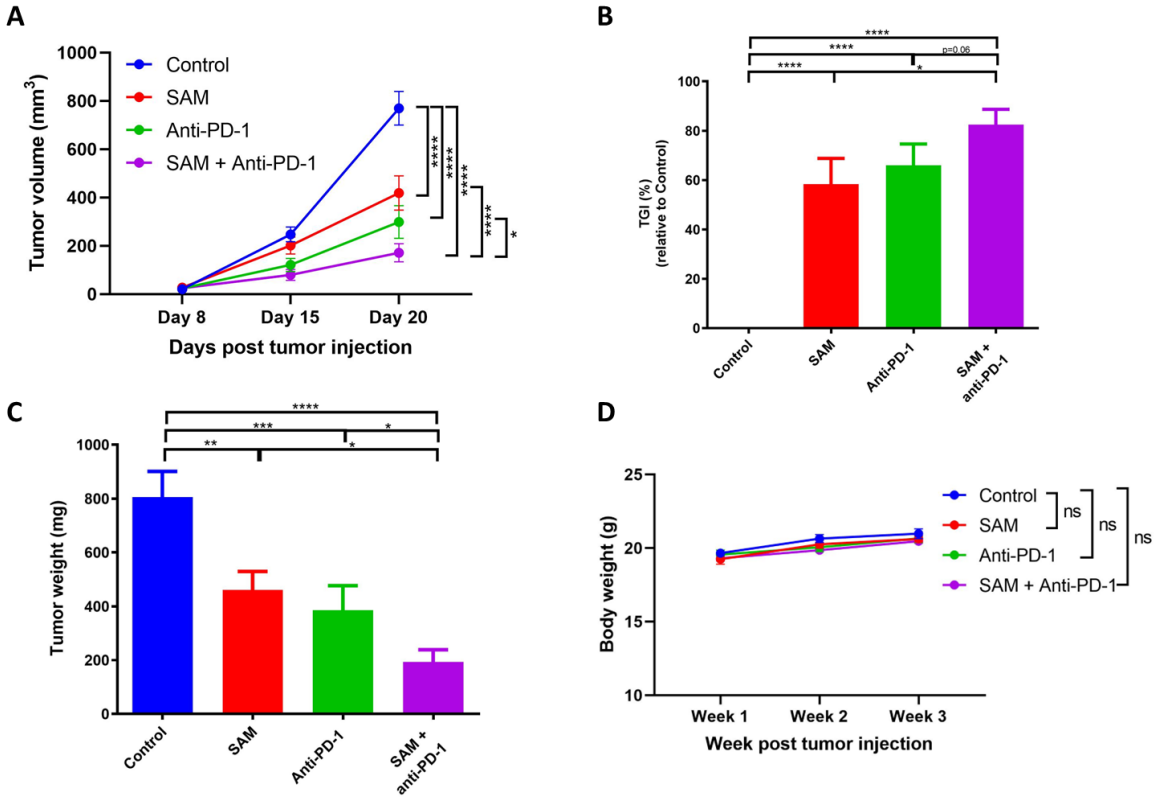

Figure 3. SAM, anti-PD-1 antibody, and the combination treatment decreased primary tumor growth in Eo771 tumor-bearing mice. (**A**) Eo771 (2×10^5 cells) were injected at the 4th m.f.p in B6 mice to induce tumor formation. The animals were treated with either the control (isotype matched IgG and PBS), SAM (80 mg/kg/day), anti-PD-1 antibody (5 mg/kg, twice per week), or combination. Tumor volumes were assessed at day 8, 15, and 20, and the animals were sacrificed at day 20. Results are presented as the mean ± SEM of tumor volume ($n \geq 7$/group). (**B**) Percentage tumor growth inhibition (TGI) was calculated from tumor volumes at day 15 to day 20, relative to the control. (**C**) Tumor weight (mg ± SEM) was measured after tumor harvest on day 20. (**D**) Body

weight (g ± SEM) of the mice was measured once a week. Statistical significance was determined by (**A**, **D**) two-way ANOVA; (**B**, **C**) one-way ANOVA in GraphPad prism. Significance values are represented by asterisks (ns, not significant; * $p < 0.05$; ** $p < 0.01$; *** $p < 0.001$ and **** $p < 0.0001$).

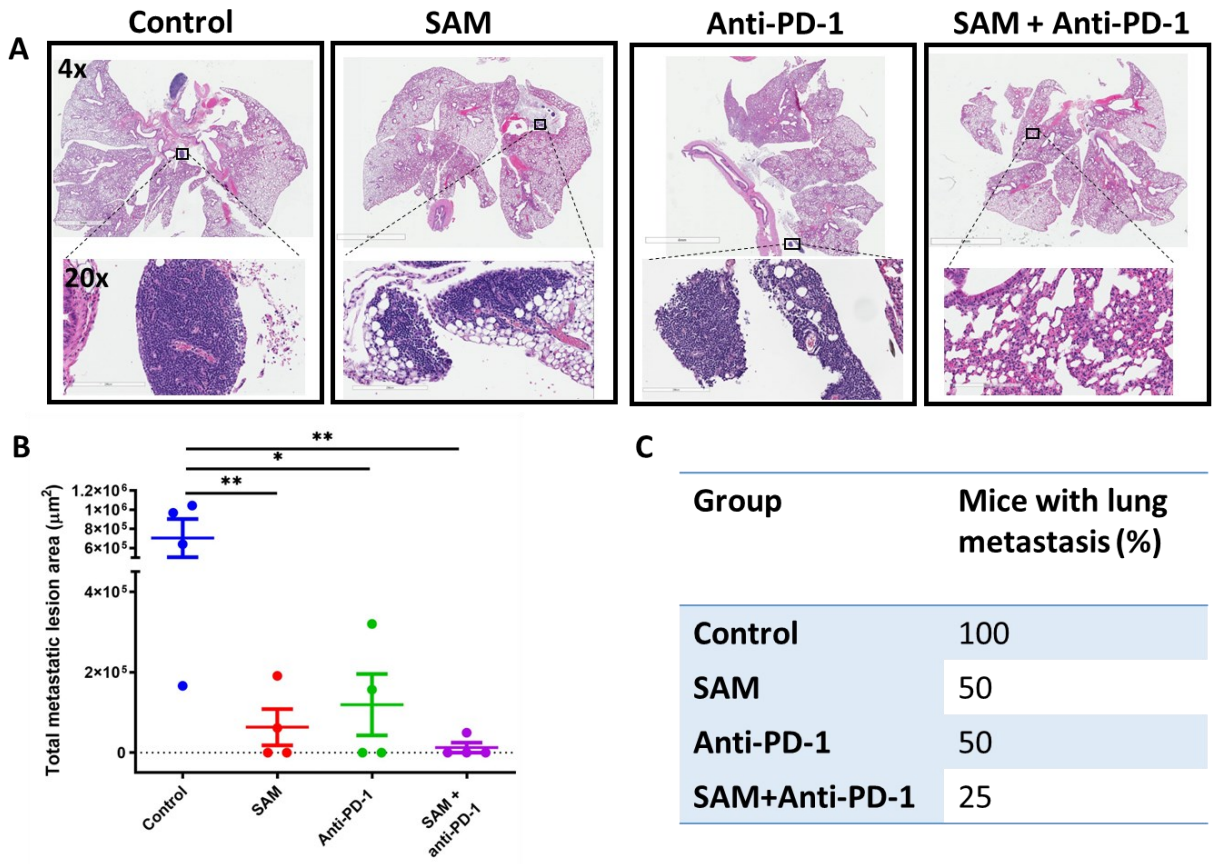

Group	Mice with lung metastasis (%)
Control	100
SAM	50
Anti-PD-1	50
SAM+Anti-PD-1	25

Figure 4. SAM, anti-PD-1 antibody, and the combination treatment decreased lung metastasis in Eo771 tumor-bearing mice. Briefly, mice were injected with Eo771 cells orthotopically at the m.f.p and treated with the four treatments indicated. At the end of the study, lungs of the mice were harvested, fixed using formalin, embedded in paraffin, sliced, and stained with H&E. (**A**) Representative histology images of mouse lung showing the whole lung and magnified images to show metastatic lesions from each group except the SAM+anti-PD-1 antibody combination group, which had no lesions in this sample. Lens: top; 4×; bottom; 20×. Magnification: top; 40×; bottom; 200×. (**B**) Total metastatic lesion area (μm^2 ± SEM) for each group (n = 4/group). Total metastatic lesion area was calculated by annotating all the metastatic lesions in the entire lung of a mouse using the ImageScope annotation tool, which gives the selected area. Then, all the lesion areas

were added together. (**C**) Percentage of mice with lung metastasis in each group. Statistical significance was determined by (B) one-way ANOVA in GraphPad prism. Significance values are represented by asterisks (* $p < 0.05$; ** $p < 0.01$).

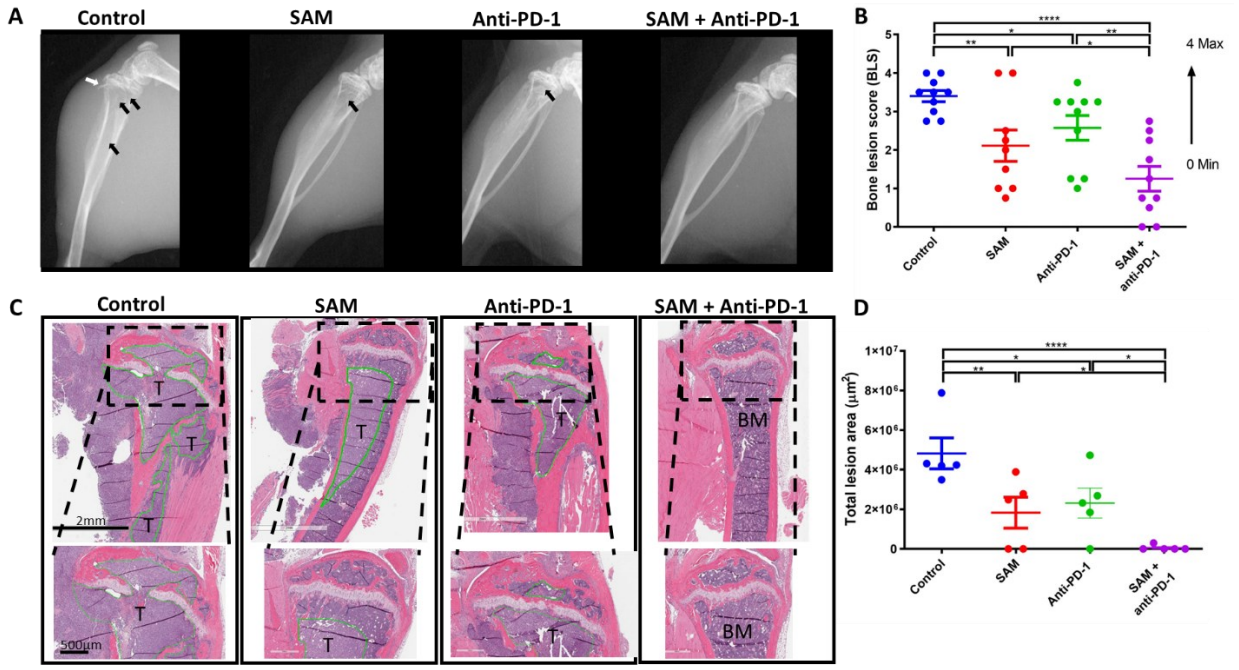

E

Group	Control	SAM	Anti-PD-1	SAM + Anti-PD-1
Mice with bone metastasis (%)	100	60	80	20

Figure 5. The SAM and anti-PD-1 antibody combination decreases bone metastasis and protects the bone from damage caused by aggressively growing tumor lesions. Briefly, mice were injected with Eo771 cells intra-tibially and treated with either control (isotype matched IgG and PBS, n = 10/group), SAM (80 mg/kg/day, n = 9/group), anti-PD-1 antibody (5 mg/kg, twice per week, n = 10/group), or the combination (n = 10/group). (**A**) Representative X-ray images showing the anatomy of the lower limb. The tibia, fibula, and femur (in part) along with the knee joint are shown. X-rays of the mice were taken at day 21 post-tumor injection. Black arrows indicate tumors, while white arrows indicate a broken cortical bone margin. (**B**) X-ray images were used to calculate a bone lesion score (BLS) for each group in increments from 0 to 4, where 0 represents no tumor lesions with the highest bone integrity (no breaks in the peripheral margin) and 4 represents the maximum tumor lesion area with the lowest bone integrity and with major breaks in the peripheral margin (n = 10/group, except SAM (n = 9/group)). (**C**) Representative histology images of mouse tibias 21 days post-tumor injection. Briefly, mice were sacrificed at day 21, and

tibias were extracted, fixed, decalcified, embedded, sliced, and subjected to H&E staining, as described in Materials and Methods. T, tumor; BM, bone marrow. The black bar at the bottom left represents the scale in each image: top, 2 mm; below, 500 μm. (**D**) Total bone lesion area (μm^2) for each group (n = 5/group). Briefly, the tumor lesion area in the whole tibia image was measured using the ImageScope annotation tool, added and plotted in GraphPad Prism. (**E**) Percentage of mice with bone metastasis in each group. Statistical significance was determined by (**B**, **D**) one-way ANOVA in GraphPad prism. Significance values are represented by asterisks (* $p < 0.05$; ** $p < 0.01$; *** $p < 0.001$; **** $p < 0.0001$).

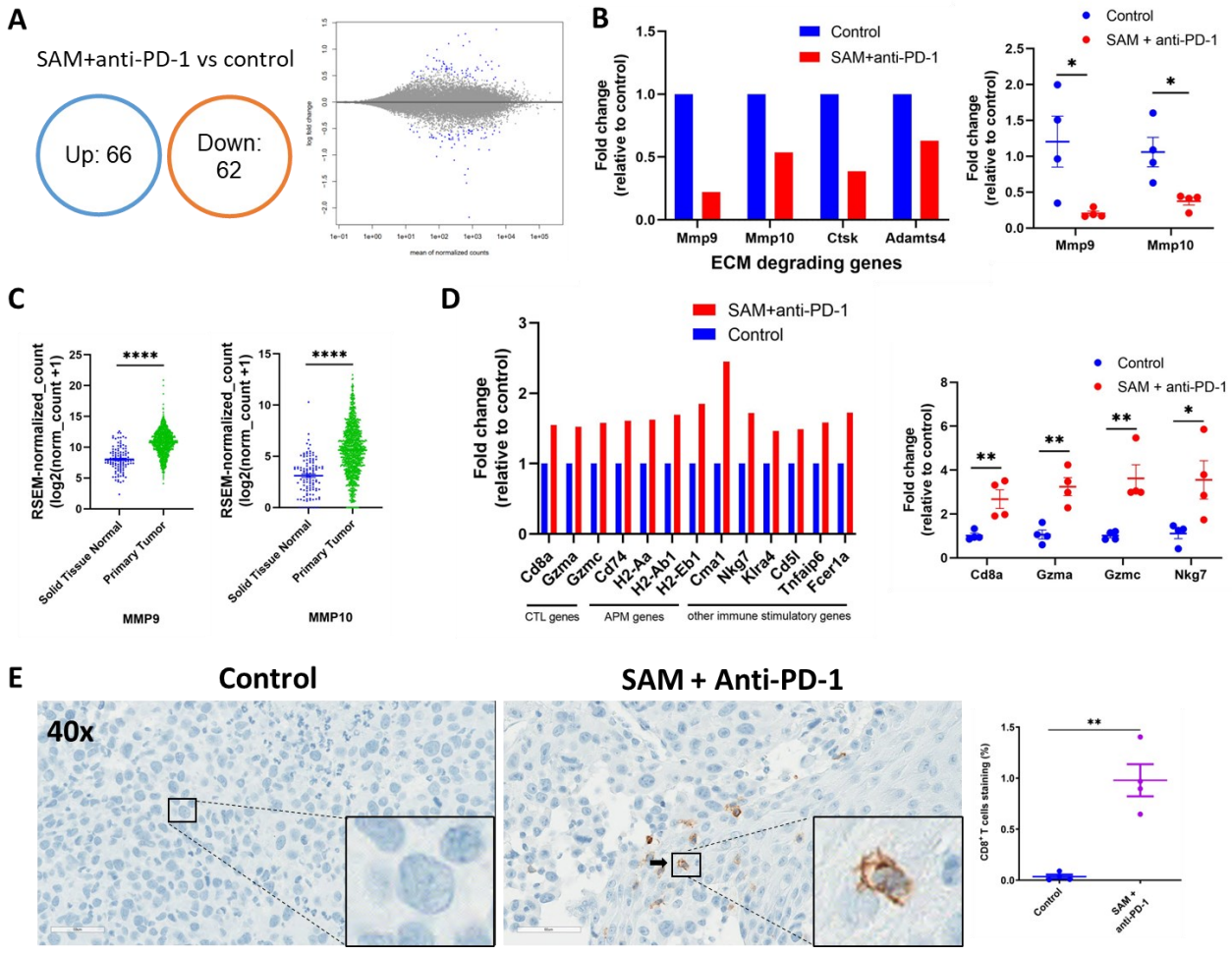

Figure 6. Tumors treated with the SAM and anti-PD-1 antibody combination show reduced expression of key oncogenes and pro-metastasis genes, and elevated expression of immunostimulatory genes. (**A**) Venn diagram (left) and MA plot (right) showing significant DEGs ($p < 0.001$) in SAM and anti-PD-1 antibody combination-treated Eo771 tumors versus control

Eo771 tumors. Up, upregulated genes; down, downregulated genes. (**B**) Change in expression of significantly downregulated genes in the combination-treated versus control tumors extracted from RNA-seq data (left, n = 3/group) and validated with RT-qPCR (right, n = 4/group). The data are presented as fold change in expression in the treatment group relative to the control. The value of the control was set at 1. (**C**) Expression of key pro-metastatic genes *MMP9* and *MMP10* in human solid normal tissue and primary tumor tissue of breast cancer patients derived from GTEx and TCGA databases (n = 1391 samples) using the Xena platform. Expression values are depicted in RSEM, which is RNA-Seq by Expectation Maximization. (**D**) Change in expression of top significantly upregulated genes in combination-treated versus control tumors extracted from RNA-seq data (left, n = 3/group) and validated with RT-qPCR (right, n = 4/group). Data is presented as fold change in the treatment group relative to the control. The value of the control was set at 1. CTL, cytotoxic T lymphocytes; APM, antigen processing and presentation machinery. (**E**) Immunohistochemistry with $CD8a^+$ T cell marker staining of Eo771 tumors treated with the combination treatment and the controls. (**E**, left) Representative images (lens, 40×; magnification, 400×) of the primary Eo771 tumors stained with murine antibody against $CD8a^+$ marker (brown) from the control and SAM+anti-PD-1 antibody combination-treated tumors. The nuclei are stained blue and a $CD8^+$ T cell is indicated by a black arrow. Enlarged images at the bottom right show the absence and presence of $CD8^+$ T cells in the control and SAM+anti-PD-1 antibody group, respectively. (**E**, right) $CD8a^+$ T cell positive staining area percentage (n = 4 samples/group). Statistical significance was determined using (**C**,**E**) T-test in GraphPad prism and (**A**,**B**,**D**) by Wald test with BH FDR (≤ 0.2) correction. Significance values are represented by asterisks (* $p < 0.05$; ** $p < 0.01$; **** $p < 0.0001$).

Declarations and other statements

Author Contributions: Conceptualization, A.M., C.A.P., M.S., and S.A.R.; Data curation, A.M.; Formal analysis, A.M.; Funding acquisition, S.A.R.; Investigation, A.M., M.A., and A.A.; Methodology, A.M.; Resources, S.A.R.; Software, A.M.; Supervision, M.S. and S.A.R.; Validation, A.M. and A.A.; Visualization, A.M.; Writing—original draft, A.M.; Writing—review and editing, A.M., M.A., C.A.P., M.S., and S.A.R. All authors have read and agreed to the published version of the manuscript.

Funding: The study was supported by the Canadian Institutes of Health Research (CIHR) grants, PJT-156225 and PJT-148821, awarded to Shafaat A. Rabbani and Ciriaco A. Piccirillo, respectively.

Institutional Review Board Statement: The study was conducted according to the guidelines of the Facility Animal Care Committee (FACC) of McGill University (protocol code 2891 and approved in April 2019).

Informed Consent Statement: Not applicable.

Data Availability Statement: The data analyzed or generated is available within the main file and in the supplementary files.

Acknowledgments: Ali Mehdi is a recipient of the Fonds de recherche du Québec-Santé (FRQ-S) scholarship.

Conflicts of Interest: The authors declare no potential conflicts of interest.

Simple Summary: Breast cancer (BCa) is a devastating disease, which has a high prevalence and mortality in women. BCa metastasis is a major cause of mortality, and bone metastasis accounts for the majority of BCa-associated deaths. The luminal B subtype of BCa is immunogenically low and has the highest propensity to form bone metastasis compared to other BCa subtypes. Recent efforts have targeted BCa with immune checkpoint inhibitor (CPI) therapy. Although some clinical success in other BCa subtypes, luminal BCas had limited success. This has led to combining immune-stimulating therapies with CPIs to enhance the effectiveness of CPI therapy. We have demonstrated that a natural methyl donor, S-adenosylmethionine (SAM), has significant anti-cancer effects in various cancer models including all subtypes of BCa. Here, we show that SAM in combination with anti-PD-1 antibody has an enhanced anti-cancer efficacy compared to SAM, anti-PD-1 antibody, and control. The combination significantly reduced primary tumor growth and

metastasis to lungs and bone. Hence, combining SAM with CPI has the potential to treat luminal B BCa.

References

1. Brenner, D.R.; Weir, H.K.; Demers, A.A.; Ellison, L.F.; Louzado, C.; Shaw, A.; Turner, D.; Woods, R.R.; Smith, L.M.; Canadian Cancer Statistics Advisory Committee. Projected estimates of cancer in Canada in 2020. *CMAJ* **2020**, *192*, E199–E205. https://doi.org/10.1503/cmaj.191292.
2. Sung, H.; Ferlay, J.; Siegel, R.L.; Laversanne, M.; Soerjomataram, I.; Jemal, A.; Bray, F. Global Cancer Statistics 2020: GLOBOCAN Estimates of Incidence and Mortality Worldwide for 36 Cancers in 185 Countries. *Cancer J. Clin.* **2021**, *71*, 209–249. https://doi.org/10.3322/caac.21660.
3. Siegel, R.L.; Miller, K.D.; Jemal, A. Cancer statistics, 2017. *Cancer J. Clin.* **2018**, *67*, 7–30. https://doi.org/10.3322/caac.21387.
4. Seyfried, T.N.; Huysentruyt, L.C. On the origin of cancer metastasis. *Crit. Rev. Oncog.* **2013**, *18*, 43–73. https://doi.org/10.1615/critrevoncog.v18.i1-2.40.
5. Chaffer, C.L.; Weinberg, R.A. A perspective on cancer cell metastasis. *Science* **2011**, *331*, 1559–1564. https://doi.org/10.1126/science.1203543.
6. Yersal, O.; Barutca, S. Biological subtypes of breast cancer: Prognostic and therapeutic implications. *World J. Clin. Oncol.* **2014**, *5*, 412–424. https://doi.org/10.5306/wjco.v5.i3.412.
7. Cardoso, F.; Kyriakides, S.; Ohno, S.; Penault-Llorca, F.; Poortmans, P.; Rubio, I.T.; Zackrisson, S.; Senkus, E.; on behalf of the ESMO Guidelines Committee. Early breast cancer: ESMO Clinical Practice Guidelines for diagnosis, treatment and follow-updagger. *Ann. Oncol.* **2019**, *30*, 1194–1220. https://doi.org/10.1093/annonc/mdz173.
8. Viale, G.; Hanlon Newell, A.E.; Walker, E.; Harlow, G.; Bai, I.; Russo, L.; Dell'Orto, P.; Maisonneuve, P. Ki-67 (30-9) scoring and differentiation of Luminal A- and Luminal B-like breast cancer subtypes. *Breast Cancer Res. Treat.* **2019**, *178*, 451–458. https://doi.org/10.1007/s10549-019-05402-w.

9. Wu, Q.; Li, J.; Zhu, S.; Wu, J.; Chen, C.; Liu, Q.; Wei, W.; Zhang, Y.; Sun, S. Breast cancer subtypes predict the preferential site of distant metastases: A SEER based study. *Oncotarget* **2017**, *8*, 27990–27996. https://doi.org/10.18632/oncotarget.15856.
10. Yang, M.; Liu, C.; Yu, X. Skeletal-related adverse events during bone metastasis of breast cancer: Current status. *Discov. Med.* **2019**, *27*, 211–220.
11. Kane, C.M.; Hoskin, P.; Bennett, M.I. Cancer induced bone pain. *BMJ* **2015**, *350*, h315. https://doi.org/10.1136/bmj.h315.
12. Harris, S.R. Differentiating the Causes of Spontaneous Rib Fracture After Breast Cancer. *Clin. Breast Cancer* **2016**, *16*, 431–436. https://doi.org/10.1016/j.clbc.2016.07.001.
13. Alsaab, H.O.; Sau, S.; Alzhrani, R.; Tatiparti, K.; Bhise, K.; Kashaw, S.K.; Iyer, A.K. PD-1 and PD-L1 Checkpoint Signaling Inhibition for Cancer Immunotherapy: Mechanism, Combinations, and Clinical Outcome. *Front. Pharmacol.* **2017**, *8*, 561. https://doi.org/10.3389/fphar.2017.00561.
14. Pardoll, D.M. The blockade of immune checkpoints in cancer immunotherapy. *Nat. Rev. Cancer* **2012**, *12*, 252. https://doi.org/10.1038/nrc3239.
15. Schadendorf, D.; van Akkooi, A.C.J.; Berking, C.; Griewank, K.G.; Gutzmer, R.; Hauschild, A.; Stang, A.; Roesch, A.; Ugurel, S. Melanoma. *Lancet* **2018**, *392*, 971–984. https://doi.org/10.1016/s0140-6736(18)31559-9.
16. Kalbasi, A.; Ribas, A. Tumour-intrinsic resistance to immune checkpoint blockade. *Nat. Rev. Immunol.* **2020**, *20*, 25–39. https://doi.org/10.1038/s41577-019-0218-4.
17. Barrueto, L.; Caminero, F.; Cash, L.; Makris, C.; Lamichhane, P.; Deshmukh, R.R. Resistance to Checkpoint Inhibition in Cancer Immunotherapy. *Transl. Oncol.* **2020**, *13*, 100738. https://doi.org/10.1016/j.tranon.2019.12.010.
18. Alexandrov, L. B., S. Nik-Zainal, D. C. Wedge, S. A. Aparicio, S. Behjati, A. V. Biankin, G. R. Bignell, N. Bolli, A. Borg, A. L. Borresen-Dale, S. Boyault, B. Burkhardt, A. P. Butler, C. Caldas, H. R. Davies, C. Desmedt, R. Eils, J. E. Eyfjord, J. A. Foekens, M. Greaves, F. Hosoda, B. Hutter, T. Ilicic, S. Imbeaud, M. Imielinski, N. Jager, D. T. Jones, D. Jones, S. Knappskog, M. Kool, S. R. Lakhani, C. Lopez-Otin, S. Martin, N. C. Munshi, H. Nakamura, P. A. Northcott, M. Pajic, E. Papaemmanuil, A. Paradiso, J. V. Pearson, X. S. Puente, K. Raine, M. Ramakrishna, A. L. Richardson, J. Richter, P. Rosenstiel, M. Schlesner, T. N. Schumacher, P. N. Span, J. W. Teague, Y. Totoki, A. N. Tutt, R. Valdes-Mas, M. M. van

Buuren, L. van 't Veer, A. Vincent-Salomon, N. Waddell, L. R. Yates, Initiative Australian Pancreatic Cancer Genome, Icgc Breast Cancer Consortium, Icgc Mmml- Seq Consortium, Icgc PedBrain, J. Zucman-Rossi, P. A. Futreal, U. McDermott, P. Lichter, M. Meyerson, S. M. Grimmond, R. Siebert, E. Campo, T. Shibata, S. M. Pfister, P. J. Campbell, and M. R. Stratton. "Signatures of Mutational Processes in Human Cancer." *Nature* 500, no. 7463 (2013): 415-21.

19. Yarchoan, M.; Hopkins, A.; Jaffee, E.M. Tumor Mutational Burden and Response Rate to PD-1 Inhibition. *N. Engl. J. Med.* **2017**, *377*, 2500–2501. https://doi.org/10.1056/NEJMc1713444.
20. Planes-Laine, G.; Rochigneux, P.; Bertucci, F.; Chretien, A.S.; Viens, P.; Sabatier, R.; Goncalves, A. PD-1/PD-L1 Targeting in Breast Cancer: The First Clinical Evidences Are Emerging. A Literature Review. *Cancers* **2019**, *11*, 1033. https://doi.org/10.3390/cancers11071033.
21. Plitas, G.; Konopacki, C.; Wu, K.; Bos, P.D.; Morrow, M.; Putintseva, E.V.; Chudakov, D.M.; Rudensky, A.Y. Regulatory T Cells Exhibit Distinct Features in Human Breast Cancer. *Immunity* **2016**, *45*, 1122–1134. https://doi.org/10.1016/j.immuni.2016.10.032.
22. Dieci, M.V.; Griguolo, G.; Miglietta, F.; Guarneri, V. The immune system and hormone-receptor positive breast cancer: Is it really a dead end? *Cancer Treat. Rev.* **2016**, *46*, 9–19. https://doi.org/10.1016/j.ctrv.2016.03.011.
23. Dieci, M.V.; Guarneri, V.; Tosi, A.; Bisagni, G.; Musolino, A.; Spazzapan, S.; Moretti, G.; Vernaci, G.M.; Griguolo, G.; Giarratano, T.; et al. Neoadjuvant Chemotherapy and Immunotherapy in Luminal B-like Breast Cancer: Results of the Phase II GIADA Trial. *Clin. Cancer Res.* **2022**, *28*, 308–317. https://doi.org/10.1158/1078-0432.CCR-21-2260.
24. Miller, L. D., J. A. Chou, M. A. Black, C. Print, J. Chifman, A. Alistar, T. Putti, X. Zhou, D. Bedognetti, W. Hendrickx, A. Pullikuth, J. Rennhack, E. R. Andrechek, S. Demaria, E. Wang, and F. M. Marincola. "Immunogenic Subtypes of Breast Cancer Delineated by Gene Classifiers of Immune Responsiveness." *Cancer Immunol Res* 4, no. 7 (2016): 600-10.
25. Jung, H.; Kim, H.S.; Kim, J.Y.; Sun, J.M.; Ahn, J.S.; Ahn, M.J.; Park, K.; Esteller, M.; Lee, S.H.; Choi, J.K. DNA methylation loss promotes immune evasion of tumours with high mutation and copy number load. *Nat. Commun.* **2019**, *10*, 4278. https://doi.org/10.1038/s41467-019-12159-9.

26. Pakneshan, P.; Szyf, M.; Farias-Eisner, R.; Rabbani, S.A. Reversal of the hypomethylation status of urokinase (uPA) promoter blocks breast cancer growth and metastasis. *J. Biol. Chem.* **2004**, *279*, 31735–31744. https://doi.org/10.1074/jbc.M401669200.
27. Shukeir, N.; Pakneshan, P.; Chen, G.; Szyf, M.; Rabbani, S.A. Alteration of the methylation status of tumor-promoting genes decreases prostate cancer cell invasiveness and tumorigenesis in vitro and in vivo. *Cancer Res.* **2006**, *66*, 9202–9210. https://doi.org/10.1158/0008-5472.CAN-06-1954.
28. Mahmood, N.; Cheishvili, D.; Arakelian, A.; Tanvir, I.; Khan, H.A.; Pepin, A.S.; Szyf, M.; Rabbani, S.A. Methyl donor S-adenosylmethionine (SAM) supplementation attenuates breast cancer growth, invasion, and metastasis in vivo; therapeutic and chemopreventive applications. *Oncotarget* **2018**, *9*, 5169–5183. https://doi.org/10.18632/oncotarget.23704.
29. Mahmood, N.; Arakelian, A.; Cheishvili, D.; Szyf, M.; Rabbani, S.A. S-adenosylmethionine in combination with decitabine shows enhanced anti-cancer effects in repressing breast cancer growth and metastasis. *J. Cell. Mol. Med.* **2020**, *24*, 10322–10337. https://doi.org/10.1111/jcmm.15642.
30. Mahmood, N.; Arakelian, A.; Muller, W.J.; Szyf, M.; Rabbani, S.A. An enhanced chemopreventive effect of methyl donor S-adenosylmethionine in combination with 25-hydroxyvitamin D in blocking mammary tumor growth and metastasis. *Bone Res.* **2020**, *8*, 28. https://doi.org/10.1038/s41413-020-0103-6.
31. Mahmood, N.; Rabbani, S.A. Targeting DNA Hypomethylation in Malignancy by Epigenetic Therapies. *Adv. Exp. Med. Biol.* **2019**, *1164*, 179–196. https://doi.org/10.1007/978-3-030-22254-3_14.
32. Hote, P.T.; Sahoo, R.; Jani, T.S.; Ghare, S.S.; Chen, T.; Joshi-Barve, S.; McClain, C.J.; Barve, S.S. Ethanol inhibits methionine adenosyltransferase II activity and S-adenosylmethionine biosynthesis and enhances caspase-3-dependent cell death in T lymphocytes: Relevance to alcohol-induced immunosuppression. *J. Nutr. Biochem.* **2008**, *19*, 384–391. https://doi.org/10.1016/j.jnutbio.2007.05.010.
33. Tobena, R.; Horikawa, S.; Calvo, V.; Alemany, S. Interleukin-2 induces gamma-S-adenosyl-L-methionine synthetase gene expression during T-lymphocyte activation. *Biochem. J.* **1996**, *319*, 929–933.

34. LeGros, H.L., Jr.; Geller, A.M.; Kotb, M. Differential regulation of methionine adenosyltransferase in superantigen and mitogen stimulated human T lymphocytes. *J. Biol. Chem.* **1997**, *272*, 16040–16047.
35. Kotb, M.; Dale, J.B.; Beachey, E.H. Stimulation of S-adenosylmethionine synthetase in human lymphocytes by streptococcal M protein. *J. Immunol.* **1987**, *139*, 202–206.
36. De La Rosa, J.; Geller, A.M.; LeGros, H.L., Jr.; Kotb, M. Induction of interleukin 2 production but not methionine adenosyltransferase activity or S-adenosylmethionine turnover in Jurkat T-cells. *Cancer Res.* **1992**, *52*, 3361–3366.
37. De La Rosa, J.; Kotb, M.; Kredich, N.M. Regulation of S-adenosylmethionine synthetase activity in cultured human lymphocytes. *Biochim. Biophys. Acta* **1991**, *1077*, 225–232.
38. German, D.C.; Bloch, C.A.; Kredich, N.M. Measurements of S-adenosylmethionine and L-homocysteine metabolism in cultured human lymphoid cells. *J. Biol. Chem.* **1983**, *258*, 10997–11003.
39. Zeng, Z.; Yang, H.; Huang, Z.Z.; Chen, C.; Wang, J.; Lu, S.C. The role of c-Myb in the up-regulation of methionine adenosyltransferase 2A expression in activated Jurkat cells. *Biochem. J.* **2001**, *353*, 163–168.
40. Kotb, M.; Kredich, N.M. S-Adenosylmethionine synthetase from human lymphocytes. Purification and characterization. *J. Biol. Chem.* **1985**, *260*, 3923–3930.
41. Sahin, E.; Sahin, M. Epigenetical Targeting of the FOXP3 Gene by S-Adenosylmethionine Diminishes the Suppressive Capacity of Regulatory T Cells Ex Vivo and Alters the Expression Profiles. *J. Immunother.* **2019**, *42*, 11–22. https://doi.org/10.1097/cji.0000000000000247.
42. Bian, Y.; Li, W.; Kremer, D.M.; Sajjakulnukit, P.; Li, S.; Crespo, J.; Nwosu, Z.C.; Zhang, L.; Czerwonka, A.; Pawlowska, A.; et al. Cancer SLC43A2 alters T cell methionine metabolism and histone methylation. *Nature* **2020**, *585*, 277–282. https://doi.org/10.1038/s41586-020-2682-1.
43. Ulanovskaya, O.A.; Zuhl, A.M.; Cravatt, B.F. NNMT promotes epigenetic remodeling in cancer by creating a metabolic methylation sink. *Nat. Chem. Biol.* **2013**, *9*, 300–306. https://doi.org/10.1038/nchembio.1204.
44. Larroquette, M.; Domblides, C.; Lefort, F.; Lasserre, M.; Quivy, A.; Sionneau, B.; Bertolaso, P.; Gross-Goupil, M.; Ravaud, A.; Daste, A. Combining immune checkpoint inhibitors with

chemotherapy in advanced solid tumours: A review. *Eur. J. Cancer* **2021**, *158*, 47–62. https://doi.org/10.1016/j.ejca.2021.09.013.

45. Hanahan, D. Hallmarks of Cancer: New Dimensions. *Cancer Discov.* **2022**, *12*, 31–46. https://doi.org/10.1158/2159-8290.CD-21-1059.
46. Escors, D.; Gato-Cañas, M.; Zuazo, M.; Arasanz, H.; García-Granda, M.J.; Vera, R.; Kochan, G. The intracellular signalosome of PD-L1 in cancer cells. *Signal Transduct. Target. Ther.* **2018**, *3*, 26. https://doi.org/10.1038/s41392-018-0022-9.
47. Dong, P.; Xiong, Y.; Yue, J.; Hanley, S.J.B.; Watari, H. Tumor-Intrinsic PD-L1 Signaling in Cancer Initiation, Development and Treatment: Beyond Immune Evasion. *Front. Oncol.* **2018**, *8*, 386. https://doi.org/10.3389/fonc.2018.00386.
48. Mehdi, A.; Attias, M.; Mahmood, N.; Arakelian, A.; Mihalcioiu, C.; Piccirillo, C.A.; Szyf, M.; Rabbani, S.A. Enhanced Anticancer Effect of a Combination of S-adenosylmethionine (SAM) and Immune Checkpoint Inhibitor (ICPi) in a Syngeneic Mouse Model of Advanced Melanoma. *Front. Oncol.* **2020**, *10*, 1361. https://doi.org/10.3389/fonc.2020.01361.
49. Le Naour, A.; Rossary, A.; Vasson, M.P. EO771, is it a well-characterized cell line for mouse mammary cancer model? Limit and uncertainty. *Cancer Med.* **2020**, *9*, 8074–8085. https://doi.org/10.1002/cam4.3295.
50. Le Naour, A.; Koffi, Y.; Diab, M.; Le Guennec, D.; Rouge, S.; Aldekwer, S.; Goncalves-Mendes, N.; Talvas, J.; Farges, M.C.; Caldefie-Chezet, F.; et al. EO771, the first luminal B mammary cancer cell line from C57BL/6 mice. *Cancer Cell. Int.* **2020**, *20*, 328. https://doi.org/10.1186/s12935-020-01418-1.
51. Gialeli, C.; Theocharis, A.D.; Karamanos, N.K. Roles of matrix metalloproteinases in cancer progression and their pharmacological targeting. *FEBS J.* **2011**, *278*, 16–27. https://doi.org/10.1111/j.1742-4658.2010.07919.x.
52. Jiang, H.; Li, H. Prognostic values of tumoral MMP2 and MMP9 overexpression in breast cancer: A systematic review and meta-analysis. *BMC Cancer* **2021**, *21*, 149. https://doi.org/10.1186/s12885-021-07860-2.
53. Goldman, M.J.; Craft, B.; Hastie, M.; Repecka, K.; McDade, F.; Kamath, A.; Banerjee, A.; Luo, Y.; Rogers, D.; Brooks, A.N.; et al. Visualizing and interpreting cancer genomics data via the Xena platform. *Nat. Biotechnol.* **2020**, *38*, 675–678. https://doi.org/10.1038/s41587-020-0546-8.

54. Zhang, M.; Fujiwara, K.; Che, X.; Zheng, S.; Zheng, L. DNA methylation in the tumor microenvironment. *J. Zhejiang Univ. Sci. B* **2017**, *18*, 365–372. https://doi.org/10.1631/jzus.B1600579.
55. Ostrand-Rosenberg, S. Immune Surveillance: A Balance Between Pro- and Anti-tumor Immunity. *Curr. Opin. Genet. Dev.* **2008**, *18*, 11–18. https://doi.org/10.1016/j.gde.2007.12.007.
56. Sukari, A.; Nagasaka, M.; Al-Hadidi, A.; Lum, L.G. Cancer Immunology and Immunotherapy. *Anticancer Res.* **2016**, *36*, 5593–5606. https://doi.org/10.21873/anticanres.11144.
57. Gibney, G.T.; Weiner, L.M.; Atkins, M.B. Predictive biomarkers for checkpoint inhibitor-based immunotherapy. *Lancet Oncol.* **2016**, *17*, e542–e551. https://doi.org/10.1016/S1470-2045(16)30406-5.
58. Ji, R.R.; Chasalow, S.D.; Wang, L.; Hamid, O.; Schmidt, H.; Cogswell, J.; Alaparthy, S.; Berman, D.; Jure-Kunkel, M.; Siemers, N.O.; et al. An immune-active tumor microenvironment favors clinical response to ipilimumab. *Cancer Immunol. Immunother.* **2012**, *61*, 1019–1031. https://doi.org/10.1007/s00262-011-1172-6.
59. Ilisso, C.P.; Sapio, L.; Delle Cave, D.; Illiano, M.; Spina, A.; Cacciapuoti, G.; Naviglio, S.; Porcelli, M. S-Adenosylmethionine Affects ERK1/2 and Stat3 Pathways and Induces Apotosis in Osteosarcoma Cells. *J. Cell. Physiol.* **2016**, *231*, 428–435. https://doi.org/10.1002/jcp.25089.
60. Ilisso, C.P.; Delle Cave, D.; Mosca, L.; Pagano, M.; Coppola, A.; Mele, L.; Caraglia, M.; Cacciapuoti, G.; Porcelli, M. S-Adenosylmethionine regulates apoptosis and autophagy in MCF-7 breast cancer cells through the modulation of specific microRNAs. *Cancer Cell. Int.* **2018**, *18*, 197. https://doi.org/10.1186/s12935-018-0697-6.
61. Cave, D.D.; Desiderio, V.; Mosca, L.; Ilisso, C.P.; Mele, L.; Caraglia, M.; Cacciapuoti, G.; Porcelli, M. S-Adenosylmethionine-mediated apoptosis is potentiated by autophagy inhibition induced by chloroquine in human breast cancer cells. *J. Cell. Physiol.* **2018**, *233*, 1370–1383. https://doi.org/10.1002/jcp.26015.
62. Parashar, S.; Cheishvili, D.; Arakelian, A.; Hussain, Z.; Tanvir, I.; Khan, H.A.; Szyf, M.; Rabbani, S.A. S-adenosylmethionine blocks osteosarcoma cells proliferation and invasion in

vitro and tumor metastasis in vivo: Therapeutic and diagnostic clinical applications. *Cancer Med.* **2015**, *4*, 732–744. https://doi.org/10.1002/cam4.386.

63. Shukeir, N.; Stefanska, B.; Parashar, S.; Chik, F.; Arakelian, A.; Szyf, M.; Rabbani, S.A. Pharmacological methyl group donors block skeletal metastasis in vitro and in vivo. *Br. J. Pharmacol.* **2015**, *172*, 2769–2781. https://doi.org/10.1111/bph.13102.
64. Liu, Y.; Bi, T.; Yuan, F.; Gao, X.; Jia, G.; Tian, Z. S-adenosylmethionine induces apoptosis and cycle arrest of gallbladder carcinoma cells by suppression of JAK2/STAT3 pathways. *Naunyn Schmiedebergs Arch. Pharmacol.* **2020**, *393*, 2507–2515. https://doi.org/10.1007/s00210-020-01858-6.
65. Stagg, J.; Divisekera, U.; McLaughlin, N.; Sharkey, J.; Pommey, S.; Denoyer, D.; Dwyer, K.M.; Smyth, M.J. Anti-CD73 antibody therapy inhibits breast tumor growth and metastasis. *Proc. Natl. Acad. Sci. USA* **2010**, *107*, 1547–1552. https://doi.org/10.1073/pnas.0908801107.
66. Hoover, R.G.; Gullickson, G.; Kornbluth, J. Natural killer lytic-associated molecule plays a role in controlling tumor dissemination and metastasis. *Front. Immunol.* **2012**, *3*, 393. https://doi.org/10.3389/fimmu.2012.00393.
67. Singh, G.; Rabbani, A.S. *Bone Metastasis*; Human Press Inc.: Totowa, NJ, USA, 2005.
68. Sun, X.; Li, K.; Hase, M.; Zha, R.; Feng, Y.; Li, B.Y.; Yokota, H. Suppression of breast cancer-associated bone loss with osteoblast proteomes via Hsp90ab1/moesin-mediated inhibition of TGFbeta/FN1/CD44 signaling. *Theranostics* **2022**, *12*, 929–943. https://doi.org/10.7150/thno.66148.
69. Feng, Y.; Liu, S.; Zha, R.; Sun, X.; Li, K.; Robling, A.; Li, B.; Yokota, H. Mechanical Loading-Driven Tumor Suppression Is Mediated by Lrp5-Dependent and Independent Mechanisms. *Cancers* **2021**, *13*, 267. https://doi.org/10.3390/cancers13020267.
70. Pakneshan, P.; Tetu, B.; Rabbani, S.A. Demethylation of urokinase promoter as a prognostic marker in patients with breast carcinoma. *Clin. Cancer Res.* **2004**, *10*, 3035–3041.
71. Beatty, G.L.; Gladney, W.L. Immune escape mechanisms as a guide for cancer immunotherapy. *Clin. Cancer Res.* **2015**, *21*, 687–692. https://doi.org/10.1158/1078-0432.ccr-14-1860.
72. Mehdi, A.; Rabbani, S.A. Role of Methylation in Pro- and Anti-Cancer Immunity. *Cancers* **2021**, *13*, 545. https://doi.org/10.3390/cancers13030545.

73. Hung, M.H.; Lee, J.S.; Ma, C.; Diggs, L.P.; Heinrich, S.; Chang, C.W.; Ma, L.; Forgues, M.; Budhu, A.; Chaisaingmongkol, J.; et al. Tumor methionine metabolism drives T-cell exhaustion in hepatocellular carcinoma. *Nat. Commun.* **2021**, *12*, 1455. https://doi.org/10.1038/s41467-021-21804-1.
74. Chik, F.; Machnes, Z.; Szyf, M. Synergistic anti-breast cancer effect of a combined treatment with the methyl donor S-adenosyl methionine and the DNA methylation inhibitor 5-aza-2'-deoxycytidine. *Carcinogenesis* **2014**, *35*, 138–144. https://doi.org/10.1093/carcin/bgt284.
75. Shukeir, N.; Arakelian, A.; Chen, G.; Garde, S.; Ruiz, M.; Panchal, C.; Rabbani, S.A. A synthetic 15-mer peptide (PCK3145) derived from prostate secretory protein can reduce tumor growth, experimental skeletal metastases, and malignancy-associated hypercalcemia. *Cancer Res.* **2004**, *64*, 5370–5377. https://doi.org/10.1158/0008-5472.can-04-0788.
76. Black, M.; Barsoum, I.B.; Truesdell, P.; Cotechini, T.; Macdonald-Goodfellow, S.K.; Petroff, M.; Siemens, D.R.; Koti, M.; Craig, A.W.; Graham, C.H. Activation of the PD-1/PD-L1 immune checkpoint confers tumor cell chemoresistance associated with increased metastasis. *Oncotarget* **2016**, *7*, 10557–10567. https://doi.org/10.18632/oncotarget.7235.
77. Bernardo, M.; Tolstykh, T.; Zhang, Y.A.; Bangari, D.S.; Cao, H.; Heyl, K.A.; Lee, J.S.; Malkova, N.V.; Malley, K.; Marquez, E.; et al. An experimental model of anti-PD-1 resistance exhibits activation of TGFss and Notch pathways and is sensitive to local mRNA immunotherapy. *Oncoimmunology* **2021**, *10*, 1881268. https://doi.org/10.1080/2162402X.2021.1881268.
78. Bourgeois-Daigneault, M.C.; Roy, D.G.; Aitken, A.S.; El Sayes, N.; Martin, N.T.; Varette, O.; Falls, T.; St-Germain, L.E.; Pelin, A.; Lichty, B.D.; et al. Neoadjuvant oncolytic virotherapy before surgery sensitizes triple-negative breast cancer to immune checkpoint therapy. *Sci. Transl. Med.* **2018**, *10*. https://doi.org/10.1126/scitranslmed.aao1641.
79. Gao, M.; Wang, T.; Ji, L.; Bai, S.; Tian, L.; Song, H. Therapy with Carboplatin and Anti-PD-1 Antibodies Before Surgery Demonstrates Sustainable Anti-Tumor Effects for Secondary Cancers in Mice With Triple-Negative Breast Cancer. *Front. Immunol.* **2020**, *11*, 366. https://doi.org/10.3389/fimmu.2020.00366.
80. Rastelli, L.; Valentino, M.L.; Minderman, M.C.; Landin, J.; Malyankar, U.M.; Lescoe, M.K.; Kitson, R.; Brunson, K.; Souan, L.; Forenza, S.; et al. A KDR-binding peptide (ST100,059)

can block angiogenesis, melanoma tumor growth and metastasis in vitro and in vivo. *Int. J. Oncol.* **2011**, *39*, 401–408. https://doi.org/10.3892/ijo.2011.1040.

81. Rabbani, S.A.; Ateeq, B.; Arakelian, A.; Valentino, M.L.; Shaw, D.E.; Dauffenbach, L.M.; Kerfoot, C.A.; Mazar, A.P. An anti-urokinase plasminogen activator receptor antibody (ATN-658) blocks prostate cancer invasion, migration, growth, and experimental skeletal metastasis in vitro and in vivo. *Neoplasia* **2010**, *12*, 778–788. https://doi.org/10.1593/neo.10296.
82. Yang, M.; Burton, D.W.; Geller, J.; Hillegonds, D.J.; Hastings, R.H.; Deftos, L.J.; Hoffman, R.M. The bisphosphonate olpadronate inhibits skeletal prostate cancer progression in a green fluorescent protein nude mouse model. *Clin. Cancer Res.* **2006**, *12*, 2602–2606. https://doi.org/10.1158/1078-0432.CCR-05-2050.
83. Rabbani, S.A.; Arakelian, A.; Farookhi, R. LRP5 knockdown: Effect on prostate cancer invasion growth and skeletal metastasis in vitro and in vivo. *Cancer Med.* **2013**, *2*, 625–635. https://doi.org/10.1002/cam4.111.

Supplementary Material

Supplementary Table S1: List of primers utilized in the study.

Gene	**Forward**	**Reverse**
Pdl1	ACAGCCAGGGCAAAACCA	GGATGTGTTGCAGGCAGTTCT
Mmp9	CCGACTTTTGTGGTCTTCCC	TAGCGGTACAAGTATGCCTCTG
Mmp10	TCAATCCCTGTATGGAGCCG	TTGTCTGGGGTCTCAGGTCT
Cd8a	GGAGAACTGCCTTTAGCGGT	GTACCGCTCCACTAGACTGC
Gzma	GGACTCCTGCAATGGGGATT	AAAAGAGGTGATGCCTCGCA
Gzmc	GGAGCTTCCTTTGAGGAGGATT	GTTTGCCCGTAGGAGACGAT
Nkg7	CATGGCTTTTTCTGCAGCTCT	GTCTGGCTCCATCTCATACTGG

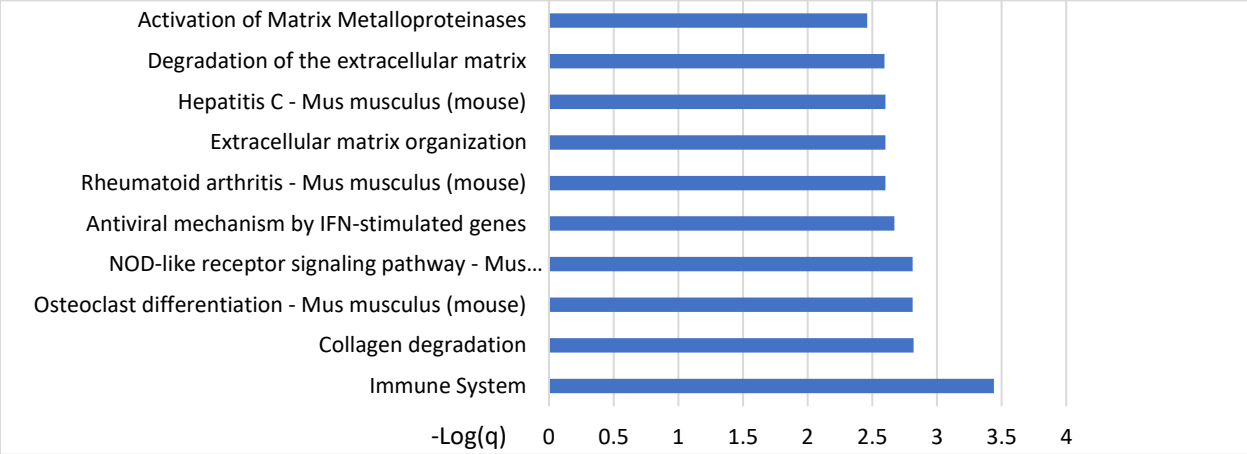

Supplementary Figure S1: Top 10 significantly downregulated pathways obtained from downregulated genes in SAM and anti-PD-1 antibody combination treated Eo771 tumors versus control tumors.

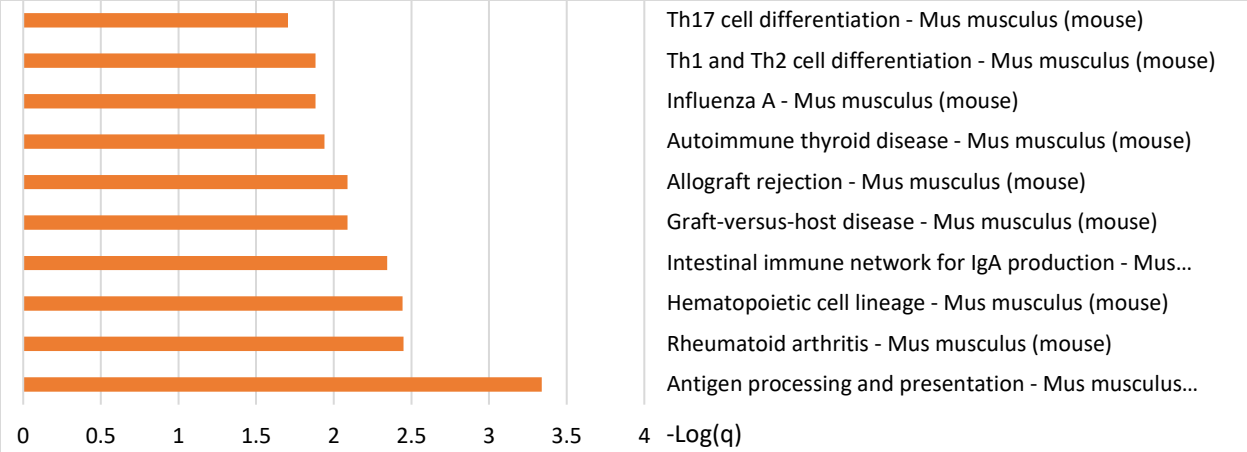

Supplementary Figure S2: Top 10 significantly upregulated pathways related to immunity obtained from upregulated genes in SAM and anti-PD-1 antibody combination treated Eo771 tumors versus control tumors.

Other supplementary files can be downloaded from the following link (supplementary additional files).

CHAPTER SIX: General Discussion

Early diagnosis of cancer is essential as it would allow early therapeutic intervention and significantly increase survival of patients. This is true for multiple cancer types as the 5-year survival rate decreases drastically for a localized tumor to a cancer which has metastasized [77]. For instance, the 5-year survival rate decreases from 99% for a localized/regional PCa to only 30% for distant metastasis warranting the need to develop of strategies for early detection of PCa and other cancers [77].

DNA methylation changes occur at the earliest stages of initiation and progression of cancer. Aberrant DNA methylation patterns was the first epigenetic mechanisms to be associated with cancer. Studying DNA methylation changes offers several advantages [81, 82]. Sampling DNA methylation changes can be carried out from fresh frozen and formalin-fixed-paraffin-embedded tissues [81, 82]. Additionally, technologies for detecting genome-wide and loci specific DNA methylation levels are well-established, highly sensitive and can detect either quantitatively or qualitatively. Moreover, DNA methylation aberrations are robust and have a higher frequency than genetic mutations [81, 82]. Furthermore, DNA methylation changes are not limited to tumor tissues but can be detected in liquid biopsies including circulating tumor cells, cell-free DNA, circulating tumor DNA, and exosomes. For instance, several studies have examined DNA methylation of pi-class glutathione-S-transferase (*GSTP1*) gene promoter in bodily fluids [81, 82]. The *GSTP1* gene promoter is hypermethylated in 90% of the tumor tissue of PCa patients. *GSTP1* gene was found to be highly sensitive and the degree of methylation at *GSTP1* correlated with aggressiveness of PCa in prostatic secretions and serum samples [81, 82]. Methylation levels of several other genes (including *RARβ*, *CD44*, *ECAD*, *RASSF1A*) alone or in combination with *GSTP1* gene have been studied to improve diagnosis of the PCa [81, 82].

In the past decades DNA methylation studies have focused on tumor, TME, and liquid biopsies derived from tumors. However, all these strategies require the tumor to be of a particular lesion size or stage in order to be detected. Therefore, to diagnose cancer even earlier than the stage where it can be detected by liquid biopsies, novel strategies leveraging the power of cancer immunosurveillance system are warranted. Cancer immunosurveillance system plays a vital role in regressing and eliminating transformed, pre-malignant and malignant cells. In fact, it is now well established that cancer immunosurveillance system shapes the evolution of cancer in a phenomenon called cancer immunoediting [83, 84]. Since components of the cancer

immunosurveillance system such as the T cells are the first to recognize and eliminate pre-cancer and cancer cells they can be leveraged as cancer biomarkers including diagnosis and risk stratification of cancer patients.

An intriguing question of whether the DNA methylation patterns would be altered in peripheral T cells in response to presence of cancer (such as PCa) and progressiveness of cancer has not been addressed extensively. Answering this question is crucial as it has significant implications in diagnostic, prognostic, and therapeutic setting. Our laboratory previously showed that DNA methylation changes in T cells can also be used to identify healthy individuals from BCa patients. Along these lines, the power of DNA methylation changes was leveraged in cancer immunosurveillance system to provide a potential for development of a non-invasive test for detecting cancers or stratify patients into cancer risk categories. In this proof of principle study (Chapter 2), we also show that DNA methylation changes do occur in the host peripheral T cells of healthy individuals compared to PCa patients. Validating the hypothesis further, the DNA methylation changes in T cell occurred in the genes/pathways that are involved in immunosurveillance of tumor cells. Previous studies have identified DNA methylation patterns linked to PCa in blood cells or whole blood [81, 82]. However, these approaches were confounded by analyzing DNA from multiple cell types in blood. In contrast, this thesis focused on T cells which are adaptive in recognizing tumor cells in an Ag-specific manner and can improve themselves to fight cancer more effectively.

The current diagnosis of PCa involves invasive sampling of the prostate multiple times (around 12 times) with the help of transrectal ultrasound (TRUS) to confirm PCa. Apart from being invasive, prostate biopsies can provide false negatives, require the tumor lesion to be large enough to be sampled, and increase the risk of metastasis. The current thesis also attempted to resolve this issue by proposing a non-invasive or minimally invasive strategy of using peripheral T cells which can be easily extracted from blood drawn from subjects.

Although the strategy proposed here has immense potential, our study had limitations. Our sample size was small and therefore it was not feasible to stratify subjects into different categories including racial backgrounds, genetic subtypes, androgen sensitivity, history of smoking, and alcohol intake, which can alter the T cell DNA methylome [215-217]. However, the samples that were utilized had strict inclusion criteria. For instance, the samples were only obtained from age-

matched subjects that had no other immune-related disorder and had not undergone any prior therapy which would alter T cell DNA methylome.

The current study (Chapter 2) utilized Illumina Infinium MethylationEPIC array which covers more than 850,000 methylation sites providing an epigenome-wide quantitative analysis at single-nucleotide resolution [218]. Although EPIC array provides a comprehensive genome-wide coverage, the EPIC array does not cover the entire genome. Since the EPIC array doesn't particularly include CpGs specific to T cell biology, it is possible that some CpGs associated with genes that are essential in recognition, activation and effector functions of the T cells could have been missed in our EPIC array analysis. For example, when epigenome-wide methylation analysis of T cells was carried out in low gleason PCa patients versus healthy controls in a previous smaller cohort using lesser number of array probes (Illumina 450K probes), we couldn't find differentially methylated probes that were significant after multiple correction (FDR< 0.05). Therefore, caution must be taken while drawing conclusions as even with these comprehensive epigenome-wide analysis no significant data doesn't mean there is no biological methylation difference but rather it maybe a limitation of the methodologies. Alternatively, whole-genome bisulfite sequencing technology can be utilized to cover DNA methylation changes of the entire epigenome of T cells.

After identifying that DNA methylation changes occur not only in cancer cells but also in components of immunosurveillance system like T cells (Chapter 2), targeting these mechanisms were justified in shifting the balance towards cancer regression and elimination (Chapter 3-5). Both melanoma and BCa have a high prevalence and cancer-related deaths globally warranting the need for effective anti-cancer therapeutics. Due to the urgency of improving the overall survival rate and reducing morbidity and mortality rates of patients, further efforts focused on developing strategies that not only have high anti-cancer efficacy but also have immense translational potential (Chapter 3-5). Several studies have demonstrated the lack of SAM within the TME [212, 213]. The decrease in SAM levels restricts the ability of the rapidly dividing tumor cells to methylate immune evasive genes which are present typically in the late-replicating regions of the DNA [176, 210, 211]. This causes DNA hypomethylation and increases the expression of silenced immune evasive genes ultimately increasing the resistance to immunity generally and to CPIs specifically [214]. In addition, methionine (pre-cursor of SAM) supplementation was demonstrated to increase the methylation potential of $CD8^+$ T cells within the TME which ultimately led to $CD8^+$ T cells

becoming functional and responsive to CPIs [212]. In contrast, rodents fed with methyl-deficient diet had reduced SAM levels, decreased SAM/SAH ratio, had global DNA hypomethylation, and developed liver tumors [18, 24, 40]. Indeed, several studies have established the requirement of SAM for T cells' activation, clonal expansion (proliferation), effector functions and survival [200-204]. Apart from the role of DNA hypomethylation in immunity, global DNA hypomethylation is a well-established cancer initiation and progression mechanism documented for decades [9, 17-19]. It has been demonstrated extensively that DNA hypomethylation results in activation of oncogenes and repetitive elements and causes genome instability which ultimately leads to tumorigenesis [9, 17-19]. Despite the crucial role of DNA hypomethylation in tumorigenesis, there is currently not a single FDA approved therapeutic drug that could target DNA hypomethylation. Our laboratory has demonstrated the ability of SAM to target DNA hypomethylation and block DNA demethylation. Therefore, this study provided treatment with SAM to immunocompetent tumor bearing mice in melanoma and BCa models.

Multiple global transcriptome analysis (RNA-sequencing) and gene-specific expression analysis were carried out in melanoma and BCa cells and tumors (Chapter 3-5) treated with SAM alone or in combination with anti-PD-1 antibody. We have also carried out transcriptome analysis upon SAM treatment in BCa previously [30, 54, 71]. Regardless of the cancer type or gene expression technique used, SAM significantly reduced and induced expression of genes (and proteins) and related pathways involved in progressing and suppressing the cell cycle, respectively. For instance, expression of the cell-cycle inhibitor, p21, was significantly upregulated by SAM in melanoma cells and vice versa for cell cycle progressive genes including cyclin dependent kinases 1 and 2, and cyclins B1 and B2 (Chapter 4). Consistently, SAM induced protein expression of p21 and p53, decreased expression of cyclins (including A, B, D, and E), and caused cell cycle arrest at the G_2M phase of osteosarcoma, PCa and BCa cell lines [62, 64, 73-75]. Uncontrolled cellular proliferation is a major hallmark of cancer. Parallel to this, SAM caused significant reduction of cellular proliferation in multiple cancer cell lines (Chapters 3-5). Ki67 is an essential and most widely used proliferation clinical marker which has been strongly associated with various tumor parameters including growth, progression, clinical tumor stage, and metastasis [219]. SAM caused significant reduction in the Ki67 proliferation marker in melanoma and breast tumors (Chapter 4 and [30, 54, 71]). Collectively, results from the studies herein and previously published literature,

it is evident that one the major mechanisms by which SAM causes significant reduction in tumor growth and progression is by supressing proliferation and inhibiting cell cycle progression.

The heterogeneity of melanoma tumors is well documented. Several studies carrying out bulk RNA-sequencing, single-cell RNA sequencing and immunohistochemical analysis have pointed to the different cell types present in the tumor samples of melanoma patients which has led to the phenotype switching model of melanoma [220-224]. Phenotype switching of melanoma tumor cells occurs constantly allowing them to switch between the proliferative, invasive, and differentiated states. The proliferative state allows the tumors to grow rapidly while the invasive state helps in invasion and metastasis. MITF regulates essential genes and pathways involved in differentiation, proliferation, and survival of melanocytes and melanoma. Furthermore, MITF is also essential in melanogenesis. MITF acts as a rheostat and regulates phenotype switching and this model is well-established [220-224]. High expression of MITF results in differentiation of melanoma cells followed by cell cycle arrest induced by p21 and p16 whereas low expression of MITF results in stem-cell like cells that have increased invasive and metastatic ability. The dedifferentiated melanomas that are characterized by low expression of MITF and MDAs are intrinsically resistant to immunotherapies (anti-PD-1 and anti-CTLA-4 antibodies) and targeted therapies (BRAFi), often persist, and have the highest ability to form tumors and metastasize [220, 222-227]. The low MITF expressing tumor cells are also responsible for tumor recurrence after drug exposure, represent minimal residual disease, and have been associated with low overall survival. Therefore, various anti-melanoma strategies have been proposed to direct phenotype switching from the invasive and proliferative state towards the differentiated state by inducing MITF expression [222, 228]. The present study first identified SAM directed phenotype switching of invasive and proliferative cells into differentiated melanocyte-like cells. This switching occurs through inducing expression of *Mitf* and transcription factors *Sox10* and *Creb1,* which are direct activators of *Mitf* gene. The differentiated cells had low proliferative rates, increased expression of melanocyte differentiation enzymes, elevated melanin and melanosome synthesis, melanocyte-like morphology, and low expression of stemness marker genes (Chapter 4).

Interestingly, a recent study has demonstrated that MITF can downregulate expression of extracellular matrix (ECM), focal adhesion and EMT genes [225]. In this way, MITF hinders the EMT process thereby reducing invasive and metastatic ability of the melanoma cells [225]. Role

of SAM in repressing invasion and metastasis by reducing expression of pro-metastatic genes including *uPA* and *MMPs* (*MMP2*, *MMP9*) has been extensively demonstrated by us in osteosarcoma, BCa, and PCa [30, 54, 62, 64, 67, 71]. Expectedly luminal B BCa showed downregulation of MMPs (*MMP9* and *MMP10*) and related genes in the tumors that were treated with SAM (Chapter 5). Intriguingly in melanoma cells, we also found significant downregulation of several essential cancer stem-cell marker genes, including *Nanog*, *Wnt*, *Sox2, Slug (Snai2) and Brn2* (Chapter 4), that allow cancer cells to invade and metastasize [229-234]. In fact, the reduction in expression of these genes was due to SAM-medicated increase in MITF expression because knock-down of MITF using siRNA targeting *Mitf* resulted in increase in expression of these genes (Chapter 4).

During melanogenesis, melanoma cells become less aggressive indicating that melanin synthesis upregulates certain genes that suppress cells' invasive ability, and furthermore, melanin pigmentation was demonstrated to inhibit metastasis (*in vivo*) [235-237]. In addition to melanin, melanosomes dramatically modify elastic properties and inhibit transmigration abilities of melanoma cells mechanistically [237, 238]. In line with the evidence that SAM decreased invasion and metastasis, SAM also increased both melanogenesis and melanosome generation (Chapter 4). Moreover, SAM increased the expression of enzymes and transcription factors involved in melanogenesis and structural components of melanosomes including Tyr and related genes (converting tyrosine into melanin), Melan-A (Mart-1), Pmel (Gp100), Sox10 and Creb1 (Chapter 4). Parallel to this, SAM decreased invasion and metastasis of melanoma and BCa cells and tumors, *in vitro* and *in vivo* (Chapter 3-5 and [30, 54, 71]). Collectively, the above data indicate that SAM significantly suppresses invasion and metastasis of melanoma and BCa.

One important unanswered question was to determine the effect of SAM on enhancing the susceptibility of cancer cells to anti-cancer immunity, and to determine if SAM can elevate anti-cancer immune responses which has not been carried out in-depth in any cancer type in the past. SAM was found to increase the immunogenicity of the melanoma cells and tumors by inducing expression of several MDAs including *Mart-1*, *Pmel*, *Tyr*, *Tyrp1* and *Tyrp2*, and MAAs, and pathways that increase neoepitope generation (Chapter 4). Increase in MDAs expression is essential as vaccination, CAR-T cell directed immunotherapy, knock-out/knock-down studies targeting only one of the MDAs have demonstrated the power of MDA-specific cytotoxic T cell

mediated killing of tumor cells. For instance, recently, it was shown that lack of Mart-1 or Tyr led to increase in melanoma tumor growth in mouse models [239-241]. Moreover, T cells targeting MDAs resulted in regression of tumors in human melanoma patients [242]. Parallel to treating melanoma by increasing MITF expression, numerous pre-clinical and clinical studies have demonstrated that the success of BRAFi therapy is partially due to elevating MITF levels that upregulates MDAs which subsequently increases immunogenicity of tumor cells thereby eliciting a superior cytotoxic response from tumor infiltrating $CD8^+$ T cells [152, 153, 243, 244]. MDAs also function in increasing melanogenesis and melanosome generation, and consistently, differentiated dark stained tumors were also found to be immunologically hot, that is, infiltrated with higher frequency of immune cells [223]. Therefore, SAM increasing MDAs' expression would eventually increase the recognition of the melanoma cells by the cytotoxic $CD8^+$ T cells. In addition, SAM also increased the susceptibility of the melanoma cells to cell death as it upregulated the expression of FAS and TRIAL death receptors which are utilized by the NK and $CD8^+$ T cells to cause instant tumor cell death (Chapter 4).

SAM alone did not cause a significant increase in recruitment of $CD8^+$ T cells and various $CD8^+$ T cells' activation, proliferation, and effector functions in B16-B6 mouse model (Chapter 3). However, SAM alone significantly increased the $CD45^+$ immune cells infiltration, $CD3^+$, $CD4^+$ (Th1 and Th17) and $CD8^+$ T cell infiltration, and $CD8^+$ T cells' activation in YUMMER1.7-B6 mouse model (Chapter 4). The difference in the effect of SAM on different melanoma mouse models could be attributed to several reasons related to the biology of the YUMMER1.7 and B16 tumors. Firstly, the B16 tumors have a low MHC class I expression compared to other tumors, including methylcholanthrene-induced (MCA) sarcomas, Renca and YUMMER1.7, derived from black B6 mice [245]. B16-B6 mouse models are typically considered as substantially less immunogenic as it has been difficult to cause protection in this model even with vaccines (like BCG), pathogenic bacterium (*Corynebacterium parvum)* and high doses of IL-2 which are typically curative in other mouse models like Renca and MCA sarcomas [245]. Moreover, strategies employed in order to make other tumors models more immunogenic from non-immunogenic such as stably expressing co-stimulatory molecule B7-1, do not work well in B16 model [245, 246]. On the other hand, the YUMMER1.7 tumors are highly immunogenic, are infiltrated with high number of immune cells (immunologically hot) and recapitulate the somatic TMB of tumor from human melanoma patients [247]. Therefore, it is predicted that SAM alone

can induce anti-cancer immunity in tumors that have some degree of immune infiltration and activation within the TME. This is evident from effect of SAM alone on the YUMMER1.7 tumors (Chapter 4), and from the effect of SAM in combination with anti-PD-1 antibody that caused significant increase in $CD3^+$ and $CD8^+$ T cell infiltration, and $CD8^+$ T cells' activation, proliferation, cytokine production and polyfunctionality even in low immunogenic B16 tumors (Chapter 3). Furthermore, these results are in parallel with low immunogenic luminal B BCa subtype (Chapter 5). Additionally, type I IFNα/β signalling pathways were induced in melanoma and BCa tumors treated with SAM alone (Chapter 3 and [71]).

There are several unique benefits of using SAM as an anti-cancer agent. Firstly, we and others have demonstrated that the orally given SAM is bioavailable in mice and humans [30, 71, 248]. Moreover, we didn't find short- and long-term adverse events due to SAM in these studies and previous published studies from our laboratory [24, 30, 71]. In contrast, previous *in vitro* work has suggested that high levels of SAM are metabolized to adenine and methylthioadenosine (MTA) which may have the opposite action to SAM and inhibit methylation [58-61]. However, this was not observed *in vivo* and, parallel to our work, both SAM and MTA showed significant anti-cancer effects in reducing tumor growth *in vivo*. Indeed, MTA can be converted back to SAM by the salvage pathway [58-61]. Furthermore, SAM is already available as a natural supplement for depression, joint pain and other disorders and has been consumed by humans for a long time [59]. SAM has been tested in more than 100 clinical trials for multiple disorders [59, 249, 250]. There are currently three clinical trails in the early phases of testing the efficacy of SAM as an anti-cancer agent in hepatocellular carcinoma. In line with this, we have not found development of pharmacological resistance to long-term treatment of SAM in this study or any other cancer model (*in vitro* and *in vivo*) [24, 30, 64, 71, 251].

CPIs have led to a paradigm shift in cancer treatment, and this is reflective from the high number of FDA approvals and clinical trials evaluating CPIs against multiple cancer types for several indications. However, two-third of the patients do not respond to CPIs and there is a high variability in response. For instance, the response rate generally is only around 30-40% for anti-PD-1 antibody treatment in metastatic melanoma. Furthermore, CPIs are limited due to irAEs. To counter these problems, numerous pre-clinical and clinical trials are being conducted using combinatorial strategies, however, each combination has its limitations. For instance, most

chemotherapies which are currently approved in the clinic are unable to stimulate immunity by immunogenic cell death, or are immunosuppressive, or have heightened AEs limiting their use in combining with CPI [111, 169]. Furthermore, epi-therapy such as DNMTi in combination with CPI therapy has challenges. For example, DNMTi have a low overall response in solid tumors and are being reported to elevate expression of key silenced oncogenes and pro-metastatic (including *uPA* and *SALL4*) that would essentially increase the ability of the tumor cells to progress and metastasize to distant organs, which is a major risk factor for mortality. Herein, we propose targeting cancers with SAM and anti-PD-1 antibody. As mentioned above, SAM alone showed some potential in elevating the anti-cancer immunity. However, the combined effect of SAM and anti-PD-1 antibody caused significant reduction in tumor growth and progression in both melanoma mouse models compared to monotherapies (Chapter 3 and 4). Hence, we investigated the effect of SAM, anti-PD-1 antibody, and combination on cancer immunosurveillance system using flow cytometry. We utilized the next generation multiplex BD Fortessa LSR-X20 which can simultaneously analyze 20 different fluorescence-conjugated antibodies bound to both extracellular and intracellular proteins or markers. This allowed us to study various lymphoid and myeloid immune cells within TME including $CD8^+$ T cells, major subtypes of $CD4^+$ T cells (Th1, Th2, Th17 and Tregs), macrophages, monocytes, dendritic cells, NK cells, and neutrophils. Moreover, we also studied the viability, activation (T-bet, ICOS), proliferation (ki67) and effector functions (including IFNγ, TNFα, IL2). In parallel, we also investigated the effect of treatments on immune cells in draining and non-draining lymph nodes and spleens of the tumor-bearing mice to answer questions regarding the recruitment of immune cells to the TME. Indeed, a major effect of anti-cancer efficacy of the combination treatment was due to enhanced infiltration, activation (upregulated T-bet, ICOS), and effector functions (elevated IFNγ, TNFα) of $CD8^+$ T cells (Chapter 3 and 4). Furthermore, in the YUMMER1.7-B6 model, Th1 and Th17 cells contributed to the elevation of adaptive immune responses of the cytotoxic $CD8^+$ T cells (Chapter 4). Importantly, we found high levels of cytotoxic polyfunctional $CD8^+$ T cells in the TME of combination treated group, compared to control which had none or very low levels (Chapter 3 and 4). Polyfunctional cytotoxic $CD8^+$ T cells are the most potent effector $CD8^+$ T cells that can cause direct tumor lysis due to production of large amounts of cytokines and proteases (granzymes and perforins). Consist with melanoma tumors, we also observed elevation of immunostimulatory genes and pathways,

and increased $CD8^+$ T cells recruitment in BCa TME treated with SAM and anti-PD-1 antibody combination (Chapter 5).

Metastasis to distant organs is a major complication which significantly increases the morbidity and mortality rates of the melanoma and BCa patients. For instance, for both melanoma and BCa, the 5-year survival rate decreases from 99% for a localized to only 27-28% for distant metastasis [77]. In fact, cancer associated metastasis account for about 90% of cancer related deaths [134, 135]. Therefore, we studied the effect of SAM and anti-PD-1 antibody combination on skeletal and non-skeletal metastasis. The combination significantly reduced the metastasis to lungs in melanoma and BCa lung metastasis models (Chapter 4 and 5). Since skeletal metastasis is a major complication of BCa that ultimately leads to skeletal related events (SREs) [139-142], we established a bone metastasis model by injecting Eo771 cells via intra-tibial route [252, 253]. The combination had marked reduction in lesion area, or no lesion in most cases, and showed superior integrity indicating rapid clearance of tumor cells from the bone microenvironment (Chapter 5).

As all studies have certain limitation, the studies involving SAM and anti-PD-1 antibody had some limitations as well. For the B16-B6 mouse model, we couldn't evaluate long term effects including survival probabilities of SAM and anti-PD-1 antibody monotherapies and combination. This is because at day 16 post tumor inoculation, B16-B6 mouse model has an exponential tumor growth reaching humane endpoints quickly, and tumors become necrotic in the center and form ulceration and start bleeding (Chapter 3-4). Similarly, for the Eo771-B6 mouse model, we couldn't investigate the long-term effects and survival probabilities of the monotherapies and combination as this model starts to form ulceration at day 22-24 post-tumor inoculation and must be euthanized accordingly (Chapter 5). Nevertheless, long term effects were studied for the monotherapies and combination in YUMMER1.7-B6 mouse model (Chapter 4). And the effect of SAM alone in MMTV-PyMT mice has been studied previously in our laboratory. Another technical challenge occurred during the immunophenotyping analysis using flow cytometry (Chapter 3-4). Although numerous immune cells were studied in the TME (including $CD8^+$ T cells, $CD4^+$ Th1, Th2, Th17 and Tregs, macrophages, monocytes, dendritic cells, NK cells, and neutrophils) using cell-specific surface markers; functional markers were not investigated for all immune cells. This was due to limited number of protein/markers that can be analyzed with flow cytometry at one time and

limitation of the tumor material, especially the combination tumors that were significantly smaller compared to other groups. Nevertheless, it is previously established that the major effect of CPI blockade is on adaptive immune responses. Therefore, we focused on the effector function markers of $CD4^+$ and $CD8^+$ T cells including their activation (T-bet, PD-1, ICOS), proliferation (ki67), infiltration (CXCR3), and effector function markers (IFNγ, TNFα, IL-2). Indeed, monotherapies and combination caused significant differences in the markers related to $CD4^+$ and $CD8^+$ T cells biology (Chapter 3-4).

Another limitation of the studies herein (Chapters 3-5) is the in-depth determination of the adverse effects of SAM and anti-PD-1 antibody combination. However, we have tested SAM using various physical (including body weight, mouse grooming, hydration, and activity), biochemical (such as liver and renal function test), and behavioral assays (such as novel object recognition test and open field test) in the current studies and previous studies in our laboratory (Chapters 3-5 and [6, 24, 30, 54, 71]). SAM did not cause significant abnormal physical changes (e.g. body weight), detrimental behavioral defects, or toxicity for the dose currently used in the study. Indeed, SAM being an approved nutraceutical supplement has shown no severe adverse effects in other pre-clinical and clinical studies except a transient adverse behavioral effect in an individual [24, 30, 59, 64, 71, 248, 251]. Moreover, significant physical changes (including body weight, mouse grooming, hydration, and activity) were not observed between combination group and other groups (Chapters 3-5). Therefore, we predict that SAM and CPI combination will have a similar safety profile to CPI alone. Nevertheless, it is imperative to carry out toxicology screenings for the combination treatment in the future.

Although marked improvements in treatment of cancer have been demonstrated in the recent years, there is still high prevalence and cancer-related deaths globally. Therefore, there is an urgent need to develop affordable anti-cancer therapeutics especially the ones that targets metastasis. Drug re-purposing has become attractive in recent times as it drastically reduces time needed to test, evaluate, and develop a new drug but also allows for efficient availability of it at a much-reduced cost. In this regard, our strategy of using SAM is appealing, as we show that SAM, an approved natural nutraceutical agent, given orally can target cancer either alone or in combination with FDA approved CPIs such as anti-PD-1 antibody. Since both SAM and anti-PD-

1 antibody are approved agents, this novel strategy can be translated to clinic at an accelerated pace to reduce cancer associated morbidity and mortality.

CHAPTER SEVEN: Conclusions and Future Directions

Future studies analyzing the DNA methylation signature in the peripheral T cells may have a large number of subjects. This will allow inclusion of various variables including patient's racial background, genetic subtypes, gene fusions linked to PCa, history of smoking and alcohol intake [215-217]. The current study had peripheral T cells of patients before any treatment. It would be interesting to study the effect on DNA methylation patterns before and after standard of care treatment. This will allow identification of prognostic markers in peripheral T cells of patients that benefit from a treatment. Along these lines, our laboratory has already planned to study DNA methylation changes in the peripheral T cells of melanoma patients before and after CPI therapy, and to identify prognostic markers that could distinguish responders from non-responders. Integrative analysis combining DNA methylation and transcriptome analysis of the T cells would further delineate the link between the methylation patterns and gene expression. Integrative analysis will also dissect the effect that the cancer/tumor cells have on the transcriptome of peripheral T cells.

The present study evaluated the effect of SAM, anti-PD-1 antibody and combination on tumor and immune cells. However, there is a spectrum of cell types that are present in the TME. In the future studies, effect of monotherapies and combination may be studied by subjecting tumors to single-cell RNA-sequencing analysis. Accordingly, this will help to uncover the molecular pathways affected in more depth, and the different cell types affected by monotherapies and combination. Since SAM seemed to affect Th17 cells biology, it would also be interesting to unveil the effect of SAM on activation, differentiation, and function of Th17 cells.

SAM is a universal methyl donor that donates methyl groups to various components of cell including RNA and histone proteins. There is an increasing knowledge of gene regulation by m^6A RNA methylation and methylation of histones. Future studies should also investigate the effect of SAM on m^6A RNA methylation and histone modifications and its link to transcriptional regulation.

The current study combined SAM with only one CPI, that is, anti-PD-1 antibody. It would be interesting to combine SAM with other CPIs and one promising candidate is anti-CTLA-4 antibody. Anti-CTLA-4 antibody acts by upregulating the proliferation of $CD4^+$ Th1 cells and $CD8^+$ T cells. SAM was reported to be essential for T cells activation and proliferation [200-204]. Therefore, combining SAM with anti-CTLA-4 antibody might also enhance the anti-cancer immunity. Another promising combination would be to combine SAM with dual CPIs, anti-PD-1

and anti-CTLA-4 antibodies. Dual CPIs therapy has shown promise in clinical trials; however, it is largely limited by irAEs. It is anticipated that the triple combination would have even superior anti-cancer efficacy than SAM and anti-PD-1 antibody combination. However, triple combinations might result in a higher irAEs resulting from dual CPIs, and a more complicated therapeutic regime. Nevertheless, lower dose of both CPIs might reduce irAEs as reported in the past. Toxicology screening would further help to evaluate adverse effects and irAEs of the SAM and CPI combinations [254-256].

One important treatment strategy utilized in the clinic is surgical removal of solid tumors including melanoma and breast tumors. However, in a proportion of patients, the cancer relapse. It would be interesting to study if SAM and anti-PD-1 antibody can prevent tumor recurrence after surgical removal of the tumors from mice. Along these lines, it would also be intriguing to study if after complete elimination of the tumors (such as in a proportion of YUMMER1.7-B6 mouse model), the combination treatment can avoid tumor rechallenge with same or a higher dose of YUMMER1.7 cells.

All the studies (Chapter 3-5) were carried out using unaltered syngeneic melanoma and BCa cell lines and immunocompetent mouse models, instead of immune-deficient xenograft models. This way we could recapitulate human pathophysiology of cancers which is driven by tumorigenesis and cancer evolution, and through immunoediting by the immune cells [84, 222, 257]. However, one prominent limitation of the syngeneic models is that they reach humane end point in a short period of time. This limits the evaluation of long-term effects of a particular therapy. Although we studied the effects of SAM, anti-PD-1 antibody, and combination for 65 days in YUMMER1.7-B6 model, there is still room for improvements. Genetically engineered mouse models (GEMMs) provide an alternative to syngeneic model for testing long-term effects of SAM. The GEMMs are driven by cancer specific mutations and develop tumors in several weeks to months. Moreover, GEMMs can also be used to study effects of CPI therapies as they are also immunocompetent. One such example is the GEMM with the *Braf* mutation (and KO of either p53 or Ink4a/Arf) which is linked to the promoter of the *Tyr* gene [258]. These GEMMs develop tumors in 14-21 weeks with around 80-95% penetrance. Similarly, MMTV-PyMT BCa GEMMs can be an alternative to the Eo771-B6 luminal B BCa mouse model. Future studies evaluating long-term effect of either SAM, CPIs or combination can utilize these GEMMs.

Another alternative mouse model which may represent human disease are the humanized mouse models. Humanized mice are highly specialized wherein their own mouse immune system is not developed, but have a complete functional human immune system established from human hematopoietic stem cells or human PBMCs [259]. Future studies could take advantage of humanized mice injected with human cancer cells or patient xenografts providing relevant pre-clinical model for SAM and CPI therapies. Using a xenograft derived from a particular patient could allow patient-specific evaluation of the combination therapy. However, humanized mouse models are technically challenging to establish, are costly, require specialized care, and may develop graft-versus-host-disease (GVHD) [259].

Past few decades have yielded significant improvements in quality of life and life expectancy of cancer patients. This was mostly due to development of better therapeutic strategies including chemotherapy, surgical methods, radiotherapy, and targeted therapy. Immunotherapy including CPI therapy has revolutionized the treatment of cancer providing long-lasting effect and has given hope for a cure instead of a mere extension of treating devastating chronic condition [111, 260]. CPIs have brought forward the idea of targeting the immune cells instead of cancer cells [260]. This change in perspective would allow researchers to select therapies that can uplift cancer immunosurveillance system. Apart from targeting cancer cells, various chemotherapies and targeted therapies regulate the immune system. As such, this thesis provides a good example of an anti-cancer agent, SAM, that not only targets the cancer cells but also the immune surveillance system complementing CPI therapy, thereby boosting the anti-cancer efficacy and anti-cancer immunity. Due to the urgency of improving the overall survival rate and reducing morbidity and mortality rates of cancer patients, it is reasonable to initiate clinical trials with SAM alone or with anti-PD-1 antibody combination. In fact, the testing of anti-cancer efficacy of SAM in liver cancer patients is already in the early phases of three clinical trials. Based on the current findings (Chapters 3-5) and previously published pre-clinical findings by our laboratory, we are also planning early phase clinical trials for testing the anti-cancer efficacy of SAM in melanoma and BCa patients.

In summary, this thesis provides proof of principle study which demonstrates that DNA methylation alterations occur in peripheral T cells of PCa patients and can be leveraged for the diagnosis or risk stratification of PCa patients. The thesis also provides first direct evidence of the

beneficial anti-cancer effects of SAM against melanoma (Figure 1). This is also first evidence in the superior anti-cancer efficacy of a novel combination of SAM with anti-PD-1 antibody via alteration of key genes/pathways implicated in cancer and elevating adaptive immune responses against melanoma, BCa and potentially against other cancers (Figure 1). Since both SAM and anti-PD-1 antibody are approved agents, the novel therapeutic strategy provides immense potential to be translated into clinic to reduce cancer associated morbidity and mortality.

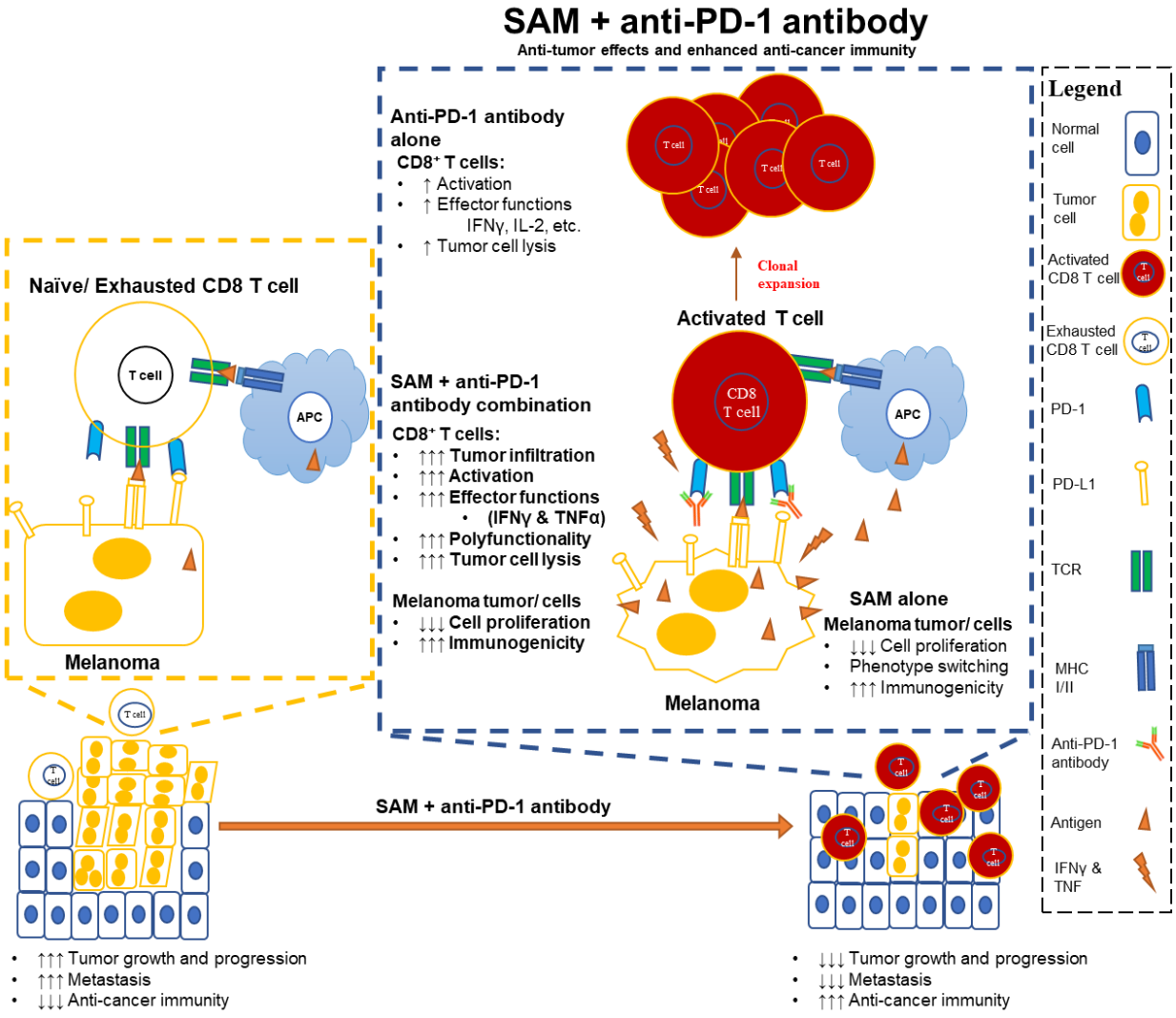

Figure 1: SAM and anti-PD-1 antibody combination reduces tumor growth, progression, and metastasis, and enhances the anti-cancer immunity in melanoma. SAM induces phenotype switching, decreases cell proliferation, and increases immunogenicity of melanoma cells, resulting in tumor growth inhibition. Anti-PD-1 antibody alone restores $CD8^+$ T cells effector functions.

SAM in combination with anti-PD-1 antibody results in higher $CD8^+$ T cells tumor infiltration, higher activation, effector functions and polyfunctionality of $CD8^+$ T cells compared to monotherapies which ultimately leads to higher tumor cell lysis and death. The combination also results in superior control of tumor growth, progression, and metastasis.

BIBLIOGRAPHY

1. Hanahan, D. and R.A. Weinberg, *Hallmarks of cancer: the next generation.* Cell, 2011. **144**(5): p. 646-74.
2. Sharma, S., T.K. Kelly, and P.A. Jones, *Epigenetics in cancer.* Carcinogenesis, 2010. **31**(1): p. 27-36.
3. Sandoval, J. and M. Esteller, *Cancer epigenomics: beyond genomics.* Curr Opin Genet Dev, 2012. **22**(1): p. 50-5.
4. Allis, C.D. and T. Jenuwein, *The molecular hallmarks of epigenetic control.* Nature Reviews Genetics, 2016. **17**: p. 487-500.
5. Bird, A., *DNA methylation patterns and epigenetic memory.* 2002.
6. Mehdi, A. and S.A. Rabbani, *Role of Methylation in Pro- and Anti-Cancer Immunity.* Cancers (Basel), 2021. **13**(3).
7. Feinberg, A.P. and B. Vogelstein, *Hypomethylation distinguishes genes of some human cancers from their normal counterparts.* Nature, 1983. **301**(5895): p. 89-92.
8. Hsieh, J. and F.H. Gage, *Epigenetic control of neural stem cell fate.* Curr Opin Genet Dev, 2004. **14**(5): p. 461-9.
9. Robertson, K.D., *DNA methylation and human disease.* Nature Reviews Genetics, 2005. **6**(8): p. 597-610.
10. Jones, P.A. and S.B. Baylin, *The fundamental role of epigenetic events in cancer.* Nature Reviews Genetics, 2002. **3**(6): p. 415-428.
11. Patil, V., R.L. Ward, and L.B. Hesson, *The evidence for functional non-CpG methylation in mammalian cells.* Epigenetics, 2014.
12. Saxonov, S., P. Berg, and D.L. Brutlag, *A genome-wide analysis of CpG dinucleotides in the human genome distinguishes two distinct classes of promoters.* Proc Natl Acad Sci U S A, 2006. **103**(5): p. 1412-7.
13. Luo, C., P. Hajkova, and J.R. Ecker, *Dynamic DNA methylation: In the right place at the right time.* Science, 2018. **361**(6409): p. 1336-1340.
14. Neri, F., et al., *Intragenic DNA methylation prevents spurious transcription initiation.* Nature, 2017. **543**(7643): p. 72-77.
15. Schultz, M.D., et al., *Human body epigenome maps reveal noncanonical DNA methylation variation.* Nature, 2015. **523**(7559): p. 212-6.

16. McGuire, M.H., et al., *Pan-cancer genomic analysis links 3'UTR DNA methylation with increased gene expression in T cells.* EBioMedicine, 2019. **43**: p. 127-137.
17. Biswas, S. and C.M. Rao, *Epigenetics in cancer: Fundamentals and Beyond.* Pharmacol Ther, 2017. **173**: p. 118-134.
18. Ehrlich, M., *DNA hypomethylation in cancer cells.* Epigenomics, 2009. **1**(2): p. 239-59.
19. Wajed, S.A., P.W. Laird, and T.R. DeMeester, *DNA methylation: an alternative pathway to cancer.* Ann Surg, 2001. **234**(1): p. 10-20.
20. Wong, D.J., et al., *p16INK4a promoter is hypermethylated at a high frequency in esophageal adenocarcinomas.* Cancer Res, 1997. **57**(13): p. 2619-22.
21. Feinberg, A.P. and B. Vogelstein, *Hypomethylation of ras oncogenes in primary human cancers.* Biochem Biophys Res Commun, 1983. **111**(1): p. 47-54.
22. Gama-Sosa, M.A., et al., *The 5-methylcytosine content of DNA from human tumors.* Nucleic Acids Res, 1983. **11**(19): p. 6883-94.
23. Feinberg, A.P. and B. Tycko, *The history of cancer epigenetics.* Nat Rev Cancer, 2004. **4**(2): p. 143-53.
24. Mahmood, N. and S.A. Rabbani, *Targeting DNA Hypomethylation in Malignancy by Epigenetic Therapies.* Adv Exp Med Biol, 2019. **1164**: p. 179-196.
25. Pakneshan, P., et al., *Reversal of the hypomethylation status of urokinase (uPA) promoter blocks breast cancer growth and metastasis.* J Biol Chem, 2004. **279**(30): p. 31735-44.
26. Pulukuri, S.M., et al., *Demethylation-linked activation of urokinase plasminogen activator is involved in progression of prostate cancer.* Cancer Res, 2007. **67**(3): p. 930-9.
27. Shukeir, N., et al., *Alteration of the methylation status of tumor-promoting genes decreases prostate cancer cell invasiveness and tumorigenesis in vitro and in vivo.* Cancer Res, 2006. **66**(18): p. 9202-10.
28. Kuo, H.C., et al., *Epigenetic hypomethylation and upregulation of matrix metalloproteinase 9 in Kawasaki disease.* Oncotarget, 2017. **8**(37): p. 60875-91.
29. Couillard, J., et al., *The role of DNA hypomethylation in the control of stromelysin gene expression.* Biochem Biophys Res Commun, 2006. **342**(4): p. 1233-9.
30. Mahmood, N., et al., *Methyl donor S-adenosylmethionine (SAM) supplementation attenuates breast cancer growth, invasion, and metastasis in vivo; therapeutic and chemopreventive applications.* Oncotarget, 2018. **9**(4): p. 5169-5183.

31. Chernov, A.V., et al., *Epigenetic Control of the Invasion-promoting MT1-MMP/MMP-2/TIMP-2 Axis in Cancer Cells.* J Biol Chem, 2009. **284**(19): p. 12727-34.
32. Holm, T.M., et al., *Global loss of imprinting leads to widespread tumorigenesis in adult mice.* Cancer Cell, 2005. **8**(4): p. 275-85.
33. Kulis, M. and M. Esteller, *DNA methylation and cancer.* Adv Genet, 2010. **70**: p. 27-56.
34. Roman-Gomez, J., et al., *Repetitive DNA hypomethylation in the advanced phase of chronic myeloid leukemia.* Leuk Res, 2008. **32**(3): p. 487-90.
35. Wolff, E.M., et al., *Hypomethylation of a LINE-1 promoter activates an alternate transcript of the MET oncogene in bladders with cancer.* PLoS Genet, 2010. **6**(4): p. e1000917.
36. Hanahan, D., *Hallmarks of Cancer: New Dimensions.* Cancer Discov, 2022. **12**(1): p. 31-46.
37. Ehrlich, M., *DNA methylation in cancer: too much, but also too little.* Oncogene, 2002. **21**(35): p. 5400-13.
38. Chen, R.Z., et al., *DNA hypomethylation leads to elevated mutation rates.* Nature, 1998. **395**(6697): p. 89-93.
39. Gaudet, F., et al., *Induction of tumors in mice by genomic hypomethylation.* Science, 2003. **300**(5618): p. 489-92.
40. Pogribny, I.P., et al., *Irreversible global DNA hypomethylation as a key step in hepatocarcinogenesis induced by dietary methyl deficiency.* Mutat Res, 2006. **593**(1-2): p. 80-7.
41. Pogribny, I.P., et al., *Breaks in genomic DNA and within the p53 gene are associated with hypomethylation in livers of folate/methyl-deficient rats.* Cancer Res, 1995. **55**(9): p. 1894-901.
42. Szyf, M., *Epigenetics, DNA methylation, and chromatin modifying drugs.* Annu Rev Pharmacol Toxicol, 2009. **49**: p. 243-63.
43. Szyf, M., *DNA methylation properties: consequences for pharmacology.* Trends Pharmacol Sci, 1994. **15**(7): p. 233-8.
44. Morales-Nebreda, L., F.S. McLafferty, and B.D. Singer, *DNA methylation as a transcriptional regulator of the immune system.* Transl Res, 2019. **204**: p. 1-18.

45. Silverman, L.R., et al., *Randomized controlled trial of azacitidine in patients with the myelodysplastic syndrome: a study of the cancer and leukemia group B.* J Clin Oncol, 2002. **20**(10): p. 2429-40.
46. Kantarjian, H., et al., *Decitabine improves patient outcomes in myelodysplastic syndromes: results of a phase III randomized study.* Cancer, 2006. **106**(8): p. 1794-803.
47. Derissen, E.J., J.H. Beijnen, and J.H. Schellens, *Concise drug review: azacitidine and decitabine.* Oncologist, 2013. **18**(5): p. 619-24.
48. Nervi, C., E. De Marinis, and G. Codacci-Pisanelli, *Epigenetic treatment of solid tumours: a review of clinical trials.* Clin Epigenetics, 2015. **7**: p. 127.
49. Koch, A., et al., *Analysis of DNA methylation in cancer: location revisited.* Nat Rev Clin Oncol, 2018. **15**(7): p. 459-466.
50. Gnyszka, A., Z. Jastrzebski, and S. Flis, *DNA methyltransferase inhibitors and their emerging role in epigenetic therapy of cancer.* Anticancer Res, 2013. **33**(8): p. 2989-96.
51. Giri, A.K. and T. Aittokallio, *DNMT Inhibitors Increase Methylation in the Cancer Genome.* Front Pharmacol, 2019. **10**: p. 385.
52. Subramaniam, D., et al., *DNA methyltransferases: a novel target for prevention and therapy.* Front Oncol, 2014. **4**: p. 80.
53. Ateeq, B., et al., *Pharmacological inhibition of DNA methylation induces proinvasive and prometastatic genes in vitro and in vivo.* Neoplasia, 2008. **10**(3): p. 266-78.
54. Mahmood, N., et al., *S-adenosylmethionine in combination with decitabine shows enhanced anti-cancer effects in repressing breast cancer growth and metastasis.* J Cell Mol Med, 2020.
55. Liu, Y.C., et al., *Demethylation and Up-Regulation of an Oncogene after Hypomethylating Therapy.* N Engl J Med, 2022. **386**(21): p. 1998-2010.
56. Tatetsu, H., et al., *SALL4, the missing link between stem cells, development and cancer.* Gene, 2016. **584**(2): p. 111-9.
57. Ehrlich, M., *DNA hypermethylation in disease: mechanisms and clinical relevance.* Epigenetics, 2019. **14**(12): p. 1141-1163.
58. Lu, S.C. and J.M. Mato, *S-Adenosylmethionine in cell growth, apoptosis and liver cancer.* J Gastroenterol Hepatol, 2008. **23**(Suppl 1): p. S73-7.

59. Bottiglieri, T., *S-Adenosyl-L-methionine (SAMe): from the bench to the bedside--molecular basis of a pleiotrophic molecule.* Am J Clin Nutr, 2002. **76**(5): p. 1151s-7s.
60. Lu, S.C., *S-Adenosylmethionine.* Int J Biochem Cell Biol, 2000. **32**(4): p. 391-5.
61. Loenen, W.A., *S-adenosylmethionine: jack of all trades and master of everything?* Biochem Soc Trans, 2006. **34**(Pt 2): p. 330-3.
62. Shukeir, N., et al., *Pharmacological methyl group donors block skeletal metastasis in vitro and in vivo.* Br J Pharmacol, 2015. **172**(11): p. 2769-81.
63. Murín, R., et al., *Role of S-adenosylmethionine cycle in carcinogenesis.* General Physiology and Biophysics, 2017. **36**(5): p. 513-520.
64. Parashar, S., et al., *S-adenosylmethionine blocks osteosarcoma cells proliferation and invasion in vitro and tumor metastasis in vivo: therapeutic and diagnostic clinical applications.* Cancer Med, 2015. **4**(5): p. 732-44.
65. Chik, F., Z. Machnes, and M. Szyf, *Synergistic anti-breast cancer effect of a combined treatment with the methyl donor S-adenosyl methionine and the DNA methylation inhibitor 5-aza-2'-deoxycytidine.* Carcinogenesis, 2014. **35**(1): p. 138-44.
66. Luo, J., et al., *S-adenosylmethionine inhibits the growth of cancer cells by reversing the hypomethylation status of c-myc and H-ras in human gastric cancer and colon cancer.* Int J Biol Sci, 2010. **6**(7): p. 784-95.
67. Schmidt, T., A. Leha, and G. Salinas-Riester, *Treatment of prostate cancer cells with S-adenosylmethionine leads to genome-wide alterations in transcription profiles.* Gene, 2016. **595**(2): p. 161-167.
68. Zhao, Y., et al., *Inhibitory effect of S-adenosylmethionine on the growth of human gastric cancer cells in vivo and in vitro.* Chin J Cancer, 2010. **29**(8): p. 752-60.
69. Hussain, Z., et al., *S-adenosylmethionine, a methyl donor, up regulates tissue inhibitor of metalloproteinase-2 in colorectal cancer.* Genet Mol Res, 2013. **12**(2): p. 1106-18.
70. Li, T.W., et al., *Effects of S-adenosylmethionine and methylthioadenosine on inflammation-induced colon cancer in mice.* Carcinogenesis, 2012. **33**(2): p. 427-35.
71. Mahmood, N., et al., *An enhanced chemopreventive effect of methyl donor S-adenosylmethionine in combination with 25-hydroxyvitamin D in blocking mammary tumor growth and metastasis.* Bone Res, 2020. **8**: p. 28.

72. Wang, Y., Z. Sun, and M. Szyf, *S-adenosyl-methionine (SAM) alters the transcriptome and methylome and specifically blocks growth and invasiveness of liver cancer cells.* Oncotarget, 2017. **8**(67): p. 111866-111881.
73. Ilisso, C.P., et al., *S-Adenosylmethionine regulates apoptosis and autophagy in MCF-7 breast cancer cells through the modulation of specific microRNAs.* Cancer Cell Int, 2018. **18**: p. 197.
74. Ilisso, C.P., et al., *S-Adenosylmethionine Affects ERK1/2 and Stat3 Pathways and Induces Apotosis in Osteosarcoma Cells.* J Cell Physiol, 2016. **231**(2): p. 428-35.
75. Cave, D.D., et al., *S-Adenosylmethionine-mediated apoptosis is potentiated by autophagy inhibition induced by chloroquine in human breast cancer cells.* J Cell Physiol, 2018. **233**(2): p. 1370-1383.
76. Hapach, L.A., et al., *Engineered models to parse apart the metastatic cascade.* NPJ Precis Oncol, 2019. **3**: p. 20.
77. Siegel, R.L., et al., *Cancer Statistics, 2021.* CA Cancer J Clin, 2021. **71**(1): p. 7-33.
78. Tomasi, M.L., et al., *S-adenosylmethionine and methylthioadenosine inhibit cancer metastasis by targeting microRNA 34a/b-methionine adenosyltransferase 2A/2B axis.* Oncotarget, 2017. **8**(45): p. 78851-78869.
79. Ilisso, C.P., et al., *The methyl donor S-adenosylmethionine potentiates doxorubicin effects on apoptosis of hormone-dependent breast cancer cell lines.* Endocrine, 2015. **50**(1): p. 212-22.
80. Luzhna, L. and O. Kovalchuk, *Modulation of DNA methylation levels sensitizes doxorubicin-resistant breast adenocarcinoma cells to radiation-induced apoptosis.* Biochem Biophys Res Commun, 2010. **392**(2): p. 113-7.
81. Majumdar, S., et al., *Aberrant DNA methylation and prostate cancer.* Curr Genomics, 2011. **12**(7): p. 486-505.
82. Locke, W.J., et al., *DNA Methylation Cancer Biomarkers: Translation to the Clinic.* Front Genet, 2019. **10**: p. 1150.
83. Dunn, G.P., L.J. Old, and R.D. Schreiber, *The immunobiology of cancer immunosurveillance and immunoediting.* Immunity, 2004. **21**(2): p. 137-48.

84. Smyth, M.J., G.P. Dunn, and R.D. Schreiber, *Cancer immunosurveillance and immunoediting: the roles of immunity in suppressing tumor development and shaping tumor immunogenicity.* Adv Immunol, 2006. **90**: p. 1-50.
85. Li, L., et al., *DNA Methylation in Peripheral Blood: A Potential Biomarker for Cancer Molecular Epidemiology.* J Epidemiol, 2012. **22**(5): p. 384-94.
86. Terry, M.B., et al., *DNA methylation in white blood cells: Association with risk factors in epidemiologic studies.* Epigenetics, 2011. **6**(7): p. 828-37.
87. Parashar, S., et al., *DNA methylation signatures of breast cancer in peripheral T-cells.* BMC Cancer, 2018. **18**(1): p. 574.
88. Zhang, Y., et al., *The signature of liver cancer in immune cells DNA methylation.* Clin Epigenetics, 2018. **10**: p. 8.
89. Ostrand-Rosenberg, S., *Immune Surveillance: A Balance Between Pro- and Anti-tumor Immunity.* Curr Opin Genet Dev, 2008. **18**(1): p. 11-8.
90. Page, D.B., et al., *Tumor immunology and cancer immunotherapy: summary of the 2014 SITC primer.* Journal for Immunotherapy of Cancer, 2015. **3**(1): p. 1-10.
91. Pandya, P.H., et al., *The Immune System in Cancer Pathogenesis: Potential Therapeutic Approaches.* J Immunol Res, 2016. **2016**.
92. Dunn, J. and S. Rao, *Epigenetics and immunotherapy: The current state of play.* Mol Immunol, 2017. **87**: p. 227-239.
93. Zhang, M., et al., *DNA methylation in the tumor microenvironment*.* J Zhejiang Univ Sci B, 2017. **18**(5): p. 365-72.
94. Tian, Y., L. Meng, and Y. Zhang, *Epigenetic Regulation of Dendritic Cell Development and Function.* Cancer J, 2017. **23**(5): p. 302-307.
95. Gordon, S., *Alternative activation of macrophages.* Nat Rev Immunol, 2003. **3**(1): p. 23-35.
96. Wyckoff, J.B., et al., *Direct visualization of macrophage-assisted tumor cell intravasation in mammary tumors.* Cancer Res, 2007. **67**(6): p. 2649-56.
97. Lin, E.Y., et al., *Macrophages regulate the angiogenic switch in a mouse model of breast cancer.* Cancer Res, 2006. **66**(23): p. 11238-46.
98. Gaud, G., R. Lesourne, and P.E. Love, *Regulatory mechanisms in T cell receptor signalling.* Nat Rev Immunol, 2018. **18**(8): p. 485-497.

99. Wargo, J.A., et al., *Immune Effects of Chemotherapy, Radiation, and Targeted Therapy and Opportunities for Combination With Immunotherapy.* Semin Oncol, 2015. **42**(4): p. 601-16.
100. Pardoll, D.M., *The blockade of immune checkpoints in cancer immunotherapy.* Nature Reviews Cancer, 2012. **12**(4): p. 252.
101. Sukari, A., et al., *Cancer Immunology and Immunotherapy.* Anticancer Res, 2016. **36**(11): p. 5593-5606.
102. Zou, W., *Regulatory T cells, tumour immunity and immunotherapy.* Nat Rev Immunol, 2006. **6**(4): p. 295-307.
103. Ralainirina, N., et al., *Control of NK cell functions by CD4+CD25+ regulatory T cells.* J Leukoc Biol, 2007. **81**(1): p. 144-53.
104. Ye, J., R.S. Livergood, and G. Peng, *The role and regulation of human Th17 cells in tumor immunity.* Am J Pathol, 2013. **182**(1): p. 10-20.
105. McKinney, E.F. and K.G. Smith, *T cell exhaustion and immune-mediated disease-the potential for therapeutic exhaustion.* Curr Opin Immunol, 2016. **43**: p. 74-80.
106. Emran, A.A., et al., *Targeting DNA Methylation and EZH2 Activity to Overcome Melanoma Resistance to Immunotherapy.* Trends Immunol, 2019. **40**(4): p. 328-344.
107. Wherry, E.J. and M. Kurachi, *Molecular and cellular insights into T cell exhaustion.* Nat Rev Immunol, 2015. **15**(8): p. 486-99.
108. Raval, R.R., et al., *Tumor immunology and cancer immunotherapy: summary of the 2013 SITC primer.* J Immunother Cancer, 2014. **2**: p. 14.
109. Demaria, O., et al., *Harnessing innate immunity in cancer therapy.* Nature, 2019. **574**(7776): p. 45-56.
110. Gorentla, B.K. and X.P. Zhong, *T cell Receptor Signal Transduction in T lymphocytes.* J Clin Cell Immunol. **2012**(Suppl 12): p. 005-.
111. Galluzzi, L., et al., *Immunological Effects of Conventional Chemotherapy and Targeted Anticancer Agents.* Cancer Cell, 2015. **28**(6): p. 690-714.
112. Beatty, G.L. and W.L. Gladney, *Immune escape mechanisms as a guide for cancer immunotherapy.* Clin Cancer Res, 2015. **21**(4): p. 687-92.
113. Galon, J. and D. Bruni, *Approaches to treat immune hot, altered and cold tumours with combination immunotherapies.* Nat Rev Drug Discov, 2019. **18**(3): p. 197-218.

114. McCarthy, E.F., *The toxins of William B. Coley and the treatment of bone and soft-tissue sarcomas.* Iowa Orthop J, 2006. **26**: p. 154-8.
115. Esfahani, K., et al., *A review of cancer immunotherapy: from the past, to the present, to the future.* Curr Oncol, 2020. **27**(Suppl 2): p. S87-S97.
116. Keir, M.E., et al., *PD-1 and its ligands in tolerance and immunity.* Annu Rev Immunol, 2008. **26**: p. 677-704.
117. Keir, M.E., L.M. Francisco, and A.H. Sharpe, *PD-1 and its ligands in T-cell immunity.* Curr Opin Immunol, 2007. **19**(3): p. 309-14.
118. Koyama, S., et al., *Adaptive resistance to therapeutic PD-1 blockade is associated with upregulation of alternative immune checkpoints.* Nat Commun, 2016. **7**: p. 10501.
119. Dong, H., et al., *Tumor-associated B7-H1 promotes T-cell apoptosis: a potential mechanism of immune evasion.* Nat Med, 2002. **8**(8): p. 793-800.
120. Sheppard, K.A., et al., *PD-1 inhibits T-cell receptor induced phosphorylation of the ZAP70/CD3zeta signalosome and downstream signaling to PKCtheta.* FEBS Lett, 2004. **574**(1-3): p. 37-41.
121. Parry, R.V., et al., *CTLA-4 and PD-1 receptors inhibit T-cell activation by distinct mechanisms.* Mol Cell Biol, 2005. **25**(21): p. 9543-53.
122. Alsaab, H.O., et al., *PD-1 and PD-L1 Checkpoint Signaling Inhibition for Cancer Immunotherapy: Mechanism, Combinations, and Clinical Outcome.* Front Pharmacol, 2017. **8**: p. 561.
123. Couzin-Frankel, J., *Breakthrough of the year 2013. Cancer immunotherapy*, in *Science*. 2013: United States. p. 1432-3.
124. Schadendorf, D., et al., *Melanoma.* Lancet, 2018. **392**(10151): p. 971-984.
125. Rebecca, V.W., R. Somasundaram, and M. Herlyn, *Pre-clinical modeling of cutaneous melanoma.* Nat Commun, 2020. **11**(1): p. 2858.
126. Network, T.C.G.A., *Genomic Classification of Cutaneous Melanoma.* Cell, 2015. **161**(7): p. 1681-96.
127. Rogiers, A., et al., *Long-Term Survival, Quality of Life, and Psychosocial Outcomes in Advanced Melanoma Patients Treated with Immune Checkpoint Inhibitors.* J Oncol, 2019. **2019**: p. 5269062.

128. Asmar, R., J. Yang, and R.D. Carvajal, *Clinical utility of nivolumab in the treatment of advanced melanoma.* Ther Clin Risk Manag, 2016. **12**: p. 313-25.
129. Larkin, J., et al., *Five-Year Survival with Combined Nivolumab and Ipilimumab in Advanced Melanoma.* N Engl J Med, 2019. **381**(16): p. 1535-1546.
130. Ballotti, R., Y. Cheli, and C. Bertolotto, *The complex relationship between MITF and the immune system: a Melanoma ImmunoTherapy (response) Factor?* Mol Cancer, 2020. **19**(1): p. 170.
131. Brenner, D.R., et al., *Projected estimates of cancer in Canada in 2020.* CMAJ, 2020. **192**(9): p. E199-E205.
132. Sung, H., et al., *Global Cancer Statistics 2020: GLOBOCAN Estimates of Incidence and Mortality Worldwide for 36 Cancers in 185 Countries.* CA Cancer J Clin, 2021. **71**(3): p. 209-249.
133. Siegel, R.L., K.D. Miller, and A. Jemal, *Cancer statistics, 2017.* CA: A Cancer Journal for Clinicians, 2018. **67**(1): p. 7-30.
134. Seyfried, T.N. and L.C. Huysentruyt, *On the origin of cancer metastasis.* Crit Rev Oncog, 2013. **18**(1-2): p. 43-73.
135. Chaffer, C.L. and R.A. Weinberg, *A perspective on cancer cell metastasis.* Science, 2011. **331**(6024): p. 1559-64.
136. Yersal, O. and S. Barutca, *Biological subtypes of breast cancer: Prognostic and therapeutic implications.* World J Clin Oncol, 2014. **5**(3): p. 412-24.
137. Cardoso, F., et al., *Early breast cancer: ESMO Clinical Practice Guidelines for diagnosis, treatment and follow-updagger.* Ann Oncol, 2019. **30**(8): p. 1194-1220.
138. Viale, G., et al., *Ki-67 (30-9) scoring and differentiation of Luminal A- and Luminal B-like breast cancer subtypes.* Breast Cancer Res Treat, 2019. **178**(2): p. 451-458.
139. Wu, Q., et al., *Breast cancer subtypes predict the preferential site of distant metastases: a SEER based study.* Oncotarget, 2017. **8**(17): p. 27990-27996.
140. Yang, M., C. Liu, and X. Yu, *Skeletal-related adverse events during bone metastasis of breast cancer: current status.* Discov Med, 2019. **27**(149): p. 211-220.
141. Kane, C.M., P. Hoskin, and M.I. Bennett, *Cancer induced bone pain.* BMJ, 2015. **350**: p. h315.

142. Harris, S.R., *Differentiating the Causes of Spontaneous Rib Fracture After Breast Cancer.* Clin Breast Cancer, 2016. **16**(6): p. 431-436.
143. Alexandrov, L.B., et al., *Signatures of mutational processes in human cancer.* Nature, 2013. **500**(7463): p. 415-21.
144. Yarchoan, M., A. Hopkins, and E.M. Jaffee, *Tumor Mutational Burden and Response Rate to PD-1 Inhibition.* N Engl J Med, 2017. **377**(25): p. 2500-2501.
145. Planes-Laine, G., et al., *PD-1/PD-L1 Targeting in Breast Cancer: The First Clinical Evidences Are Emerging. A Literature Review.* Cancers (Basel), 2019. **11**(7).
146. Plitas, G., et al., *Regulatory T Cells Exhibit Distinct Features in Human Breast Cancer.* Immunity, 2016. **45**(5): p. 1122-1134.
147. Dieci, M.V., et al., *The immune system and hormone-receptor positive breast cancer: Is it really a dead end?* Cancer Treat Rev, 2016. **46**: p. 9-19.
148. Polk, A., et al., *Checkpoint inhibitors in breast cancer - Current status.* Cancer Treat Rev, 2018. **63**: p. 122-134.
149. Dieci, M.V., et al., *Neoadjuvant Chemotherapy and Immunotherapy in Luminal B-like Breast Cancer: Results of the Phase II GIADA Trial.* Clin Cancer Res, 2022. **28**(2): p. 308-317.
150. Gibney, G.T., L.M. Weiner, and M.B. Atkins, *Predictive biomarkers for checkpoint inhibitor-based immunotherapy.* Lancet Oncol, 2016. **17**(12): p. e542-e551.
151. Yan, X., et al., *Prognostic Factors for Checkpoint Inhibitor Based Immunotherapy: An Update With New Evidences.* Front Pharmacol, 2018. **9**: p. 1050.
152. Vafaei, S., et al., *Combination therapy with immune checkpoint inhibitors (ICIs); a new frontier.* Cancer Cell Int, 2022. **22**(1): p. 2.
153. Prieto, P.A., et al., *Targeted Therapies Combined With Immune Checkpoint Therapy.* Cancer J, 2016. **22**(2): p. 138-46.
154. Taube, J.M., et al., *Association of PD-1, PD-1 ligands, and other features of the tumor immune microenvironment with response to anti-PD-1 therapy.* Clin Cancer Res, 2014. **20**(19): p. 5064-74.
155. Larkin, J., et al., *Combined Nivolumab and Ipilimumab or Monotherapy in Untreated Melanoma.* N Engl J Med, 2015. **373**(1): p. 23-34.

156. Mahoney, K.M. and M.B. Atkins, *Prognostic and predictive markers for the new immunotherapies.* Oncology (Williston Park), 2014. **28 Suppl 3**: p. 39-48.
157. Tumeh, P.C., et al., *PD-1 blockade induces responses by inhibiting adaptive immune resistance.* Nature, 2014. **515**(7528): p. 568-71.
158. Ji, R.R., et al., *An immune-active tumor microenvironment favors clinical response to ipilimumab.* Cancer Immunol Immunother, 2012. **61**(7): p. 1019-31.
159. Jorgovanovic, D., et al., *Roles of IFN-gamma in tumor progression and regression: a review.* Biomark Res, 2020. **8**: p. 49.
160. Bhat, P., et al., *Interferon-gamma derived from cytotoxic lymphocytes directly enhances their motility and cytotoxicity.* Cell Death Dis, 2017. **8**(6): p. e2836.
161. Shen, J., et al., *Anti-cancer therapy with TNFalpha and IFNgamma: A comprehensive review.* Cell Prolif, 2018. **51**(4): p. e12441.
162. Johnson, D.B., et al., *Melanoma-specific MHC-II expression represents a tumour-autonomous phenotype and predicts response to anti-PD-1/PD-L1 therapy.* Nat Commun, 2016. **7**: p. 10582.
163. Seidel, J.A., A. Otsuka, and K. Kabashima, *Anti-PD-1 and Anti-CTLA-4 Therapies in Cancer: Mechanisms of Action, Efficacy, and Limitations.* Front Oncol, 2018. **8**.
164. Buchbinder, E.I. and A. Desai, *CTLA-4 and PD-1 Pathways: Similarities, Differences, and Implications of Their Inhibition.* Am J Clin Oncol, 2016. **39**(1): p. 98-106.
165. Koustas, E., et al., *The Resistance Mechanisms of Checkpoint Inhibitors in Solid Tumors.* Biomolecules, 2020. **10**(5).
166. Sharma, P., et al., *Primary, Adaptive, and Acquired Resistance to Cancer Immunotherapy.* Cell, 2017. **168**(4): p. 707-723.
167. Ribas, A., et al., *Phase I study combining anti-PD-L1 (MEDI4736) with BRAF (dabrafenib) and/or MEK (trametinib) inhibitors in advanced melanoma.* Journal of Clinical Oncology, 2015. **33**(15_suppl): p. 3003-3003.
168. Catenacci, D.V.T., et al., *Margetuximab plus pembrolizumab in patients with previously treated, HER2-positive gastro-oesophageal adenocarcinoma (CP-MGAH22-05): a single-arm, phase 1b-2 trial.* Lancet Oncol, 2020. **21**(8): p. 1066-1076.
169. Bezu, L., et al., *Combinatorial strategies for the induction of immunogenic cell death.* Front Immunol, 2015. **6**: p. 187.

170. Wang, Y., et al., *Combining Immunotherapy and Radiotherapy for Cancer Treatment: Current Challenges and Future Directions.* Front Pharmacol, 2018. **9**: p. 185.
171. Drake, C.G., *Combination immunotherapy approaches.* Ann Oncol, 2012. **23 Suppl 8**: p. viii41-6.
172. Apetoh, L., et al., *Toll-like receptor 4-dependent contribution of the immune system to anticancer chemotherapy and radiotherapy.* Nat Med, 2007. **13**(9): p. 1050-9.
173. Higgins, J.P., M.B. Bernstein, and J.W. Hodge, *Enhancing immune responses to tumor-associated antigens.* Cancer Biol Ther, 2009. **8**(15): p. 1440-9.
174. Chakraborty, M., et al., *Irradiation of tumor cells up-regulates Fas and enhances CTL lytic activity and CTL adoptive immunotherapy.* J Immunol, 2003. **170**(12): p. 6338-47.
175. Reits, E.A., et al., *Radiation modulates the peptide repertoire, enhances MHC class I expression, and induces successful antitumor immunotherapy.* J Exp Med, 2006. **203**(5): p. 1259-71.
176. Romero-Garcia, S., H. Prado-Garcia, and A. Carlos-Reyes, *Role of DNA Methylation in the Resistance to Therapy in Solid Tumors.* Front Oncol, 2020. **10**: p. 1152.
177. Sigalotti, L., et al., *Epigenetic drugs as immunomodulators for combination therapies in solid tumors.* Pharmacol Ther, 2014. **142**(3): p. 339-50.
178. Heninger, E., T.E. Krueger, and J.M. Lang, *Augmenting antitumor immune responses with epigenetic modifying agents.* Front Immunol, 2015. **6**: p. 29.
179. Terranova-Barberio, M., S. Thomas, and P.N. Munster, *Epigenetic modifiers in immunotherapy: a focus on checkpoint inhibitors.* Immunotherapy, 2016. **8**(6): p. 705-19.
180. Chiappinelli, K.B., et al., *Combining Epigenetic and Immunotherapy to Combat Cancer.* Cancer Res, 2016. **76**(7): p. 1683-9.
181. Larkin, J., F.S. Hodi, and J.D. Wolchok, *Combined Nivolumab and Ipilimumab or Monotherapy in Untreated Melanoma.* N Engl J Med, 2015. **373**(13): p. 1270-1.
182. Bao, L., K. Dunham, and K. Lucas, *MAGE-A1, MAGE-A3, and NY-ESO-1 can be upregulated on neuroblastoma cells to facilitate cytotoxic T lymphocyte-mediated tumor cell killing.* Cancer Immunol Immunother, 2011. **60**(9): p. 1299-307.
183. Ishibashi, K., et al., *Epigenetic modification augments the immunogenicity of human leukocyte antigen G serving as a tumor antigen for T cell-based immunotherapy.* Oncoimmunology, 2016. **5**(6): p. e1169356.

184. Krishnadas, D.K., et al., *A phase I trial combining decitabine/dendritic cell vaccine targeting MAGE-A1, MAGE-A3 and NY-ESO-1 for children with relapsed or therapy-refractory neuroblastoma and sarcoma.* Cancer Immunol Immunother, 2015. **64**(10): p. 1251-60.

185. Xu, P., et al., *DNA methyltransferase inhibitors: an updated patent review (2012-2015).* Expert Opin Ther Pat, 2016. **26**(9): p. 1017-30.

186. Mikyskova, R., et al., *DNA demethylating agent 5-azacytidine inhibits myeloid-derived suppressor cells induced by tumor growth and cyclophosphamide treatment.* J Leukoc Biol, 2014. **95**(5): p. 743-753.

187. Terracina, K.P., et al., *DNA methyltransferase inhibition increases efficacy of adoptive cellular immunotherapy of murine breast cancer.* Cancer Immunol Immunother, 2016. **65**(9): p. 1061-73.

188. Lucarini, V., et al., *Combining Type I Interferons and 5-Aza-2'-Deoxycitidine to Improve Anti-Tumor Response against Melanoma.* J Invest Dermatol, 2017. **137**(1): p. 159-169.

189. Covre, A., et al., *Epigenetics meets immune checkpoints.* Semin Oncol, 2015. **42**(3): p. 506-13.

190. Tellez, C.S., et al., *SGI-110 and entinostat therapy reduces lung tumor burden and reprograms the epigenome.* Int J Cancer, 2014. **135**(9): p. 2223-31.

191. Zhang, F., et al., *Epigenetic manipulation restores functions of defective CD8(+) T cells from chronic viral infection.* Mol Ther, 2014. **22**(9): p. 1698-706.

192. Ghoneim, H.E., et al., *De Novo Epigenetic Programs Inhibit PD-1 Blockade-Mediated T Cell Rejuvenation.* Cell, 2017. **170**(1): p. 142-157 e19.

193. Chiappinelli, K.B., et al., *Inhibiting DNA Methylation Causes an Interferon Response in Cancer via dsRNA Including Endogenous Retroviruses.* Cell, 2015. **162**(5): p. 974-86.

194. Stone, M.L., et al., *Epigenetic therapy activates type I interferon signaling in murine ovarian cancer to reduce immunosuppression and tumor burden.* Proc Natl Acad Sci U S A, 2017. **114**(51): p. E10981-E10990.

195. Yang ML , e.a., *Lupus autoimmunity altered by cellular methylation metabolism. - PubMed - NCBI.* Autoimmunity, 2018. **46**(1).

196. Ara, A.I., et al., *S-Adenosylmethionine Inhibits Lipopolysaccharide-Induced Gene Expression via Modulation of Histone Methylation.* Hepatology, 2008. **47**(5): p. 1655-66.

197. Ding, W., et al., *s-adenosylmethionine levels govern innate immunity through distinct methylation-dependent pathways.* Cell Metab, 2015. **22**(4): p. 633-45.
198. Bardag-Gorce, F., et al., *SAMe Prevents the Up Regulation of Toll-Like Receptor Signaling in Mallory-Denk Body Forming Hepatocytes.* Exp Mol Pathol, 2010. **88**(3): p. 376-9.
199. Gomez-Santos, L., et al., *Inhibition of natural killer cells protects the liver against acute injury in the absence of glycine N-methyltransferase.* Hepatology, 2012. **56**(2): p. 747-759.
200. Hote, P.T., et al., *Ethanol inhibits methionine adenosyltransferase II activity and S-adenosylmethionine biosynthesis and enhances caspase-3-dependent cell death in T lymphocytes: relevance to alcohol-induced immunosuppression.* J Nutr Biochem, 2008. **19**(6): p. 384-91.
201. Tobena, R., et al., *Interleukin-2 induces gamma-S-adenosyl-L-methionine synthetase gene expression during T-lymphocyte activation.* Biochem J, 1996. **319 (Pt 3)**: p. 929-33.
202. LeGros, H.L., Jr., A.M. Geller, and M. Kotb, *Differential regulation of methionine adenosyltransferase in superantigen and mitogen stimulated human T lymphocytes.* J Biol Chem, 1997. **272**(25): p. 16040-7.
203. Kotb, M., J.B. Dale, and E.H. Beachey, *Stimulation of S-adenosylmethionine synthetase in human lymphocytes by streptococcal M protein.* J Immunol, 1987. **139**(1): p. 202-6.
204. De La Rosa, J., et al., *Induction of interleukin 2 production but not methionine adenosyltransferase activity or S-adenosylmethionine turnover in Jurkat T-cells.* Cancer Res, 1992. **52**(12): p. 3361-6.
205. De La Rosa, J., M. Kotb, and N.M. Kredich, *Regulation of S-adenosylmethionine synthetase activity in cultured human lymphocytes.* Biochim Biophys Acta, 1991. **1077**(2): p. 225-32.
206. German, D.C., C.A. Bloch, and N.M. Kredich, *Measurements of S-adenosylmethionine and L-homocysteine metabolism in cultured human lymphoid cells.* J Biol Chem, 1983. **258**(18): p. 10997-1003.
207. Zeng, Z., et al., *The role of c-Myb in the up-regulation of methionine adenosyltransferase 2A expression in activated Jurkat cells.* Biochem J, 2001. **353**(Pt 1): p. 163-168.
208. Kotb, M. and N.M. Kredich, *S-Adenosylmethionine synthetase from human lymphocytes. Purification and characterization.* J Biol Chem, 1985. **260**(7): p. 3923-30.

209. Sahin, E. and M. Sahin, *Epigenetical Targeting of the FOXP3 Gene by S-Adenosylmethionine Diminishes the Suppressive Capacity of Regulatory T Cells Ex Vivo and Alters the Expression Profiles.* J Immunother, 2019. **42**(1): p. 11-22.
210. Shipony, Z., et al., *Dynamic and static maintenance of epigenetic memory in pluripotent and somatic cells.* Nature, 2014. **513**(7516): p. 115-9.
211. Zhou, W., et al., *DNA methylation loss in late-replicating domains is linked to mitotic cell division.* Nat Genet, 2018. **50**(4): p. 591-602.
212. Bian, Y., et al., *Cancer SLC43A2 alters T cell methionine metabolism and histone methylation.* Nature, 2020.
213. Ulanovskaya, O.A., A.M. Zuhl, and B.F. Cravatt, *NNMT promotes epigenetic remodeling in cancer by creating a metabolic methylation sink.* Nat Chem Biol, 2013. **9**(5): p. 300-6.
214. Jung, H., et al., *DNA methylation loss promotes immune evasion of tumours with high mutation and copy number load.* Nat Commun, 2019. **10**(1): p. 4278.
215. Varela-Rey, M., et al., *Alcohol, DNA Methylation, and Cancer.* Alcohol Res, 2013. **35**(1): p. 25-35.
216. Wilson, L.E., et al., *Alcohol and DNA Methylation: An Epigenome-Wide Association Study in Blood and Normal Breast Tissue.* Am J Epidemiol, 2019. **188**(6): p. 1055-1065.
217. Lee, K.W. and Z. Pausova, *Cigarette smoking and DNA methylation.* Front Genet, 2013. **4**: p. 132.
218. Moran, S., C. Arribas, and M. Esteller, *Validation of a DNA methylation microarray for 850,000 CpG sites of the human genome enriched in enhancer sequences.* Epigenomics, 2016. **8**(3): p. 389-99.
219. Li, L.T., et al., *Ki67 is a promising molecular target in the diagnosis of cancer (review).* Mol Med Rep, 2015. **11**(3): p. 1566-72.
220. Rambow, F., J.C. Marine, and C.R. Goding, *Melanoma plasticity and phenotypic diversity: therapeutic barriers and opportunities.* Genes Dev, 2019. **33**(19-20): p. 1295-1318.
221. Hoek, K.S., et al., *In vivo switching of human melanoma cells between proliferative and invasive states.* Cancer Res, 2008. **68**(3): p. 650-6.
222. Cheli, Y., et al., *Mitf is the key molecular switch between mouse or human melanoma initiating cells and their differentiated progeny.* Oncogene, 2011. **30**(20): p. 2307-18.

223. Wiedemann, G.M., et al., *Microphthalmia-Associated Transcription Factor (MITF) Regulates Immune Cell Migration into Melanoma.* Transl Oncol, 2019. **12**(2): p. 350-360.
224. Cheli, Y., et al., *Hypoxia and MITF control metastatic behaviour in mouse and human melanoma cells.* Oncogene, 2012. **31**(19): p. 2461-70.
225. Dilshat, R., et al., *MITF reprograms the extracellular matrix and focal adhesion in melanoma.* Elife, 2021. **10**.
226. Rambow, F., et al., *Toward Minimal Residual Disease-Directed Therapy in Melanoma.* Cell, 2018. **174**(4): p. 843-855 e19.
227. Travnickova, J., et al., *Zebrafish MITF-Low Melanoma Subtype Models Reveal Transcriptional Subclusters and MITF-Independent Residual Disease.* Cancer Res, 2019. **79**(22): p. 5769-5784.
228. Saez-Ayala, M., et al., *Directed phenotype switching as an effective antimelanoma strategy.* Cancer Cell, 2013. **24**(1): p. 105-19.
229. Fane, M.E., et al., *BRN2, a POUerful driver of melanoma phenotype switching and metastasis.* Pigment Cell Melanoma Res, 2019. **32**(1): p. 9-24.
230. Ganesan, R., E. Mallets, and J. Gomez-Cambronero, *The transcription factors Slug (SNAI2) and Snail (SNAI1) regulate phospholipase D (PLD) promoter in opposite ways towards cancer cell invasion.* Mol Oncol, 2016. **10**(5): p. 663-76.
231. Sinnberg, T., et al., *Wnt-signaling enhances neural crest migration of melanoma cells and induces an invasive phenotype.* Mol Cancer, 2018. **17**(1): p. 59.
232. Zhang, S., X. Xiong, and Y. Sun, *Functional characterization of SOX2 as an anticancer target.* Signal Transduct Target Ther, 2020. **5**(1): p. 135.
233. Saito, M., et al., *Effect of Nanog overexpression on the metastatic potential of a mouse melanoma cell line B16-BL6.* Mol Cell Biochem, 2021. **476**(7): p. 2651-2661.
234. Girouard, S.D., et al., *SOX2 contributes to melanoma cell invasion.* Lab Invest, 2012. **92**(3): p. 362-70.
235. Hoek, K.S., et al., *Metastatic potential of melanomas defined by specific gene expression profiles with no BRAF signature.* Pigment Cell Res, 2006. **19**(4): p. 290-302.
236. Carreira, S., et al., *Mitf regulation of Dia1 controls melanoma proliferation and invasiveness.* Genes Dev, 2006. **20**(24): p. 3426-39.

237. Sarna, M., et al., *Melanin presence inhibits melanoma cell spread in mice in a unique mechanical fashion.* Sci Rep, 2019. **9**(1): p. 9280.
238. Sarna, M., et al., *Cell elasticity is an important indicator of the metastatic phenotype of melanoma cells.* Exp Dermatol, 2014. **23**(11): p. 813-8.
239. Huang, F., et al., *Inhibiting the MNK1/2-eIF4E axis impairs melanoma phenotype switching and potentiates antitumor immune responses.* J Clin Invest, 2021. **131**(8).
240. Saran, A., et al., *Loss of tyrosinase activity confers increased skin tumor susceptibility in mice.* Oncogene, 2004. **23**(23): p. 4130-5.
241. Srour, N., et al., *PRMT7 ablation stimulates anti-tumor immunity and sensitizes melanoma to immune checkpoint blockade.* Cell Rep, 2022. **38**(13): p. 110582.
242. Johnson, L.A., et al., *Gene therapy with human and mouse T-cell receptors mediates cancer regression and targets normal tissues expressing cognate antigen.* Blood, 2009. **114**(3): p. 535-46.
243. Hsiao, J.J. and D.E. Fisher, *The roles of microphthalmia-associated transcription factor and pigmentation in melanoma.* Arch Biochem Biophys, 2014. **563**: p. 28-34.
244. Boni, A., et al., *Selective BRAFV600E inhibition enhances T-cell recognition of melanoma without affecting lymphocyte function.* Cancer Res, 2010. **70**(13): p. 5213-9.
245. Overwijk, W.W. and N.P. Restifo, *B16 as a mouse model for human melanoma.* Curr Protoc Immunol, 2001. **Chapter 20**: p. Unit 20.1.
246. Wu, T.C., et al., *A reassessment of the role of B7-1 expression in tumor rejection.* J Exp Med, 1995. **182**(5): p. 1415-21.
247. Wang, J., et al., *UV-induced somatic mutations elicit a functional T cell response in the YUMMER1.7 mouse melanoma model.* Pigment Cell Melanoma Res, 2017. **30**(4): p. 428-435.
248. Goren, J.L., et al., *Bioavailability and lack of toxicity of S-adenosyl-L-methionine (SAMe) in humans.* Pharmacotherapy, 2004. **24**(11): p. 1501-7.
249. Galizia, I., et al., *S-adenosyl methionine (SAMe) for depression in adults.* Cochrane Database Syst Rev, 2016. **10**: p. CD011286.
250. Papakostas, G.I., J.E. Alpert, and M. Fava, *S-adenosyl-methionine in depression: a comprehensive review of the literature.* Curr Psychiatry Rep, 2003. **5**(6): p. 460-6.

251. Mehdi, A., et al., *Enhanced Anticancer Effect of a Combination of S-adenosylmethionine (SAM) and Immune Checkpoint Inhibitor (ICPi) in a Syngeneic Mouse Model of Advanced Melanoma.* Front Oncol, 2020. **10**: p. 1361.
252. Sun, X., et al., *Suppression of breast cancer-associated bone loss with osteoblast proteomes via Hsp90ab1/moesin-mediated inhibition of TGFbeta/FN1/CD44 signaling.* Theranostics, 2022. **12**(2): p. 929-943.
253. Feng, Y., et al., *Mechanical Loading-Driven Tumor Suppression Is Mediated by Lrp5-Dependent and Independent Mechanisms.* Cancers (Basel), 2021. **13**(2).
254. Double, J., et al., *Toxicity testing in the development of anticancer drugs.* Lancet Oncol, 2002. **3**(7): p. 438-42.
255. Kumar, S., S. Bajaj, and R.B. Bodla, *Preclinical screening methods in cancer.* Indian J Pharmacol, 2016. **48**(5): p. 481-6.
256. Parasuraman, S., *Toxicological screening.* J Pharmacol Pharmacother, 2011. **2**(2): p. 74-9.
257. Bertolotto, C., et al., *Microphthalmia gene product as a signal transducer in cAMP-induced differentiation of melanocytes.* J Cell Biol, 1998. **142**(3): p. 827-35.
258. Goel, V.K., et al., *Melanocytic nevus-like hyperplasia and melanoma in transgenic BRAFV600E mice.* Oncogene, 2009. **28**(23): p. 2289-98.
259. Yin, L., et al., *Humanized mouse model: a review on preclinical applications for cancer immunotherapy.* Am J Cancer Res, 2020. **10**(12): p. 4568-4584.
260. Shekarian, T., et al., *Paradigm shift in oncology: targeting the immune system rather than cancer cells.* Mutagenesis, 2015. **30**(2): p. 205-11.
261. Information, N.C.f.B. PubChem *Compound Summary for CID 34755, S-adenosylmethionine*. 2023 January 17, 2023]; Available from: https://pubchem.ncbi.nlm.nih.gov/compound/S-adenosylmethionine.